

VOLUME 78

AUGUST 15, 1974

✓ NUMBER 17

JPCHAx

THE JOURNAL OF

PHYSICAL
CHEMISTRY

PUBLISHED BIWEEKLY BY THE AMERICAN CHEMICAL SOCIETY

THE JOURNAL OF PHYSICAL CHEMISTRY

BRYCE CRAWFORD, Jr., *Editor*

WILMER G. MILLER, *Associate Editor*

ROBERT W. CARR, Jr., **FREDERIC A. VAN-CATLEDGE**, *Assistant Editors*

EDITORIAL BOARD: A. O. ALLEN (1970-1974), C. A. ANGELL (1973-1977),
F. C. ANSON (1974-1978), V. A. BLOOMFIELD (1974-1978), J. R. BOLTON (1971-1975),
L. M. DORFMAN (1974-1978), M. FIXMAN (1970-1974), H. S. FRANK (1970-1974),
R. R. HENTZ (1972-1976), W. J. KAUZMANN (1974-1978), R. L. KAY (1972-1976),
D. W. McCLURE (1974-1978), R. M. NOYES (1973-1977), J. A. POPLE (1971-1975),
B. S. RABINOVITCH (1971-1975), H. REISS (1970-1974), S. A. RICE (1969-1975),
F. S. ROWLAND (1973-1977), R. L. SCOTT (1973-1977), A. SILBERBERG (1971-1975),
J. B. STOTHERS (1974-1978), W. A. ZISMAN (1972-1976)

AMERICAN CHEMICAL SOCIETY, 1155 Sixteenth St., N.W., Washington, D. C. 20036

Books and Journals Division

JOHN K. CRUM *Director*

RUTH REYNARD *Assistant to the Director*

CHARLES R. BERTSCH *Head, Editorial Processing Department*

D. H. MICHAEL BOWEN *Head, Journals Department*

BACIL GUILLEY *Head, Graphics and Production Department*

SELDON W. TERRANT *Head, Research and Development Department*

©Copyright, 1974, by the American Chemical Society. Published biweekly by the American Chemical Society at 20th and Northampton Sts., Easton, Pa. 18042. Second-class postage paid at Washington, D. C., and at additional mailing offices.

All manuscripts should be sent to *The Journal of Physical Chemistry*, Department of Chemistry, University of Minnesota, Minneapolis, Minn. 55455.

Additions and Corrections are published once yearly in the final issue. See Volume 77, Number 26 for the proper form.

Extensive or unusual alterations in an article after it has been set in type are made at the author's expense, and it is understood that by requesting such alterations the author agrees to defray the cost thereof.

The American Chemical Society and the Editor of *The Journal of Physical Chemistry* assume no responsibility for the statements and opinions advanced by contributors.

Correspondence regarding accepted copy, proofs, and reprints should be directed to Editorial Processing Department, American Chemical Society, 20th and Northampton Sts., Easton, Pa. 18042. Department Head: CHARLES R. BERTSCH. Assistant Department Head: MARIANNE C. BROGAN. Assistant Editor: CELIA B. McFARLAND. Editorial Assistant: JOSEPH E. YURVATI.

Advertising Office: Centcom, Ltd., 50 W. State St., Westport, Conn. 06880.

Business and Subscription Information

Send all new and renewal subscriptions *with payment* to Office of the Controller, 1155 16th Street, N.W., Washington, D. C. 20036. Subscriptions should be renewed promptly to avoid a break in your

series. All correspondence and telephone calls regarding changes of address, claims for missing issues, subscription service, the status of records, and accounts should be directed to Manager, Membership and Subscription Services, American Chemical Society, P. O. Box 3337, Columbus, Ohio 43210. Telephone (614) 421-7230.

On changes of address, include both old and new addresses with ZIP code numbers, accompanied by mailing label from a recent issue. Allow four weeks for change to become effective.

Claims for missing numbers will not be allowed (1) if loss was due to failure of notice of change in address to be received before the date specified, (2) if received more than sixty days from date of issue plus time normally required for postal delivery of journal and claim, or (3) if the reason for the claim is "issue missing from files."

Subscription rates (1974): members of the American Chemical Society, \$20.00 for 1 year; to nonmembers, \$60.00 for 1 year. Those interested in becoming members should write to the Admissions Department, American Chemical Society, 1155 Sixteenth St., N.W., Washington, D. C. 20036. Postage to Canada and countries in the Pan-American Union, \$5.00; all other countries, \$6.00. Air freight rates available on request. Single copies for current year: \$3.00. Rates for back issues from Volume 56 to date are available from the Special Issues Sales Department, 1155 Sixteenth St., N.W., Washington, D. C. 20036.

Subscriptions to this and the other ACS periodical publications are available on microfilm. Supplementary material not printed in this journal is now available in microfiche form on a current subscription basis. For information on microfilm or microfiche subscriptions, write Special Issues Sales Department at the address above.

THE JOURNAL OF
PHYSICAL CHEMISTRY

Volume 78, Number 17 August 15, 1974

JPCHAx 78(17) 1681-1774 (1974)

ISSN 0022-3654

- Role of Singlet Oxygen in Some Chemiluminescence and Enzyme Oxidation Reactions
..... **Robert Nilsson and David R. Kearns*** 1681
- Theory of Electron Transfer Reactions in Simple Dielectric Fluids **P. P. Schmidt** 1684
- Redox Mechanism in an Ionic Matrix. IV. Catalytic Effects of Peroxide and Superoxide on the
Oxidation of Nitrite by Molecular Oxygen in Molten Alkali Nitrates
..... **F. Paniccia and P. G. Zamboni*** 1693
- Laser Flash Photolytic Study of Mercury(II) Iodide in Aqueous Solution
..... **Philippe Fornier de Violet,* Roland Bonneau, and Samuel R. Logan** 1698
- Entropies of the Hydrates of Sodium Hydroxide. III. Low-Temperature Heat Capacities and
Heats of Fusion of the α and β Crystalline Forms of NaOH·4H₂O
..... **S. C. Mraw and W. F. Giauque*** 1701
- Mixtures of Trifluoroacetic Acid with Acetic Acid and Carbon Tetrachloride
..... **Friedrich Kohler,* G. H. Findenegg, and M. Bobik** 1709■
- Electrochemical Studies and Molecular Energy Levels in Furanquinones
..... **J. E. Kuder,* D. Wychick, R. L. Miller, and M. S. Walker** 1714
- Hydrophobic Interactions in Mixtures of *N,N*-Dimethylformamide and Water. Model
Calculations and Enthalpies of Solution **C. de Visser and G. Somsen*** 1719
- Hydrogen Bonding of Water in Organic Solvents. I **O. D. Bonner* and Y. S. Choi** 1723
- Hydrogen Bonding of Water in Organic Solvents. II. The Change of Water Structure with
Composition **O. D. Bonner* and Y. S. Choi** 1727
- Coordination and Ionic Solvation **B. G. Cox, A. J. Parker, and W. E. Waghorne*** 1731■
- Effect of Structure on the Mesomorphic Properties of Cholesteryl Alkanoates. V. Electric Field
Effects on a Uniaxial Smectic Phase of Mixtures of Cholesteryl Alkanoates
..... **John M. Pochan* and Harry W. Gibson** 1740
- Dipole Moment and Far-Infrared Studies on the Dimethyl Sulfoxide-Iodine Complex
..... **A. Eugene Pekary** 1744
- Nuclear Magnetic Resonance Studies of the Interaction of Molecular Oxygen with
Organic Compounds **M. Polak and G. Navon*** 1747
- Cation Radical Salts of *N*-Methylphenothiazine and Its Analogs. Synthesis and Characterization
..... **M. H. Litt* and J. Radovic** 1750
- Structure of Aqueous Solutions. Structure Making and Structure Breaking in Solutions of
Sucrose and Urea **David W. James* and Ray L. Frost** 1754
- Self-Diffusion Coefficients for Chloride Ion in Aqueous Solutions of Sodium Polyacrylate
Containing Sodium Chloride **Shelini Menezes-Affonso and Paul Ander*** 1756
- Effect of Ethanol on Hydrophobic Interactions. A Conductometric Study of Ion-Pair Formation
by Double-Long-Chain Electrolytes **D. G. Oakenfull* and D. E. Fenwick** 1759
- Matrix Isolation Infrared Study of the Reaction between Germanium Vapor and Molecular
Oxygen. The Characterization and Mechanism of Formation of Molecular Germanium
Dioxide and Ozone **A. Bos, J. S. Ogden,* and L. Orgee** 1763

COMMUNICATIONS TO THE EDITOR

- Electron Spin Resonance Study of Chlorine Dioxide Adsorbed on the Alkali-Cation-Exchanged X-Type Zeolites **K. Shimokoshi,* H. Sugihara, and I. Yasumori** 1770
- Equilibrium Studies by Electron Spin Resonance. VIII. The Use of Time Averaged Coupling Constants to Determine Free Ion-Ion Pair Equilibrium Constants **Gerald R. Stevenson* and Antonio E. Alegria** 1771
- On the Negative Temperature Dependence of Slow Ion-Molecule Reactions **M. Meot-Ner, J. J. Solomon, F. H. Field, and H. Gershinowitz*** 1773

■ Supplementary material for this paper is available separately, in photocopy or microfiche form. Ordering information is given in the paper.

* In papers with more than one author, the asterisk indicates the name of the author to whom inquiries about the paper should be addressed.

AUTHOR INDEX

- | | | | |
|---------------------------|---------------------------|------------------------|------------------------|
| Alegria, A. E., 1771 | Gershinowitz, H., 1773 | Navon, G., 1747 | Schmidt, P. P., 1684 |
| Ander, P., 1756 | Giauque, W. F., 1701 | Nilsson, R., 1681 | Shimokoshi, K., 1770 |
| Bobik, M., 1709 | Gibson, H. W., 1740 | Oakenfull, D. G., 1759 | Solomon, J. J., 1773 |
| Bonneau, R., 1698 | James, D. W., 1754 | Ogden, J. S., 1763 | Somsen, G., 1719 |
| Bonner, O. D., 1723, 1727 | Kearns, D. R., 1681 | Orgee, L., 1763 | Stevenson, G. R., 1771 |
| Bos, A., 1763 | Kohler, F., 1709 | | Sugihara, H., 1770 |
| Choi, Y. S., 1723, 1727 | Kuder, J. E., 1714 | Paniccia, F., 1693 | Waghorne, W. E., 1731 |
| Cox, B. G., 1731 | Litt, M. H., 1750 | Parker, A. J., 1731 | Walker, M. S., 1714 |
| de Violet, P. F., 1698 | Logan, S. R., 1698 | Pekary, A. E., 1744 | Wychick, D., 1714 |
| de Visser, C., 1719 | Menezes-Affonso, S., 1756 | Pochan, J. M., 1740 | |
| Fenwick, D. E., 1759 | Meot-Ner, M., 1773 | Polak, M., 1747 | Yasumori, I., 1770 |
| Field, F. H., 1773 | Miller, R. L., 1714 | Radovic, J., 1750 | |
| Findenegg, G. H., 1709 | Mraw, S. C., 1701 | | Zambonin, P. G., 1693 |
| Frost, R. L., 1754 | | | |

THE JOURNAL OF PHYSICAL CHEMISTRY

Registered in U. S. Patent Office © Copyright, 1974, by the American Chemical Society

VOLUME 78, NUMBER 17 AUGUST 15, 1974

Role of Singlet Oxygen in Some Chemiluminescence and Enzyme Oxidation Reactions

Robert Nilsson and David R. Kearns*

Department of Chemistry, University of California, Riverside, California 92502 (Received January 31, 1974)

Publication costs assisted by the National Institute of General Medical Sciences

In this paper we have investigated the possible role of singlet oxygen in (i) the sensitized luminescence of fluorescein induced by the decomposition of hydrogen peroxide, (ii) the decomposition of superoxide ion by hydroxylic solvents, and (iii) the oxidation of linoleic acid by lipoxidase. Through the use of the previously reported deuterium isotope effect on singlet oxygen lifetimes we are able to confirm the participation of singlet oxygen in the hydrogen peroxide induced fluorescence of fluorescein. We found no evidence for the presence of singlet oxygen in the decomposition of superoxide ion or in the oxidation of linoleic acid catalyzed by lipoxidase.

Introduction

The participation of singlet oxygen has been implied in a number of liquid systems including photosensitized oxidations,¹⁻³ decomposition of hydrogen peroxide by chlorine and hypochlorite,^{4,5} thermal decomposition of transannular peroxides of anthracene derivatives,^{6,7} reactions catalyzed by the enzyme lipoxidase,⁸ and in reactions of the superoxide ion radical, O_2^- .⁹ Determination of the absolute lifetime of singlet oxygen in solution and the development of diagnostic tests based on the large deuterium effects on the lifetime of singlet oxygen, as well as on the correlation between the lifetime and the intensity of the infrared absorption of the solvent by us, has opened a way of reassessing the participation of singlet oxygen in various homogeneous¹⁰⁻¹³ as well as heterogeneous systems.¹⁴ Employing these tools together with kinetic spectroscopy and azide as quencher,¹⁵ conclusive evidence for the participation of singlet oxygen in the photosensitized oxidation of the free amino acids histidine, tryptophan, and methionine was obtained.¹⁶ In an extension of this work the participation of singlet oxygen in the photodynamic inactivation of the enzymes alcohol dehydrogenase and trypsin was established.¹⁷ Identical results have now been obtained for the photodynamic destruction of lysozyme in two other laboratories using different sensitizers.^{18,19} In this laboratory it has recently been demonstrated that the red chemiluminescence from the hydrogen peroxide-hypochlorite system is dramatically enhanced in D_2O , although the peroxide decomposition rate is retarded in this medium. In this way direct spectroscopic evidence for a deuterium effect on the lifetime of singlet oxygen was obtained.²⁰ In the present communication we have used this

deuterium effect to investigate three different systems which reportedly involve singlet oxygen. These include (i) the sensitized luminescence of fluorescein induced by the decomposition of hydrogen peroxide, (ii) the decomposition of the superoxide radical by hydroxylic solvents, and (iii) the oxidation of linoleic acid catalyzed by lipoxidase.

Experimental Section

Chemiluminescence Measurements. (a) H_2O_2 - $NaOCl$ Sensitized Fluorescence of Fluorescein. The device for measuring the chemiluminescence consisted of a cuvette placed in a light-tight compartment situated in front of a sensitive photomultiplier equipped with a filter eliminating the red light originating from singlet oxygen itself. The photocurrent from the photomultiplier was measured directly by a storage oscilloscope. Since the peroxide decomposition is very rapid, the photocurrent was integrated by charging a $1\text{-}\mu\text{F}$ condenser coupled between the input of the oscilloscope and ground. A 0.39 M solution of $NaOCl$ (0.25 ml) in water or in 50% D_2O was placed in the cuvette together with various amounts of fluorescein and 2 ml of a 0.3% solution of H_2O_2 in H_2O or D_2O was injected into the cuvette by means of a syringe connected to the inside of the light-tight chamber by a bent metal tube.

The yield of sensitized luminescence was found to be strongly dependent on the fluorescein concentration (Table I). Even at 10^{-3} M , where dimerization of the dye is considerable, an increase of the concentration of the dye increases the emission yield. The slight decrease observed around 10^{-2} M is therefore probably due to self quenching. The extremely high concentrations of dye required to

TABLE I: Influence of the Fluorescein Concentration on the Integrated, Sensitized Chemiluminescence Induced in the Peroxide-Hydrochlorite System

Fluorescein concn, M	Relative integrated luminescence intensity
2×10^{-4}	25
6×10^{-4}	160
1.8×10^{-3}	240
6×10^{-3}	500
1.2×10^{-2}	440

achieve optimal luminescence seem to support the concept of a termolecular mechanism of energy transfer.²⁵ In Figure 1 the enhancement of the integrated luminescence is listed together with the expected lifetime of singlet oxygen at two concentrations of D_2O .

(b) *Superoxide Sensitized Fluorescence of Fluorescein.* The superoxide sensitized fluorescence of fluorescein was studied using the same apparatus described above. When solutions of dry dimethyl sulfoxide containing KO_2 were examined for luminescence none could be detected either from solutions containing fluorescein or from solutions containing no fluorescein. However, with the injection of a small amount of water (0.25 ml) or dimethyl sulfoxide containing water, a weak light emission could be observed in the presence of fluorescein. Since the replacement of H_2O by D_2O should enhance the lifetime of singlet oxygen in the mixed DMSO- H_2O water solution, the experiments were repeated using D_2O instead of H_2O , but no difference between the D_2O and H_2O experiments could be detected.

Chemical Oxidation by Superoxide Ion. The oxidation of the singlet oxygen acceptor tetramethylene (TME) by KO_2 was studied in the following way. A $3.5 \times 10^{-2} M$ solution of TME was prepared in dry dimethyl sulfoxide saturated with KO_2 . After 24 hr, either in a closed vessel or in an open container which permitted the slow absorption of moisture from the air, we were unable to detect any oxidation of the TME as analyzed by gas chromatography.

Under the above reaction conditions the decomposition of the KO_2 is rather slow so to accelerate it either water or ethanol was added. Even in the systems where immediate decomposition was induced by injection of water or ethanol, no oxidation of TME or another singlet oxygen acceptor, 1,3-diphenylisobenzofuran, was observed when they were added to the solution.

The Lipoxidase Catalyzed Oxidation of Linoleic Acid. The assay medium for measuring the activity of lipoxidase consisted of 100- μM suspension of linoleic acid in 0.2 M borate buffer pH 9 to which 0.05 mg of soybean lipoxidase (Sigma, lyophilized, 50,000 units/mg) was added. The oxidation of the fatty acid was monitored spectrophotometrically as an increase in absorption at 234 nm. Exchanging H_2O for D_2O had no effect on the rate of oxidation of linoleic acid under these conditions.

Discussion

(1) *Sensitized Fluorescence from Fluorescein Produced by Decomposition of Hydrogen Peroxide by Hypochlorite.* One of the most interesting aspects of the hydrogen peroxide-hypochlorite system is that it is capable of sensitizing the luminescence from various organic compounds which are present during the peroxide decomposition. Such luminescence has been obtained in presence of substances such as anthracene, acridine, eosin, fluorescein, quinine

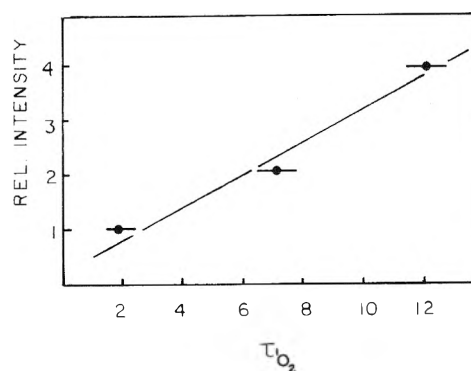


Figure 1. Variation of the integrated intensity of luminescence in the fluorescein-hydrogen peroxide-hypochlorite system with the lifetime of singlet oxygen, τ , in solution. Different lifetimes were obtained by using solutions containing different relative amounts of H_2O and D_2O . The lifetime in H_2O is 2 μsec , whereas in a solution containing 6% H_2O and 94% D_2O the lifetime is calculated to be 12 μsec .

sulfate, aesculin, violanthrone, and rubrene.²¹⁻²⁴ Since the energy available from $^1\Delta_g$ which is generated by the decomposition of H_2O_2 is insufficient to excite these molecules by energy transfer between two molecules, Khan and Kasha suggested a mechanism involving energy transfer from molecular pairs of excited oxygen.²⁵ The pathway by which energy pooling occurs is uncertain and a two-step successive excitation mechanism²³ as well as a termolecular mechanism²⁵ has been proposed.

In order to test for the involvement of singlet oxygen in the H_2O_2 - $NaOCl$ sensitized chemiluminescence of fluorescein we have examined the effect of D_2O on the luminescence intensity. The basis for the experiment lies in the fact the lifetime of singlet oxygen in D_2O is about 20 μsec , but it is a factor of 10 shorter in H_2O . Thus, if the chemiluminescence sensitized by the peroxide decomposition is due to the formation of singlet oxygen molecules, the luminescence should be much brighter in D_2O than H_2O , simply because the singlet oxygen molecules live longer and therefore have a better opportunity to sensitize the luminescence. The only complicating factor is that the decomposition of the H_2O_2 is slower in D_2O so that it would be possible to have no enhancement, or even a decrease in the intensity even though it involves a singlet oxygen sensitized process. If D_2O enhances the luminescence, however, then it is safe to conclude that singlet oxygen is involved.

The results of our experiments are summarized in Figure 1, where it can be seen that relative to the H_2O solution there is a fourfold enhancement of the fluorescein chemiluminescence when the reaction is run in 94% D_2O . In view of the singlet oxygen lifetime measurements reported by Merkel and Kearns,¹¹ we can compute that the singlet oxygen lifetime is about a factor of 6 longer in the 94% D_2O solution. Depending upon whether the mechanism involved the singlet oxygen concentration to the first, second, or third power, we might have expected a 6-, 36-, or 216-fold increase in the intensity. Unfortunately we are not able to distinguish between these three possibilities because of the fact that the decomposition of H_2O_2 is slower in D_2O than in H_2O . If we had accurate values for the decomposition rate, then we could evaluate this possibility. Nevertheless, the involvement of singlet oxygen in the luminescence is clearly established.

(2) *Decomposition of Potassium Superoxide in Dimethyl Sulfoxide.* When the singlet oxygen acceptor 2,5-di-

methylfuran was added to a solution of KO_2 in dimethyl sulfoxide Khan obtained a reaction product giving the characteristic peroxide test with potassium iodide. Further, this solution was found to induce sensitized luminescence from anthracene. The results were interpreted in terms of production of singlet oxygen from O_2^- .⁹ Since the chemical test hardly could be considered as conclusive for proving the generation of singlet oxygen, we undertook a study of the D_2O effect on the luminescence using the same equipment as described in the previous section. Whereas no luminescence could be detected from dry dimethyl sulfoxide containing KO_2 with or without fluorescein, injection of a small amount of water or dimethyl sulfoxide containing water induced a weak light emission. The addition of a small amount of water to dimethyl sulfoxide will drastically reduce the lifetime of any singlet oxygen produced in the system due to the large differences in lifetimes in the two solvents: 2 μsec in H_2O vs. 30 μsec in dimethyl sulfoxide. The replacement of H_2O by D_2O ($\tau_{\text{D}_2\text{O}} = 20 \mu\text{sec}$) would therefore be expected to greatly enhance the emission if the luminescence was actually caused by singlet oxygen. No such effect was observed. Furthermore, no oxidation of the singlet oxygen acceptor tetramethylethylene could be detected in KO_2 containing dry dimethyl sulfoxide after letting the reaction mixture stand for 24 hr, either in a closed vessel, or in an open container permitting the slow absorption of moisture from the air. Even adding water or ethanol to promote the decomposition of the KO_2 did not result in oxidation of TME or DPBF. In view of these results it seems unlikely that singlet oxygen is produced in any appreciable amounts in this system.

(3) Oxidation of Linoleic Acid Catalyzed by Lipoxidase.

On the basis of oxidation of tetraphenylcyclopentadienone and 1,3-diphenylisofuran during the catalytic action of soybean lipoxidase the participation of singlet oxygen has been proposed.⁸ If this intermediate is involved as an active oxidizing species during the catalytic cycle, the overall oxidation rate should be speeded up by a tenfold increase in lifetime of singlet oxygen caused by substituting H_2O for D_2O .

In our experiments we observed no change in the rate of the lipoxidase catalyzed oxidation of linoleic acid when D_2O instead of H_2O was used as the solvent. Thus, the

participation of singlet oxygen in the normal catalytic cycle of lipoxidase seems to be excluded. This finding is in line with the observation that tetraphenylcyclopentadienone, one of the substrates used for identifying singlet oxygen in the above work,⁸ is readily oxidized by nonsinglet oxygen pathways yielding the same products.²⁶

Acknowledgments. The support of the U. S. Public Health Service (Grant No. CA 11459) and the Swedish Atomic Research Council is most gratefully acknowledged. We are also indebted to Mr. Ron Galloway and Professor M. Gibian for aid in carrying out the measurement of lipoxidase activity.

References and Notes

- (1) H. Kautsky, *Trans. Faraday Soc.*, **35**, 216 (1939).
- (2) C. S. Foote and S. Wexler, *J. Amer. Chem. Soc.*, **86**, 3880 (1964).
- (3) E. J. Corey and W. C. Taylor, *J. Amer. Chem. Soc.*, **86**, 3881 (1964).
- (4) A. U. Khan and M. Kasha, *J. Chem. Phys.*, **39**, 2105 (1963).
- (5) C. S. Foote and S. Wexler, *J. Amer. Chem. Soc.*, **86**, 3879 (1964).
- (6) H. H. Wasserman and J. R. Scheffer, *J. Amer. Chem. Soc.*, **89**, 3073 (1967).
- (7) D. R. Kearns and A. L. Khan, *Photochem. Photobiol.*, **10**, 193 (1969).
- (8) H. W.-S. Chan, *J. Amer. Chem. Soc.*, **93**, 2357 (1971).
- (9) A. U. Khan, *Science*, **168**, 476 (1970).
- (10) P. B. Merkel and D. R. Kearns, *Chem. Phys. Lett.*, **12**, 120 (1971).
- (11) P. B. Merkel and D. R. Kearns, *J. Amer. Chem. Soc.*, **94**, 1029 (1972).
- (12) P. B. Merkel, R. Nilsson, and D. R. Kearns, *J. Amer. Chem. Soc.*, **94**, 1030 (1972).
- (13) P. B. Merkel and D. R. Kearns, *J. Amer. Chem. Soc.*, **94**, 7244 (1972).
- (14) R. Nilsson and D. R. Kearns, *Photochem. Photobiol.*, **19**, 181 (1974).
- (15) N. Hasty, P. B. Merkel, P. Radlick, and D. R. Kearns, *Tetrahedron Lett.*, **1**, 49 (1972).
- (16) R. Nilsson, P. B. Merkel, and D. R. Kearns, *Photochem. Photobiol.*, **16**, 117 (1972).
- (17) R. Nilsson and D. R. Kearns, *Photochem. Photobiol.*, **17**, 65 (1973).
- (18) H. Schmidt and P. Z. Rosenkranz, *Z. Naturforsch. B.*, **27**, 1436 (1972).
- (19) A. G. Kepka and L. I. Grossweiner, *Photochem. Photobiol.*, **18**, 49 (1973).
- (20) T. Kajiwara and D. R. Kearns, *J. Amer. Chem. Soc.*, **95**, 5886 (1973).
- (21) L. Mallet, *C. R. Acad. Sci.*, **185**, 352 (1927).
- (22) R. B. Kurtz, *Ann. N. Y. Acad. Sci.*, **16**, 399 (1954).
- (23) E. A. Ogryzlo and A. E. Pearson, *J. Phys. Chem.*, **72**, 2913 (1968).
- (24) T. Wilson, *J. Amer. Chem. Soc.*, **91**, 2387 (1969).
- (25) A. U. Khan and M. Kasha, *J. Amer. Chem. Soc.*, **92**, 3293 (1970).
- (26) J. E. Baldwin, J. C. Swallow, and H. W.-S. Chan, *Chem. Commun.*, 1407 (1971).

Theory of Electron Transfer Reactions in Simple Dielectric Fluids

P. P. Schmidt¹

Department of Chemistry, Oakland University, Rochester, Michigan 48063 and William Ramsay and Ralph Forster Laboratories, University College, London, England (Received December 10, 1973)

Publication costs assisted by Oakland University

Existing theories of electron transfer reactions develop from two separate points of view: the transition state theory of Marcus and the quantum mechanical theory of Levich and Dogonadze. Both approaches have their merits. However, neither possesses the generality afforded a theory based on the fundamental premise of statistical mechanics, the Liouville theorem. Recently, a new approach to the examination of the solution electron transfer reaction system was advanced. This new approach employs an analysis based on the application of Yamamoto's general statistical mechanical reaction rate theory. The purpose of this paper is to continue the examination of the electron transfer reaction system from this general point of view. In particular, this paper investigates the relationship between the simple Levich-Dogonadze outer-sphere electron transfer reaction theory and the more general approach. The analysis presented reveals the Levich-Dogonadze theory to be a special case of a more general approach. In particular, the result, the rate constant expression, is the same for the general statistical mechanical and perturbation theory treatments in the nonadiabatic limit. In the adiabatic limit the results differ. The comparison of the rate constant expression in the adiabatic limit and the result obtained here provides greater insight into the nature of that limit. The analysis presented here, moreover, shows that the rate constant expression depends on a type of momentum space Van Hove correlation function. This dependence suggests types of more general analyses which, hopefully, may get around the use of the simple dielectric continuum representation of the solvent modes of the system and proceed to an analysis more explicitly revealing the dependence of reaction rate processes on individual molecular dynamical contributions.

Introduction

In the last 15 years, largely through the efforts of a small number of individuals, the theory of electron transfer reactions has advanced to a fairly sophisticated and useful level. At this time there are two major theories for these reactions. On one hand, there is the equilibrium statistical mechanical, transition state theory originally formulated by Marcus^{2a} and Hush,^{2b} and in recent years brought to a high level of development by Marcus.³ On the other hand, Levich and Dogonadze⁴ some time ago introduced a quantum mechanically based theory which they and their coworkers continue to develop.⁵ Recently, we introduced a new theoretical approach.⁶ This new theory is based on the direct application of nonequilibrium statistical mechanics⁷ to the electron transfer reaction system. In many of its mathematical aspects this new theory bears close resemblances to both the Levich-Dogonadze and Marcus-Hush theories. However, because this theory is based on the use of nonequilibrium statistical mechanics, in principle it possesses greater rigor and generality than the previous theories. Even in its present early state of development this new approach is able to reproduce all the general features of both the Marcus theory and the Levich-Dogonadze theory. This has been shown already in the case of the Marcus theory.⁸

The purpose of this report is to present a reformulation of the Levich-Dogonadze theory⁴ in terms of the more general nonequilibrium statistical mechanical theory.⁶ Specifically, the analysis contained in this paper represents an examination of the Levich-Dogonadze model from a new theoretical point of view. Although the results obtained are of the same form as those obtained for the

simple electron transfer system considered by Levich and Dogonadze, these new results are not physically identical. The distinction lies in the theoretical approach; that is, the use of the nonequilibrium statistical mechanical approach imparts to the rate constant expressions a far greater generality and range of applicability.

There are several reasons for examining the Levich-Dogonadze model system in spite of its oversimplicity. First, in its simple form it is mathematically tractable. Interesting, physically useful expressions result for the rate constant. Sufficient detail of the mathematical development is contained here to reveal this facet of the theory. Second, both the Levich-Dogonadze and the general, nonequilibrium statistical mechanical theories cast the general rate constant expression into a form which depends on a time-dependent correlation function. It is a momentum space correlation function analogous to the Van Hove correlation function familiar from neutron, electron, and X-ray scattering theory.⁹ By virtue of this dependence of the rate constant expression on a momentum space correlation function there is available potentially a considerable amount of physically interesting information about the dynamics of the electron transfer act. This aspect of the theory appears at this time to be the key to further theoretical development the goal of which is to account for more complicated inner-sphere reactions.

Finally, certain aspects of both the Marcus-Hush^{2,3} and the Levich-Dogonadze⁴ theories recently have come under critical attack.¹⁰ In particular, the use of the dielectric continuum representation of the solvent has been discredited as overly simplistic to the extent of being useless, thus rendering the existing theories invalid. When

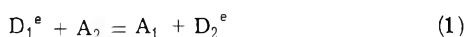
indiscriminately applied, this is certainly so. However, there are a number of aspects of the dielectric continuum representation which are useful. In particular, it is an excellent physical concept with which to examine the nature and influence of solvent fluctuations important in the activation process. Clearly, the dielectric continuum representation needs improvement, modification, or perhaps even (if possible) replacement. Nevertheless, it is not at all clear that without proper modification this representation of the solvent system cannot be more extensively and accurately used: for example, as a semicontinuum representation.

This paper makes use of the dielectric continuum representation. It is important to stress, however, that the generality of the expressions for the rate constant subsequently obtained depend heavily on this approximation. This, of course, is also true of the Levich–Dogonadze theory.

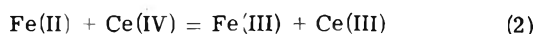
The Nature of the Simple Electron Transfer System

This section initiates the formal analysis which is the subject of this paper. There are two objectives for this section: one, the physical description of the model system, and two, the derivation and transformation to useful form of the Hamiltonian operator essential to the subsequent analysis resulting in the rate constant expressions. The system requires little more than a brief description of the now well-known Levich–Dogonadze model.⁴

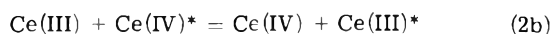
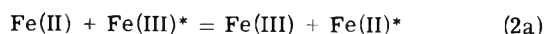
Consider a system of (usually) ionic conjugate electron donor and acceptor pairs. A chemical reaction representation of such a system is the following



In eq 1 A_1 is the acceptor conjugate to the donor D_1^e . For example, for the heteronuclear exchange



Fe(II) and Fe(III) are conjugate donor and acceptor pairs. A similar description applied to the Ce(III) and Ce(IV) entities. The reaction system symbolized by eq 1 represents the basic system of interest in this paper. However, it is necessary to be aware of two competing reactions, the homonuclear electron exchange reactions involving the Fe(II), Fe(III) and Ce(III), Ce(IV) pairs respectively



Such a symbolic representation is suited to simple outer-sphere type electron transfer reactions. But, in general, and especially for more complicated redox reactions, not all reactions reduce to this form. For purposes of this paper, however, this representation has a useful clarity.

The electron donor and acceptor pair systems are in solution in some suitable solvent system, perhaps with supporting electrolyte. This solvent system is represented as a dielectric continuum. In selecting a dielectric continuum representation one generally stipulates that during the course of the electron transfer there is no formation or destruction of chemical bonds and no gross alteration of the solvent system immediately surrounding the reactants and products. With these stipulations, the resulting theory necessarily applies only to outer-sphere type reactions. The succeeding analysis assumes exactly these stipulations.

Both the Levich–Dogonadze quantum mechanical⁴ and the general nonequilibrium statistical mechanical theories of simple electron transfer reactions require the use of a dynamic representation of the dielectric continuum. This in turn requires that one examine the dynamics, or equations of motion, of the solvent polarization field, \mathbf{P} , by which the dielectric continuum is characterized. It is well known from the polaron theory,¹¹ and now accepted in the solution electron transfer theory (as a result of Levich and Dogonadze's contributions) that the Hamiltonian operator for the dielectric continuum in the absence of interaction with the electron transfer system of interest is⁴

$$H_D = (2\pi/C) \int dV [\mathbf{P}^2 + \omega^{-2} \dot{\mathbf{P}}^2] \quad (3)$$

In particular, this Hamiltonian operator is the operator associated with the equilibrium dielectric continuum. The expression (3) already contains an assumption, namely that the dielectric continuum be regarded as dispersion free. That is only one frequency is assigned to all the energy modes of the dielectric. This is equivalent to the Einstein representation for the dielectric continuum. This is, moreover, a drastic assumption, but one which can be dropped in a more refined treatment of the theory. Indeed, this has been done recently by Dogonadze, Kuznetsov, Levich, and Vorotyntsev.¹² However, for immediate expository purposes we consider only the Einstein approximation of one frequency. The consequence of considering dispersion is found in the Appendix.

The factor C in eq 3 is

$$1/C = 1/\epsilon_\infty - 1/\epsilon_0 \quad (4)$$

where ϵ is the optical dielectric constant for the solvent. The static dielectric constant is given by ϵ_0 .

As it stands, the Hamiltonian operator, (3), is not in tractable form. However, by means of a Fourier series expansion the operator simplifies subject to the requirement that the expansion coefficients satisfy the boson commutation condition: *viz.*

$$\mathbf{P} = \left[\frac{\hbar}{\gamma V \omega} \right]^{1/2} \sum_{\mathbf{k}} \hat{e}_{\mathbf{k}} [q_{\mathbf{k}} \cos(\mathbf{k} \cdot \mathbf{r}) - p_{\mathbf{k}} \sin(\mathbf{k} \cdot \mathbf{r})] \quad (5)$$

with

$$[q_{\mathbf{k}}, p_{\mathbf{k}'}] = i\delta_{\mathbf{k}\mathbf{k}'} \quad (6)$$

Thus, the solvent Hamiltonian operator transforms to

$$H_D = \frac{\hbar\omega}{2} \sum_{\mathbf{k}} [p_{\mathbf{k}}^2 + q_{\mathbf{k}}^2] \quad (7)$$

It is important to note that, in spite of the fact the solvent Hamiltonian operator has the form associated with the quantum harmonic oscillator, it does not specifically imply that physical harmonic oscillations of the solvent medium play a singular role in the activation process. Some confusion has arisen with respect to this point.¹⁰ The process of Fourier transformation and the requirement that the Fourier transform coefficients satisfy boson commutation rules implies *only* that all motions of the solvent system together behave energetically as bosons. It is certainly true that physical libratory motions of molecules in the solvent system contribute to the state of polarization of the system. However, all motions contribute

to some degree. It is only the choice of the magnitude of the frequency ω^s which limits the representation in the sense of stressing the contribution of a particular class of molecular motions. Thus, Levich¹³ in particular states that it is librations of the solvent molecules which in large measure contribute to the activation process. Levich has underplayed the fact that other molecular motions contribute as well. Certainly in a complete analysis one must account for the contributions from all motions of the solvent as well as the interactions coupling the various degrees of freedom. Such an analysis has been carried out by Dogonadze, Kuznetsov, and Levich.¹² This analysis requires a large scale diagonalization which isolates a number of system "normal modes." One finds that certain of these normal modes contribute predominantly to the activation process. Moreover, the frequencies and associated energies of these modes are different from the frequencies associated with the individual molecular degrees of freedom. In a crude manner, with the Einstein model of the dielectric one does just this type of diagonalization, without performing the calculation, by guessing a reasonable frequency to associate with the activating solvent modes.

Continuing with the development of the system Hamiltonian operator it is necessary to consider the effect on the solvent due to the presence of the electron transfer system. Originally, Levich and Dogonadze expressed this as⁴

$$V_{es} = \int dV \mathbf{D}_e \cdot (\mathbf{P} + \mathbf{P}_e) \quad (8)$$

where \mathbf{D}_e is the induction field due to the transfer electron. This representation, however, is only a first approximation, and it ignores the fact that the electron remains tightly bound to the donor center during much of the time. In fact, even in the transition state the electron is reasonably tightly associated with several atomic centers; in that state it is associated generally with both the donor and acceptor centers. Accordingly, a better representation of the interaction is

$$V_{es} = 2\pi \int dV \mathbf{E}_m \cdot \mathbf{P} \quad (9)$$

for which E_m is the complete electric field vector associated with the donor center and contains monopole as well as higher order contributions. The predominate contribution is likely to be a dipolar one. No detailed development of the interaction V_{es} is attempted (such a treatment will be reported shortly by McKinley and Schmidt). The interaction is left general, specified only by V_{es} .

We now come to the consideration of the contributions due to electronic degrees of freedom. The typical expression of the electronic contributions is contained in the following terms

$$-\frac{\hbar^2}{2m_e} \nabla_e^2 + U(R, r) \quad (10)$$

Here $U(R, r)$ is the potential energy operator which accounts for the interaction of the exchange electron with the donor and acceptor centers as well as accounting for direct Coulombic interaction between the species. R is the set of coordinates for the interaction between ionic centers, and r is the set of electronic coordinates.

Following Levich and Dogonadze's development⁴ of the system Hamiltonian operator, it is possible to write

$$\mathcal{H} = -\frac{\hbar^2}{2m_e} \nabla_e^2 + U(R, r) + \frac{\hbar\omega}{2} \sum_k [p_k^2 + q_k^2] + \frac{\epsilon_\infty - 1}{8\pi\epsilon_\infty} \int dV (\mathbf{D}_1^2 + \mathbf{D}_2^2) + V_{es}(q_k) \quad (11)$$

in which the terms containing the induction field contributions, \mathbf{D}_1 and \mathbf{D}_2 , represent the Born contribution to the ionic solvation energy. Equation 11 is the basic Hamiltonian operator necessary for the succeeding analysis. Indeed, the further analysis requires simplification of this expression to a useful form. This is accomplished by means of the Born-Oppenheimer adiabatic separation analysis.

Let the electronic Hamiltonian operator be given by

$$H_{el} = -\frac{\hbar^2}{2m_e} \nabla_e^2 + U(R, r) + V_{es}(q_k) \quad (12)$$

The adiabatic electronic wave functions, which depend parametrically on both R and q_k , are solutions to the following eigenvalue problem

$$H_{el} \phi_i(R, r, q_k) = E_i(R, q_k) \phi_i(R, r, q_k) \quad (13)$$

As usual, one seeks a solution to the total problem in terms of an expansion in a known set of basis functions. In this case the known basis set is the set of electronic wave functions which are solutions to (13). The general solution is of the form

$$\Psi = \sum_i \chi_i \phi_i$$

The χ_i are the expansion coefficients, but in the usual interpretation they are regarded as the vibrational wave functions. The problem now reduces to finding some equation which determines these wave functions.

The Born-Oppenheimer separation scheme defines an adiabatic vibrational Hamiltonian operator as

$$H_{ad}^i = \frac{\hbar\omega}{2} \sum_k [p_k^2 + q_k^2] + E_i(R, q_k) \quad (14)$$

Note, however, that the energy $E_i(R, q_k)$ depends parametrically on q_k . (We shall not be concerned in this paper with the dynamics of the parametric R dependence.) This dependence of E_i on q_k is a result of the presence of the electron transfer system in what was originally an isolated dielectric continuum. As a result, the equilibrium values of the q_k operators, which characterize in part the states of the dielectric continuum, are shifted. Assume the presence of the electron transfer system induces only small displacements of the solvent system from its equilibrium positions. Thus, by means of a Taylor's series expansion, truncated with the first-order term, we find

$$H_{ad}^i = \frac{\hbar\omega}{2} \sum_k [p_k^2 + q_k^2] + E_i(R, q_{ik}^0) + \left[\frac{\partial E_i}{\partial q_k} \right]_{q_{ik}^0} (q_k - q_{ik}^0) \quad (15)$$

In a straightforward manner the expression for the adiabatic vibrational Hamiltonian operator simplifies to

$$H_{ad}^i = \frac{\hbar\omega}{2} \sum_k [p_k^2 + q_k^2] + \sum_k \frac{\hbar\omega}{2} (q_{ik}^0)^2 + E_i(R, q_{ik}^0) \quad (16)$$

with

$$q_{ik}^0 = -\frac{1}{\hbar\omega} \left[\frac{\partial E_i(P, q_k)}{\partial q_k} \right]_{q_k = q_{ik}^0} \quad (17)$$

which follows from the condition that the solvent and donor-acceptor system together are in an equilibrium state. As a result of the above manipulations, we make the following identification

$$\frac{\hbar\omega}{2} \sum_k (q_{ik}^0)^2 = \frac{\epsilon_\infty - 1}{8\pi\epsilon_\infty} \int dV \mathbf{D}_i^2 \quad (18)$$

With the notational simplification

$$\mathbf{J}_i = E_i(P, q_{ik}^0) + \frac{\epsilon_\infty - 1}{8\pi\epsilon_\infty} \int dV \mathbf{D}_i^2 \quad (19)$$

we find the adiabatic vibrational Hamiltonian operator assumes the form

$$H_{ad}^i = \frac{\hbar\omega}{2} \sum_k [p_k^2 + q_k^2] + J_i \quad (20)$$

In addition to the adiabatic terms, the Born-Oppenheimer separation analysis provides terms which mix system states. These terms are signified as non-Born-Oppenheimer, or nonadiabatic, contributions and for this particular system they are expressed as

$$H_{na}^i = \frac{\hbar\omega}{2} \sum_{k,j} \langle \phi_i | p_k^2 | \phi_j \rangle + \hbar\omega \sum_{k,j} \langle \phi_i | p_k | \phi_j \rangle p_k + \sum_j \langle \phi_i | U(R, r) | \phi_j \rangle \quad (21)$$

There are two nonadiabatic contributions. The first two terms in eq 21 together represent vibronic coupling terms which in principle can induce a system to make a transition from one vibronic state to another. They arise naturally as a result of the parametric dependence of the electronic wave functions on the variable q_k . Normally, these terms are disregarded; they are considered to contribute insignificantly to the promotion of the system from one state to another. On the other hand, the last term in (21) can have a significant magnitude. In particular, it is the term which couples the motions of the electron on the donor center with the acceptor center; it is normally referred to as the nuclear Coulomb exchange interaction. In a perturbation theory treatment, as, for example, the Levich-Dogonadze theory,⁴ this exchange term is considered to be significantly greater in magnitude than the vibronic contributions, but still sufficiently small as to make possible the use of quantum mechanical perturbation theory. Then, as Levich and Dogonadze have done,⁴ one proceeds to evaluate the quantum mechanical expression for the probability the system makes a transition from some defined initial state to a final state. This we examine shortly.

There are now several manipulative operations which transform the total Hamiltonian operator to a more useful form. Specifically, the introduction of the occupation number operator, or second quantization, representation makes it possible in the subsequent analysis automatically to select the correct energies and operators which figure in the rate constant expression.

Associate the following operators with the designated states: the creation and annihilation operators a_n^* and a_n create and annihilate donor states on a species 1 at a site n in the system (the associated conjugate donor and acceptor pairs are D_1^e and A_1); the creation and annihilation

operators b_n^* and b_n similarly create and annihilate donor states for the species 2 (conjugate donor and acceptor pairs are D_2^e and A_2). The vacuum state at a system site n , $|0\rangle$, is an acceptor state. Thus, the eigenvalue 0 for the occupation number operator $a_n^*a_n$ operating on $|0\rangle$ indicates that at the site n species 1 is an acceptor, or oxidized, state. For example, $a_n^*a_n|0\rangle = 0|0\rangle$. Conversely, the eigenvalue 1 in $a_n^*a_n|1\rangle = 1|1\rangle$, indicates the species 1 at the site n is in a donor state, *i.e.*, it is a reduced species. Similar arguments apply to the 2 species. As a result, the total Hamiltonian operator is now

$$\mathcal{H} = \sum_n (S_{an} + J_{an'} a_n^* a_n) + \sum_{n'} (S_{bn'} + J_{bn'} b_n^* b_n) + \frac{\hbar\omega}{2} \sum_{\substack{n, n' \\ i, k}} (a_n^* a_n + b_n^* b_n) [p_k^2 + (q_k - q_{ik}^0)^2] + \sum_{n, n'} C_{nn'}^{(1)} a_n^* a_{n'} + \sum_{n, n'} C_{nn'}^{(2)} b_n^* b_{n'} + \sum_{n, n'} C_{nn'}^{(3)} a_n^* b_{n'} \quad (22)$$

The energy S_{an} is given by

$$S_{an} = \frac{\epsilon_\infty - 1}{8\pi\epsilon_\infty} \int dV \mathbf{D}_1^2(\text{ox}) \quad (23)$$

and it is the Born solvation energy of an a species. The energy term $J_{an'}$ is defined by

$$J_{an'} = \epsilon_a + \frac{\epsilon_\infty - 1}{8\pi\epsilon_\infty} \int dV (\mathbf{D}_1^2(\text{ox}) - \mathbf{D}_1^2(\text{red})) \quad (24)$$

As a result of the operation of the occupation number operators $a_n^*a_n$ and $b_n^*b_n$, the following energy term appears as part of the enthalpy of reaction

$$J_{in} = \epsilon_i + (C/8\pi) \int dV (\mathbf{D}_1^2(\text{red}) + \mathbf{D}_2^2(\text{ox})) \quad (25)$$

Similar terms apply to the b species. The various Coulombic nuclear exchange interactions in eq 22 are

$$\begin{aligned} C^{(1)} &= \langle \phi_{an} | U(R, r) | \phi_{an'} \rangle \\ C^{(2)} &= \langle \phi_{bn} | U(R, r) | \phi_{bn'} \rangle \\ C^{(3)} &= \langle \phi_{an} | U(R, r) | \phi_{bn'} \rangle \end{aligned} \quad (26)$$

Note, as indicated earlier, the total Hamiltonian operator contains terms which account for the heteronuclear as well as the homonuclear electron transfer reactions. This is a direct result of the microscopic consideration of the individual electron transfer possibilities. Of course, only those terms of the total Hamiltonian operator which yield the appropriate rate constant expression are used, *i.e.*, either the homonuclear or heteronuclear examples.

In a quantum mechanical analysis, which employs time-dependent perturbation theory, the terms expressing the exchange interaction act as the perturbations to induce the system to make a transition.

The following unitary transformation of the total Hamiltonian operator simplifies the calculations in both the quantum mechanical perturbation theory analysis and the nonequilibrium statistical mechanical analysis leading to the rate constant expression. The transformation is

$$\tilde{\mathcal{H}} = e^{-iS} \mathcal{H} e^{iS} \quad (27)$$

with

$$S = \sum_{\substack{n, n' \\ i, k}} (a_n^* a_n + b_{n'}^* b_{n'}) q_{\{i\}k}^0 p_k \quad (28)$$

Carrying out the operations, we find

$$\begin{aligned} \tilde{\mathcal{K}} = & \sum_n J_{an} a_n^* a_n + \\ & \sum_{n'} J_{bn'} b_{n'}^* b_{n'} + \frac{\hbar\omega}{2} \sum_{\substack{n, n' \\ i, k}} (a_n^* a_n + b_{n'}^* b_{n'}) [p_k^2 + q_k^2] + \\ & \sum_{n, n'} C^{(1)} \exp[-i \sum_k (q_{ank}^0 - q_{an'k}^0) p_k] a_n^* a_{n'} + \\ & \sum_{n, n'} C^{(2)} \exp[-i \sum_k (q_{bnk}^0 - q_{bn'k}^0) p_k] b_n^* b_{n'} + \\ & \sum_{n, n'} C^{(3)} \exp[-i \sum_k (q_{ank}^0 - q_{bn'k}^0) p_k] a_n^* b_{n'} \quad (29) \end{aligned}$$

The purpose of this transformation has been to eliminate the linear contributions to the solvent part of the Hamiltonian operator. As a consequence of this operation, the change in state of the solvent, which takes place as the system makes its transition to the electron transfer transition state, is displayed together with the perturbation terms which induce the transition.

In the following analysis leading to rate constant expressions interest is restricted to the heteronuclear exchange case. Therefore, we retain only the $C^{(3)}$ contribution. In order to further simplify the analysis the displacement of the solvent coordinate variable is defined as

$$\zeta_k = q_{ank}^0 - q_{bn'k}^0 \quad (30)$$

The heteronuclear nonadiabatic transition term simplifies to

$$\sum_{nn'} C^{(3)} \exp[-i \sum_k \zeta_k p_k] a_n^* b_{n'}$$

Perturbation Theory Approach

In order to reveal the similarity between the nonequilibrium statistical mechanical and quantum mechanical perturbation theories of electron transfer reactions, in this section we cast the Levich-Dogonadze theory⁴ into a form suitable for comparison.

The starting point in the Levich-Dogonadze analysis is the quantum mechanical expression for the transition probability

$$w = \frac{2\pi}{\hbar} \sum_{i, f} e^{-\beta E_i} |\langle \phi_i | H' | \phi_f \rangle|^2 \delta(E_f - E_i) \quad (31)$$

where H' is a general perturbation; we do not yet specify it to be $C^{(3)}$. This expression is suitably averaged over all possible initial solvent states and summed over all possible final solvent states. As it stands, however, the summations in eq 28 are difficult to evaluate. This problem can be rectified provided by some means the dependence of the energy terms on the summation indices disappears. This indicial dependence vanishes in the following manner. Introduce the Fourier transform representation of the Dirac delta function

$$\delta(E) = \frac{1}{2\pi\hbar} \int_{-\infty}^{\infty} dt e^{iEt/\hbar} \quad (32)$$

Then by means of the operator theorem

$$e^{\alpha H} \phi_i = e^{\alpha E_i} \phi_i \quad \text{for} \quad H\phi_i = E_i \phi_i \quad (33)$$

The transition probability is

$$w = \frac{1}{\hbar^2} \sum_{i, f} \int_{-\infty}^{\infty} dt \langle \phi_i | H' | \phi_f \rangle \times \langle \phi_f | e^{iHt/\hbar} (H')^* e^{-(t-i\hbar\beta)H/\hbar} | \phi_i \rangle \quad (34)$$

As a result of the above manipulations, quantum mechanical operators replace the energy terms. It is important to note that the Hamiltonian operator which appears in eq 31 for the transition probability is the total Hamiltonian operator.

Next, by means of the closure condition

$$\sum_f |\phi_f\rangle \langle \phi_f| = 1 \quad (35)$$

the summation over the final states can be carried out.

In the Heisenberg representation the time dependence of a quantum mechanical operator appears as

$$H'(t) = e^{iHt/\hbar} H'(0) e^{-iHt/\hbar} \quad (36)$$

The expectation value for any operator, Op, is

$$\langle \text{Op} \rangle = \text{Tr}\{e^{-\beta H} \text{Op}\} = \sum_i \langle \phi_i | e^{-\beta H} \text{Op} | \phi_i \rangle \quad (37)$$

Thus, we obtain the final form for the transition probability

$$w = \frac{1}{\hbar^2} \int_{-\infty}^{\infty} dt \langle H'(0) (H'(t))^* \rangle \quad (38)$$

At this point we specify the perturbation

$$H' = C^{(3)} \exp[-i \sum_k \zeta_k p_k] a_n^* b_{n'} \quad (39)$$

Thus, the transition probability is

$$w = \frac{1}{\hbar^2} \int_{-\infty}^{\infty} dt \langle C^{(3)}(0) e^{-i \sum_k \zeta_k p_k} C^{(3)}(t)^* e^{i \sum_k \zeta_k p_k} \rangle \times \exp[i(J_b - J_a)t/\hbar] \quad (40)$$

Here it is necessary to point out that to the lowest order in the interaction, expressed here by (36), the adiabatic part of the Hamiltonian operator replaces the total Hamiltonian operator. Thus, the time dependence of the operators in eq 37 is specified by the adiabatic Hamiltonian operator.

One final point worth noting at this stage is the consequence of the neglect of the interaction terms in the Hamiltonian operator in the specification of the time dependence in the Heisenberg representation. The consequence of retaining these terms is simple. Further application of perturbation theory is implied. When the manipulations are carried out, one finds contributions due to the involvement of virtual states. In particular, one finds with an even more detailed Hamiltonian operator contributions of a bridge transfer character which involve virtual states of other (possibly bridge) species in the system. By neglecting these terms, then, we restrict our considerations to the direct electron transfer cases. This applies as well to the analysis which follows based on nonequilibrium statistical mechanics.

The $C^{(3)}$ matrix elements depend on time in eq 37. Strictly speaking, because these matrix elements depend parametrically on both R and q_k , the time dependence appears as $R(t)$ and $q_k(t)$ in $C^{(3)}$. However, the usual treatment, also followed here, assumes that the dependence of $C^{(3)}$ on both R and q_k is a slowly varying one. As

a result of this slowly varying dependence, one is often justified in taking the matrix elements outside the averaging brackets. This is the Condon approximation. Effecting it here results in the following expression for the transition probability

$$w = \frac{|C|^2}{\hbar^2} \int_{-\infty}^{\infty} dt \langle \Pi_k e^{-i\zeta_k p_k(0)} e^{i\zeta_k p_k(t)} \rangle \times \exp[i(J_b - J_a)t/\hbar] \quad (41)$$

There is one very important physical restriction which applies to the transition probability expressed in eq 38. Namely, eq 38, and any subsequent expression for the rate constant derived from it, is valid only for values of the exchange matrix element sufficiently small as to satisfy the restrictions inherent in the use of perturbation theory. In physical and chemical terms the above transition probability applies only to chemically nonadiabatic reactions. That is, it applies to reaction systems for which the separation between adiabatic potential energy surfaces is small. Therefore, in these nonadiabatic systems there is a probability much reduced from unity that the system once in the transition state will pass to the final state. As the Yamamoto rate theory shows,⁷ this restriction is absent in the nonequilibrium statistical mechanical treatment.

Statistical Mechanical Expression for the Rate Constant

Yamamoto⁷ posed the problem of calculating the rate constant for a chemical reaction in the following way. Given a system displaced from equilibrium in a small amount, the affinity accounts for the tendency of the system to relax to the equilibrium state. Thus, in order to account quantitatively for this relaxation process one adds to the equilibrium system Hamiltonian operator a term in the generalized potential associated with the nonequilibrium restoring force. Such a Hamiltonian operator is

$$H_T = H + AN \quad A = \text{affinity} \quad (42)$$

Yamamoto's theory⁷ then proceeds to the development of the equations of motion for the density operator in order to determine the linear response of the chemical system to the imposed, internal nonequilibrium force. In the linear response limit the rate constant expression is

$$k = \frac{V}{\beta \langle N_a \rangle_0 \langle N_b \rangle_0} \int_0^{\infty} dt \int_0^{\beta} d\lambda \langle \dot{N}(0) \dot{N}(t + i\hbar\lambda) \rangle \quad (43)$$

where N is an occupation number operator for a particular species undergoing reaction^{6,14}

$$N = \sum_n a_n^* a_n \quad (44)$$

In eq 40 $\langle N_1 \rangle_0$ and $\langle N_2 \rangle_0$ are the equilibrium numbers of reactant species. The time derivative of the occupation number operator which appears in eq 40 is found by means of the Heisenberg equation of motion

$$i\hbar \dot{N} = [H_T, N] \quad (45)$$

Although eq 43 is in a useful form, it can be transformed to an expression which more nearly corresponds to that found by means of the perturbation theory

$$k = \frac{\pi \hbar V}{Z \langle N_a \rangle_0 \langle N_b \rangle_0} \sum_{l, l'} e^{-\beta E_l} |\langle l | \dot{N} | l' \rangle|^2 \delta(E_{l'} - E_l) = \frac{V}{2 \langle N_a \rangle_0 \langle N_b \rangle_0} \int_{-\infty}^{\infty} dt \langle \dot{N}(0) \dot{N}(t) \rangle \quad (46)$$

The final expression in (46) is the one we shall use in the subsequent analysis in this paper.

The equation of motion of the N operator for a 1 species follows with the use of eq 26 and 45. It is

$$\dot{N} = -\frac{i}{\hbar} \sum_{n'} C^{(3)} \exp[-i \sum_k (q_{ank}^0 - q_{bn'k}^0) p_k] a_n^* b_{n'} + hc \quad (47)$$

Substituting eq 47 into 43 and taking into consideration the combinatorial factors, we find

$$k = \frac{|C^{(3)}|^2}{\hbar^2} \int_{-\infty}^{\infty} dt \exp[i(J_b - J_a)t/\hbar] \times \langle \Pi_k \exp[-i\zeta_k p_k(0)] \exp[i\zeta_k p_k(t)] \rangle \quad (48)$$

This is essentially the same as eq 41 found by the application of quantum mechanical perturbation theory. There is an essential difference, however, in that this expression is one of far greater generality. It applies, in principle, to all reaction limits from those termed chemically adiabatic to the nonadiabatic cases.

At this point one readily sees that with the evaluation of the correlation function, which is the same in eq 41 and 48, the evaluation of the rate constant expression in either case can be completed.

The Correlation Function and the Rate Constant

The evaluation of correlation functions of the form appearing in (48) has been reported a number of times. In several places in the physics literature (including chemical physics) it is outlined in some detail.¹⁵ However, in only scattered instances is it outlined in any detail in connection with the electron transfer problem in solution. In view of the importance of these averaging methods in this type of theory it is worthwhile to sketch the averaging process here.

The following analysis pays attention to quantum mechanical operator restrictions. The result obtained, therefore, is valid for all temperature ranges. In the end, however, we concentrate on the high temperature limit as it is the limit of greatest immediate interest to the practicing chemist.

Given any two quantum mechanical operators A and B , a corollary of the Baker-Hausdorff theorem states¹⁶

$$\exp[A + B] = e^A e^B \exp(-[A, B]/2) \quad (49)$$

subject to $[A, B] = \text{constant}$. Equation 49 is important in the evaluation of the average in either eq 41 and 48, as it is not possible, except in the classical limit, to combine or separate arguments of the exponential function (operator). The time dependence of the momentum variable which satisfies the harmonic oscillator Heisenberg equation of motion in dimensionless coordinates is

$$p(t) = p(0) \cos \omega t - q(0) \sin \omega t$$

with

$$[q, p] = i$$

The use of eq 49 together with the quantum commuta-

tor relation allows us to write

$$\begin{aligned} \exp[-i\zeta_k p_k(0)] \exp[i\zeta_k p_k(t)] = \\ \exp[-i\zeta_k p_k(0)(1 - \cos \omega t)] \times \\ \exp[-i\zeta_k q_k(0) \sin \omega t] \exp[(i/2)\zeta_k^2 \sin \omega t \cos \omega t] \end{aligned} \quad (50)$$

The averaging operation can be expressed in a continuous basis as¹⁵

$$\begin{aligned} \langle \exp[-i\zeta_k p_k(0)] \exp[i\zeta_k p_k(t)] \rangle = \\ dx_1 dx_2 \langle x_1 | \rho | x_2 \rangle \langle x_2 | \exp[-i\zeta_k p_k(0)] \times \\ \exp[i\zeta_k p_k(t)] | x_1 \rangle \end{aligned} \quad (51)$$

where

$$\begin{aligned} \langle x_1 | \rho | x_2 \rangle = \left[\frac{\tanh(\hbar\omega\beta/2)}{2\pi} \right]^{1/2} \times \\ \exp \left[-\frac{1}{4} [(x_1 + x_2)^2 \tanh(\hbar\omega\beta/2) + \right. \\ \left. (x_1 - x_2)^2 \coth(\hbar\omega\beta/2)] \right] \end{aligned} \quad (52)$$

is the normalized quantum mechanical density matrix for the harmonic oscillator. With the use of eq 51, the expectation value of the quantity inside the averaging brackets is

$$\begin{aligned} \langle x_2 | \exp[-i\zeta_k p_k(0)] \exp[i\zeta_k p_k(t)] | x_1 \rangle = \\ \exp[i(\zeta_k^2/2) \sin \omega t \cos \omega t - i\zeta_k x_1 \sin \omega t] \times \\ \delta(x_2 - \zeta_k(1 - \cos \omega t) - x_1) \end{aligned} \quad (53)$$

The substitution of eq 52 and 53, followed by the simplification of the result of the integration yields

$$\begin{aligned} \langle \exp[-i\zeta_k p_k(0)] \exp[i\zeta_k p_k(t)] \rangle = \\ \exp \left[-\frac{\zeta_k^2}{2} \coth(\hbar\omega\beta/2) + \right. \\ \left. \frac{\zeta_k^2}{2} \operatorname{csch}(\hbar\omega\beta/2) \cos(\omega t - i\hbar\omega\beta/2) \right] \end{aligned} \quad (54)$$

This is the result quoted by Levich and Dogonadze⁴ who obtained it by equivalent means through the use of the Feynman operator calculus techniques.¹⁷ The route outlined above is considerably simpler.

At this point we note that by means of a simple reformulation of the argument of the exponential in (54) one can identify the generating function for the Bessel function $I_n(\dots)$

$$\begin{aligned} \langle \exp[-i\zeta_k p_k(0)] \exp[i\zeta_k p_k(t)] \rangle = \\ \exp \left[-\frac{\zeta_k^2}{2i} \coth(\hbar\omega\beta/2) \right] \times \\ \sum_{n=-\infty}^{\infty} I_n \left[\frac{\zeta_k^2}{2} \operatorname{csch}(\hbar\omega\beta/2) \right] \exp[in\omega t + n\hbar\omega\beta/2] \end{aligned} \quad (55)$$

If this expression is substituted in either (41) or (48), and the time integrations carried out, the result is an infinite series of delta functions. Energy conservation conditions automatically require the selection of one of these functions. After the Bessel function corresponding to the transition is identified, either the high or low temperature expansion yields the results first reported by Levich and Dogonadze.⁴

An easier route to the final, high-temperature form of the rate constant is the following. Returning to eq 54 we

take the high-temperature limit and as well we expand the cosine function for small time arguments. This is valid as long as the lifetime of the transition state is within the quantum mechanical uncertainty limit. The uncertainty limit, then defines the time bounds on the lifetime of the transition state. This is a standard procedure employed frequently in the theoretical treatment of neutron, electron, and X-ray scattering.⁹ Moreover, it is equivalent to the use of the asymptotic forms of the Bessel function. The result is

$$\begin{aligned} \langle \exp[-i\zeta_k p_k(0)] \exp[i\zeta_k p_k(t)] \rangle_{c1} \approx \\ \exp \left[-\frac{\zeta_k^2 \omega}{2\hbar\beta} t^2 + i \frac{\zeta_k^2 \omega}{2} t \right] \end{aligned} \quad (56)$$

This expression can be substituted in eq 48 and the time integrations immediately carried out. We find

$$\begin{aligned} k = |C|^2 \left[\frac{\pi\beta}{\hbar^2 E_s} \right]^{1/2} \exp \left[-\frac{[J_b - J_a + E_s]^2 \beta}{4E_s} \right] \\ E_s = \frac{\hbar\omega}{k^2} \zeta_k^2 \end{aligned} \quad (57)$$

An alternate procedure, which has a number of advantages for physical interpretation, employs the methods of steepest descents to evaluate the time integrals. Fischer has used this extensively in his examination of molecular nonradiative processes. Recently, he has used it in connection with the electron transfer problem with some striking results. In particular, he has found Marcus's predictions of the behavior of the rate constant *vs.* the free energy of the reaction in the abnormal region (*i.e.*, very exothermic reactions) is wrong. In the normal region the steepest descents methods yield results identical with those found here and elsewhere.

Equation 57 is based on the evaluation of eq 48, and has the same form as that obtained with the use of eq 41. The difference, as mentioned, is that the above result is generally valid.

Finally, we remark that eq 57 becomes the expression for the rate constant only after averaging over all possible separations between reactant species. This averaging process has been discussed in some detail by Levich in his review article.¹³

Discussion

The fact that the form of the rate constant (57) is general poses an interesting problem. We know, on the basis of the use of the Landau-Zener theory, as well as more general arguments, that in the adiabatic limit (for the Levich-Dogonadze model system) the rate constant expression should have the form^{2a,3,13,18}

$$k = \frac{\omega}{2\pi} \exp \left[-\frac{[J_b - J_a + E_s]^2 \beta}{4E_s} \right] \quad (58)$$

There is no means whereby eq 57 directly reduces to (58). We conclude that for a certain critical strength of the interaction matrix element C coupling the initial and final states, and thus being responsible for the splitting of the reaction potential energy surfaces, the rate constant expression assumes the form of eq 58. That is, for values of the interaction matrix element satisfying

$$|C|^2 \geq \frac{\hbar\omega}{2\pi} (E_s/\pi\beta)^{1/2} \quad (59)$$

the rate constant must be given by eq 58. This, of course, is exactly what has been meant by the chemical adiabatic limit all along. Specifically, the conclusion is that past a certain separation between the potential energy surfaces the dynamics of the system must be governed entirely by the dynamics of the slow system, in this case by the fluctuations in the polarization modes. Unfortunately, except for making the rigorous statement (59), nothing more can be said concerning the very important problem of determining whether indeed a reaction is adiabatic or not. More importantly, it is not clear how one may get the adiabatic result from the general theory. Hopefully, this is merely a temporary impasse. In view of the generality of the nonequilibrium statistical mechanical approach, it seems entirely possible that there should be some discernible, theoretically based distinction between the limits, and that some future formulation will show this in a smooth manner.

The one very important, and potentially powerful, facet of the analysis of the rate constant presented here is the manner in which the dependence of the rate constant has been cast on a momentum space correlation function. A considerable effort is being made in several research groups to generalize the formulation of the electron transfer reaction rate problem. In particular, steps away from the dielectric continuum approximation are being attempted. We anticipate that some more general analysis of the correlation function should be possible by which more detailed and specific information about the dynamical nature of the solution can be introduced. In particular, a general analysis based on the examination of the motions of all the particles in the system shows that the rate constant expression depends on a set of correlation functions similar in form to the one found here for the dielectric continuum polarization modes. As previously indicated in this paper, these correlation functions represent a momentum space analog of the Van Hove correlation function. In fact, they are formally the same as the intermediate function $I(k, t)$ introduced in scattering theory.⁹ It therefore seems entirely likely that some form of analysis of the equations of motion for these general correlation functions should introduce a more general picture of the effect of solvent and supporting electrolyte into the theoretical analysis leading to the rate constant expression for the solution electron transfer reaction.

The strong point of the analysis outlined in this paper, whether applied to the dielectric continuum representation model or to some more general treatment, lies in the fact that it does not depend directly on transition state arguments. These, of course, enter in a tacit and natural manner; although, care must be exercised in connection with the incorporation of the transition state energy minimum condition (to be discussed in a note, now in preparation). The evaluation of the contribution of system dynamics to the rate process depends on an examination of the operator equations of motion for the appropriate dynamical operators. Most importantly, the analysis depends on an averaging process which uses only the system equilibrium density matrix. Thus, if the state of the system is characterized in equilibrium, the state of the system at the transition point follows automatically from the time development of the dynamical operators. These time-dependent operators when averaged over the initial equilibrium state, yield the average of the operators in the transition state. This is a well known and powerful con-

cept, and its validity rests on the validity of the statistical mechanical ergodic hypothesis.¹⁹

Summary

The purpose of this paper has been to report an examination of the model of the simple electron transfer reaction originally defined and examined from a quantum mechanical point of view by Levich and Dogonadze.⁴ The analysis reported here depends on the use of the nonequilibrium statistical mechanical theory of chemical reaction rates formulated by Yamamoto.⁷

In this paper we carefully formulated the system Hamiltonian operator through the use of the Born-Oppenheimer adiabatic separation scheme. This Hamiltonian operator was simplified by means of a unitary transformation. The perturbation terms generally regarded as responsible for inducing the system transition from an initial reactant state to a final product state were cast into a form which allowed an unambiguous choice of dynamical contributions to the rate process. This technique can be used in either the quantum mechanical perturbation theory of Levich and Dogonadze, or in the more general statistical mechanical treatment. Both forms of the rate constant expression were given here.

The results for both the quantum mechanically derived rate constant and the rate constant which follows on application of the statistical mechanical treatment have an identical form. For nonadiabatic reactions these two rate constants are indeed physically identical. However, the expression obtained on the basis of the Yamamoto theory is physically general, it applies to the adiabatic limit as well. We know, however, that in the adiabatic limit the rate constant should have the form of eq 58. Comparison of the general result, eq 57, with eq 58 yields the exact condition for the existence of an adiabatic reaction.

The nonequilibrium statistical mechanical formulation of the theory of electron transfer reaction rates is developing. In this development the theory grows increasingly complex. Already, it has been possible to consider the influence of internal molecular vibronic contributions on the reaction rate constant.^{20, 21-23} A number of other dynamical contributions have been examined. Even in the simple harmonic oscillator representation for the dielectric solvent and for the vibrational contributions within the reactant molecules the resulting rate constant expressions are very complicated. It is our hope that this brief look at the very simple electron transfer system, as well as the comparison to the relatively well-known Levich-Dogonadze theory, will serve as an introduction to the more complicated analyses soon to appear.

Acknowledgment. I wish to thank Professor A. G. Davies and Dr. T. Thirunamachandran for their hospitality in providing me the opportunity to carry out this work at University College London. I also wish to express my appreciation to Professor R. A. Marcus for a number of encouraging discussions.

Appendix

The simple Einstein limit representation of the dielectric continuum does not adequately account for the contribution of all significant molecular dynamical degrees of freedom to the activation energy. As indicated in the text, Dogonadze and his associates¹² have developed a phe-

nomenological theory of the dielectric continuum which includes dispersion effects. The inclusion of these effects improves the theory to the point where the activation repolarization and solvation energies reflect this expanded consideration of the solution dynamics.

The purpose of this Appendix is to indicate the manner by which the expanded dielectric continuum representation enters the analysis presented in the text.

The form of the Hamiltonian operator which includes dielectric dispersion is^{12,24}

$$H_s = \sum_k \frac{\hbar \omega_k^{\parallel}}{2} [p_k^2 + q_k^2] \quad (\text{A1})$$

where the frequencies ω_k^{\parallel} are found from the inequality²⁴

$$\text{Im} \epsilon_{\alpha\beta}^{-1}(\omega, \mathbf{k}) \neq 0 \quad (\text{A2})$$

In the above expression $\epsilon_{\alpha\beta}(\omega, \mathbf{k})$ is the complex dielectric permittivity tensor of the medium (α and β are cartesian coordinate indices, $\alpha, \beta = x, y, z$). The origin of the above Hamiltonian operator is in an expanded phenomenological Hamiltonian operator expressed originally in terms of canonically conjugate polarization vector quantities.¹² Equation A1 follows after application of a Fourier series expansion and quantization of the expansion coefficients. All this has been reported in papers by Dogonadze.¹²

There is very little difference in the analysis which employs (A1) instead of eq 7 leading to the expression for the rate constant. The single important difference is that the solvent repolarization energy (and similarly for the ion solvation energy) is

$$E_r = \frac{\hbar}{2} \sum_k \omega_k^{\parallel} [q_k^{0f} - q_k^{0i}]^2 \quad (\text{A3})$$

It is a relatively straightforward matter to show that this form of the repolarization energy, (A3), can be recast into a Fourier convolution integral

$$E_r = \frac{1}{8\pi} \sum_{\alpha, \beta} \int d^3 R_1 \int d^3 R_2 \Delta E_{\alpha}(\mathbf{R}_1) \times \Delta E_{\beta}^*(\mathbf{R}_2) C_{\alpha\beta}^n(\mathbf{R}_1, \mathbf{R}_2) = \frac{\pi}{2(2\pi)^3} \times \sum_{\alpha, \beta} \int d^3 k C_{\alpha\beta}^n(\mathbf{k}) \Delta E_{\alpha}(\mathbf{k}) \Delta E_{\beta}^*(\mathbf{k}) e^{i\mathbf{k} \cdot \mathbf{R}} \quad (\text{A4})$$

where $\Delta E_{\alpha}(k)$ is the change in the molecular field for the two states of the reactant, R is the interreactant separation, and $C^n(k)$ is^{2b}

$$C_{\alpha\beta}^n(k) = \frac{\hat{k}_{\alpha} \hat{k}_{\beta}}{k^2} \left[\frac{1}{\epsilon_n^{\parallel}(k)} - \frac{1}{\epsilon_{st}^{\parallel}(k)} \right] \quad (\text{A5})$$

The ϵ quantities are the Fourier transforms of the optical (n) and static (st) dielectric permittivities. This form of the repolarization energy has been investigated in connection with several detailed studies of the phenomenological theory of the interactions between reactants and the polar medium surrounding them.^{24,25} In a general sense, the repolarization energy has been found by Dogonadze and co-workers¹² to be

$$E_r = \frac{1}{\pi} \sum_k (E_k^{(i)} - E_k^{(f)})^2 \int_0^{\omega_c} d\omega \omega^{-1} \text{Im} \chi(\mathbf{k}, \omega) \quad (\text{A6})$$

and this energy is usually about 80% of the energy calculated in the simple Einstein limit. In the above expression $\chi(\mathbf{k}, \omega)$ is the generalized susceptibility for the solvent system.

References and Notes

- (1) Address correspondence to Oakland University, Rochester, Mich. 48063.
- (2) (a) R. A. Marcus, *J. Chem. Phys.*, **24**, 966 (1956); (b) N. S. Hush, *ibid.*, **28**, 962 (1958).
- (3) R. A. Marcus, *J. Chem. Phys.*, **43**, 679 (1965).
- (4) V. G. Levich and R. R. Dogonadze, *Collect. Czech. Chem. Commun.*, **29**, 193 (1961).
- (5) R. R. Dogonadze in "Reactions of Molecules at Electrodes," N. S. Hush, Ed., Wiley, New York, N. Y., 1971.
- (6) P. P. Schmidt, *J. Chem. Phys.*, **56**, 2775 (1972).
- (7) T. Yamamoto, *J. Chem. Phys.*, **33**, 281 (1960).
- (8) P. P. Schmidt, *J. Chem. Phys.*, **57**, 3749 (1972).
- (9) L. van Hove, *Phys. Rev.*, **95**, 249 (1954).
- (10) J. O. M. Bockris, K. L. Mittal, and R. K. Sen, *Nature (London)*, *Phys. Sci.*, **234**, 118 (1971).
- (11) H. Fröhlich, *Advan. Phys.*, **3**, 325 (1954).
- (12) R. R. Dogonadze, A. M. Kuznetsov, and V. G. Levich, *Dokl. Akad. Nauk SSSR*, **188**, 603 (1969).
- (13) V. G. Levich, *Advan. Electrochem. Electrochem. Eng.*, **4**, 249 (1965).
- (14) S. Fischer, *J. Chem. Phys.*, **53**, 3195 (1970).
- (15) R. Zwanzig, *Annu. Rev. Phys. Chem.*, **16**, 67 (1965).
- (16) Wm. Louisell, "Radiation and Noise in Quantum Electronics," McGraw-Hill, New York, N. Y., 1964.
- (17) R. P. Feynman, *Phys. Rev.*, **84**, 108 (1951).
- (18) P. P. Schmidt, *J. Phys. Chem.*, **77**, 488 (1973).
- (19) R. M. Mazo, "Statistical Mechanical Theories of Transport Processes," Pergamon Press, London, 1967.
- (20) M. A. Vorolyntsev and A. M. Kuznetsov, *Vestn. Mosk. Univ., Ser. Phys.*, **2**, 146 (1970).
- (21) P. P. Schmidt, *J. Chem. Soc., Faraday Trans. 2*, **69**, 1104 (1973).
- (22) P. P. Schmidt, *Z. Naturforsch.*, submitted for publication.
- (23) P. P. Schmidt and H. B. Mark, Jr., *J. Chem. Phys.*, **58**, 4290 (1973).
- (24) R. R. Dogonadze and A. A. Kornyshev, *Phys. Status Solidi*, **53**, 439 (1972).
- (25) P. P. Schmidt and J. M. McKinley, to be submitted for publication.

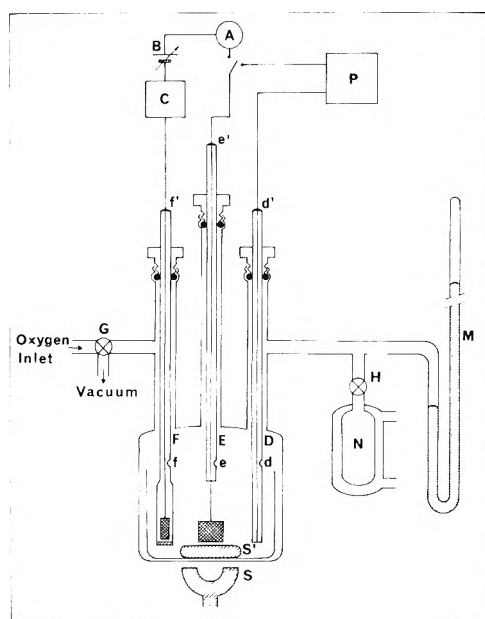
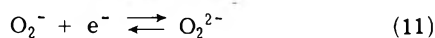
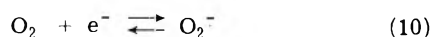


Figure 1. Reaction cell: (A) ammeter, (B) dc generator, (C) coulometer, (D, E, F) electrodes, (G, H) stopcocks, (M) manometer, (N) calibration bulb, (P) polarograph, (S, S') magnetic stirrer, (d, e, f) holes for rapid pressure equilibration, (d', e', f') vacuum seal.

tained in a Teflon beaker placed in a Pyrex cell holding three O-ring joints (Ace Glass Co. Vineland, N. J.) which allowed the vacuum-tight insertion of three electrodes. Under conditions of controlled magnetic stirring a disk microelectrode (D) coupled with a quasi-reference platinum electrode (E) permitted us to record voltammograms of the electroactive species present in solution. In the course of the production of peroxide by massive electrolysis the same electrode (E) worked as a large-area cathode while the anode was another platinum electrode (F) placed in a fritted glass compartment. All glass surfaces in contact with the solution were protected by thin platinum foils. Electrode wires were sealed in d', e', and f' with low vapor-pressure resin (Torr Seal, Varian Associates, Palo Alto, Calif.); holes d, e, and f permitted rapid pressure equilibrations.

The cell was connected with a mercury manometer, a vacuum line, and the apparatus for the purification of oxygen.

Calibrations. Some preliminary electroanalytical and volumetric calibrations were necessary to obtain quantitative information on the various species involved in the chemical processes. (a) Preparation of plots in which voltammetric limiting currents (obtained under controlled magnetic stirring) were reported as a function of the concentrations of the species superoxide, peroxide, and oxygen which are electroactive according to the reversible^{1b,9} processes



Similar calibrations were performed by using nitrite¹⁰ as a depolarizing agent. Under present working conditions the accuracy and precision limits for this "flux-voltammetric" technique were around 2-3% for concentrations $\approx 10^{-3}$ M. (b) Calculation of a correlation between the number of moles of oxygen present in the free volume over the melt and the actual pressure read on the manometer. This was

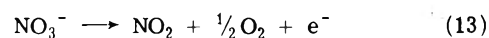
done by expanding in the reaction cell a known volume of an inert gas contained in a thermostated bulb (N). The calibration leads to the relationship

$$n_{\text{O}_2} = A(T)P_{\text{O}_2} \quad (12)$$

where n_{O_2} is the number of moles of oxygen present in the cell, P_{O_2} the experimental pressure, and $A(T)$ a constant (at a given temperature of the melt) which takes into account all possible temperature gradients present in the experimental system. For more information on these manometric techniques see ref 11.

Procedures. A typical experiment was carried out as follows. A good vacuum was applied to the cell until disappearance of the reduction water wave¹² (water concentration not exceeding 10^{-5} M). Then by maintaining the system under vacuum, the electroproduction (reactions 7 and 8) of peroxide was performed to the desired concentration (coulometric control).

Gas produced at the anode (F) according¹³ to the overall reaction



was immediately pumped off via hole f and the vacuum system (see Figure 1).

At the end of the massive electrolysis, after stirring of the melt was discontinued, a desired amount of oxygen was introduced into the cell. After reading the initial pressure, magnetic stirring was reactivated. The reaction kinetics was followed by detecting the decrease of oxygen pressure (manometrically) and the variation of the peroxide and superoxide concentrations (voltammetrically).

Results and Discussion

Description of Experimental Findings. The results obtained in the course of a typical experiment performed at 505 K are shown in Figure 2, where, as a function of time, the value of oxygen pressure over the reacting system (Figure 2A) and the actual concentrations of the species peroxide and superoxide (Figure 2B) are plotted. The origin of the time axis corresponds to the introduction of oxygen in the reaction cell.

It is apparent from the figure that the concentration of peroxide rapidly decreases in the initial interval AB while it remains approximately constant in the successive interval BC. When the concentration of peroxide decreases some superoxide is produced. The variation of the two concentrations was correlated by the expression

$$-2\Delta[\text{O}_2^{2-}] = \Delta[\text{O}_2^-] \quad (14)$$

An example of a current-potential profile recorded during the period BC is reported in Figure 3A; the concentrations of superoxide and peroxide are proportional^{1b,8} to h_1 and h_2 , respectively.

After the "steady-state" period BC the concentration of peroxide and superoxide reached a minimum (close to zero) and a maximum value, respectively, by following S-shaped kinetic curves (interval CD). The large prevalence of superoxide over peroxide which characterized interval DE was present as long as an appreciable oxygen pressure was maintained over the reacting system. An example of a voltammogram recorded under these experimental conditions is reported in Figure 3B. The limiting currents h_3 and h_4 are proportional to the concentrations of superoxide and oxygen, respectively.

The effect obtained by pumping-off oxygen from the

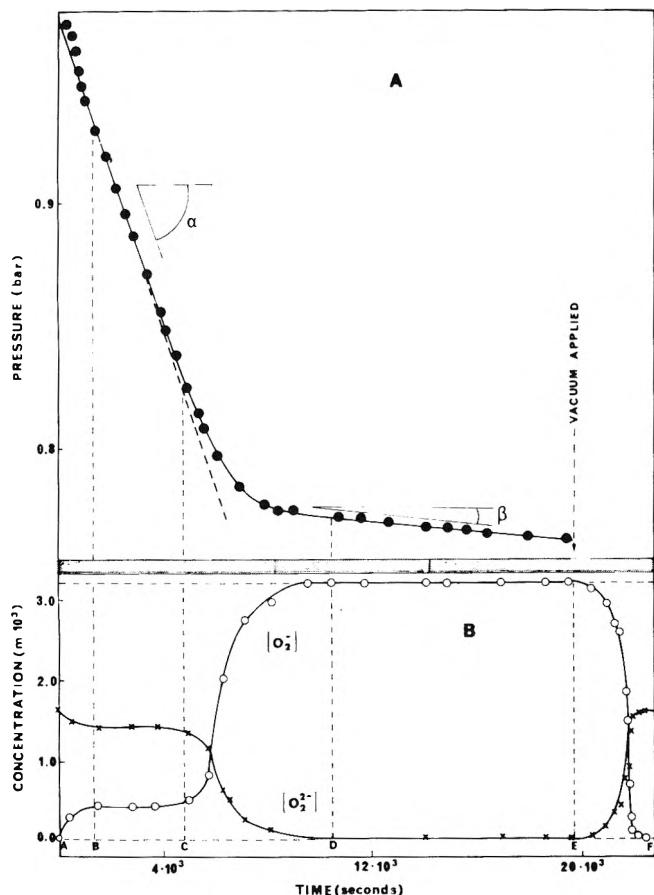
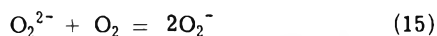


Figure 2. Variation of the oxygen pressure (●) and of the concentrations of peroxide (×) and superoxide (○) as a function of time in the course of a typical experiment presenting a marked "steady-state" period (interval BC) for the $[O_2^{2-}]$ and $[O_2^-]$. Working conditions described in Table I (run 3).

system (interval EF) will be described in a separate paragraph since it represents a side aspect of the problem.

Let us consider the rate of oxygen disappearance described in Figure 2A. It is approximately constant (slope α) during the "steady-state" interval BC when consumption of oxygen is solely due to the oxidation of nitrite according to reaction 6. The constancy of superoxide and peroxide concentrations exclude, in fact, the other possible oxygen-consuming overall reaction



On the contrary, process 15 certainly parallels reaction 6 at the beginning of the reaction (interval \overline{AB}) when part of the peroxide initially present is converted to superoxide.

The rate of oxygen consumption gets markedly smaller and smaller as the peroxide concentration decreases (interval \overline{CD}). After complete conversion to superoxide of all the initially present peroxide the pressure-time curve again resumes a linear shape (slope β).

The prevalence of superoxide in \overline{DE} is in agreement with the high value of the equilibrium constant⁹ for reaction 15

$$[O_2^-]^2/[O_2][O_2^{2-}] = K_{15} = 2 \times 10^6 \quad (15a)$$

and the probably high concentration of oxygen in the melt (of the order of $10^{-7} m$). A reasonable estimation of the relevant value is possible on the basis of the partition coefficient¹¹ for the process

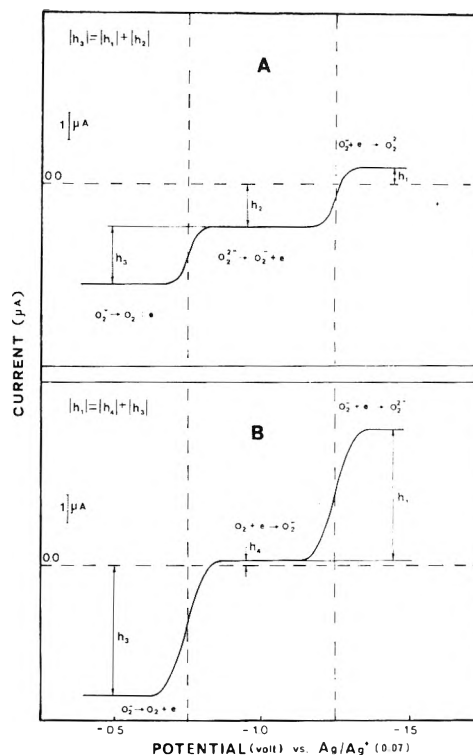


Figure 3. Voltammograms (corrected for residual current) indicative of the melt situation in correspondence to interval BC (profile A) and DE (profile B) of the experiment described in Figure 2. Diameter of indicator disk electrode is 0.5 mm.



$$K_H = 4 \times 10^{-6} \text{ mol}^{-1} \text{ kg atm}^{-1} \quad (16a)$$

since consumption of oxygen is relatively slow and the melt stirred (*vide infra*).

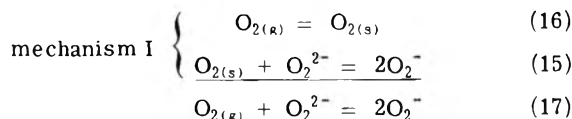
The length of the "steady-state" period was strongly dependent on the initial peroxide concentration. Compare, for example, the two experiments described in Figures 2 and 4, which were performed (all the other conditions being the same) in the presence of initial peroxide concentrations equal to 1.6 and 0.55 *m*, respectively. In the case of the experiment described in Figure 4, no straight line corresponding to the one with the α slope in Figure 2 can be found. In both Figures 2 and 4, on the contrary, the "final" intervals of the pressure-time curves present well-defined linear shapes (slopes equal to β and β' , respectively).

Effect of Vacuum on the Reacting System. As mentioned in the previous paragraph only the species O_2^- , O_2 , and NO_2^- (large concentration) were present in the melt after point D in Figure 2. By applying, under these conditions, a vacuum to eliminate oxygen (which stabilized the superoxide species even in the presence of a large concentration of nitrite: see eq 9a and 16a) complete reconversion of superoxide to peroxide was observed. The disappearance of superoxide and the corresponding formation of peroxide followed S-shaped curves (see interval EF in Figure 2B) characteristic^{1c} of the autocatalytic mechanism expressed by eq 4a. This confirms the conclusion drawn from previous kinetic studies on reaction 4 performed^{1c} under an inert-gas atmosphere.

Analysis of Data and Proposed Mechanism. The most interesting conclusion which can be drawn from the de-

scribed experimental results is that the presence of both peroxide and superoxide ions strongly catalyzes reaction 6. For example, the rate of oxygen consumption at any point of the kinetic curves reported in Figures 2A and 4A is several orders of magnitude (from three to five) larger than it should be, *ceteris paribus*, in the absence of O_2^{2-} and O_2^- . This has been directly tested by following (for several months) the relevant slow kinetics by a suitable manometric technique.^{7,11}

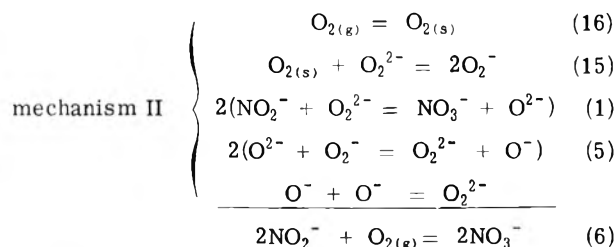
By considering the results reported in Figure 2 one notes that the first period of the reaction is characterized by a certain prevalence of the well-known^{1b} process



which leads to the disappearance of O_2^{2-} and to the production of O_2^- . The rate of the overall process 17, however, rapidly decreases and a "steady-state" situation for the concentration of peroxide and superoxide is reached (interval BC) which can be expressed by the relation

$$[O_2^{2-}]/[O_2^-] \approx \text{constant} \quad (18)$$

This finding raises, in effect, the question why the formation of superoxide remains "frozen" for an appreciable period of time (interval BC) while the actual oxygen pressure is theoretically sufficient (see relations 15a and 16a) to shift reaction 17 far to the right. The apparently paradoxical situation can be explained on a kinetic basis. Superoxide produced according to the overall reaction 17 must be consumed *via* a "destructive" parallel process. This last possibility can be expressed, for example, by the set of reactions involved in the autocatalytic mechanisms 4a relevant to reaction 4. By combining mechanism 1 with the sequence 4a one obtains



In effect mechanism II can explain the "steady-state" period BC, during which the production of superoxide is balanced by its consumption, and the oxygen disappearance is solely due to the oxidation of nitrite. The proposed mechanism also rationalizes the catalytic action (on the process 6) of peroxide.

Reaction 1 was supposed to be the rate-determining step of mechanism II and the disappearance of nitrite was expressed by the rate expression

$$v_1 = -d[NO_2^-]/dt = k_1[NO_2^-][O_2^{2-}] \quad (19)$$

This hypothesis was made by considering Figure 2 which shows that as long as $[O_2^{2-}]$ does not vary, the rate of oxygen consumption (according to reaction 6) remains constant within the limits of constancy of the nitrite concentration (present in excess). See the shape of curve 2A in the interval BC.

In this interval the actual nitrite concentration, at a given time t , can be obtained by subtracting from its initial concentration the nitrite consumed *via* reaction 6.

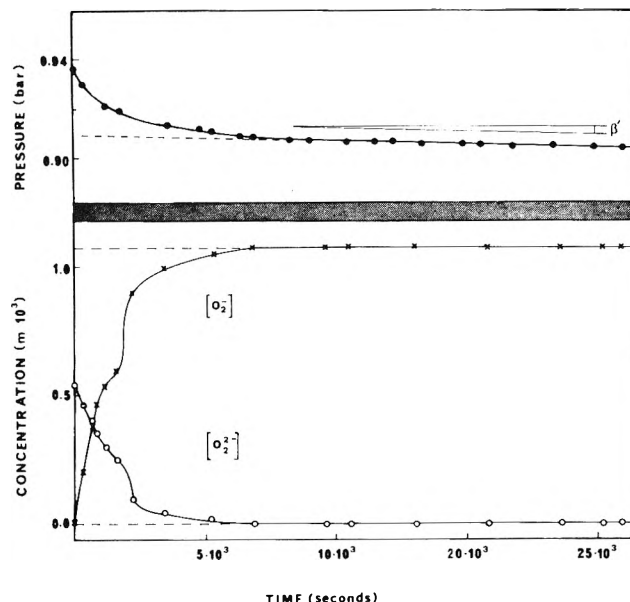


Figure 4. Kinetic curves relevant to a typical experiment (run 4 of Table I) not showing a "steady-state" period for concentrations of peroxide and superoxide (presence of a flex in correspondence to interval BC in Figure 2). Symbols as in Figure 2.

The relevant calculation can be made on the basis of oxygen disappearance.

$$[NO_2^-]_t = [NO_2^-]_{t_1} - 2 \left[\frac{(n_{O_2})_{t_1} - (n_{O_2})_t}{W} + ([O_2^{2-}]_{t_1} - [O_2^{2-}]_t) \right] \quad (20)$$

where $[NO_2^-]_{t_1}$, $[O_2^{2-}]_{t_1}$, and $(n_{O_2})_{t_1}$ are the initial concentrations of nitrite and superoxide and the initial moles of oxygen, respectively; $[NO_2^-]_t$, $[O_2^{2-}]_t$, and $(n_{O_2})_t$ are the same quantities at the time t and W is the weight, in kilograms, of the melt. The term $2([O_2^{2-}]_{t_1} - [O_2^{2-}]_t)$ takes into account that a small fraction of the consumed oxygen was used to convert (during the interval AB) peroxide to superoxide according to reaction 17. The concentration of peroxide (constant in the interval BC) can be readily obtained from the limiting current of the relevant voltammetric wave (see Figure 3 and the Experimental Section).

For small time intervals the rate v_1 (eq 19) can be expressed by the ratio

$$v_1 \approx - \frac{\Delta[NO_2^-]}{\Delta t} = \frac{[NO_2^-]_{t_1} - [NO_2^-]_{t_2}}{t_1 - t_2} \quad (21)$$

Values of the kinetic constant k , calculated by using eq 19-21, are given in Table I, column 2. It can be seen that reliable k_1 values could be estimated only for some of the experiments described in Table I; this is because of the mentioned absence of a "steady-state" interval when the initial $[O_2^{2-}]$ is too low. See, for example, Figure 4 which describes experiment 4 in Table I.

The average value $k_1 = 1.9 \times 10^{-2} \text{ mcl}^{-1} \text{ kg sec}^{-1}$ obtained from the results reported in Table I is very close to the value of $1.7 \times 10^{-2} \text{ mol}^{-1} \text{ kg sec}^{-1}$ obtained^{1c} by direct measurement of the rate constant of reaction 1 under the same experimental conditions. This coincidence of kinetic data confirms *a posteriori* the assumption that process 1 is the rate-determining step of mechanism II. In

TABLE I: Data Relevant to Kinetic Experiments Performed at 505 K^a

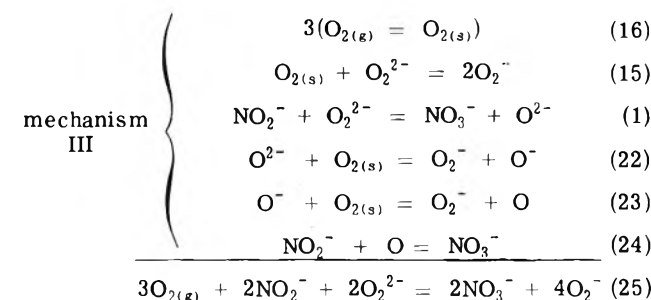
Run	$k_1 \times 10^3$, mol ⁻¹ kg sec ⁻¹	$k_2 \times 10^4$, mol ⁻¹ kg sec ⁻¹	$[\text{O}_2^{2-}]_{\text{init}} \times 10^3$, mol kg ⁻¹	$[\text{O}_2^{2-}]_{\text{plat}} \times 10^3$, mol kg ⁻¹	$[\text{NO}_2^-]_i$, mol kg ⁻¹	$[\text{NO}_2^-]_e$, mol kg ⁻¹
1	1.8	2.0	1.0	0.90	0.447	0.410
2		1.8	0.40			0.402
3	2.0	2.1	1.60	1.40	0.362	0.304
4		1.9	0.55			0.388
5		1.4	0.80	0.60		0.275
6	2.3	1.8	4.35	4.05	0.223	0.172
7	1.4	2.3	1.10	0.95	0.477	0.474

Average k values 1.9 1.9

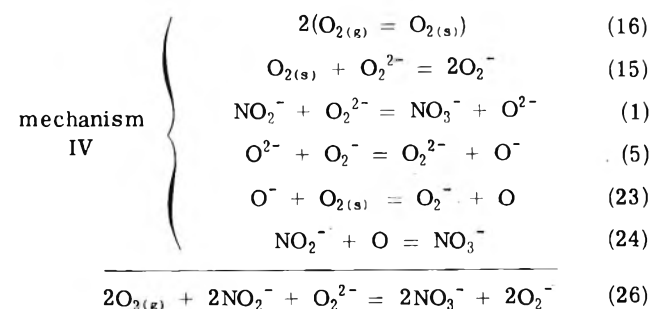
^a $[\text{NO}_2^-]_i$ = nitrite concentrations at the beginning of the plateau (for example, point B in Figure 2). $[\text{NO}_2^-]_e$ = nitrite concentrations at the beginning of the reaction period at maximum O_2^{2-} concentration (for example, point D in Figure 2). $[\text{O}_2^{2-}]_{\text{final}} = 2[\text{O}_2^{2-}]_{\text{initial}}$.

particular, it can be excluded that the rate of the process is controlled by the diffusion of oxygen. Process 16 represents a fast step even if the actual oxygen concentration in the course of the reaction may be lower than the equilibrium concentration: *i.e.*, that required by the relevant Henry's coefficient. Reaction 15 (whose direct and reverse kinetic constants^{1d} are quite high) represents a quasi-equilibrium situation prior to the rate-determining step.

Of course mechanism II is just a simplified representation of the chemical dynamics relevant to the "steady state" interval \overline{BC} . Other processes, leading to a net production of superoxide, must parallel mechanism II. Such mechanisms, initially negligible, must become more and more competitive with mechanism II as the reaction proceeds. This can be expressed, in the simplest way, as follows



and/or



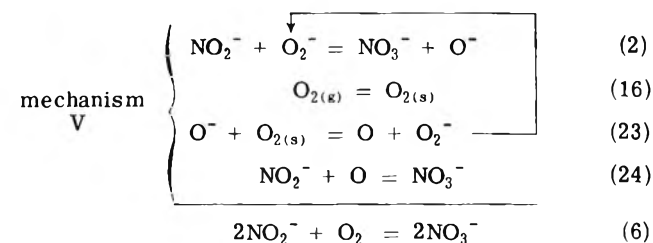
In fact, besides with superoxide as in mechanism II, products of steps 1 and 5 can react with molecular oxygen present in solution according to reactions 22 and 23. The formulation of the final step 24 is suggested by the large concentration of nitrite present in solution.

Mechanisms III and IV justify¹⁴ the net production of superoxide and the consequent disappearance of peroxide which occurs in interval \overline{CD} in Figure 2A. The increasing prevalence of these processes can be expressed (reaction 15, *vide ante*, represents a quasi-equilibrium situation) by the relation

$$[\text{O}_2] = \frac{1}{K_{15}} \frac{[\text{O}_2^-]^2}{[\text{O}_2^{2-}]} \quad (27)$$

In this context the reaction time BC is considered the equivalent of an induction period for the seemingly autocatalytic nature of the kinetics in the time interval \overline{CD} .

Another point of interest related to the present work is the rate of oxygen consumption in the presence of superoxide only (see the reaction intervals \overline{DE} in Figures 2A and 4A). In this case the consumption of oxygen uniquely occurs *via* reaction 6 which is strongly accelerated by the presence of superoxide (comparison with a blank). This accelerating effect can be expressed, in the simplest way, by the scheme



By hypothesising that reaction 2 plays the role of the rate-determining step, the relevant kinetic law can be expressed by

$$v_2 = -d[\text{NO}_2^-]/dt = k_2[\text{NO}_2^-][\text{O}_2^-] \quad (28)$$

By following the same criteria used for the evaluation of k_1 , the values of k_2 have been computed for all experiments described in Table I. The data reported in this table are effectively constant within the limits of experimental uncertainty. Their average value ($k = 1.9 \times 10^{-4}$ mol⁻¹ kg sec⁻¹) is in agreement with the corresponding datum ($k_2 < 5 \times 10^{-4}$ kg sec⁻¹) previously calculated^{1c} on the basis of completely different experiments. All this indirectly confirms the proposed mechanism V.

The reader's attention is drawn to the fact that the values of the kinetic constants k_2 and k_3 (relevant to the "direct" reaction between NO_2^- and O_2) are comparable. This indicates that the large acceleration of process 6 in the presence of superoxide (Figures 2 and 4) is uniquely due to the higher concentration of O_2^- respective to the one which can be obtained for oxygen under pressures of the order of 1 atm (partition coefficient: $K_H = 4 \times 10^{-6}$ mol kg⁻¹ atm). For example, under the pressure of 1 atm of oxygen and in the presence of a superoxide concentration of 10^{-3} m the rate of process 6 is approximately the same as that under a pressure of 10^3 atm in absence of catalysts.

In conclusion, by considering the conditions of the

"complete" experiment described in Figure 2 one can say that mechanism I prevails only at the beginning of the reaction (close to point A). When appreciable superoxide concentrations are formed, mechanism II takes on more and more importance and largely prevails in the interval BC. Mechanisms such as III and IV become competitive with II only in interval CD when, again, a net production of superoxide can be observed. The prevalence of mechanism V occurs when practically all the peroxide initially present is converted to superoxide.

Generally speaking the results presented in this paper appear self-consistent and in good agreement with previous studies. They satisfactorily support the hypotheses made on the existence of catalytic effect, by O_2^{2-} and O_2^- , on reaction 6 even if some phenomena could be explained only on a semiquantitative basis because of system complexity. On the other hand, this is the limit often found for molten salt studies because of the few analytical techniques which can be conveniently employed and because of several experimental restrictions which characterize the use of these high-temperature solvents.

References and Notes

- (1) (a) P. G. Zambonin and J. Jordan, *J. Amer. Chem. Soc.*, **89**, 6365 (1967); (b) *ibid.*, **91**, 2225 (1969); (c) P. G. Zambonin and A. Cavaggioni, *ibid.*, **93**, 2854 (1971); (d) P. G. Zambonin, F. Paniccia, and A. Bufo, *J. Phys. Chem.*, **76**, 422 (1972).
- (2) J. M. Schlegel and D. Priore, *J. Phys. Chem.*, **76**, 2841 (1972).
- (3) H. Lux, R. Kuhm, and T. Niedermeier, *Z. Anorg. Allg. Chem.*, **286** (1959).
- (4) J. Goret and B. Tremillon, *Bull. Soc. Chim. Fr.*, **67** (1966).
- (5) E. P. Mignosin, L. Martinot, and G. Duyckaerts, *Inorg. Nucl. Chem. Lett.*, **3**, 511 (1967).
- (6) F. L. Whiting, G. Mamontov, and J. P. Young, *J. Inorg. Nucl. Chem.*, **34**, 2475 (1972).
- (7) F. Paniccia and P. G. Zambonin, *J. Phys. Chem.*, **77**, 1810 (1973).
- (8) P. G. Zambonin, *J. Electroanal. Chem.*, **24**, 365 (1970).
- (9) P. G. Zambonin, *J. Electroanal. Chem.*, **33**, 243 (1971).
- (10) P. G. Zambonin, *Anal. Chem.*, **41**, 868 (1969).
- (11) E. Desimoni, F. Paniccia, and P. G. Zambonin, *J. Electroanal. Chem.*, **38**, 373 (1972).
- (12) P. G. Zambonin, V. L. Cardetta, and G. Signorile, *J. Electroanal. Chem.*, **28**, 237 (1970).
- (13) W. E. Triaca and A. J. Arvia, *Electrochim. Acta*, **9**, 1055 (1969).
- (14) It is to be noted that the present experiments cannot give sufficient information to distinguish (on the basis of the overall stoichiometries) between mechanisms III and IV or any other reaction path which can be written to rationalize period CD. This is mainly because of the difficulty in estimating (at various times of interval CD) the extract contribution of mechanisms II and V to the total oxygen consumption.

Laser Flash Photolytic Study of Mercury(II) Iodide in Aqueous Solution

Philippe Fournier de Violet,*¹ Roland Bonneau, and Samuel R. Logan

Laboratoire de Chimie Physique A, Université de Bordeaux I, 33405 Talence, France (Received February 4, 1974)

Publication costs assisted by Centre National de la Recherche Scientifique

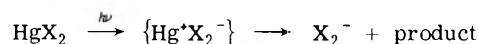
Absorption spectra and kinetics of formation of transient species produced by laser flash photolysis of mercury(II) iodide in aqueous solutions are reported. An analysis of the results shows that the primary process in the photolysis of HgI_2 is the formation of atomic iodine and of a transient species absorbing at 340 nm which has been tentatively assigned to HgI . In the presence of small quantities of I^- ions, the I_2^- radical anion is formed as a result of a secondary dark reaction. A previously speculated mechanism is hereby directly confirmed. The primary quantum yield of photodissociation has been evaluated as 0.04 and the rate constants of the equilibrium reaction $I + I^- \rightleftharpoons I_2^-$ as $k_1 2 \times 10^{10} M^{-1} sec^{-1}$ and $k_2 1.7 \times 10^6 sec^{-1}$. These data are obtained from a simplified kinetic scheme.

Introduction

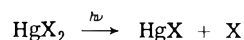
Studies of the photochemistry of mercury(II) halides, HgX_2 , and of the related complexes, HgX_4^{2-} , were previously undertaken by Langmuir and Hayon² using a flash photolysis system capable of following the events occurring subsequent to 20 μsec after the photolytic pulse. They found that on photolysis $HgCl_2$, $HgCl_4^{2-}$, $HgBr_2$, $HgBr_4^{2-}$, and HgI_4^{2-} gave rise to the corresponding radical anions, Cl_2^- , Br_2^- , and I_2^- . The only transient detected in the photolysis of HgI_2 absorbed at 330 nm and it was not identified. I_2^- , with λ_{max} at 385 nm, was detected when small quantities of I^- ions were added.

Several possible primary processes were considered by Langmuir and Hayon.² The participation of hydroxyl radicals, formed by charge transfer from a water solvent molecule to a mercuric ion, was discounted because of the ab-

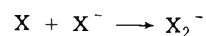
sence of an effect by OH radical scavengers and because of the slight effect of pH on the yields of X_2^- . Two other mechanisms were considered: (I) an intramolecular rearrangement of the electronic charge followed by direct formation of X_2^-



and (II) the dissociation of a mercury-halogen bond



followed by the reaction of a halogen atom with a halide ion

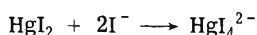


However, it was not found possible to distinguish between these two mechanisms.

The main purpose of the present study has to determine whether X_2^- was a primary product of the photolysis of these compounds (mechanism I) or produced by a secondary reaction (mechanism II) as suggested in ref 2. The technique of laser flash photolysis was applied in a previous study³ to the photochemistry of I_2 in water and the time resolution was fully adequate to distinguish the initial product, the charge transfer complex $I \cdot H_2O$, from the I_2^- radical ion formed subsequently by a thermal reaction with I^- . In this work we seek to make a similar distinction for HgI_2 .

Experimental Section

The experimental set-up, using a collinear arrangement, has been described elsewhere.⁴ The flash excitation is provided by a Q switched neodymium glass laser (C.G.E. instrument) associated with two KDP frequency doublers, delivering approximately 50 mJ at 265 nm in 30 nsec. The analyzing light source is a pulsed xenon discharge lamp giving pulses having a flat part of 10 μ sec. The cell has a 5-cm path length and aqueous HgI_2 solutions in the range of $6 \times 10^{-5} M$ were used, giving an optical density at 265 nm of approximately unity. Transient absorption spectra were obtained point by point at a given time after the laser pulse. When I^- ions were required in the HgI_2 solution, measured quantities of standard KI were added. The resulting concentration of free I^- ions was then deduced, taking account of the equilibrium



Results

When $6 \times 10^{-5} M$ aqueous solutions of HgI_2 were excited with laser pulses of 265-nm light, a transient absorption was detected with a maximum at 340 nm. The spectrum, calculated from the transmittances observed just after the laser pulse, is given in Figure 1, spectrum 1. This transient decays uniformly and by a first-order process, as if due to a single species. At both 340 and 385 nm, the rate constant was found to be $2.5 \times 10^5 \text{ sec}^{-1}$.

The addition of small quantities of iodide ion causes both the spectral and the kinetic characteristics to be modified. Immediately after the laser pulse, the extent of the transient absorption is considerably diminished in the spectral regions below 350 nm and below 335 nm the measured $\Delta(\text{OD})$ becomes negative. However, 1 μ sec after the laser pulse the transient absorption has changed so that it now shows a maximum at 385 nm (Figure 1, spectra 2 and 3).

In Figure 2, we compare the changes in the OD at 385 nm over the 1.5 μ sec following the laser pulse for HgI_2 alone (curve 1) with those for various amounts of added KI (curves 2a, 2b, 2c, and 2d). In the presence of I^- , we observe the same initial transient absorption as for HgI_2 alone, followed by a slow increase, the extent and the rate of which depend on the iodide concentration.

Interpretation and Discussion

The transient absorption spectrum shown in Figure 1 curve 1 is similar to that previously reported but is not positively identified; it is most probably a primary photochemical product since it is not observed to grow subsequent to the laser pulse. This transient absorption could be attributed to HgI since, in the gas phase, this species has an electronic transition around 300 nm.⁵ The formation of Hg_2I_2 observed as an end product in this system is

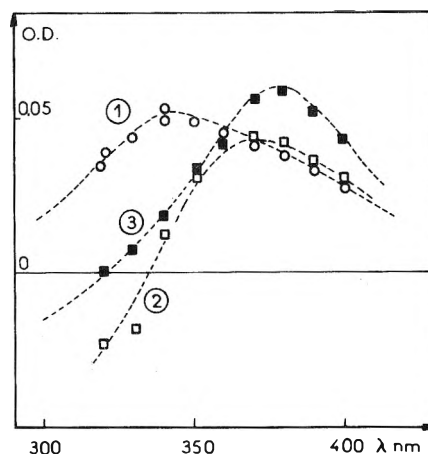


Figure 1. Transient optical density changes produced by laser flash photolysis of (1) $[HgI_2] \approx 6 \times 10^{-5} M$ immediately after the laser pulse; (2, 3) $[HgI_2] \approx 6 \times 10^{-5} M$ in presence of $[I^-] \approx 10^{-5} M$; (2) immediately after the laser pulse and (3) 1 μ sec after the laser pulse.

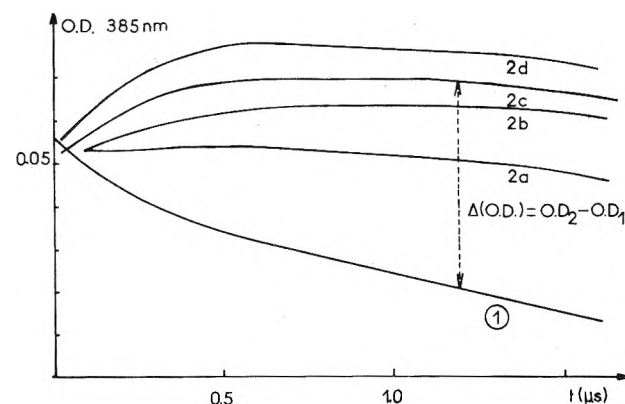


Figure 2. Transient optical density at 385 nm vs. time: (1) $[HgI_2] = 6 \times 10^{-5} M$; (2) $[HgI_2] = 6 \times 10^{-5} M$ in presence of (a) $[I^-] = 2 \times 10^{-5} M$, (b) $[I^-] = 3.8 \times 10^{-5} M$, (c) $[I^-] = 5.4 \times 10^{-5} M$, and (d) $[I^-] = 7.7 \times 10^{-5} M$.

in support of such an assignment. The transient absorption appearing in the presence of I^- in the spectral region 380–400 nm is assigned to the well-known diiodide ion I_2^- .⁵ In the spectral region 320–360 nm, the negative $\Delta(\text{OD})$ does not necessarily imply that I_2^- or I^- reacts with the product absorbing at 340 nm as has been previously suggested.² An alternative possibility is a decrease of the concentration of HgI_4^{2-} (which absorbs in the spectral region in question with $\lambda_{\text{max}} 325 \text{ nm}$ and $\epsilon_{\text{max}} 20,000 M^{-1} \text{ cm}^{-1}$) by direct photolysis since this species is reported² to have a large absorption at 265 nm.

Since this spectral region is extremely complex to analyze, we examined only the kinetic behavior of the transient absorption at 385 nm. In Figure 2, we measured the difference in optical density, $\Delta(\text{OD})$, between the curves 2a, b, c, d, and curves 1, that is

$$\Delta(\text{OD}) = \text{OD}_{2a, b, c} - \text{OD}_1$$

The increase in $\Delta(\text{OD})$ is clearly attributable to the formation of I_2^- , and this quantity may be taken as a measure of I_2^- concentration, subject to the assumption that the rate of disappearance of the initial transient, having a λ_{max} at 340 nm, is unaffected by the presence of I^- ions.

If the only reactions involving I_2^- that need be considered are



and



then we have

$$d[I_2^-]/dt = k_1[I][I^-] - k_2[I_2^-] \quad (3)$$

Since in these experiments $[I_2^-] \ll [I^-]$, we may write

$$dx/dt = k_1b(a - x) - k_2x$$

where $a = [I]_0$ and $b = [I^-]_0$. After integration and the substitution of optical density changes for concentrations, we obtain

$$\log \{ \Delta(\text{OD})_{\text{max}} - \Delta(\text{OD}) \} = \log \Delta(\text{OD})_{\text{max}} - \frac{k_1[I^-] + k_2}{2.303} t \quad (4)$$

where $\Delta(\text{OD})_{\text{max}}$ represents the plateau value of $\Delta(\text{OD})$ which is assumed to correspond to equilibrium between reactions 1 and 2.

In Figure 3, we show the graphical test of eq 4 for $[I^-] = 5.7 \times 10^{-5} M$. From the slope, we obtain $\{k_1[I^-] + k_2\}$ and the variation of this function with I^- concentration is shown in Figure 4. The poor linearity of this plot is attributable to the neglect of other reactions of I_2^- such as



and



These become more significant at the higher concentrations of I^- , so in Figure 4 we have drawn a straight line through the points at low $[I^-]$ and ignored these at higher $[I^-]$ where the kinetic analysis is least valid. The slope and intercept give $k_1 = 1.0 \times 10^{10} M^{-1} \text{sec}^{-1}$ and $k_2 = 1.7 \times 10^6 \text{sec}^{-1}$. These values and the ratio $k_1/k_2 = 1.2 \times 10^4 M^{-1}$ are in good agreement with those previously reported^{4,6} ($k_1/k_2 \approx 1.4 \times 10^4 M^{-1}$ and $k_1/k_2 \geq 1.1 \times 10^4 M^{-1}$).

Our data show quantitative agreement with a scheme whereby the I_2^- is produced by an equilibrium reaction between an iodine atom formed in a primary photochemical step and an iodide ion. The existence of a charge transfer excited state $\text{Hg}^+I_2^-$ of HgI_2 , which could also be a source of delayed I_2^- formation, can be ruled out by the I^- dependence of the I_2^- formation. Thus, the finding not only substantiates mechanism II but indicates that any contribution from mechanism I can only be negligible.

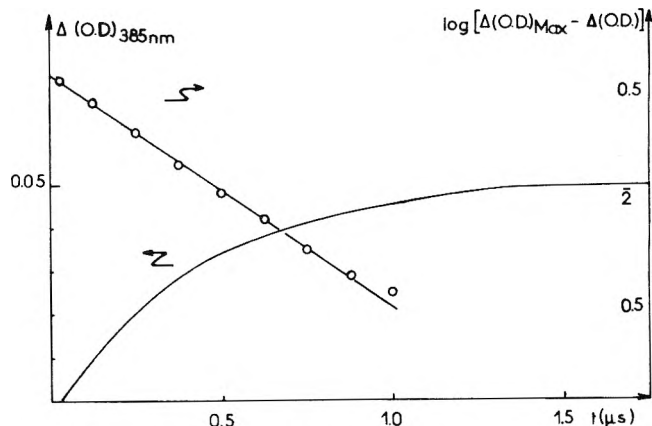
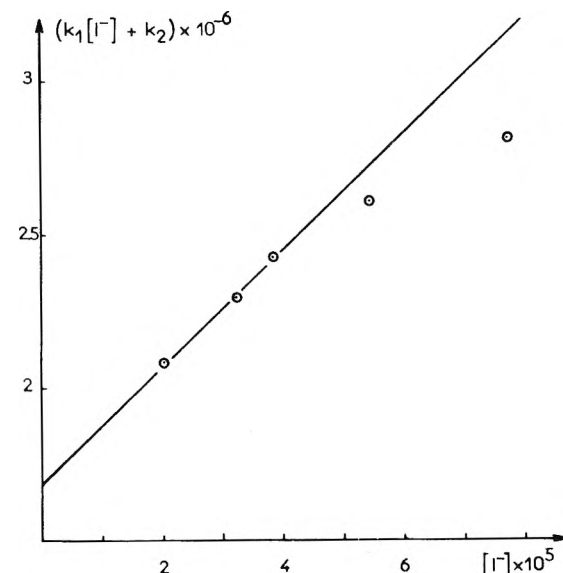
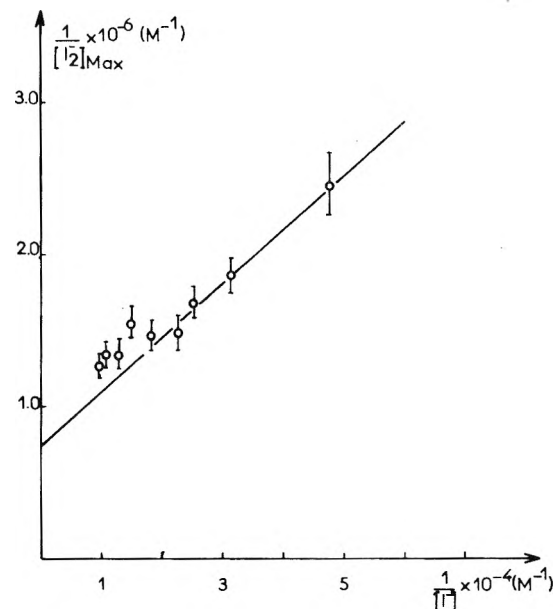
The dependence on I^- concentration of the plateau concentration of I_2^- , when reactions 1 and 2 are in equilibrium, also permits the evaluation of the initial concentration of I atoms. At equilibrium, eq 3 becomes

$$dx/dt = k_1(a - x_{\text{max}})(b - x_{\text{max}}) - k_2x_{\text{max}} = 0$$

Neglecting the term in x_{max} , we obtain

$$\frac{1}{x_{\text{max}}} = \frac{1}{a} + \left(1 + \frac{k_2}{k_1a}\right) \frac{1}{b} \quad (7)$$

When $1/[I_2^-]_{\text{max}}$ is plotted against $1/[I^-]$ (Figure 5), a straight line is obtained from which we obtain $[I] \approx 1.4 \times 10^{-6} M$ and $k_1/k_2 \approx 2 \times 10^4 M^{-1}$. Since during the laser pulse the volume of the irradiated solution absorbs about 3.5×10^{-5} einstein l^{-1} , the primary quantum yield of I atoms is approximately 0.04. However, the values obtained for the constants k_1 , k_2 , the ratio k_1/k_2 , and ϕ are only indicative since reactions 5 and 6 have been neglect-

Figure 3. Kinetics of formation of I_2^- at 385 nm.Figure 4. Plot of the slope of curves of the type shown in Figure 3 against concentration of I^- , that is, of $\{k_1[I^-] + k_2\}$ against $[I^-]$.Figure 5. Plot of the reciprocal maximum concentration of I_2^- against the reciprocal of the concentration of I^- .

ed for high concentration of I^- to simplify the kinetic scheme.

Although we have shown that the mechanism of photolysis involves I atoms production in the primary step, in agreement with the work of Langmuir and Hayon,² we have not observed these directly. This is chiefly because the absorption maximum³ of the charge transfer complex at 255 nm lies in the region of the HgI_2 absorption. In any case, the low quantum yield means that a very small transient would be produced, a concentration of $1 \mu M$ producing an OD of 0.005.

At present, we cannot be sure that the mechanism proposed in the case of HgI_2 , applies also to other mercury(II) halides. Flash photolysis of aqueous solutions of $HgCl_2$ and $HgBr_2$ have shown the formation of Cl_2^- and Br_2^- .

However, hydrolysis and dissociation reactions of these compounds are important in water (2% for $HgCl_2$ and 1%

for $HgBr_2$) so that halide ions are always present in solution. Under these conditions, it is not unlikely that Cl_2^- and Br_2^- radical anions are produced by a subsequent thermal reaction of halogen atom with halide ion. However, confirmation of this is difficult with our apparatus because the absorptions of $HgCl_2$ and $HgBr_2$ are very weak at 265 nm.

References and Notes

- (1) Author to whom correspondence should be addressed.
- (2) M. E. Langmuir and E. Hayon, *J. Phys. Chem.*, **71**, 3808 (1967).
- (3) P. Fournier de Violet, R. Bonneau, and J. Joussot-Dubien, *Chem. Phys. Lett.*, **19**, 251 (1973).
- (4) P. Fournier de Violet, R. Bonneau, and J. Joussot-Dubien, *J. Chim. Phys.*, **70**, 1404 (1973).
- (5) G. Herzberg, Ed., "Molecular Spectra and Molecular Structure." Vol. I, Van Nostrand, Princeton, N. J., 1967, p 539.
- (6) L. I. Grossweiner and M. S. Matheson, *J. Phys. Chem.*, **61**, 1089 (1957).

Entropies of the Hydrates of Sodium Hydroxide. III. Low-Temperature Heat Capacities and Heats of Fusion of the α and β Crystalline Forms of $NaOH \cdot 4H_2O$

S. C. Mraw and W. F. Giauque*

Low Temperature Laboratory, Departments of Chemistry and Chemical Engineering, University of California, Berkeley, California 94720
(Received March 29, 1974)

Publication costs assisted by the National Science Foundation

$NaOH \cdot 4H_2O$ can exist in two crystalline forms labeled α (stable) and β (unstable). The heat capacity of $NaOH \cdot 4H_2O \cdot \alpha$ has been measured from 20 to 280.7°K, its unstable melting point, and its heat of fusion at this temperature was found to be 6467 ± 20 cal/mol. The heat capacity of $NaOH \cdot 4H_2O \cdot \beta$ has been determined from 15 to $271.32 \pm 0.05^\circ K$, its congruent melting point, and its heat of fusion at this temperature was measured as 4601 ± 15 cal/mol. The heat capacity of the liquid, including a supercooled region, was measured from 257 to 313°K. The $\int_{0^\circ K}^{298.15^\circ K} C_p d \ln T$ was found to be 76.17 ± 0.1 gibbs/mol for liquid tetrahydrate using the β form and 76.13 ± 0.1 gibbs/mol using the α form. These values not only agree with each other but also agree with a previously known value, 76.17 gibbs/mol at 298.15°K. Thus both forms approach 0°K without frozen-in entropy, such as can result from disordered hydrogen bonding or other structural defects. The thermodynamic properties of $NaOH \cdot 4H_2O \cdot \alpha$, $NaOH \cdot 4H_2O \cdot \beta$, and their liquid, have been tabulated. ΔH°_0 for the reaction $\alpha(s) = \beta(s)$ was calculated as +822 cal/mol. At 1 atm the β form is thermodynamically unstable with respect to the α form at all temperatures. When sodium hydroxide tetrahydrate crystallizes, the sequence appears to be β , which has considerable kinetic stability; and then α , which has final thermodynamic stability. It is shown that this is in accordance with Robinson's rule which pointed out that the higher entropy form is to be expected first in the mechanism sequence. It was found that the spontaneous transformation of β to α occurs with a volume increase of about 6%, and its initiation is most probable in the approximate temperature range, 210–250°K. It was also found that the α form floats on its liquid. Due to this expansion it is suggested that caution should be exercised in storing or shipping sodium hydroxide solutions near the tetrahydrate composition during winter weather. A special heavy calorimeter was devised and used to resist the effect of the solid–solid expansion. A more satisfactory light-weight fluted-type calorimeter, which was shown easily to undergo repeated expansions followed by a return to its original dimensions, has been described for future use in similar circumstances.

The research reported here is part of a program designed to disclose the extent to which residual entropy occurs at limiting low temperatures. This sometimes exists in solids due to "frozen-in" nonequilibrium structural disorder. The

present results are part of a series on the hydrates of sodium hydroxide to ascertain the facts concerning possible ordered or disordered hydrogen bonding. An understanding of the various types of such residual entropy is of consider-

able practical importance because they can interfere with the accurate application of the third law of thermodynamics.

Giauque and Ashley (Giauque)¹ considered available $\int_0^T C_p d \ln T$ data on ice, as compared to a reliable entropy value based on spectroscopic data of gaseous water, less the well-known entropy increments due to changes of state. It was shown that ice retained an entropy of 0.9 ± 0.1 gibbs/mol (1 gibbs \equiv 1 defined cal/defined deg) due to some type of frozen-in structural disorder. In the then absence of structural data on ice, they suggested (as it turned out—incorrectly) that the $\frac{3}{4}$ mol of ortho molecules in H_2O gas retained equal proportions of random clockwise and counterclockwise internal rotations in ice at low temperatures, leading to a discrepancy of $(3/4)R \ln 2 = 1.03$ gibbs/mol.

The importance of water in chemical thermodynamics made it desirable to perform a definitive investigation on the low-temperature properties of ice. This was undertaken by Giauque and Stout.² They found that ice retained 0.82 ± 0.05 gibbs/mol at limiting low temperatures. On the basis of this information,² Pauling³ then offered what we believe to be the correct explanation of the above discrepancy in terms of disordered hydrogen bonding leading to the value $R \ln (3/2) = 0.806$ gibbs/mol as a close theoretical approximation.

Long and Kemp⁴ showed that D_2O also had a similar residual entropy of 0.77 gibbs/mol.

Pitzer and Coulter⁵ found a discrepancy of about $R \ln 2$ in $Na_2SO_4 \cdot 10H_2O$, which was explained by Ruben, Templeton, Rosenstein, and Olovsson,⁶ whose X-ray structural investigation disclosed details leading to a disorder of $R \ln 2$. Their results indicate a random clockwise and counterclockwise ordering of hydrogen-bonded rings each consisting of four water molecules/mol of $Na_2SO_4 \cdot 10H_2O$.

Water is such a common component of solid compounds that it is important to make a systematic survey of the extent to which hydrogen bonding or other structural arrangements cause residual entropy discrepancies. This should enable the development of methods of detecting such effects and, by various types of structural investigations, hopefully making calculated corrections where necessary. For example, Ruben, *et al.*,⁶ also showed by their X-ray structural measurements that the similar structures of $Na_2CrO_4 \cdot 10H_2O$ and $Na_2SO_4 \cdot 10H_2O$ make it appear practically certain that the similar four-member H_2O ring in $Na_2CrO_4 \cdot 10H_2O$ would also retain disorder equivalent to a nonequilibrium entropy of $R \ln 2$ gibbs/mol at low temperatures.

However, we may quote from a considerable variety of low-temperature investigations carried out in this laboratory, which show that all of the following substances and probably most other hydrates attain perfect order at limiting low temperatures: NH_3 ;⁷ $NH_3 \cdot H_2O$, $(NH_3)_2 \cdot H_2O$;⁸ $NH_3 \cdot 2H_2O$;⁹ HNO_3 , $HNO_3 \cdot H_2O$, $HNO_3 \cdot 3H_2O$;¹⁰ H_2SO_4 , $H_2SO_4 \cdot H_2O$, $H_2SO_4 \cdot 2H_2O$, $H_2SO_4 \cdot 3H_2O$, $H_2SO_4 \cdot 4H_2O$, $H_2SO_4 \cdot 6.5H_2O$;¹¹ $CdSO_4$, $CdSO_4 \cdot H_2O$, $(CdSO_4)_3 \cdot 8H_2O$;¹² $CoSO_4 \cdot 6H_2O$, $CoSO_4 \cdot 7H_2O$;¹³ $NiSO_4 \cdot 6H_2O$, $NiSO_4 \cdot 7H_2O$.¹⁴ However, as a warning against any overconfidence, Stavely and his coworkers have recently found that $Na_2HPO_4 \cdot 12H_2O$ ¹⁵ retains an entropy of 3.5 ± 0.5 gibbs/mol; $Na_2CO_3 \cdot 10H_2O$ ¹⁶ retains 1.5 ± 0.5 gibbs/mol; and $ZnF_2 \cdot 4H_2O$ ¹⁷ retains 2.1 ± 0.4 gibbs/mol of nonequilibrium entropy at limiting low temperatures.

Murch and Giauque¹⁸ measured the low-temperature heat capacities of NaOH and NaOH·H₂O. Siemens and

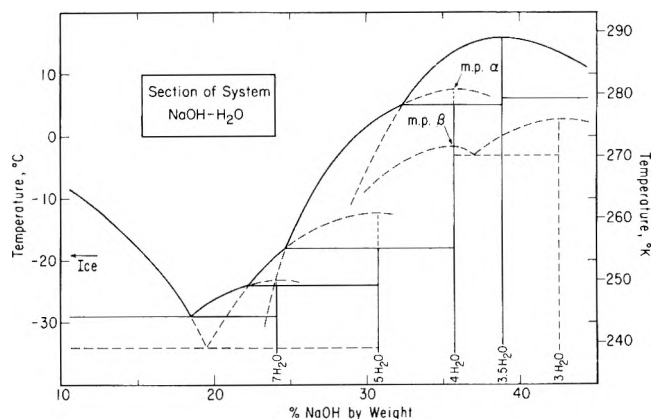


Figure 1. Central portion of the phase diagram for the system sodium hydroxide–water after Pickering²⁰ and Cohen-Adad, *et al.*²¹ Several previously observed invariant points have been deleted because the phases have not been identified.

Giauque¹⁹ extended the investigation to include $NaOH \cdot 2H_2O$ and $NaOH \cdot 3.5H_2O$. In each case the entropy of formation of the above sodium hydroxide hydrate compounds, calculated by assuming perfect order at 0°K, agreed with the equilibrium values derived at 298.15°K by use of the second law of thermodynamics.

The present work covers the α (stable) and β (unstable) crystalline forms of $NaOH \cdot 4H_2O$. We may say at once that they also have been found to approach zero entropy and, thus, perfect order at limiting low temperatures.

A partial phase diagram, based on the work of Pickering,²⁰ and its confirmation by Cohen-Adad, Tranquard, Péronne, Negri, and Rollet,²¹ is shown as Figure 1. From the diagram it may be seen that both tetrahydrate melting points are thermodynamically unstable but that the α form is stable at a peritectic at which it splits to form $NaOH \cdot 3.5H_2O$ and solution. However, it was shown by Pickering that the α and β forms each have sufficient individual stability to permit the measurement of the melting curves as a function of solution composition. Pickering also noted that the unstable β form was the easier to obtain.

Preparation and Analysis of the Sample

The sodium hydroxide used was made from reagent grade metallic sodium containing less than 0.01% impurity. The method of preparation was closely similar to that described by Murch and Giauque.¹⁸ Briefly, clean pieces of sodium were mounted on a platinum screen above a platinum dish and allowed to react with water vapor carried by a stream of pure nitrogen in a Monel glove box with a Plexiglas window. The nitrogen was humidified by distilled water which had been freed of carbon dioxide by boiling. The resulting sodium hydroxide solution, about 50% by weight, was transferred to a Teflon bottle and diluted to about 38% for storage. It was titrated from a weight buret, against standard sulfuric acid, prepared from a constant-boiling mixture as described by Kunzler.²² The stock solution was then diluted to $NaOH \cdot 4H_2O$. A final analysis of the sample gave $NaOH \cdot 4.0002 \pm 0.0010H_2O$. A test for carbonate in the final solution was carried out by acidifying the solution and sweeping out CO_2 by a stream of nitrogen, followed by absorption of the CO_2 in a known amount of alkali. This was back-titrated to evaluate the difference. The carbonate present was evaluated at $(2 \pm 1) \times 10^{-5}$ mol of CO_3^{2-} /mol of NaOH.

Measurements with Gold Calorimeter VI

It had been planned to carry out the research in the same calorimeter, "gold calorimeter VI," used in the previous work on the sodium hydroxide hydrates.^{18,19} A description of this calorimeter has been given previously.¹⁸ It contains eight radial gold vanes to improve thermal conductivity and a well to accommodate a Leeds and Northrup strain-free platinum thermometer, No. 1215333, calibrated at the National Bureau of Standards. A new insulated thermometer-heater of gold wire, 0.0031 in. in diameter, containing about 0.1% silver, was wound on the outer cylindrical surface as described previously,¹⁸ except that a third lead was taken off near the midpoint of the thermometer-heater. The purpose of the third lead was to enable heat introduction in the lower portion of the calorimeter to produce convection stirring of the liquid if necessary.

The NaOH·4H₂O sample was transferred from a weight buret to the gold calorimeter in the nitrogen-filled glove box. It weighed 169.178 g *in vacuo* equivalent to 1.50973 mol. The molecular weight was taken as 112.0584. The unoccupied space in the sample chamber was filled with helium gas at 1 atm to assist thermal conduction. The auxiliary low-temperature apparatus was of a type described in considerable detail by Giauque and Egan,²³ except that there was no external tube leading into the calorimeter. A heavy cylindrical copper and lead "block," within which the calorimeter was suspended, served as a stable-temperature environment at any temperature within the experimental range. With the evacuated apparatus immersed in liquid nitrogen, the cooling rate of the calorimeter could be controlled by admitting various pressures of helium to the vacuum space and by the temperature difference between the block and calorimeter. Since temperature control can be important, in producing and preserving unstable states, a record was kept.

At temperatures above the melting point of the β form, 271.32°K, the supercooled liquid was cooled at approximately 2°/min. The rate was then reduced to about 0.4°/min until the temperature was about 262°K after which it was reduced to about 0.02°/min. Starting at some temperature between 259 and 258°K the temperature rose rapidly to the melting point of the thermodynamically unstable β form. After standing at this temperature for about 0.5 hr, it was cooled at an average rate of about 3°/min to about 200°K and continued cooling to the temperatures of liquid hydrogen without incident.

We were completely unaware that we had set a trap which would destroy the calorimeter. A typical series of heat capacity measurements was started and proceeded uneventfully to 212°K. Sufficient heat was then added to reach a temperature of about 220°K. However, after an expected 10-min equilibrium period, with the block colder than the calorimeter, the calorimeter was still heating slowly and the rate increased to an average of 0.2°/min over a period of 8 min. Suddenly, the external gold thermometer-standard platinum thermometer circuit, which used a common stabilized current, was open. When a current was reestablished in the platinum thermometer alone, some 60 min later, it was found that the calorimeter had been warmed some 22° to 242°K, equivalent to the addition of some 1200 cal/mol of NaOH·4H₂O.

The apparatus was disassembled and it was found that the gold calorimeter had expanded sufficiently to split the gold thermometer-heater, which was encased in silk cloth

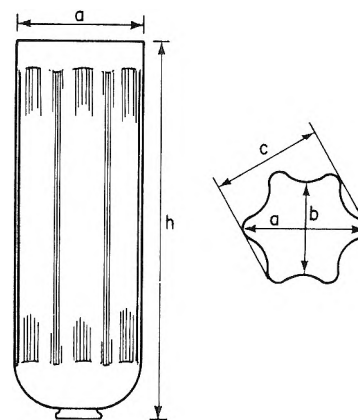


Figure 2. Side view and cross section of the electroformed flexible nickel sample chamber, designed to survive the expansion of solid sodium hydroxide tetrahydrate. The top of the shell is cylindrical, and the bottom contains a bellows convolution. Distances: $a = 36.3$ mm, $b = 28.7$ mm, $c = 31.8$ mm, $h = 11.1$ cm.

and Formvar, from top to bottom. A measurement of the gap width along the split led to a rough estimate that a transition had occurred with a volume increase of about 6–8%. The unstable β form had evidently transformed to the solid α .

The heat capacities obtained with gold calorimeter VI are given as series I in Table I.

The Second Calorimeter

It was evident that a continuation of the work would require a calorimeter which could survive the expansion from the β to the α form and enable heat capacity measurements. Two general types of solution to the problem were considered: (a) flexible containers which could expand easily without rupture, within a rigid helium-filled copper shell, to assist the distribution of heat, and serve as a support for the thermometer-heater and the strain-free platinum thermometer; (b) containers sufficiently strong to resist rupture or appreciable deformation by the expansion, with subsequent annealing of the stable crystalline form to eliminate residual strains. Again a helium-filled copper enclosing shell seemed desirable.

As examples of type (a) the transition was caused to occur in Teflon bottles, which survived the increase in volume and returned closely to their original dimensions when the solid was melted. This method would probably have been successful but was not used because of the poor thermal conductivity of Teflon.

Another type of calorimeter was based somewhat on a fluted design used by Brickwedde, Hoge, and Scott,²⁴ to solve an expansion problem, at or just below the melting point of UF₆. They used a fluted copper structure inside a cylindrical copper shell. At the end of their experiments it was found that the inner container had a permanent increase in volume of about 10%. Giauque and Stout² had used a simple double-walled copper calorimeter in connection with the expansion during the freezing of water, but it also was rejected for the present work, because it was desirable to have a design that would always restore itself to the original shape and size after repeated expansions. It was decided to try a conventional electroforming technique in which nickel is deposited on an aluminum mandrel to make a fluted container as shown in Figure 2. The Servometer Corp.²⁵ produces very flexible nickel bellows tubing by this

TABLE I: Heat Capacities of NaOH·4H₂O-β (Experimental)^a

T _{av} , °K	C _{p,av}	T _{av} , °K	C _{p,av}	T _{av} , °K	C _{p,av}	T _{av} , °K	C _{p,av}	T _{av} , °K	C _{p,av}
Series I ^b									
15.794	0.700	51.506	10.031	129.643	28.794	255.891	46.972	257.512	48.926
17.901	1.022	57.121	11.730	137.457	30.212	260.888	47.926	262.067	51.159
19.937	1.313	63.189	13.508	145.108	31.531	265.760	49.582	266.485	59.038
22.126	1.810	70.373	15.524	152.394	32.778				
24.765	2.373	78.177	17.610	160.130	34.013				
27.571	3.081	85.915	19.598	168.199	35.234				
30.634	3.846	93.688	21.460	176.178	36.436				
33.908	4.777	101.135	23.090	184.060	37.616	280.904	91.410	281.321	91.564
37.731	5.886	108.296	24.586	191.888	38.698	287.832	92.038	288.852	92.217
41.974	7.159	115.334	26.034	200.092	39.811	294.754	92.513		
46.508	8.521	122.243	27.389	208.216	40.802				
Series III ^c									
				Melted				Melted	

a) Units of C_p are gibbs per mole (gibbs = defined cal/defined degree).

b) Measurements made in the gold calorimeter on 1.50973 moles of sample (mol wt 112.0584 gm/mole).

c) Measurements made in the TWN calorimeter on 0.70028 moles of sample.

process and they agreed to deposit nickel on an aluminum mandrel supplied by our shop, after which the aluminum mandrel was dissolved. The top was left open, to be closed by welding on a lid. The wall thickness was 0.2 mm. The container flexed very well and returned to its original dimensions. In trial transformations of NaOH·4H₂O-β → NaOH·4H₂O-α its performance was excellent; however, we were unsuccessful in welding a lid onto the unnecessarily thin wall at the top, and the idea was abandoned only to save time. During one of the transition experiments it was found that dimension *b* (Figure 2) increased from 28.7 to 29.3 mm and we accept this measurement as a rather rough estimate of the average linear expansion of the tetrahydrate solid. This corresponds to a volume expansion of about 6.4%. If a 0.5 mm thick lid, including a heavy threaded inlet tube, had been electroformed on the original thin-walled vessel, it would probably have been an excellent sample chamber.

In the meantime experiments were progressing on type (b) containers. A bottom closure was welded onto an ordinary piece of steel pipe, with an o.d. of 38.2 mm and a wall thickness of 1.5 mm, and successive transformations were caused to occur. The pipe acquired a small permanent bulge but never broke and it was evident that the expansion was not far above the elastic limit. A rod of "nickel 200" was bored with a drill, leaving the conical shape at the bottom corresponding to the drill bite. The exterior of the bottom was rounded, except that a flat circular portion was left (as shown in Figure 3) for soldering on a convection-stirrer hotplate. The cylinder diameter was 27.7-mm i.d. with a wall 2 mm thick. Two trial transition expansions were caused to occur and no bulging could be detected within 0.2 mm. This container, which had an i.d. approximately 12 cm long, was incorporated into a calorimeter as shown in Figure 3, which is largely self-explanatory. Although nickel is generally reported to be inert in solutions of sodium hydroxide, a sample of "nickel 200" was tested in 36% NaOH at about 50°. A loss in weight of about (1-2) × 10⁻⁶ g/(cm² day) was found, which was about the limit of error of the measurement. In the expansion trials it was evident that the strong cylinder did not prevent the expansion but forced the solid to move upward. For this reason the standard platinum thermometer well was located outside the nickel vessel. The triangular-vane structure (Figure 3), which was planned to act as a chimney for convection stirring, was left loose in the sample chamber so that it could return to the bottom each time after the sample was melted. The calorimeter was designated the thick-walled nickel (TWN) calorimeter. The nickel filling tube was welded into the nickel lid, and the assembly was welded

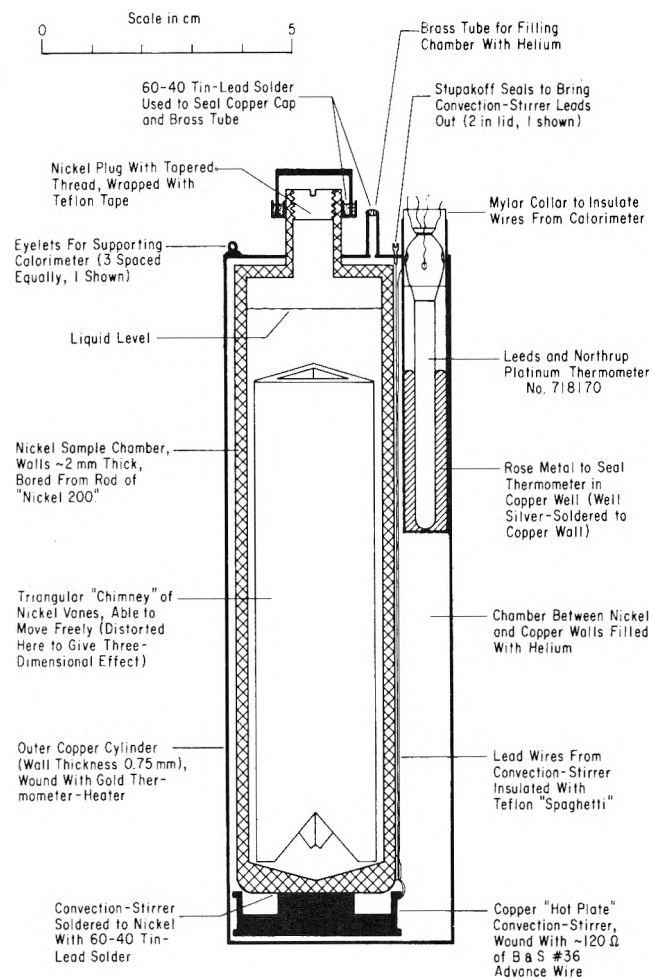


Figure 3. Thick-walled nickel (TWN) calorimeter designed to survive expansion of solid sodium hydroxide tetrahydrate.

onto the nickel cylinder. The copper exterior lid was joined to the nickel filling tube with silver solder, as was the copper trough in which the cap was soldered with 60:40 tin-lead solder. The brass tube, for introducing helium gas, and the three support eyelets were silver-soldered to the copper lid. The copper lid itself was joined to the copper cylinder with 95:5 Sn-Sb refrigeration solder, which was also used to seal the Stupakoff seals into the lid. The range of melting points of the several solders is important in the assembly sequence. The standard platinum thermometer, Leeds and Northrup No. 718170, which had been calibrated at the National Bureau of Standards, was checked at the ice point before the experiment. A gold thermometer-heater, as described earlier,¹⁸ was wound on the calorimeter outer copper wall, which was 0.75 mm thick, to assist thermal distribution.

Measurements in the TWN Calorimeter

After measuring the heat capacity of the empty calorimeter, 78.472 g of the NaOH·4.0002H₂O sample, equivalent to 0.70028 mol, was added and the apparatus reassembled. The calorimeter and contents were cooled to 251°K and held for 24 hr. No crystallization occurred and a series of heat capacities, including the supercooled region, were then measured. These results are reported in Table II.

The sample was again cooled, and near 247°K, heat evolution was observed and the sample warmed itself to the melting point of the β form. The crystallization was com-

TABLE II: Heat Capacities of NaOH·4H₂O(l) (Experimental)^a

T _{av} , °K	C _{p,av}	T _{av} , °K	C _{p,av}
260.317	89.005	286.655	91.897
266.874	89.865	293.575	92.576
272.835	90.469	300.331	92.629
279.535	91.226	306.860	93.193

a) Units of C_p are gibbs per mole (gibbs ≡ defined cal/defined degree). Measurements made on 0.70028 moles of sample (mol wt 112.0584 gm/mole) in the TWN calorimeter before any crystallization occurred.

TABLE III: Heats of Fusion of NaOH·4H₂O^a

Melting Point, °K	NaOH=4H ₂ O ^b		NaOH=4H ₂ O ^c	
	271.32	280.7	271.32	280.7
Experimental Order	1	3	2	4
T _{initial} , °K	268.520	268.938	275.997	276.350
T _{final} , °K	277.494	277.344	292.121	291.388
Premelting	18.1	95.2	15.2	42.2
Premelting near 255°K (concentration dislocation to water side of tetra)	0.0	17.0	0.0	17.0 ^b
∫C _p (s) dT	134.8	114.7	215.6	199.5
∫C _p (l) dT	560.2	546.6	1049.9	982.1
Heat added to substance	5277.9	5134.5	7737.2	7590.1
Correction for heat of mixing after concentration dislocation	0.0	-20.0	-20.0	-40.0 ^c
Correction (concentration dislocation to NaOH side of tetra--see text)	0.0	Unknown	0.0	Unknown
ΔH _f	4601.0	4565.4 ^d	6467.0	6428.0 ^d
Accepted value of ΔH _f	4601±15		6467±20	

a) All heat units are cal/mole.

b) Assumed.

c) Effect doubled to allow for two concentration dislocations.

d) Low results were expected due to small unknown corrections (see text). Thus, while second determinations were supporting evidence, they were given no numerical weight.

pleted, the β form was cooled to approximately 253°K, and measurements reported as series II in Table I were begun. Three heat capacities were determined on the solid, and then, after the first β heat of fusion was measured, three more heat capacities were completed on the liquid. The approximate lower temperature limit of 253°K for cooling the β form without inducing a transition to the α was selected after a large number of experiments, following the expansion within the gold calorimeter. Attempts to cool even a few degrees below 253°K nearly always triggered the expansion to the α form. The original cooling through the region below 253–200°K, and below, must be regarded as somewhat fortuitous. In any case we did not succeed in repeating it. The calculation of the first heat of fusion of the β form is summarized in Table III. An unsuccessful attempt was then made to cool the β form so as to fill in the gap between 212 and 253°K; however, heat evolution began near 251°K and the transformation to the α form was complete in a few minutes. To eliminate any residual strain in the sample it was heated to the region 274–275°K and held there for 36 hr. The solid α form was then cooled to liquid hydrogen temperatures and the heat capacity measurements reported as series I in Table IV were made. This series included the first α heat of fusion, detailed in Table III, and three more measurements on the liquid.

During the heat of fusion of the α form, it was necessary to consider the probability that some of the α would split at the peritectic temperature near 278°K (see Figure 1) to give NaOH·3.5H₂O plus solution. The heat capacity runs

on the solid, which terminated at 276.0°K, showed a small amount of premelting. The next heat introduction started at that temperature and continued without interruption to about 291°K. This ensured that any 3.5-hydrate, formed during the process, would be melted during the fusion run. However, it was necessary to consider that any solid NaOH·3.5H₂O, which might have fallen to the bottom of the calorimeter before melting, and any equilibrium lower density peritectic liquid, which failed to recombine with melting NaOH·3.5H₂O, would cause a concentration dislocation within the calorimeter at the end of the fusion run—a more concentrated liquid at the bottom and a more dilute liquid at the top.

The actual correction was estimated in the following manner. From the heats of solution summarized previously,¹⁹ the various heat capacities and heats of fusion involved, and the phase diagram of Cohen-Adad, *et al.*,²¹ three theoretical curves of enthalpy *vs.* temperature were plotted on the same graph corresponding to three limiting possibilities.

(1) The α form was assumed to split at the peritectic temperature and the 3.5-hydrate to settle immediately and completely to the bottom of the calorimeter. When the 3.5-hydrate layer melted at its melting point to give a dense liquid layer, with the equilibrium peritectic liquid layer above, the mixing correction was calculated to be about -90 cal/mol. This improbable situation represents the maximum correction possible.

(2) The α form was assumed to split at the peritectic temperature, but the 3.5-hydrate solid remained completely and uniformly suspended as a slurry. No correction would be necessary since complete mixing would be attained, as recombination took place along the melting curve of the 3.5-hydrate (see Figure 1).

(3) The α form could melt at its own melting point, 280.7°K. This would result in no correction.

The actual enthalpy *vs.* temperature data taken during the first heat of fusion were plotted on the same graph as the three theoretical curves for comparison. From this it was concluded that about half of the α form probably melted at its melting point, before a split occurred. From the path of the experimental enthalpy *vs.* temperature curve, an estimate of the mixing correction¹⁹ was made as -20 ± 10 cal/mol. The measured value of the heat of fusion of NaOH·4H₂O-α, at its melting point, 280.7°K, was found to be 6467 ± 20 cal/mol. This was accepted later as the final value.

Melting Points of NaOH·4H₂O-β and NaOH·4H₂O-α

Before recrystallizing the sample in the β form for a melting point determination, it was desirable to eliminate any concentration dislocation left at the end of the first β fusion. Accordingly the hotplate convection stirrer within the calorimeter was used with the intent to stir the solution and produce a uniform concentration. In all, the stirrer was on for around 3 or 4 hr each day for 2 weeks. The entire calorimeter was heated at about 8°/hr. At 50° the stirrer-heater was turned off. After several hours (often overnight), when the calorimeter had cooled 20 or 30°, the stirrer was started. Finally the calorimeter was cooled to about 247°K, the β form crystallized, and the melting point was measured carefully. Heat was added in amounts roughly corresponding to 10% of the total heat of fusion and, after each input, the calorimeter was allowed to approach equilibrium for several hours before the temperature was re-

corded. The results were as follows (f = fraction melted): $f = 0.110$, $T = 270.842^\circ\text{K}$; $f = 0.195$, $T = 271.142^\circ\text{K}$; $f = 0.281$, $T = 271.219^\circ\text{K}$; $f = 0.383$, $T = 271.257^\circ\text{K}$; $f = 0.475$, $T = 271.273^\circ\text{K}$. A plot of T vs. $1/f$ gives $271.32 \pm 0.05^\circ\text{K}$ as the melting point for $\text{NaOH}\cdot 4\text{H}_2\text{O}$. The points listed above fall on a curve rather than a straight line and suggest that the sample had not been stirred to uniform composition with respect to components of $\text{NaOH}\cdot 4\text{H}_2\text{O}$. In such a case, where the "impurity" is itself one of the components of the melting solid, a plot of T vs. $1/f$ is expected to approach the T coordinate axis at right angles and the usual extrapolation of $1/f$ to zero was done in this way. If the "impurity" had not been a component, T vs. $1/f$ should approach the T axis as a straight line at an angle. A check was made on the possibility that the "nickel 200" had begun to dissolve, more than was indicated by the initial test mentioned above, after an induction period. After the sample was removed from the calorimeter, it was found to contain only $10 \mu\text{g}$ of nickel/g of sample (approximately 0.002 mol %). This should have produced a relatively trivial premelting effect. We are forced to conclude that the stirring arrangement in the TWN calorimeter was not effective. It seems probable that the heavy bottom and walls of the nickel container prevented the establishment of a sufficient thermal head to overcome density differences within the sample, which had resulted from the peritectic splitting during the heat of fusion of the α form, as mentioned above. Subsequent measurements of heat capacity before the second fusion determinations of both α and β forms, to be mentioned later, show a considerably increased premelting. This was consistent with the considerable change of the β melting point with the fraction melted. We finally ascribed these effects to remanent concentration dislocation. Fortunately this did not affect the original heat of fusion of the β form, and an appropriate correction was applied during the calculation of the first heat of fusion of the α form.

Since it was impracticable to determine the unstable melting point of the α form in the calorimeter, it has been taken as $280.7 \pm 0.1^\circ$ from the work of Pickering.²⁰ Values of this melting point in agreement with the above value were observed with a mercury thermometer during preliminary experiments of the present work.

Second Heats of Fusion of $\text{NaOH}\cdot 4\text{H}_2\text{O}$ - β and $\text{NaOH}\cdot 4\text{H}_2\text{O}$ - α

Second heats of fusion of the β and later α form, which were only slightly lower than the first ones, were measured. As mentioned above, the heat capacities, measured in the temperature ranges before the second heats of fusion of both β and α started, showed much higher premelting than the measurements made before the first heat of fusion of the α caused the composition dislocation within the sample. Another evidence of the dislocation was a 17-cal/mol heat absorption in the α form near 255°K , the $\text{NaOH}\cdot 4\text{H}_2\text{O}$ - α - $\text{NaOH}\cdot 5\text{H}_2\text{O}$ peritectic (see Figure 1). This peritectic melting was not observed in the first fusion run on the α form and should not have been, since the tetrahydrate composition should still have been uniform.

Immediately after the melting point measurements on the β form, the sample, which had been only 50% melted, was cooled to around 255°K and the heat capacity and heat of fusion procedures were repeated. The 17-cal/mol 4-5 peritectic effect, found later before the second α fusion, was not observed before the second β fusion as the temperature was too close to the region within which the β would

TABLE IV: Heat Capacity of $\text{NaOH}\cdot 4\text{H}_2\text{O}$ - α (Experimental)^a

$T_{\text{av}}, ^\circ\text{K}$	$C_{p,\text{av}}$	$T_{\text{av}}, ^\circ\text{K}$	$C_{p,\text{av}}$	$T_{\text{av}}, ^\circ\text{K}$	$C_{p,\text{av}}$	$T_{\text{av}}, ^\circ\text{K}$	$C_{p,\text{av}}$	$T_{\text{av}}, ^\circ\text{K}$	$C_{p,\text{av}}$
Series I ^b									
21.696	1.463	69.808	13.953	158.216	30.545	246.575	42.261	252.196	46.517
23.943	1.886	77.419	15.816	166.256	31.733	254.596	43.524	256.359	44.442
26.838	2.546	85.375	17.681	174.356	32.880	262.790	44.256	260.714	44.678
30.242	3.315	93.401	19.434	182.632	34.048	270.959	45.863	265.074	45.403
33.833	4.220	101.693	21.081	190.952	35.145			269.302	46.626
37.545	5.168	109.805	22.618	199.303	36.296			273.386	49.230
41.443	6.295	117.549	24.026	207.703	37.419				
46.226	7.537	125.501	25.416	215.904	38.451				
51.333	8.970	133.464	26.716	223.659	39.442	295.428	92.570		
56.855	10.499	141.601	28.071	231.311	40.298	302.481	92.847		
62.947	12.177	150.007	29.323	238.876	40.868	309.337	93.446		
Series II									
								294.547	92.534
								301.620	93.061

a) Units of C_p are gibbs per mole (gibbs = defined cal/defined degree). Measurements made on 0.70028 moles of sample (mol wt 112.0584 gm/mole) in the TWN calorimeter.

b) Difficulty with empty calorimeter at low temperatures; see discussion in text.

TABLE V: Thermodynamic Properties of $\text{NaOH}\cdot 4\text{H}_2\text{O}$ - α (Stable Form)^a

$T, ^\circ\text{K}$	C_p^*	S^*	$\frac{(\text{H}^*-\text{H}_0^*)}{T}$	$-\frac{(\text{F}^*-\text{H}_0^*)}{T}$	$T, ^\circ\text{K}$	C_p^*	S^*	$\frac{(\text{H}^*-\text{H}_0^*)}{T}$	$-\frac{(\text{F}^*-\text{H}_0^*)}{T}$
15	(0.498)	(0.165)	(0.124)	(0.041)	190	35.077	31.789	18.160	13.629
20	1.159	0.391	0.294	0.098	200	36.420	33.623	19.039	14.583
25	2.126	0.749	0.559	0.190	210	37.723	35.431	19.898	15.533
30	3.272	1.236	0.914	0.322	220	38.984	37.215	20.737	16.478
35	4.522	1.833	1.339	0.494	230	40.200	38.975	21.557	17.418
40	5.845	2.523	1.819	0.704	240	41.396	40.731	22.359	18.353
45	7.213	3.290	2.347	0.948	250	42.566	42.425	23.144	19.281
50	8.602	4.121	2.898	1.223	260	43.766	44.119	23.914	20.204
55	9.955	5.007	3.480	1.526	270	44.926	45.792	24.671	21.121
60	11.376	5.936	4.081	1.855	273.15	45.286	46.315	24.907	21.408
65	12.716	6.900	4.694	2.206	280	46.067	47.467	25.415	22.032
70	14.008	7.889	5.313	2.576	280.7 ^b	46.148	47.562	25.467	22.095
80	16.455	9.922	6.555	3.367					
90	18.712	11.997	7.782	4.210					
100	20.786	14.072	8.980	5.092					
110	22.702	16.145	10.142	6.003	271.32 ^c	90.382	67.523	47.052	20.471
120	24.487	18.197	11.264	6.934	273.15	90.593	68.131	47.343	20.789
130	26.170	20.224	12.346	7.878	280	91.324	70.386	48.410	21.975
140	27.775	22.223	13.391	8.832	280.7 ^b	91.394	70.612	48.517	22.095
150	29.321	24.197	14.402	9.790	290	92.227	73.605	49.906	23.700
160	30.818	26.133	15.382	10.751	298.15	92.791	76.170	51.071	25.099
170	32.275	28.045	16.333	11.712	300	92.899	76.744	51.328	25.416
180	33.695	29.930	17.258	12.672	310	93.365	79.798	52.677	27.121

a) The units are gibbs per mole (gibbs = defined cal/defined degree).

b) Melting point $\text{NaOH}\cdot 4\text{H}_2\text{O}$.

c) Melting point $\text{NaOH}\cdot 4\text{H}_2\text{O}$.

probably transform. We assume that it was present and have added 17 cal/mol to the second heat of fusion of the β . This should be added whether or not $\text{NaOH}\cdot 5\text{H}_2\text{O}$ crystallized and then melted before the heat capacity measurements started a little above 255°K or if the solution supercooled and did not require melting. The heat of fusion details are included in Table III. The heat capacities taken before and after the second heat of fusion of the β form are recorded as series III of Table I.

Following the melting point and heat of fusion measurements on the β form, the convection stirrer was run for 3 more days, but in view of the later observations it is doubtful that this removed much of the concentration dislocation.

Because it was hoped that the repeated heating to 50° by the convection stirrer, over the 2-week period, might have destroyed the α nuclei, it was desirable to try one last time to cool the β into and through the range below about 253°K . The β form was crystallized in the calorimeter and cooled at approximately $0.1^\circ/\text{min}$ into the forbidden zone below 253°K . It was thought that this slow cooling (a factor of 10 less than the previous attempt) might be so gentle as to prevent the β from transforming. However, in the neighborhood of 244°K , heat began evolving, and the transformation to α occurred. The α was again warmed to approximately 274 – 275°K and held there for 36 hr to relieve any strains within the sample before it was cooled to about 250°K . Its second heat of fusion measurement, including the 17 cal/mol required at the 4- α -5 peritectic, as mentioned above, is summarized in Table III, along with that of the first.

This completed the experimental work. The heat capacities taken before and after the second heat of fusion of the α are reported as series II in Table IV.

There was no systematic difference within the experimental error that made separate consideration necessary for liquid heat capacities done before there had been any crystallization, done after β fusions, or done after α fusions. Accordingly, all measurements on the liquid were plotted on the same graph and a smooth curve put through them. The smoothed values were then used as the accepted heat capacities for NaOH·4H₂O liquid in all subsequent calculations.

Since the appearance of a small amount of 4- α -5 peritectic during the second α fusion indicates some sodium hydroxide solution below the tetrahydrate concentration, it must have been balanced by an equal amount of sodium hydroxide at an average concentration above that of the tetrahydrate. It was not surprising that some NaOH·5H₂O appeared, because this concentration is not far from that of the 3.5-4- α peritectic liquid (see Figure 1). This relatively low-density liquid should have been somewhat separated in a top layer during the first fusion of the α form. The compensating higher density region could hardly have been produced in any other way than from the bottom layer melting of NaOH·3.5H₂O, derived from splitting at the same 3.5-4- α peritectic. If the second β fusion, which terminated at 277.34°K, had included any crystalline NaOH·3.5H₂O, its late melting above 277.34°K would have been noticed during the heat capacity measurements which followed immediately. No such effect was observed. Since sodium hydroxide solutions of all pertinent concentrations supercool easily, supercooling is the most plausible explanation, especially following the 2-week heating which was partly designed to destroy all previous crystal nuclei. This would have made the second β heat of fusion somewhat low. Its deficit of 36 cal/mol (Table III) is consistent with this. One cannot eliminate the possibility of a small amount of crystalline NaOH·3H₂O (see Figure 1) during the second β fusion, but the appearance of an additional crystalline form in a small amount of displaced solution is very improbable. Its presence would have been obscured by the fact that its unknown melting heat would have been included in the second β fusion near the 3-4- β eutectic temperature (see Figure 1).

Within the possible small uncorrected differences of the α and β second heats of fusion, they strongly support the first values obtained with the original undisturbed tetrahydrate composition. However, the original determinations have been given 100% weight.

Comment on the Thick-Walled Nickel Calorimeter

Though the TWN calorimeter fulfilled its primary purpose in surviving the expansions of β to α and continuing to work, there were several drawbacks to its use that made it somewhat less than the ideal calorimeter for heat capacity measurements. Because of the massive nature of the empty calorimeter itself and the relatively small sample chamber permitted by the design, the heat capacity of the full calorimeter was approximately two-thirds due to the empty area and one-third due to the substance itself throughout most of the temperature range. In addition, equilibrium times were much longer than would have been the case in almost any other type of calorimeter. A comparison with the data books on some of the earlier work¹⁹ on NaOH hydrates showed that with liquid in the calorimeter in the

room-temperature region the gold calorimeter came to equilibrium within 8–12 min after heat input. In the case of the TWN calorimeter, the equilibrium times in the same region were 20–25 min. Furthermore, the gold calorimeter thermometer–heater wire superheated only about 1° above the average temperature during heat input in this region. In the present research, with the double-walled calorimeter, the value was around 2.5°. These difficulties had to be accepted, however, since an unusual calorimeter design was necessary to deal with the unusual properties of the tetrahydrate system.

The Entropies of NaOH·4H₂O- α and NaOH·4H₂O- β

Integration of the β heat capacities, smoothed from the experimental data, gave an entropy of 76.17 \pm 0.1 gibbs/mol of NaOH·4H₂O at 298.15°K. This included an extrapolation below 15°K, made by plotting C_p/T^2 vs. T . The region between 212 and 253°K, in which the heat capacity of the α form could not be measured, due to its spontaneous conversion to the α form, was of necessity interpolated by a reasonable curve. The error due to this was considered to be small. The similar integration of the data on the α form gave an entropy of 76.13 \pm 0.1 gibbs/mol of NaOH·4H₂O at 298.15°K. This included an extrapolation below 20°K by use of a C_p/T^2 vs. T plot. Several measurements on the empty TWN calorimeter at lower temperatures were lost due to a bad insulating vacuum, and the uncertainty of extrapolated estimates for the heavy calorimeter with its numerous varied components seemed too great to enable evaluation of the α heat capacity below 20°K.

The agreement of the entropy values of the α and β forms and especially the fact that they agree with the second-law value, 76.17 gibbs/mol, in the summary of Siemens and Giauque,¹⁹ based on anhydrous NaOH and liquid H₂O, indicate that each form approaches zero entropy (excepting nuclear spin contributions) at limiting low temperatures.

The X-ray structure of one form of NaOH·4H₂O has been given by Hemily.²⁶ It is also included in a paper by Hemily and Wunderlich,²⁷ who summarized structural data on various hydrates of sodium hydroxide. Hemily²⁶ gave the melting point as 5.4°, which would eliminate the β form (mp -1.83°). However, Hemily and Wunderlich²⁷ gave the melting point as about 0° and identified the sample as the β form. This is probably correct, since the β form usually appears first. Their structural data were obtained at -81° (192°K), and they calculated the density as 1.41 \pm 0.04 g/cm³ at that temperature.

Assuming that Hemily had the β form, it is of interest that he cooled it through the difficult 212–253° region, mentioned above. The small size would greatly reduce the chance presence of α nuclei, to trigger transition, and in all probability the cooling was rapid.

During the present work it was found that the α form floated at its melting point, 7.55°. Seeding liquid NaOH·4H₂O with α form at 0° produced crystals as large as 1 cm³. The density of the tetrahydrate liquid is known to be 1.392 g/cm³²⁸ at 7.55°. Ice cubes of 1 cm³ size average 0.9 mm above water. The α crystals seemed definitely less buoyant on a relative volume basis. If a median volume buoyancy between that of ice and zero is assumed, the density of the α crystals may be estimated as 1.33 g/cm³. Since the ice volume buoyancy is only 9%, this median estimate can hardly be in error by more than several per cent. Using the rough expansion factor of 6% given above, the density

TABLE VI: Thermodynamic Properties of NaOH·4H₂O-β (Unstable Form)^a

T, °K	C _p ^b	S ^c	$\frac{(H^{\circ}-H_0^{\circ})}{T}$	$-\frac{(F^{\circ}-H_0^{\circ})}{T}$	T, °K	C _p ^b	S ^c	$\frac{(H^{\circ}-H_0^{\circ})}{T}$	$-\frac{(F^{\circ}-H_0^{\circ})}{T}$
15	0.610	0.208	0.155	0.052	130	28.859	22.424	13.626	8.798
20	1.369	0.480	0.358	0.122	140	30.661	24.629	14.779	9.850
25	2.429	0.894	0.667	0.233	150	32.371	26.803	15.895	10.908
30	3.700	1.447	1.060	0.387	160	33.986	28.945	16.976	11.969
35	5.088	2.120	1.535	0.585	170	35.524	31.052	18.022	13.030
40	6.561	2.895	2.070	0.825	180	37.013	33.124	19.036	14.089
45	8.071	3.755	2.653	1.102	190	38.440	35.164	20.020	15.144
50	9.579	4.683	3.270	1.413	200	39.791	37.171	20.975	16.196
55	11.086	5.667	3.912	1.755	210	41.053	39.143	21.901	17.241
60	12.586	6.696	4.573	2.123	220 ^b	(22.292)	(41.081)	(22.800)	(18.281)
65	14.030	7.761	5.245	2.516	230 ^b	(23.512)	(42.988)	(23.674)	(19.314)
70	15.431	8.852	5.923	2.929	240 ^b	(24.692)	(44.865)	(24.525)	(20.340)
80	18.104	11.089	7.280	3.809	250	45.851	46.713	25.355	21.358
90	20.588	13.367	8.623	4.744	260	47.011	48.534	26.166	22.368
100	22.847	15.655	9.934	5.721	270	48.141	50.329	26.959	23.370
110	24.957	17.932	11.205	6.728	271.32 ^c	48.798	50.564	27.062	23.502
120	26.957	20.191	12.435	7.756					

For alpha(s) = beta(s), $\Delta H_0^{\circ} = 822$ cal/mole.

- a) The units are gibbs per mole (gibbs = defined cal/defined degree).
 b) No actual experimental measurements made; see discussion in text.
 c) Melting point NaOH·4H₂O.

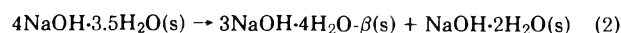
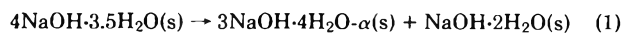
of the β form is estimated as $1.06 \times 1.33 = 1.41$ g/cm³. The density of the liquid at the β melting point, -1.83° , is 1.398 g/cm³.²⁸ The 1.41 g/cm³ β density happens to coincide with the 1.41 g/cm³ value given in ref 27, on the basis of X-ray measurements, taken at -81° . However, the broad estimated density limits, as calculated in ref 27, extend from 1.37 to 1.45 g/cm³ and could apply to either form. Nevertheless, we believe that the 1.33 g/cm³ (α) and the 1.41 g/cm³ (β) densities should be accepted within about 3% until more accurate measurements are made.

The structural details of the monoclinic crystal, as derived by Hemily,²⁷ showed an unending three-dimensional network of hydrogen bonds with no evidence of disorder.

Thermodynamic Properties of NaOH·4H₂O-α and NaOH·4H₂O-β

The thermodynamic properties of NaOH·4H₂O-α are tabulated in Table V and those of NaOH·4H₂O-β in Table VI. In order to make the entropy of each form of the tetrahydrate consistent with its second-law value at 298.15°K (taken as 76.170 gibbs/mol), the values in Tables V and VI have been adjusted by a small amount, well within the limits of error of the various measurements. In each case, the various thermodynamic properties of the solid hydrate and the heat of fusion were multiplied by a factor of 1.00051 for α and 1.00004 for β. This made the values of the β and the α forms consistent with the fact that they both must melt to give liquid NaOH·4H₂O. The ΔH°_0 for the reaction NaOH·4H₂O-α → NaOH·4H₂O-β was then calculated as +822 cal/mol. With this value and the values reported in Tables V and VI, it can be shown that solid β form is unstable with respect to solid α form at 1 atm and all temperatures.

The values in Tables V and VI were combined with those for NaOH·2H₂O and NaOH·3.5H₂O¹⁹ in order to determine whether solid NaOH·3.5H₂O could split according to either of the reactions



In order to do this, the data on NaOH·2H₂O and NaOH·3.5H₂O were multiplied by very small factors to make the entropies at 298.15°K consistent with the second-law values.¹⁹ When the calculations were made, the ΔF for reaction 1 could be seen to approach zero at low temperatures. However, the ΔF is neither negative enough nor positive enough to permit a reliable decision as to the thermo-

dynamic possibility of reaction 1. Slight changes, within experimental error, in the various heats of fusion, heat capacities, and heats of dilution involved can make the value of ΔF at low temperatures change by several calories. It can only be said, therefore, that reaction 1 is on the borderline of being thermodynamically possible. Whether there actually is a temperature at which ΔF equals zero, or exactly what that temperature is if it does exist, cannot be determined with accuracy. It should be emphasized, however, that there is little likelihood that the 3.5-hydrate would ever split by reaction 1, whether or not it is thermodynamically possible. Since the reaction would require the transport of water molecules in the solid state, it could only proceed to give microscopic phase regions of the products. These regions would have such a high free energy that they would prevent the reaction from happening in any practical macroscopic sense (see the discussions by Barieau and Giauque²⁹ and Cox, Hornung, and Giauque³⁰ regarding ZnSO₄²⁹ and MgSO₄³⁰ hydrates).

From the calculations it is apparent, however, that reaction 2 is thermodynamically impossible at all temperatures.

The temperature scales used in this research were the NBS-55 scale (below 90°K) and the ITS-48 scale (above 90°K). Conversion to the new IPTS-68 scale was considered but not made at this time, since it was desirable to keep the data on the present hydrates on the same basis as that of the others.^{18,19}

The results of the present research indicate that caution should be exercised in storing or shipping sodium hydroxide solutions in the vicinity of the tetrahydrate composition. The β form can easily crystallize from supercooled liquid at temperatures below its melting point (about -2°C or $+28^{\circ}\text{F}$) and, if kept cold after crystallization, can always transform to α anywhere below its melting point. This transformation becomes almost a certainty anywhere below about -20°C (-4°F).

The above temperatures are well within the range of winter weather in many parts of the world. Should a storage tank or a railroad tank car be at these temperatures, there is the possibility of it rupturing if it contains solid sodium hydroxide (β). It would not matter if there was room above the solid in the container, since the solid β form expands to solid α in all directions and usually does not make much use of the empty space above. An effort should be made to avoid the conditions which could produce the sequence of events: crystallization of β, transformation and expansion of β to α.

It is of interest to note that the much greater probability of crystallizing the unstable β rather than the stable α from the supercooled liquid sodium hydroxide tetrahydrate is in accordance with a rule first stated by Robinson.³¹ This ease of crystallization of the β form was observed by Pickering²⁰ and supported by many observations during the present research. Robinson's rule was stated in order to replace a faulty rule due to Ostwald, which was based on free energy, by one based on entropy.

Ostwald's rule could be stated as follows: In an isothermal system where several reactions are possible, that reaction takes place first whose products are least stable. The obvious inapplicability of this rule was soon noted in terms of such well-known cases as that of sulfur vapor, which condenses to the monoclinic form whether the temperature is above or below the rhombic-monoclinic transition point.

Robinson's rule is: "In an isothermal system where several reactions are possible, that reaction takes place first

whose products are of highest entropy." This is in accord with Boltzmann's relation that $S = k \ln(\text{probability})$. The behavior of the sodium hydroxide tetrahydrate system also illustrates this rule, as may be noted by comparing the entropy values in Tables V and VI. It is a good guide to the expected mechanism of any such system even though the rate of a subsequent reaction may eventually, and sometimes rapidly, eliminate a high-entropy intermediate form.

Acknowledgments We thank M. J. Domeniconi for assistance with the experimental measurements, Dr. R. A. Fisher for many helpful discussions, and the National Science Foundation for a graduate fellowship to S. C. M. This work was supported in part by the National Science Foundation.

References and Notes

- (1) W. F. Giauque and M. F. Ashley (Giauque), *Phys. Rev.*, **43**, 81 (1933).
- (2) W. F. Giauque and J. W. Stout, *J. Amer. Chem. Soc.*, **58**, 1144 (1936).
- (3) (a) L. Pauling, personal communication; (b) *J. Amer. Chem. Soc.*, **57**, 2680 (1935).
- (4) E. A. Long and J. D. Kemp, *J. Amer. Chem. Soc.*, **58**, 1829 (1936).
- (5) K. S. Pitzer and L. V. Coulter, *J. Amer. Chem. Soc.*, **60**, 1310 (1938).
- (6) H. W. Ruben, D. H. Templeton, R. D. Rosenstein, and I. Olovsson, *J. Amer. Chem. Soc.*, **83**, 820 (1961).
- (7) R. Overstreet and W. F. Giauque, *J. Amer. Chem. Soc.*, **59**, 254 (1937).
- (8) D. L. Hildenbrand and W. F. Giauque, *J. Amer. Chem. Soc.*, **75**, 2811 (1953).
- (9) J. P. Chan and W. F. Giauque, *J. Phys. Chem.*, **68**, 3053 (1964).
- (10) W. R. Forsythe and W. F. Giauque, *J. Amer. Chem. Soc.*, **64**, 48, 3069 (1942); **65**, 2379 (1943).
- (11) W. F. Giauque, E. W. Hornung, J. E. Kunzler, and T. R. Rubin, *J. Amer. Chem. Soc.*, **82**, 62 (1960).
- (12) M. N. Papadopolous and W. F. Giauque, *J. Phys. Chem.*, **66**, 2049 (1962).
- (13) R. V. G. Rao and W. F. Giauque, *J. Phys. Chem.*, **69**, 1272 (1965).
- (14) J. W. Stout, R. C. Archibald, G. E. Brodale, and W. F. Giauque, *J. Chem. Phys.*, **44**, 405 (1966).
- (15) C. G. Waterfield and L. A. K. Staveley, *Trans. Faraday Soc.*, **63**, 2349 (1967).
- (16) C. G. Waterfield, R. G. Linford, R. B. Goalby, T. R. Bates, C. A. Elyard, and L. A. K. Staveley, *Trans. Faraday Soc.*, **64**, 868 (1968).
- (17) R. O. Cook, A. Davies, and L. A. K. Staveley, *Trans. Faraday Soc.*, **68**, 1384 (1972).
- (18) L. E. Murch and W. F. Giauque, *J. Phys. Chem.*, **66**, 2052 (1962).
- (19) P. R. Siemens and W. F. Giauque, *J. Phys. Chem.*, **73**, 149 (1969).
- (20) S. U. Pickering, *J. Chem. Soc.*, 890 (1893).
- (21) R. Cohen-Adad, A. Tranquard, R. Péronne, P. Negri, and A. Rollet, *C. R. Acad. Sci.*, **251**, 2035 (1960).
- (22) J. E. Kunzler, *Anal. Chem.*, **25**, 93 (1953).
- (23) W. F. Giauque and C. J. Egan, *J. Chem. Phys.*, **5**, 45 (1937).
- (24) F. G. Brickwedde, H. J. Hoge, and R. B. Scott, *J. Chem. Phys.*, **16**, 429 (1948).
- (25) Servometer Corporation, Clifton, N. J.
- (26) P. W. Hemily, *Acta Crystallogr.*, **10**, 37 (1957).
- (27) P. W. Hemily and J. A. Wunderlich, *Acta Crystallogr.*, **10**, 454 (1957).
- (28) "International Critical Tables," Vol. III, McGraw-Hill, New York, N. Y., 1928, p 79.
- (29) R. E. Barieau and W. F. Giauque, *J. Amer. Chem. Soc.*, **72**, 5676 (1950).
- (30) W. P. Cox, E. W. Hornung, and W. F. Giauque, *J. Amer. Chem. Soc.*, **77**, 3935 (1955).
- (31) P. Robinson, *J. Phys. Chem.*, **34**, 207 (1930).

Mixtures of Trifluoroacetic Acid with Acetic Acid and Carbon Tetrachloride¹

Friedrich Kohler,* G. H. Findenegg, and M. Bobik

Institute of Physical Chemistry, University of Vienna, A-1090 Vienna, Austria (Received February 11, 1974)

The phase diagram (consolute curve and melting curves) of the system trifluoroacetic acid-carbon tetrachloride and the melting curves of the system trifluoroacetic acid-acetic acid have been determined. From these results the excess Gibbs energy of mixing of the two systems has been derived, using complementary data from the literature. The excess volumes and dielectric constants of the two systems have also been measured. The system trifluoroacetic acid-carbon tetrachloride resembles the system acetic acid-carbon tetrachloride, but all excess functions are more positive, which leads to phase separation below 8°. At this upper critical solution temperature the excess values of an equimolar mixture are $\Delta G^E = 336$ cal/mol, $T\Delta S^E = -47$ cal/mol, and $\Delta V = 1.91$ cm³/mol. The concentration dependence of the dielectric constant resembles that of the acetic acid system and shows the dominant influence of dimers. The phase diagram of the system trifluoroacetic acid-acetic acid exhibits a congruent melting point of a 1:1 solid compound. At 0° the excess values of an equimolar mixture are $\Delta G^E = -467$ cal/mol, $T\Delta S^E = -128$ cal/mol, and $\Delta V = -0.54$ cm³/mol. These values indicate a strong preference for the formation of heterodimers. The dielectric constant of this system has a maximum near equimolar concentration and a strongly positive temperature dependence. An equimolar mixture has also a higher electric conductance than either of the two pure acids. These results indicate that the heterodimer is strongly polar. This conclusion is also in agreement with an observed maximum of the downfield chemical shift of the acid protons.

Introduction

Recent studies on the system acetic acid-carbon tetrachloride have shown that thermodynamic,² volumetric,³ and ultrasonic absorption results⁴ for this system can be

explained consistently by a strong attractive interaction between acetic acid monomers and cyclic dimers, but it is not necessary to assume a formation of (sterically well-defined) trimers or higher chain associates.⁵ Otherwise it

would be difficult to understand the relatively large negative excess entropy of mixing of this system.

Trifluoroacetic acid has a higher dielectric constant ($\epsilon = 8.42$ at 20°) than acetic acid ($\epsilon = 6.17$ at 20°), and this might be caused by some tendency toward chain association in this liquid.

It was, therefore, of interest to study the thermodynamic and dielectric properties of the system trifluoroacetic acid-carbon tetrachloride and to compare the results with those of the system acetic acid-carbon tetrachloride. It was to be expected that the excess quantities should be more positive, mainly because of the substitution of the methyl by the trifluoromethyl group. The tendency toward chain association in pure trifluoroacetic acid should give a positive contribution to the excess entropy of this system, but this effect will be small if dimerization still plays the dominant role.

In mixtures of trifluoroacetic acid-acetic acid, a strong preference for heterodimerization has been reported both in the gas^{6,7} and in the liquid phase.⁸ If association in the two pure liquids involves mainly cyclic dimers, the mixing effects should be caused essentially by the conversion of homodimers into heterodimers. Only a small negative excess entropy of mixing should then result on account of the increased number of dimers in the mixture. Such a preference for heterodimers is thought to be related to a very polar structure of the heterodimer. Measurements of the dielectric constant, of electric conductance, and of nmr chemical shift were made in this system to investigate the character of the heterodimer.

Experimental Section

Materials. Acetic acid (purity better than 99.5%) was distilled after addition of acetic anhydride, using a column of about 80 theoretical plates and a reflux ratio of 40:1, and was then kept in a dark flask in vapor-phase contact with P_2O_5 . Melting points of different samples were between 16.43 and 16.53° ; densities at 20 and 40° were $\rho_{20} = 1.04927$ – 1.04952 and $\rho_{40} = 1.02665$ – 1.02695 g/cm³.

Carbon tetrachloride (purity better than 99.5%) was distilled and stored under similar conditions: mp -22.65° ; $\rho_{20} = 1.59410$ and $\rho_{40} = 1.55503$ g/cm³.

Trifluoroacetic acid (purity better than 98%) was also distilled under similar conditions but was kept in a glass-stoppered flask in a desiccator. It was found that the melting point of the product was lowered progressively when the liquid was kept in vapor-phase contact with P_2O_5 or other drying agents and this was attributed to a formation of anhydride. The melting point of such a product could be raised to the original value by addition of a suitable amount of water. This swift establishment of the equilibrium trifluoroacetic acid \rightleftharpoons anhydride, on the one hand, and the hygroscopic character of the acid, on the other hand, made it difficult to prepare and handle pure trifluoroacetic acid. Melting points of different samples were between -15.11 and -15.27° ; $\rho_{20} = 1.48944$ – 1.48957 , $\rho_{40} = 1.44217$ – 1.44236 g/cm³.

Techniques. Melting and consolute curves were determined as described elsewhere.^{9,10} The temperature control of the cryostat was $\pm 0.02^\circ$ down to -50° . Densities were measured as described before.¹¹ Dielectric constants and loss factors were measured with a General Radio 716-C capacitance bridge.¹² Most of the measurements were made at 100 and 400 kHz. For mixtures of high electric conductance use of an additional external resistor (GR 1434-G)

was necessary. The capacitance of this resistor was calibrated with substances of known dielectric constant and known electric conductance. As sample cells we adapted the cells MFL 1, 2, and 3 of the dipolmeter DM01 of Wissenschaftlich-Technische Werkstätten. All metal parts exposed to the liquid were protected by an electrolytic layer of rhodium which was renewed whenever necessary. The electric conductance was calculated from dielectric loss and/or measured with a conductometer of Philips (PW 9501). Nmr chemical shifts were measured with a Varian A-60A spectrometer with internal temperature regulation (40°); tetramethylsilane was used as internal standard.

Results¹³

(a) *Trifluoroacetic Acid-Carbon Tetrachloride.* The phase diagram of trifluoroacetic acid-carbon tetrachloride is shown in Figure 1. The consolute curve has been determined repeatedly with different samples of trifluoroacetic acid. Curve 2 in Figure 1 is probably due to a small water content, whereas curve 1 may correspond to a minor anhydride content of the acid. On the trifluoroacetic acid side, a slow increase of the consolute temperatures with time was observed, apparently due to the insufficient elimination of humidity. Considerable effort was made to determine the concentrations of the two coexistent liquid phases in equilibrium with solid trifluoroacetic acid, which are $x_1 = 0.081$ (0.087) and $x_1 = 0.854$ (0.857). (Throughout this paper subscript 1 refers to trifluoroacetic acid; the numbers in parentheses refer to consolute curve 2).

The activity coefficients f_i of component i in equilibrium with solid component i were evaluated from the melting curves using the equation⁹

$$\ln f_i = -\frac{L''_i \Delta T}{RTT_m} + \frac{\Delta C_{p,i}'' \Delta T^2}{2RTT_m} - \frac{\Delta H_i(T_{\text{ref}} - T)}{RT_{\text{ref}}^2} - \ln x_i$$

Here L'' denotes the heat of melting and $\Delta C_{p,i}''$ the difference in heat capacity of liquid and solid at the melting point T_m of the pure component i ; T is the equilibrium temperature of solid i and the liquid mixture of mole fraction concentration x_i , and ΔH_i is the partial molar heat of mixing; $\Delta T = T_m - T$, and T_{ref} is a reference temperature for which the activity coefficient and the excess free energy of mixing are calculated (for this system $T_{\text{ref}} = 8^\circ$ has been taken). The heat of melting can be obtained (or checked) by extrapolating the quantity $RTT_m(1 - x_i)/\Delta T$ to $x_i = 1$. Such a plot is linear for small values of $(1 - x_i)$ if $\ln f_i$ can be approximated by a parabola.⁹ For trifluoroacetic acid such a plot yields $L'' = 2250$ cal/mol (Figure 2). For carbon tetrachloride, $L'' = 602$ cal/mol was taken from the literature.¹⁴ The term containing $\Delta C_{p,i}''$ was neglected for this system. This approximation does not cause any serious error, in view of the relatively flat melting curves (small temperature differences) and the large positive values of $\ln f_i$. The partial molar heats of mixing were derived from the integral molar heats of mixing (at 30°)⁸

$$\Delta H/(\text{cal mol}^{-1}) = x_1(1 - x_1)[1160 + 172(2x_1 - 1) + 289(2x_1 - 1)^2 - 239(2x_1 - 1)^3]$$

The excess Gibbs energy was calculated as follows. The melting curve of trifluoroacetic acid was used to evaluate $\ln f_1$; the function $(\ln f_1)/x_2^2$ was plotted vs. mole fraction and

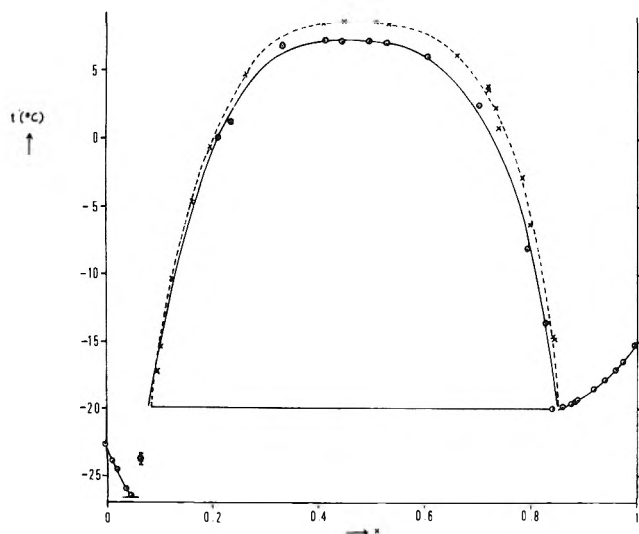


Figure 1. Phase diagram of trifluoroacetic acid (1)-carbon tetrachloride. The solid consolute curve is referred to as curve 1 in the text; the dotted curve is referred to as curve 2.

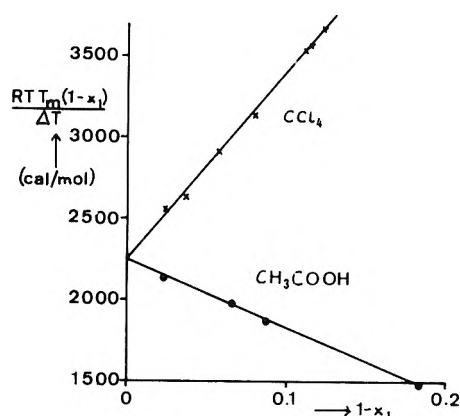


Figure 2. Extrapolation for evaluation of the heat of melting of trifluoroacetic acid.

extrapolated to the mole fraction of intersection with the consolute curve, from which the $\ln f_1$ value of the coexistent liquid mixture rich in carbon tetrachloride could be deduced. Similarly, $\ln f_2$ was evaluated from the CCl_4 branch of the melting curve and the function $(\ln f_2)/x_1^2$ extrapolated beyond the eutectic point to the corresponding mole fraction at the consolute curve. Integration of the Gibbs-Duhem equation was then performed for both homogeneous regions, using the eutectic point ($x_1 = 0.049$, $T = 246.6$ K) as a check on the consistency. ΔG^E was then evaluated¹⁵ from the consolute curve. This furnishes $\partial\Delta G^E/\partial x_1$ plus an integration constant over the heterogeneous region. The integration constant can be easily determined as ΔG^E is known for the two mole fractions at which the consolute curve intersects the melting curve. The function $\Delta G^E/x_1x_2$ thus obtained is shown in Figure 3. For an equimolar mixture at 8° , $\Delta G^E = 336$ cal/mol and $T\Delta S^E = -47$ cal/mol, indicating a similarity of this system with the system acetic acid-carbon tetrachloride² for which $\Delta G^E = 238$ cal/mol and $T\Delta S^E = -180$ cal/mol for the equimolar mixture at 30° . The negative excess entropy of both systems can be explained by the fact that the relative concentration of dimers is higher in the mixtures than in the pure acids.¹⁶

The excess molar volume of mixing ΔV is positive and

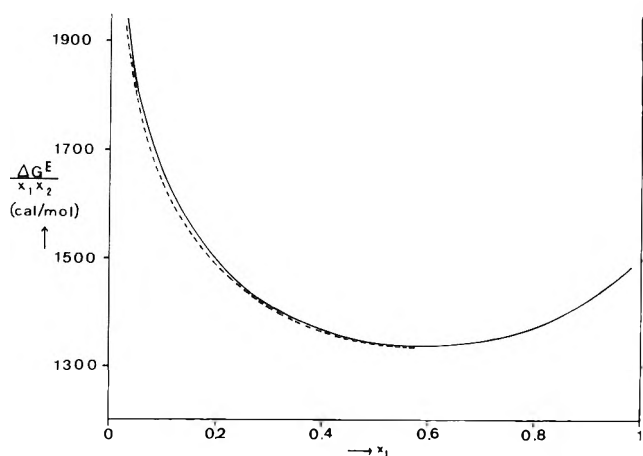


Figure 3. The excess Gibbs free energy of mixing, divided by the product of mole fractions, of trifluoroacetic acid (1)-carbon tetrachloride at 8° (the solid line is evaluated from consolute curve 1; the dotted line from consolute curve 2).

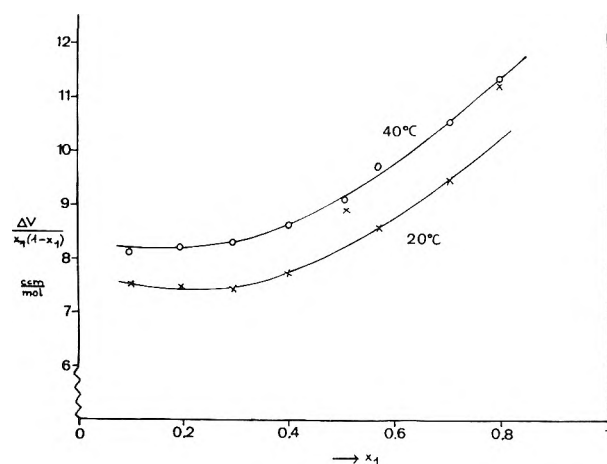


Figure 4. The excess molar volume of mixing, divided by the product of mole fractions, of trifluoroacetic acid (1)-carbon tetrachloride at 20° (crosses) and 40° (circles).

remarkably large and increases with increasing temperature (Figure 4). Here again a similarity with the acetic acid-carbon tetrachloride system³ is obvious. The volumetric behavior of both systems can be accounted for by assuming that the formation of a monomer-dimer contact is connected with a decrease in volume. The highest concentration of such "contracted" contacts will be in pure trifluoroacetic acid; the effect of diluting the acid by carbon tetrachloride will be to break up such contacts, thus causing expansion of the liquid mixture.

The dielectric constant is plotted in Figure 5 and compared with results for the acetic acid system.³ For mixtures up to a concentration of acid of $x_1 = 0.65$ the curves for the two systems are very similar, although, at very low concentration, the dielectric constant of the trifluoroacetic acid system is higher (indicating a lower dimerization constant) than that of the acetic acid system.¹⁷ For somewhat higher concentrations the acetic acid solutions exhibit a slightly higher dielectric constant. There is no obvious explanation for this fact, but it might reflect differences in the details of the monomer-dimer interaction. These differences could be caused by the different direction of the dipole moment in the two acids. The total dipole moment of the acetic acid

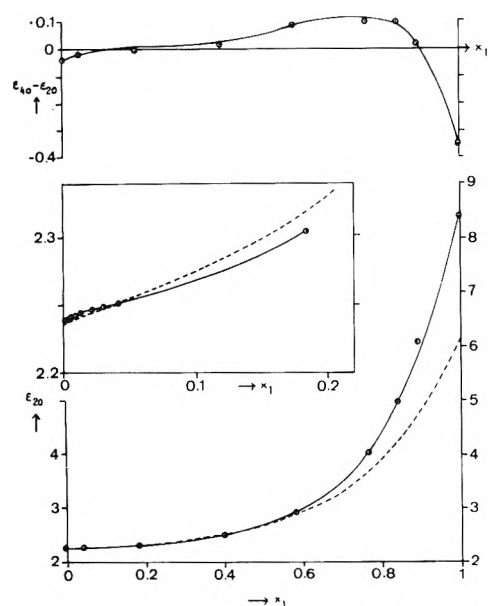


Figure 5. The dielectric constant ϵ at 20° of trifluoroacetic acid (1)-carbon tetrachloride in comparison to ϵ of acetic acid-carbon tetrachloride (dotted curve, ref 3). The region rich in carbon tetrachloride is shown in larger scale in the insert. The temperature dependence is shown as $\epsilon_{40} - \epsilon_{20}$.

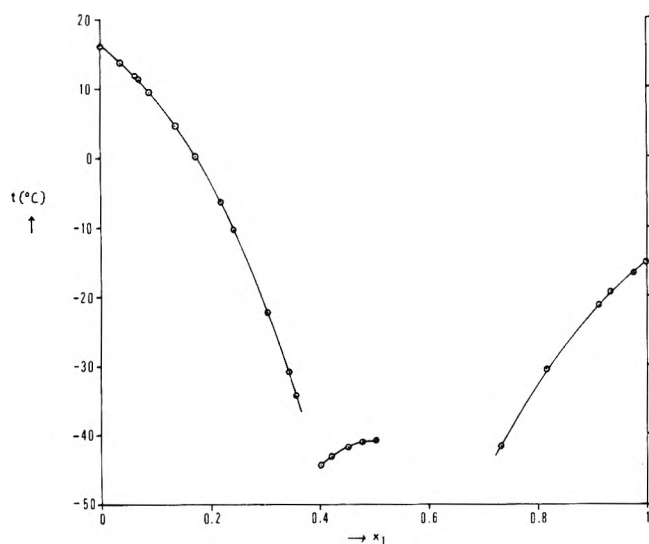


Figure 6. The melting diagram of trifluoroacetic acid (1)-acetic acid.

monomer is directed approximately parallel to the carbonyl group, while the OH bond moment is approximately opposite to this direction. By a rotation of the OH group out of the "cis" conformation the dipole moment of the molecule could thus be significantly increased. There is some indication³ that such an increase of the moment occurs in liquid acetic acid and also in mixtures with carbon tetrachloride, even at moderate concentrations of the acid. The dipole moment of the trifluoroacetic acid monomer is directed approximately halfway between the direction of the carbonyl and the CCF_3 group moments.

The increase of the dielectric constant toward pure trifluoroacetic acid and the change of sign of the temperature dependence indicate a relatively high concentration of monomers and/or some formation of chain associates in the

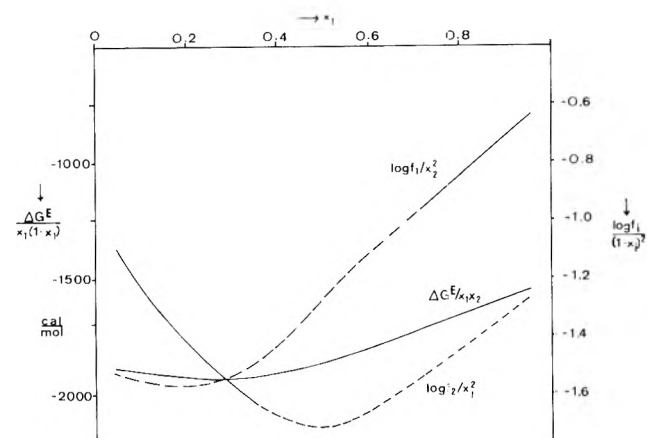


Figure 7. The functions $(\log f_i)/(1 - x_i)^2 w$ (scale on right side) and $\Delta G^E/x_1(1 - x_1)$ (scale on left side) for the system trifluoroacetic acid (1)-acetic acid at 0° . The solid part of the $(\log f_i)/(1 - x_i)^2$ curves gives the region of direct experimental observation. The scales differ by a factor of 1250, which corresponds very closely to $2.303RT$ at $T = 273.15 \text{ K}$.

pure acid. However, this conclusion is still compatible with the results of the thermodynamic investigation, i.e., that the equilibrium between monomers and cyclic dimers is dominant.

(b) *Trifluoroacetic Acid-Acetic Acid.* The melting diagram of this system is shown in Figure 6. It shows the existence of a 1:1 compound with a congruent melting point. Extrapolation of the quantity $RTT_m(1 - x_1)/\Delta T$ to $x_1 = 1$, which gives the heat of melting of trifluoroacetic acid (subscript 1), is again shown in Figure 2. For acetic acid, the corresponding plot was fairly linear, but extrapolation gave $L'' = 2870 \text{ cal/mol}$, which is considerably higher than the value of 2780 cal/mol determined previously.¹⁰ This discrepancy may introduce an error up to 5% in $\ln f_2$ or ΔG^E at concentrations corresponding to the lowest temperatures of the acetic acid melting curve. For $\Delta C_p''$ of acetic acid a value of $5.4 \text{ cal K}^{-1} \text{ mol}^{-1}$ was taken.¹⁰ For trifluoroacetic acid, $\Delta C_p''$ was set arbitrarily equal to $3 \text{ cal K}^{-1} \text{ mol}^{-1}$. An error in $\Delta C_p''$ of $\pm 1 \text{ cal K}^{-1} \text{ mol}^{-1}$ leads to a maximum error in $\ln f_1$ or ΔG^E of $\pm 1\%$ at concentrations corresponding to the lowest temperatures of the trifluoroacetic acid melting curve.

The temperature dependence of the activity coefficients was calculated by means of the following equation for the integral heat of mixing (at 30°)⁸

$$\Delta H/(\text{cal mol}^{-1}) = x_1(1 - x_1)[-2379 + 418(2x_1 - 1) + 342(2x_1 - 1)^2 - 290(2x_1 - 1)^3]$$

For the numerical integration of the Gibbs-Duhem equation it was necessary to extrapolate the activity coefficients of both components over the region of the melting curve of the 1:1 compound. Again, the function $(\ln f_i)/(1 - x_i)^2$ was used for this extrapolation (Figure 7). The smooth continuation of these functions beyond the region of the melting curve of the 1:1 compound indicates the substantial correctness of the extrapolation procedure. The resulting function $\Delta G^E/x_1(1 - x_1)$ at the reference temperature (0°) is also shown in Figure 7. For an equimolar mixture $\Delta G^E = -467 \text{ cal/mol}$ and $T\Delta S^E = -128 \text{ cal/mol}$ (at 0°). This is in agreement with the qualitative arguments given in the Introduction, that the most important process at mixing is the formation of heterodimers from homodimers,

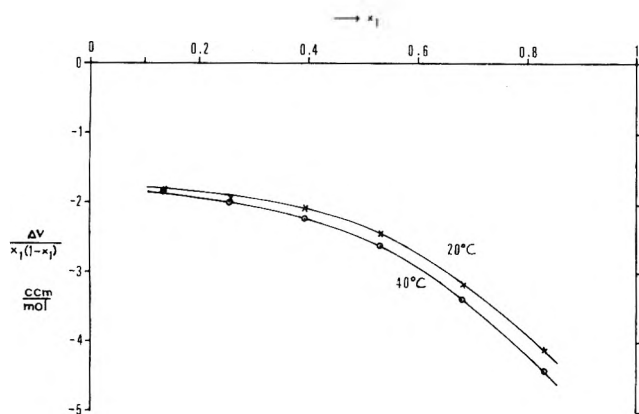


Figure 8. The excess molar volume of mixing, divided by the product of mole fractions, of trifluoroacetic acid (1)-acetic acid at 20° (crosses) and 40° (circles).

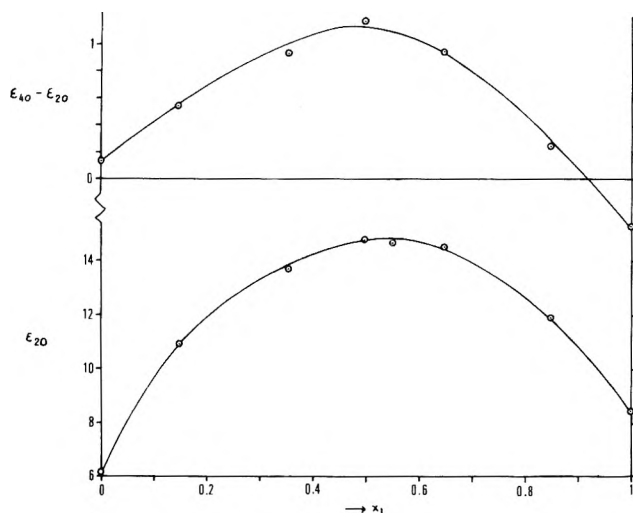


Figure 9. The dielectric constant of trifluoroacetic acid (1)-acetic acid at 20° and its temperature dependence (difference between 40 and 20°).

which should involve no major entropy change. The stronger bonds in the heterodimer and the increased concentration of dimers in the mixture contribute to a relatively small negative excess entropy.

The excess molar volume of mixing of this system is plotted as $\Delta V/x_1(1-x_1)$ in Figure 8. The negative excess volume suggests that the formation of heterodimers from homodimers is connected with a considerable decrease in volume. Furthermore, as ΔV becomes more negative with increasing temperature (in spite of some dissociation of heterodimers), the contraction connected with the formation of heterodimers seems to increase with increasing temperature (see below).

The dielectric constant of this system exhibits a pronounced maximum at mole fraction 0.5, as shown in Figure 9. This reveals a highly polar nature of the heterodimer and shows that in addition to the asymmetry of the end groups the hydrogen bonds must be strongly polarized. There is also a maximum in the temperature dependence of the dielectric constant. This is more difficult to understand, since breaking of the polar heterodimers should not increase the overall moment of the mixture. A possible explanation for this behavior might be that with increasing temperature the heterodimer assumes some zwitterion charac-

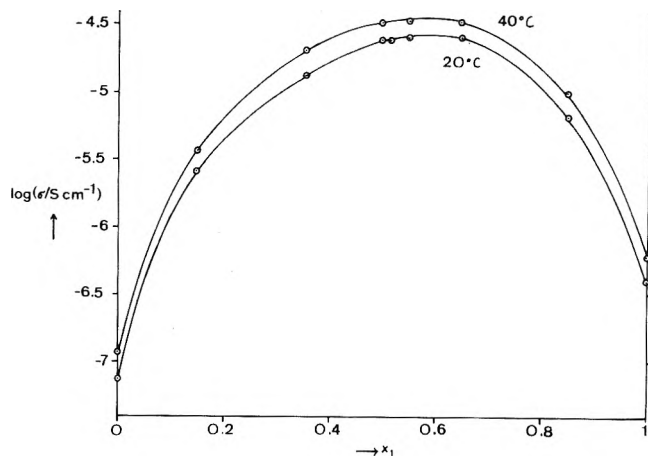


Figure 10. The logarithm (base 10) of the electric conductance of trifluoroacetic acid (1)-acetic acid at 20 and 40°.

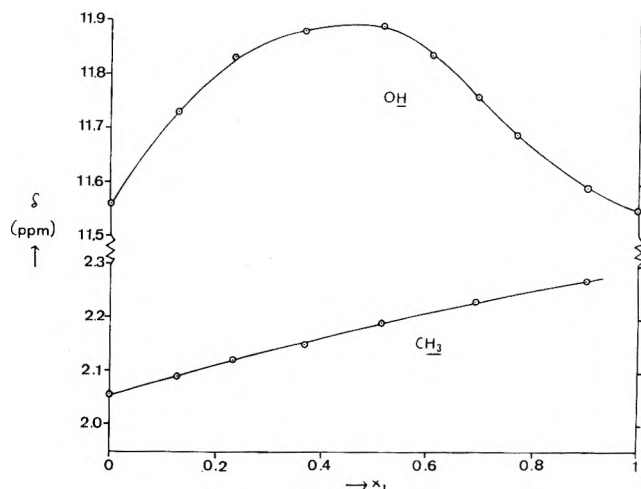


Figure 11. The nmr chemical shift in the system trifluoroacetic acid (1)-acetic acid of the acid protons and the methyl protons in ppm downfield from TMS at 40°.

ter. This would be consistent with the observed increase in electric conductance (Figure 10) and with the increase of $(-\Delta V)$ with increasing temperature.

Finally, the nmr chemical shift of the acid protons in this system is shown in Figure 11. A large downfield chemical shift of the acid protons, *i.e.*, a strong depletion of electrons, occurs at approximately equimolar concentration, where the concentration of heterodimers has its maximum. Furthermore, there is a tendency for protonation of acetic acid with increasing concentration of trifluoroacetic acid, as shown by the chemical shift of the CH_3 protons.¹⁸

Conclusions

The thermodynamic behavior of the system trifluoroacetic acid-carbon tetrachloride, like that of acetic acid-carbon tetrachloride, can be explained by the existence of cyclic dimers of trifluoroacetic acid which are relatively stable in nonpolar solutions but are distorted by the polar monomers and become less stable in the pure acid. The concentration dependence of the dielectric constant indicates the existence of polar aggregates in concentrated solutions and in the pure acid, which may be open dimers and a small (thermodynamically insignificant) fraction of higher chain associates.

The mixing properties of the system trifluoroacetic acid-acetic acid are dominated by the formation of heterodimers from the homodimers. This is confirmed by the existence of a 1:1 solid compound which exhibits a congruent melting point. Evaluation of the formation constant from the melting curve (to be dealt with in a forthcoming paper) indicates a high stability of the heterodimer. This is apparently related to the polarity of the heterodimer, as indicated by the maximum in dielectric constant, electric conductance, downfield chemical shift of the H-bonded protons, and volume contraction at or near an equimolar mixture of the two acids. The polarity of the heterodimers seems to increase with temperature.

Acknowledgment. A grant of the Hochschuljubiläumsstiftung der Stadt Wien and of the Fonds zur Förderung der wissenschaftlichen Forschung (Grant No. 1004) is gratefully acknowledged. We wish to thank Mrs. J. Schuch for help with the density measurements in the system trifluoroacetic acid-carbon tetrachloride.

Supplementary Material Available. Tables giving the experimental data (consolute curves, melting curves, densities, dielectric constants, electric conductivities, chemical shifts) and illustrating the evaluation of the consolute curve of trifluoroacetic acid-carbon tetrachloride will appear following these pages in the microfilm edition of this volume of the journal. Photocopies of the supplementary material from this paper only or microfiche (105 × 148 mm, 24× reduction, negatives) containing all of the supplementary material for the papers in this issue may be obtained from the Journals Department, American Chemical Society, 1155 16th St., N.W., Washington, D. C. 20036. Remit check or money order for \$3.00 for photocopy or \$2.00 for microfiche, referring to code number JPC-74-1709.

References and Notes

- (1) Presented in part at the 161st National Meeting of the American Chemical Society, Los Angeles, Calif., Mar 1971.
- (2) G. Miksch, F. Ratkovic, and F. Kohler, *J. Chem. Thermodyn.*, **1**, 257 (1969).
- (3) H. E. Afsprung, G. H. Findenegg, and F. Kohler, *J. Chem. Soc. A*, 1364 (1968).
- (4) G. Becker and F. Kohler, *Monatsh. Chem.*, **103**, 556 (1972).
- (5) Chain associates have been postulated recently on the basis of nmr chemical shift measurements by M. A. Goldman and M. T. Emerson, *J. Phys. Chem.*, **77**, 2295 (1973). However, their value for the chemical shift of the monomer is in disagreement with J. Jentschura and E. Lippert, *Ber. Bunsenges. Phys. Chem.*, **75**, 556 (1971).
- (6) S. D. Christian, H. E. Afsprung, and C. Ling, *J. Chem. Soc.*, 2378 (1965).
- (7) C. C. Costain and J. P. Srivastava, *J. Chem. Phys.*, **41**, 1620 (1964).
- (8) J. F. Pereira, Ph.D. Thesis, University of Oklahoma, Norman, Okla., 1963.
- (9) R. J. Munn and F. Kohler, *Monatsh. Chem.*, **91**, 381 (1960); E. Liebermann and F. Kohler, *ibid.*, **99**, 2514 (1968).
- (10) F. Kohler, E. Liebermann, G. Miksch, and C. Kainz, *J. Phys. Chem.*, **76**, 2764 (1972).
- (11) G. H. Findenegg and F. Kohler, *Trans. Faraday Soc.*, **63**, 870 (1967).
- (12) For details see M. Bobik, Doctoral Dissertation, University of Vienna, 1973.
- (13) Results given in tabular form will be included as supplementary material (see paragraph at end of paper regarding supplementary material).
- (14) L. A. K. Staveley and A. Gupta, *Trans. Faraday Soc.*, **45**, 50 (1949).
- (15) F. Kohler, *Monatsh. Chem.*, **88**, 388 (1957). An equivalent formulation has been given by A. Neckel, *ibid.*, **92**, 468 (1961).
- (16) F. Kohler, *Monatsh. Chem.*, **100**, 1151 (1969); a maximum of the relative concentration of dimers at relatively low acid concentration follows in acetic acid-carbon tetrachloride and trifluoroacetic acid-nonpolar solvent from nmr chemical shift measurements by E. Lippert, *Ber. Bunsenges. Phys. Chem.*, **67**, 267 (1963), and by U. Jentschura and E. Lippert, ref 5.
- (17) C. Ling, S. D. Christian, H. E. Afsprung, and F. W. Gray, *J. Chem. Soc. A*, 293 (1966); R. E. Kagarise, Naval Research Laboratory Report 4955, Aug 8, 1958; S. D. Christian and T. L. Stevens, *J. Phys. Chem.*, **76**, 2039 (1972).
- (18) It is difficult to make quantitative estimates about the degree of protonation (the degree of ionization of the H bonds in the dimer), because δ_{CH_3} is quite sensitive against solvent effects [U. Jentschura and E. Lippert, *J. Mol. Struct.*, **6**, 93 (1970)]. Complete protonation in "superacids" leads to δ_{CH_3} 3.12-3.18 (ppm downfield from TMS), as given by T. Birchall and R. J. Gillespie, *Can. J. Chem.*, **43**, 1045 (1965), and G. A. Olah and A. M. White, *J. Amer. Chem. Soc.*, **89**, 3591 (1967). But the conformation of this protonated acetic acid monomer is probably different from that of the acetic acid unit in the heterodimer.

Electrochemical Studies and Molecular Energy Levels in Furanquinones

J. E. Kuder,* D. Wychick, R. L. Miller, and M. S. Walker

Webster Research Center, Xerox Corporation, Rochester, New York 14603 (Received March 25, 1974)

Publication costs assisted by Xerox Corporation

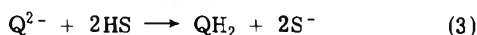
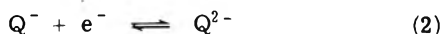
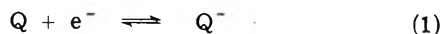
The electrochemical characteristics of dinaphtho[2,1:2',3']furan-8,13-dione (I), dinaphtho[1,2:2',3]furan-7,12-dione (II), and benzo[*b*]naphtho[2,3-*d*]furan-6,11-dione (III) in acetonitrile have been compared to those of naphthoquinone and anthraquinone in the same solvent system. Electron affinities of 1.22, 1.29, and 1.35 eV (relative to a value of 1.5 eV for *p*-benzoquinone) have been calculated from the respective one-electron reduction potentials. An estimate of the electron affinities for I and II from charge transfer spectral data gives values of 1.58 and 1.46, respectively.

Introduction

The electrochemical behavior of quinones in aqueous medium has been known for some time.¹ Under these conditions reduction to the corresponding hydroquinone usu-

ally occurs reversibly as a two-electron two-proton transfer process. The electrochemistry of quinones in nonaqueous solvents has been less extensively studied and differs from the behavior in protic solvents. Thus, in acetonitrile, di-

methylformamide,² or dimethyl sulfoxide,³ the polarograms of quinones typically show two waves corresponding to reversible one-electron transfer processes forming the dianion, which in a slow step may abstract protons from the solvent



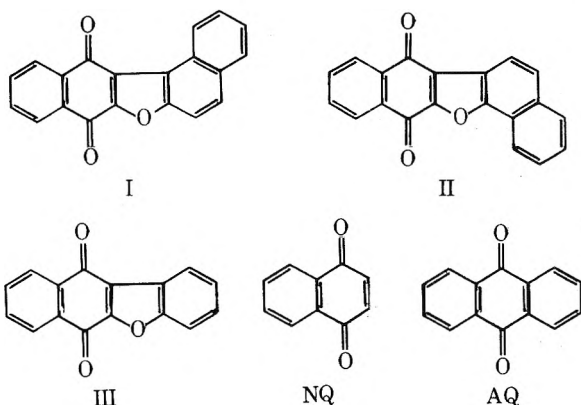
The hydroquinones QH_2 are not electrochemically oxidized in aprotic medium in the potential range of the corresponding quinones.^{2,3}

Peover demonstrated a good correlation, for a series of quinones in acetonitrile, between the electron affinities and the potential of the first polarographic reduction wave.⁴ There are, however, marked deviations due to differing degrees of solvation when the same correlations are attempted using half-wave potentials obtained in protic solvents. Peover also noted the correlation between reduction potentials of quinones and the energy of their lowest empty molecular orbitals,⁴ as well as the relation with the energy of the long wavelength charge transfer band seen in the spectra of quinones in the presence of aromatic hydrocarbon donors.⁵ The interrelationship between the various quantities related to electron affinities has been summarized in a review article by Briegleb.⁶

In previous papers^{7,8} we discussed the relative position and nature of the low-lying excited states of the furanquinones dinaphtho[2,1:2',3']furan-8,15-dione (I) and dinaphtho[1,2:2',3']furan-7,12-dione (II) as determined by their molecular absorption and emission spectra and supported by the results of Hückel molecular orbital calculations. The lowest excited singlet state of these quinones exhibits considerable charge transfer character resulting from the movement of electron density from the naphthalene portion of the molecule to the naphthoquinone moiety. In addition, two electronic transitions localized in the naphthoquinone portion of the molecules can be distinguished.

The charge generation and transport properties of a pyridylcarboxamide derivative of I have recently been reported by Tutihasi,⁹ while photoinjection and photoemission studies by Pfister and Nielsen¹⁰ on this derivative and furanquinone I itself have located the valence, conduction, and vacuum levels of these compounds in the solid state.

In this paper we report the electrochemical behavior of I and II in acetonitrile (AN) in addition to that of the related furanquinone benzo[*b*]naphtho[2,3-*d*]furan-6,11-dione (III) and of 1,4-naphthoquinone (NQ) and 9,10-anthraquinone (AQ). Electron affinities are estimated from



the reversible one-electron reduction potentials and compared to values estimated from the energies of the charge transfer absorption for anthracene-quinone complexes. These energies along with the energies of the highest occupied and lowest unoccupied molecular orbitals calculated using a HMO procedure serve to fix the molecular energy levels of the furanquinones. Finally, an estimate is made of the solid state "band gap" energy for furanquinone I and a comparison made with the measured value recently reported by Pfister and Nielsen.¹⁰

Experimental Section

Materials. The synthesis and purification of furanquinones I and II have been described previously.⁷ Compound III was synthesized¹¹ by the chromic acid oxidation of benzo[*b*]naphtho[2,3-*d*]furan in glacial acetic acid. Recrystallized twice from ethanol and once from benzene, the compound has a mp of 244–245°. 1,4-Naphthoquinone and 9,10-anthraquinone supplied by Eastman Organic were recrystallized from ethanol before use. Acetonitrile (AN) was obtained from Burdick & Jackson, and was dried over 4A molecular sieves and percolated through a 55-cm column of grade I neutral alumina immediately prior to use. Other solvents were Matheson Coleman and Bell Spectro-quality Reagent or Baker G.C. Spectrophotometric Quality Solvent. Tetraethylammonium perchlorate (TEAP), from Southwestern Analytical Chemicals, was dried 16 hr under vacuum before use.

Electrochemistry. Electrochemical data were obtained using a PAR 170 Electrochemistry System in the three-electrode mode. The auxiliary electrode was a platinum wire spiral in a compartment separated from the main cathodic compartment by a glass frit. The reference electrode was silver, silver nitrate (0.1 M), tetraethylammonium perchlorate (0.1 M) in AN. The reference compartment was connected by a glass frit to a salt bridge which terminated in a Luggin capillary located next to the working electrode. The dropping mercury electrode (dme) used had the following characteristics: $m = 1.40 \text{ mg sec}^{-1}$, $t = 3.99 \text{ sec}$ at $h = 80 \text{ cm}$, with an applied voltage of -1.00 V , when immersed in a 0.1 M solution of TEAP in AN. For cyclic voltammetry, a Beckman 39016 mercury drop electrode assembly was used. It was found that irradiation (GE Mazda sun lamp) of compound I in AN for 1 hr resulted in the disappearance of the polarographic wave at -1.6 V , possibly due to photoreduction of the quinone. Because of the photosensitivity, the samples were protected from light and voltammograms were obtained within 20 min of preparing the solutions and following a 5-min purge with purified nitrogen.

Spectroscopy. Ultraviolet and visible absorption spectra were recorded on a Cary 14 spectrophotometer using quartz cells of 1- and 10-cm path length. Solutions were prepared by dissolving the appropriate quinone in carbon tetrachloride to near saturation and then adding anthracene until the charge-transfer absorption band in the spectrum could be resolved. No attempt was made to measure equilibrium constants, etc. The following quinones, (1) methyl-*p*-benzoquinone, (2) *p*-benzoquinone, (3) chlorobenzoquinone, (4) 2,5-dichlorobenzoquinone, and (5) tetrachlorobenzoquinone, having known electron affinities,⁶ were used to determine the correlation between the frequency of the charge transfer band and the quinone electron affinity. The electron affinities of the furanquinones were then estimated from this correlation function.

TABLE I: Electrochemical Data

Compd	$E_{1/2}^a$	Polarography		Cyclic voltammetry ^c		
		$-(E_{3/4} - E_{1/4})$	I_d^b	E_{pc}	E_{pa}	i_{pa}/i_{pc}
I	-1.06	0.09	3.06	-1.09	-0.96	0.95
	-1.64	0.10	2.92	-1.68	-1.53	1.06
II	-1.02	0.08	4.17	-1.05	-0.98	0.92
	-1.60	0.08	2.71	-1.64	-1.57	0.64
III	-1.00	0.06	3.79	-1.06	-0.94	0.97
	-1.52	0.06	3.69	-1.59	-1.47	0.84
NQ	-1.02	0.06	3.45	-1.06	-0.97	1.01
	-1.45	0.06	2.68	-1.47	-1.40	0.84
AQ	-1.29	0.06	3.09	-1.33	-1.23	0.93
	-1.75	0.06	2.99	-1.75	-1.66	0.72

^a Volts vs. Ag|Ag⁺ (0.1 M). ^b $I_d = i_d/Cm^{2/3}t^{1/6}$. ^c At hmde (1- μ l drop), sweep rate 0.2 V sec⁻¹.

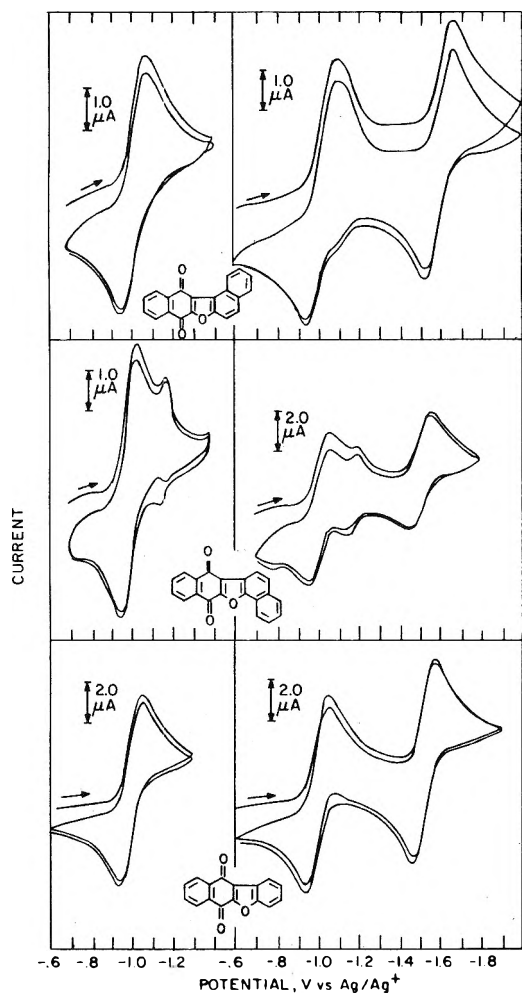


Figure 1. Cyclic voltammograms of furanquinones I, II, and III in AN. Sweep rate 0.2 V/sec: left figure, first reduction; right figure, both reductions.

Results and Discussion

Electrochemistry. The polarograms of the quinones studied here show two reduction waves of approximately equal height and separated by 0.4–0.6 V. The numerical data obtained from these curves are summarized in Table I. The values of the first reduction potentials of NQ and AQ are in good agreement with those reported by Peover⁴ and by Chatterjee¹² for these compounds when the difference of +0.337 V¹³ between the Ag|Ag⁺ reference electrode used here and the aqueous sce employed by these workers is noted. However, the second wave on NQ is found 0.1 V less cathodic and that of AQ 0.2 V less ca-

thodic than the values reported by Peover.⁴ The furanquinones I–III have their first reduction potentials located within 50 mV of the value observed for NQ. In addition, the values of the diffusion current constants I_d are in agreement with the values observed for NQ and AQ corresponding to a one-electron reduction. Our value of I_d for NQ (3.45), while higher than the value reported by Peover⁴ ($I_d = 1.71$), is in good agreement with the value reported by Chatterjee¹² ($I_d = 3.37$) and not unreasonable for a one-electron transfer in AN solution.¹⁴

The slope of a polarographic wave may be expressed by $E_{3/4} - E_{1/4}$ and is equal to $-0.0564/n$ V for a reversible process.¹⁵ As seen in Table I, the values of $E_{3/4} - E_{1/4}$ are in satisfactory agreement with the criterion for one-electron reversible processes for III, NQ, and AQ, while the values for I and II show a substantially larger deviation.

The current-potential curves obtained with the hanging mercury drop electrode are presented in Figures 1 and 2. By this technique the two reduction processes are readily seen to be reversible. The peak potentials for the cathodic and anodic directions, E_{pc} and E_{pa} , respectively, are given in Table I. Their separation is of the order expected for a reversible or quasireversible charge transfer.¹⁶ The peak current ratio i_{pa}/i_{pc} is close to unity as expected for a reversible process.¹⁶ In the cyclic voltammogram of compound II there is observed following the first cathodic peak a smaller peak at -1.18 V with a corresponding peak located at -1.16 V on reversal of the sweep direction. These peaks are still observed after an additional crystallization and sublimation of the compound, but are absent if the hmde is replaced by a stationary platinum electrode. The i - E curve is characteristic of that expected¹⁷ in cases of adsorption of reactant molecules to the electrode, as is also the lower peak current ratio i_{pa}/i_{pc} as compared to the value observed for the other quinones. There is the suggestion of adsorption peaks seen in the CV curve of I, but not in that of III. The decreasing adsorption at the hmde in the order II > I > III may be related to the qualitative observation that their solubility increases in the same order.

The reversible one-electron reduction potentials for the furanquinones may now be used to obtain an estimate of their respective gas-phase electron affinities. According to Briegleb⁶ this relationship is expressed by

$$EA = E_{1/2} + 1.41 \quad (4)$$

where the value of $E_{1/2}$ is with respect to the sce and on which scale chloranil has EA = 1.37 eV. Making the appropriate substitutions we obtain electron affinities of 0.68, 0.72, and 0.75 eV for furanquinones I, II, and III, respectively.

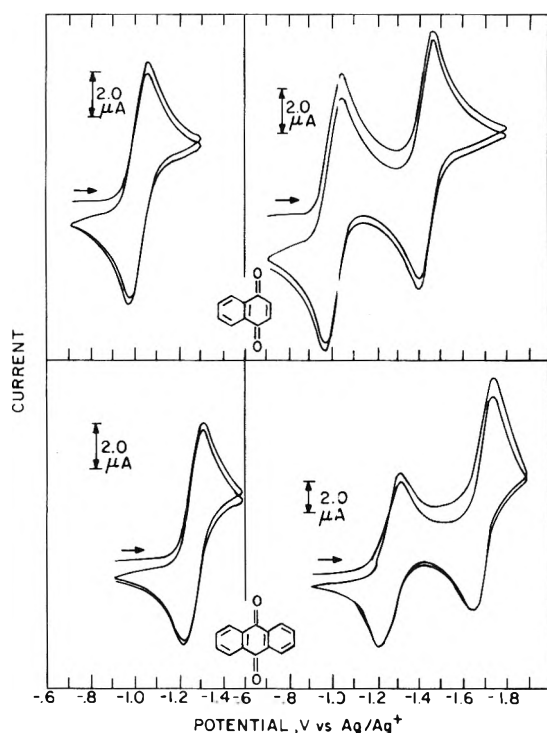


Figure 2. Cyclic voltammograms of 1,4-naphthoquinone and 9,10-anthraquinone in AN. Sweep rate 0.2 V/sec; left figure, first reduction; right figure, both reductions.

Charge Transfer Spectra. The frequency of a charge-transfer absorption band (ν_{CT}) is given by¹⁸

$$h\nu_{CT} = IP - EA - \frac{e^2}{\tau} - \Delta \quad (5)$$

where IP and EA are the gas-phase ionization potential and electron affinity of the donor and acceptor, respectively, e^2/τ is the coulombic interaction between the two, and Δ represents all other intermolecular forces. In practice, the electron affinity for an unknown acceptor may be determined by observing the variation of ν_{CT} with EA for a series of similar complexes, the third and fourth terms in the equation being considered constant for such a series. This approach to estimating electron affinities has been discussed by Briegleb.⁶ For the present study, anthracene (IP = 7.4 eV) was chosen as donor and charge transfer frequencies were obtained from the spectra of concentrated solutions, in carbon tetrachloride, of anthracene with a series of quinones of known electron affinities.⁶ The variation of ν_{CT} with acceptor electron affinity for this series of anthracene-quinone complexes, shown in Figure 3, gives the following correlation function

$$\nu_{CT} = 27.4 \times 10^3 - 8.3 \times 10^3 EA \text{ cm}^{-1} \quad (6)$$

The measured frequencies for the anthracene-quinone-I and anthracene-quinone-II charge transfer absorption bands are 20,100 and 21,200 cm^{-1} , respectively. Substitution of these values into the correlation function leads to values of 0.88 and 0.75 eV for the electron affinities of I and II, respectively, again referenced to a value of 1.37 eV for chloranil. We were unable to observe CT absorption with III, possibly due to a low value for the equilibrium constant for the anthracene-III complex.

Recently Page and Farragher¹⁹ have measured, by the magnetron technique, an absolute gas-phase electron affinity of 1.5 eV for *p*-benzoquinone. With respect to this value, absolute values for I and II as estimated from the

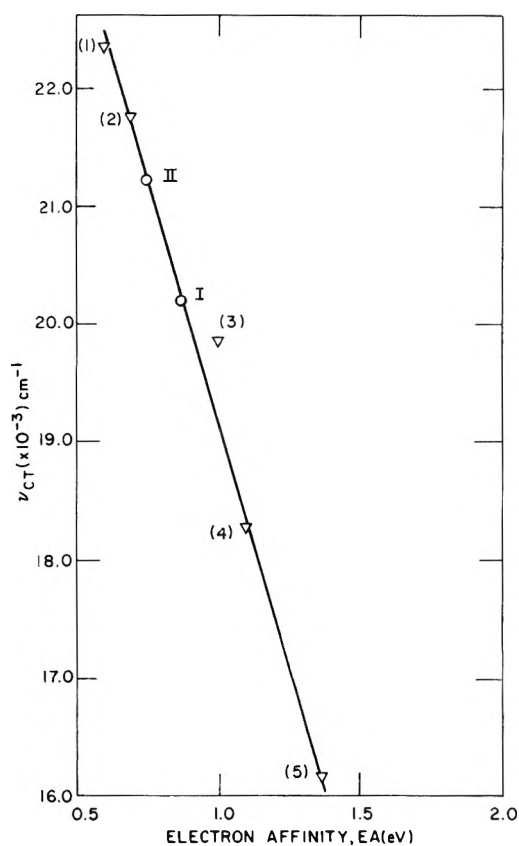


Figure 3. Charge transfer maxima vs. electron affinity for quinones in CCl_4 with anthracene donor. See Experimental Section for compounds identified by numbers in parentheses.

TABLE II: Summary of Electron Affinities and Ionization Potentials Calculated for Furanquinones I, II, and III

Compd	EA_g^a		IP_g (HMO)	IP_c (PE)
	$E_{1/2}$	$h\nu_{CT}$		
I	1.22	1.58	8.10	(6.54) ^b
II	1.29	1.46	8.20	
III	1.35		8.64	

^a Relative to *p*-benzoquinone, ref 19. ^b Data for substituted derivative, ref 21. Pfiester and Nielsen subsequently reported a similar value for I (ref 10).

charge transfer energies are 1.58 and 1.46 eV, respectively. Similarly, electron affinities estimated from the one-electron reduction potentials when referenced to the absolute value for *p*-benzoquinone are 1.22, 1.29, and 1.35 eV for I, II, and III, respectively.

These electron affinity values (see Table II) estimated by the two differing techniques are in reasonable agreement, considering the experimental uncertainties involved.

HMO Calculations. In our earlier reports^{7,8} on furanquinones I and II, the results of HMO calculations were used to correlate the spectroscopic data. In Table III are presented the energies (E) in β units of the highest occupied MO (HOMO) and lowest unoccupied MO (LUMO) of the quinones studied here. For the furanquinones the values of E_{LUMO} are essentially the same and examination of the corresponding eigenvectors reveals that the LUMO is almost completely localized on the naphthoquinone portion of the molecule. The exact values of E_{LUMO} are somewhat dependent on the input parameters chosen for

TABLE III: Energies (β Units) of the Highest Occupied and Lowest Unoccupied Molecular Orbitals^a

Compd	E_{HOMO}	E_{LUMO}
I	0.594	-0.045
II	0.624	-0.046
III	0.764	-0.039
NQ	0.985	-0.004
AQ	0.984	-0.103

^a Parameters used are those quoted in ref 7.

the furan oxygen atoms, and perfect agreement between theory and experiment is not expected. The HMO results indicate that among the furanquinones the order of electron affinities should be III > I > II, which at least for the latter two quinones is in agreement with the values calculated from the CT spectra, while from the electrochemical data the ordering is III > II > I.

The energies calculated for the HOMO's of the furanquinones are insensitive to choice of heteroatom parameters as these orbitals are essentially localized on the hydrocarbon moieties distant from the quinone portion. Under these circumstances it should be possible to apply the linear relationship obtained by Streitwieser²⁰ between ionization potential (IP) and E_{HOMO} for a series of aromatic hydrocarbons

$$\text{IP} = 3.14E_{\text{HOMO}} + 6.24 \text{ eV} \quad (7)$$

Application of this equation to the three furanquinones leads to values of gas-phase ionization potentials of 8.10, 8.20, and 8.64 eV for I, II, and III, respectively (Table II).

The differences in orbital energies ($E_{\text{LUMO}} - E_{\text{HOMO}}$) should be related to the energy of the long wavelength absorption maxima for I-III. The HMO calculations predict these should be in the order I (0.639 β), II (0.670 β), III (0.803 β). This is in agreement with the observed order of the long wavelength maxima measured in hexane, *i.e.*, I (23,300 cm^{-1}), II (24,000 cm^{-1}), and III (26,300 cm^{-1}),⁷ respectively. As previously described for I and II,^{7,8} the lowest energy $\pi-\pi^*$ transition for III also involves a movement of electron density from the benzenoid to the quinoid side of the molecule. This calculated increase in dipole moment upon excitation is in accord with the qualitative observation that the long wavelength absorption of III shifts to lower energies in dioxane or 1,2-dichloroethane.

Comparison with Solid State Data. Pfister and Nielsen¹⁰ have recently reported the energies of the valence, conduction, and vacuum levels for furanquinone I in the solid state. It is of interest therefore to estimate, using the molecular energies reported here, the energy separation of the valence and conduction bands in I and compare it to the experimentally measured value.¹⁰ To a first approximation the energies of the conduction and valence bands in an organic crystal correspond to the electron affinity (EA_c) and ionization potential (IP_c) of that crystal, respectively, with

$$EA_c = EA_g + P \quad (8)$$

and

$$IP_c = IP_g - P \quad (9)$$

where subscripts c and g refer to crystal and gas phases, respectively, and P is the crystal polarization.

The band gap energy for the crystal ΔE is then given by

$$\Delta E = IP_c - EA_c = 2IP_c - EA_g - IP_g \quad (10)$$

Leiga has measured a value of 6.54 eV for the crystal ionization potential (IP_c)²¹ of a 6-(2-pyridyl)carboxamide derivative of I, using the photoemission technique. A similar value is expected for the unsubstituted molecule due to the minor perturbation of such groups in the energy levels of this molecule.²² Substitution of the respective values for IP_c , IP_g , and EA_g from Table II into eq 10 gives a value of 3.40 eV for ΔE . This value is in excellent agreement with the value of 3.55 ± 0.13 eV reported by Pfister and Nielsen.¹⁰

Summary

The electrochemical behavior of the furanquinones is similar to that of quinones in general, the reduction potentials being close to that for naphthoquinone. Electron affinities estimated from the polarographic data are in good agreement with those obtained from charge transfer spectral studies. Finally, an estimate of the solid state "band gap energy" for furanquinone I is in excellent agreement with the experimental value reported by Pfister and Nielsen.

Acknowledgments. The authors thank Dr. A. Leiga for permission to use his photoemission data and Dr. F. Saeva for helpful discussions during the course of this work.

References and Notes

1. I. M. Kolthoff and J. J. Lingane, "Polarography," 2nd ed. Interscience, New York, N. Y., 1952, pp 699 ff.
2. S. Wawzonek, R. Berkey, E. W. Blaha, and M. E. Runner, *J. Electrochem. Soc.*, **103**, 456 (1956).
3. I. M. Kolthoff and T. B. Reddy, *J. Electrochem. Soc.*, **108**, 980 (1961).
4. M. E. Peover, *J. Chem. Soc.*, 4540 (1962).
5. M. E. Peover, *Trans. Faraday Soc.*, **58**, 1656 (1962).
6. G. Briegleb, *Angew. Chem., Int. Ed. Engl.*, **3**, 617 (1964).
7. M. S. Walker, J. E. Kuder, and R. L. Miller, *J. Phys. Chem.*, **75**, 3257 (1971).
8. M. S. Walker, R. L. Miller, and J. E. Kuder, *J. Phys. Chem.*, **76**, 2240 (1972).
9. S. Tutihasi, *J. Appl. Phys.*, **43**, 3097 (1972).
10. G. Pfister and P. Nielsen, *J. Appl. Phys.*, **43**, 3104 (1972).
11. J. N. Chatterjee, *J. Indian Chem. Soc.*, **31**, 101 (1954).
12. S. Chatterjee, *J. Chem. Soc. B*, 2194 (1971).
13. R. C. Larson, R. T. Iwamoto, and R. N. Adams, *Anal. Chim. Acta*, **25**, 371 (1961).
14. If a typical value of I_d is 1.5 n for polarography in aqueous solution (viscosity 1.01 cP), then for acetonitrile (viscosity 0.345 cP) a reasonable value of I_d would be 2.6 n.
15. L. Meites, "Polarographic Techniques," 2nd ed. Wiley-Interscience, New York, N. Y., 1965: (a) pp 165-168; (b) pp 224-228.
16. R. S. Nicholson and I. Shain, *Anal. Chem.*, **36**, 706 (1964).
17. R. H. Wopschall and I. Shain, *Anal. Chem.*, **39**, 1514 (1967).
18. R. S. Mulliken, *J. Amer. Chem. Soc.*, **72**, 600 (1950).
19. A. L. Farragher and F. M. Page, *Trans. Faraday Soc.*, **62**, 3072 (1966).
20. A. Streitwieser, Jr., "Molecular Orbital Theory for Organic Chemists," Wiley, New York, N. Y., 1962, Chapter 7.
21. A. Leiga, private communication.
22. M. S. Walker, J. Kuder, and R. Gruber, to be submitted for publication.

Hydrophobic Interactions in Mixtures of *N,N*-Dimethylformamide and Water. Model Calculations and Enthalpies of Solution

C. de Visser and G. Somsen*

Department of Chemistry, Free University of Amsterdam, de Lairesestraat 174, Amsterdam, The Netherlands (Received April 8, 1974)

Publication costs assisted by Chemical Laboratory of the Free University of Amsterdam

Enthalpies of solution of tetra-*n*-propylammonium bromide in mixtures of *N,N*-dimethylformamide and water are added to those previously measured for tetra-*n*-butylammonium bromide. The results are considered as being the consequence of two effects: one that would appear if the tetraalkylammonium ions did not show a hydrophobic interaction with water in DMF-water systems and one due to the enthalpic effect of a hydrophobic interaction. Using a simple hydration approach it is possible to calculate the number of water molecules which surround a hydrophobic alkyl group and the enthalpic effect correlated with the corresponding interactions. Moreover, the calculations fit the experimental enthalpies of solution reasonably well. The same procedure is also applied to literature values of the enthalpies of solution of tetra-*n*-butylammonium bromide in aqueous mixtures of dimethyl sulfoxide. The results are in surprisingly good agreement with the corresponding ones obtained from the present investigation.

I. Introduction

At the present the more exothermic enthalpies of solution of the larger tetraalkylammonium halides in water, as compared with those of the corresponding alkali salts, are generally¹ attributed to an enhanced hydrogen bonding in water in the vicinity of the tetraalkylammonium ions (hydrophobic interactions). This idea is substantiated by the absence of this effect in solvents such as *N,N*-dimethylformamide (DMF) where significant hydrogen bonding is not present.²⁻⁴ Moreover, it has been shown that also in *N*-methylformamide (NMF) and *N*-methylacetamide (NMA) tetraalkylammonium ions do not exhibit enthalpic effects due to "solvophobic interactions."^{5,6}

In a recent paper⁷ we reported the enthalpies of solution of tetra-*n*-butylammonium bromide (*n*-Bu₄NBr) in binary mixtures of water, formamide, NMF, and DMF. From this study it appeared that in the systems formamide-NMF and NMF-DMF the enthalpies of solution of *n*-Bu₄NBr are intermediate between those in the pure solvents and proportional to the solvent composition. However, in the amide-water mixtures the behavior is quite different and we suggested that the enthalpies of solution-composition profiles of *n*-Bu₄NBr in these systems are determined by the hydrophobic interaction of *n*-Bu₄NBr in water and in the aqueous binaries.

The effect of a cosolvent on the enthalpies of dilution of hydrophobic species has been investigated by Mastroianni, Pikal, and Lindenbaum.⁸ With the aid of a statistical model these authors explained the experimental results very well. Their model assumes that the hydrophobic effect is present when a number of water molecules cooperate in forming a hydrogen-bonded cage around the hydrophobic particles, while one or more cosolvent molecules in the hydration envelope will prevent such a formation. It will be clear that structural effects of the hydrophobic solute in the cosolvent must be absent. In this connection DMF should be an appropriate cosolvent.

In the present paper we will discuss enthalpies of solution of tetra-*n*-propylammonium bromide (*n*-Pr₄NBr) and *n*-Bu₄NBr in mixtures of DMF and water. It will be shown

that the magnitudes of the enthalpies of solution in these mixtures are the result of two effects. The first accounts for the endothermic shift of the enthalpies of solution on going from DMF to water which occurs when hydrophobic effects are absent⁴ and the second takes care of the influence of hydrophobic hydration in both pure water and the aqueous mixtures. The enthalpic effect of the hydrophobic hydration of *n*-Pr₄NBr and *n*-Bu₄NBr in pure water, which has been estimated previously,⁶ can be evaluated more precisely by comparison of several enthalpies of transfer. The hydrophobic effect in the DMF-water mixtures can be deduced by means of the cooperative model of Mastroianni, Pikal, and Lindenbaum.⁸

II. Experimental and Results

The solvent *N,N*-dimethylformamide (Baker Analyzed Reagent) and the salts *n*-Pr₄NBr and *n*-Bu₄NBr (Fluka Purum) were purified as described earlier.^{4,6} All solvent mixtures were prepared under nitrogen by weight.

Enthalpies of solution were measured with an LKB 8700-1 precision calorimetry system; the experimental procedure has been reported previously.⁶ A test of the calorimeter by measuring the enthalpy of solution of THAM (tris(hydroxymethyl)aminomethane) in 0.1 *M* aqueous HCl yielded from eight independent measurements, a mean enthalpy of solution of -29.724 ± 0.010 kJ mol⁻¹ (the uncertainty is twice the standard deviation of the mean). This value is in fair agreement with literature data as reviewed by Prosen and Kilday.⁹

Since the molalities in the aqueous mixtures (0.02-0.001 mol kg⁻¹) were close to infinite dilution, any small dependence of the enthalpies of solution on molality is within the experimental error. Consequently, the enthalpy of solution at infinite dilution $\Delta H^\circ(\text{sol})$ was taken to be the average of three or more independent observations agreeing within 150 J mol⁻¹. The final results for *n*-Pr₄NBr and for *n*-Bu₄NBr (which has been reported already in another context⁷) and their mean deviation as a function of the mole fraction of water are listed in Table I. The enthalpies of solution in pure DMF were taken from literature.⁴

TABLE I: Enthalpies of Solution $\Delta H^\circ(\text{sol})$ in kJ mol^{-1} of $n\text{-Pr}_4\text{NBr}$ and $n\text{-Bu}_4\text{NBr}$ in N,N -Dimethylformamide-Water Mixtures at 25°

$n\text{-Pr}_4\text{NBr}$		$n\text{-Bu}_4\text{NBr}$	
$X_{\text{H}_2\text{O}}$	$\Delta H^\circ(\text{sol})$	$X_{\text{H}_2\text{O}}$	$\Delta H^\circ(\text{sol})$
0	9.9	0	12.5
0.143	13.64 ± 0.02	0.192	18.48 ± 0.05
0.309	17.20 ± 0.05	0.311	22.07 ± 0.05
0.494	20.28 ± 0.01	0.488	27.12 ± 0.04
0.600	20.65 ± 0.01	0.623	29.63 ± 0.05
0.705	18.92 ± 0.02	0.695	29.77 ± 0.04
0.865	9.87 ± 0.03	0.760	27.89 ± 0.03
1	-4.25 ± 0.05	0.869	18.21 ± 0.06
		0.945	5.26 ± 0.02
		1	-8.58 ± 0.06

III. Discussion

The enthalpies of solution of $n\text{-Bu}_4\text{NBr}$ in mixtures of NMF and DMF are almost proportional to the solvent composition⁷ and may be regarded as close to ideal.¹⁰ This implies that the structure of the solvent mixtures changes gradually from one pure component to the other. The enthalpies of solution of $n\text{-Pr}_4\text{NBr}$ and $n\text{-Bu}_4\text{NBr}$ in DMF- H_2O mixtures do not display this behavior, but reach a maximum value. In view of this different behavior in NMF-DMF and in DMF- H_2O mixtures, the path of the enthalpies of solution in the latter system may be conceived as the result of two effects.

(a) When the hydrophobic interaction between tetraalkylammonium ions and water or aqueous DMF is absent, the enthalpies of solution in the mixtures $\Delta H'(M)$ could be written, analogous to the NMF-DMF mixtures, as

$$\Delta H'(M) = X_{\text{H}_2\text{O}}\Delta H'(\text{H}_2\text{O}) + (1 - X_{\text{H}_2\text{O}})\Delta H^\circ(\text{DMF}) \quad (1)$$

In this equation $\Delta H'(\text{H}_2\text{O})$ represents the enthalpy of solution in water in the absence of hydrophobic interaction.

(b) In addition to this ideal behavior allowance must be made for the enthalpic effects of hydrophobic interaction in water, $\text{Hb}(\text{H}_2\text{O})$, and in the mixtures of DMF and water, $\text{Hb}(M)$, so that the enthalpy of solution in pure water can be written as

$$\Delta H^\circ(\text{H}_2\text{O}) = \Delta H'(\text{H}_2\text{O}) + \text{Hb}(\text{H}_2\text{O}) \quad (2)$$

while the overall enthalpy of solution in a mixture of DMF and H_2O is given by

$$\Delta H^\circ(M) = \Delta H'(M) + \text{Hb}(M) \quad (3)$$

Consequently $\Delta H^\circ(M)$ can be calculated from experimental values of $\Delta H^\circ(\text{H}_2\text{O})$ and $\Delta H^\circ(\text{DMF})$ if $\text{Hb}(\text{H}_2\text{O})$ and $\text{Hb}(M)$ are known. The evaluation of these quantities will be discussed in order.

1. *The Enthalpic Effect of Hydrophobic Interaction in Pure Water, $\text{Hb}(\text{H}_2\text{O})$.* The enthalpies of transfer of both alkali bromides and tetraalkylammonium bromides from NMF and NMA to DMF are virtually constant.⁴ From water to DMF this still applies to the alkali bromides, but the transfer enthalpies of $n\text{-Pr}_4\text{NBr}$ and $n\text{-Bu}_4\text{NBr}$ deviate substantially. If this difference may be attributed to hydrophobic interaction, the corresponding enthalpic effect for $n\text{-Pr}_4\text{NBr}$ and $n\text{-Bu}_4\text{NBr}$ in water is of the order of magnitude of -50 kJ mol^{-1} .

In order to quantify this effect better, recently⁶ we have compared the enthalpies of solvation of alkali and tetraalkylammonium bromides in, among others, NMF, NMA, and

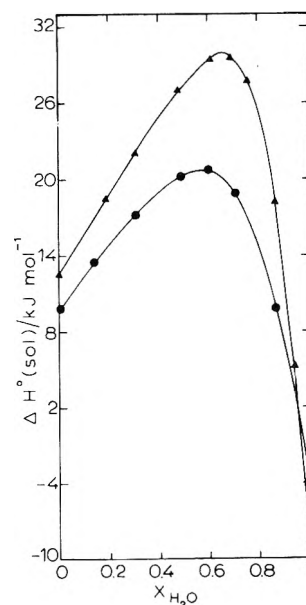


Figure 1. Enthalpies of solution $\Delta H^\circ(\text{sol})$ in mixtures of N,N -dimethylformamide and water as a function of the mole fraction of water: ●, $n\text{-Pr}_4\text{NBr}$; ▲, $n\text{-Bu}_4\text{NBr}$.

water with those in propylene carbonate (PC) as a reference solvent. This procedure yielded enthalpic effects of hydrophobic interactions in water which amount for $n\text{-Pr}_4\text{N}^+$ to -59 , and for $n\text{-Bu}_4\text{N}^+$ to -67 kJ mol^{-1} . However, these values carry large uncertainties (estimated at $\pm 20 \text{ kJ mol}^{-1}$) since the enthalpies of solvation of the salts in water and in PC are both dominated by the same large and rather uncertain lattice enthalpies.

These difficulties can be circumvented by applying the same procedure to enthalpies of transfer,¹¹ ΔH_{tr} . If in two solvents A and B all enthalpies of solvation of salts MBr are linear to the corresponding ones in PC, it can be shown that

$$\Delta H_{\text{tr}}(\text{MBr}, \text{A} \rightarrow \text{PC}) =$$

$$P + Q\Delta H_{\text{tr}}(\text{MBr}, \text{B} \rightarrow \text{PC}) \quad (4)$$

in which P and Q are constants. Equation 4 only involves enthalpies of transfer which do not contain lattice enthalpies and hence are intrinsically of greater absolute accuracy. In Figure 2 eq 4 has been visualized, B being NMF and A NMA, DMF, or water. As this figure shows, the data for A = NMA or DMF are in fair accordance with eq 4. So in these solvents the conclusions drawn before that tetraalkylammonium ions behave like large alkali ions and do not display "solvophobic interactions" are substantiated.

For A = H_2O the tetraalkylammonium bromides plot deviates strongly from the linear dependence of the alkali bromides. As in the procedure with the enthalpies of solvation,⁶ we attribute these deviations to the enthalpic effects of hydrophobic interactions. For $n\text{-Pr}_4\text{NBr}$ this effect amounts to $-50 \pm 6 \text{ kJ mol}^{-1}$, while for $n\text{-Bu}_4\text{NBr}$ it is $-55 \pm 6 \text{ kJ mol}^{-1}$. The quoted uncertainties are obtained from a least-squares technique. We shall use these values as being the enthalpic effect of hydrophobic interaction, $\text{Hb}(\text{H}_2\text{O})$, of $n\text{-Pr}_4\text{NBr}$ and $n\text{-Bu}_4\text{NBr}$ in pure water.

Figure 2 shows also that the enthalpies of transfer from any solvent to PC for all alkali ions obey a linear relationship with respect to the corresponding enthalpies of transfer from NMF to PC. Apparently, the different structural influences¹² of alkali ions in water (Li^+ and Na^+ being hy-

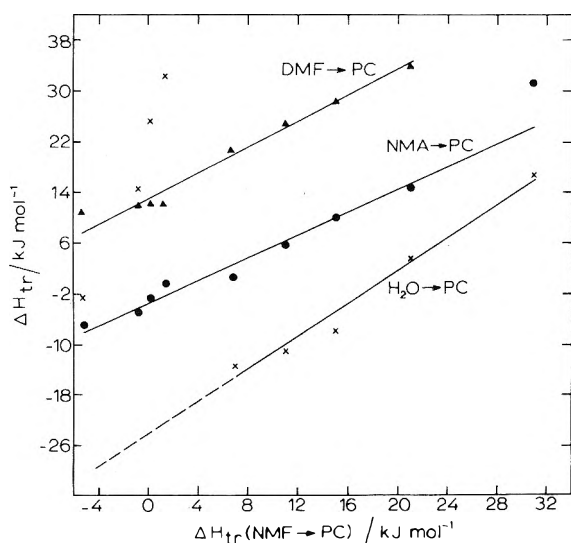


Figure 2. Enthalpies of transfer ΔH_{tr} from DMF, NMA, and H₂O to PC with respect to $\Delta H_{tr}(\text{NMF} \rightarrow \text{PC})$. From left to right values are given for Me₄N⁻, Et₄N⁻, *n*-Pr₄N⁻, *n*-Bu₄N⁻, Cs⁻, Rb⁻, K⁻, Na⁻, and LiBr.

drophilic structure makers, the other univalent alkali ions hydrophilic structure breakers) are not reflected by corresponding differences in the enthalpies of transfer and consequently purely entropic in origin.

2. *The Enthalpic Effect of Hydrophobic Interaction in the Aqueous DMF Mixtures, H_b(M).* Values of H_b(M) with increasing mole fraction of water can be calculated using the model of Mastroianni, Pikal, and Lindenbaum.⁸ Then the following assumptions must be employed.

(a) In aqueous solution a large tetraalkylammonium ion is surrounded by a cage of *N* water molecules and each alkyl group is surrounded by a subcage of *N*/4 water molecules.

(b) In a mixture of DMF and water, the distribution of solvent molecules surrounding the ion is random so that the probability of a given solvation site being occupied by a water molecule is $X_{\text{H}_2\text{O}}$.

(c) The presence of one or more DMF molecules at a solvation site of an alkyl group will prevent the formation of a subcage around this group but will not affect the structures of the subcages around the other alkyl groups.

(d) The enthalpic effect of hydrophobic interaction in DMF-water mixtures is merely the result of subcage formation around large alkyl groups. Each hydrophobic hydrated alkyl group contributes $\frac{1}{4} \text{H}_b(\text{H}_2\text{O})$.

As a result of assumption b the probability of *N*/4 sites being occupied by water molecules is $X^{N/4}$, if *X* is the mole fraction of water. Using assumption d the enthalpic contribution per mole of alkyl groups is given by $X^{N/4} \cdot \frac{1}{4} \text{H}_b(\text{H}_2\text{O})$. Consequently, the contribution with regard to 1 mol of R₄NBr amounts to

$$\text{H}_b(\text{M}) = X^{N/4} \text{H}_b(\text{H}_2\text{O}) \quad (5)$$

Exactly the same equation can be derived using the procedure of Mastroianni, Pikal, and Lindenbaum,⁸ *i.e.*

$$\text{H}_b(\text{M}) = \sum_{i=1}^4 P_i \frac{i}{4} \text{H}_b(\text{H}_2\text{O})$$

where

$$P_i = \binom{4}{i} (X^{N/4})^i (1 - X^{N/4})^{4-i}$$

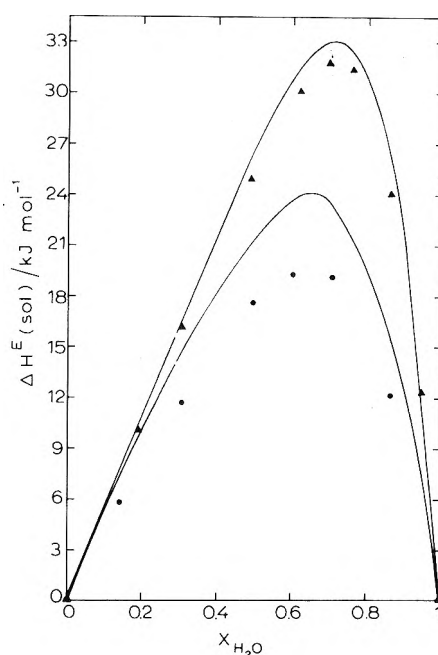


Figure 3. Excess enthalpies of solution $\Delta H^E(\text{sol})$ in mixtures of *N,N*-dimethylformamide and water as a function of the mole fraction of water. The experimental results for *n*-Pr₄NBr are given by ●, those for *n*-Bu₄NBr by ▲.

3. *Comparison with Experimental Data.* Combination of eq 3 with eq 1, 2, and 5 yields for the enthalpy of solution in a mixture of DMF and water

$$\Delta H^\circ(\text{M}) = X\{\Delta H^\circ(\text{H}_2\text{O}) - \text{H}_b(\text{H}_2\text{O})\} + (1 - X)\Delta H^\circ(\text{DMF}) + X^{N/4}\text{H}_b(\text{H}_2\text{O}) \quad (6)$$

Consequently, the excess enthalpy of solution in the mixture, $\Delta H^E(\text{M})$ is given by

$$\Delta H^E(\text{M}) = \Delta H^\circ(\text{M}) - \{X\Delta H^\circ(\text{H}_2\text{O}) + (1 - X)\Delta H^\circ(\text{DMF})\} = (X^{N/4} - X)\text{H}_b(\text{H}_2\text{O}) \quad (7)$$

Equation 7 can be checked using the values derived above of H_b(H₂O): for *n*-Pr₄NBr -50 kJ mol^{-1} and for *n*-Bu₄NBr -55 kJ mol^{-1} . The value of *N* can be evaluated from the mole fraction of water where $\Delta H^E(\text{M})$ reaches an extreme (maximum)

$$-\left(\frac{N}{4} - 1\right) \log X_{\text{max}} = \log \frac{N}{4} \quad (8)$$

For *n*-Pr₄NBr in DMF-H₂O this mole fraction is 0.63 and, consequently, *N* = 16. For *n*-Bu₄NBr the corresponding values are $X_{\text{max}} = 0.71$ and *N* = 26. The latter value is in good agreement with the value derived by Mastroianni, Pikal, and Lindenbaum (*N* = 24). It is interesting to note that solid hydrates of *n*-Bu₄NBr contain clathrate-like structures in which the *n*-Bu₄N⁺ ion is surrounded by about 32 water molecules.¹

Using eq 7 and with the aid of the derived values of H_b(H₂O) and *N*, $\Delta H^E(\text{M})$ of *n*-Pr₄NBr and *n*-Bu₄NBr in DMF-H₂O has been calculated as a function of the mole fraction of water. The results are visualized in Figure 3 (drawn line). Especially for *n*-Bu₄NBr the theoretical results are in good agreement with the experimental data.

Another approach can be applied by subjecting eq 7 to a curve-fitting program in order to search for the best fit of the experimental data by optimizing both parameters

TABLE II: Best Fit of the Experimental Excess Enthalpies of Solution in kJ mol^{-1} of $n\text{-Pr}_4\text{NBr}$ and $n\text{-Bu}_4\text{NBr}$ in DMF- H_2O Mixtures Using Eq 7 by Optimizing the Parameters N and $\text{Hb}(\text{H}_2\text{O})$

$X_{\text{H}_2\text{O}}$	$n\text{-Pr}_4\text{NBr}^a$		$n\text{-Bu}_4\text{NBr}^b$		ΔH^E_{calc}
	$\Delta H^E(\text{obsd})$	$\Delta H^E(\text{calcd})$	$X_{\text{H}_2\text{O}}$	$\Delta H^E(\text{obsd})$	
0	0	0	0	0	0
0.143	5.76	5.66	0.192	10.03	10.14
0.309	11.67	11.95	0.311	16.13	16.39
0.494	17.37	17.47	0.488	24.91	25.22
0.600	19.24	19.05	0.623	30.26	30.31
0.705	18.99	18.68	0.695	31.92	31.51
0.865	12.21	12.60	0.760	31.41	30.95
1	0	0	0.869	24.03	24.32
			0.945	12.68	13.09
			1	0	0

^a $N = 16.8$, $\text{Hb}(\text{H}_2\text{O}) = -39.6 \text{ kJ mol}^{-1}$. ^b $N = 25.6$, $\text{Hb}(\text{H}_2\text{O}) = -52.8 \text{ kJ mol}^{-1}$.

$\text{Hb}(\text{H}_2\text{O})$ and N . These calculations were performed on an IBM-1130 computing system using a general curve-fitting program¹³ ROFIT. The results are given in Table II. The mean deviations of $\Delta H^E(\text{calcd})$ from $\Delta H^E(\text{obsd})$ are for $n\text{-Pr}_4\text{NBr}$ 172 J mol^{-1} and for $n\text{-Bu}_4\text{NBr}$ 229 J mol^{-1} . Therefore, we can conclude that, using the values of N and $\text{Hb}(\text{H}_2\text{O})$ given in Table II, the fit is very good. Also the values of N agree with those derived from eq 8 by taking the enthalpic effect of hydrophobic interaction in water as being known. The best fit value of $\text{Hb}(\text{H}_2\text{O})$ for $n\text{-Pr}_4\text{NBr}$ ($-39.6 \text{ kJ mol}^{-1}$) is out of the limits derived in section III.1 ($-50 \pm 6 \text{ kJ mol}^{-1}$); the value of $\text{Hb}(\text{H}_2\text{O})$ for $n\text{-Bu}_4\text{NBr}$ given in Table II ($-52.8 \text{ kJ mol}^{-1}$) is in excellent agreement with the value given before ($-55 \pm 6 \text{ kJ mol}^{-1}$). It seems reasonable to attribute the better concordance for $n\text{-Bu}_4\text{NBr}$ as compared to $n\text{-Pr}_4\text{NBr}$ to the greater hydrophobic character of the larger $n\text{-Bu}_4\text{N}^+$ ion. On the other hand it is striking to note that the values of $\text{Hb}(\text{H}_2\text{O})$ for $n\text{-Pr}_4\text{NBr}$ and $n\text{-Bu}_4\text{NBr}$ obtained from ROFIT lead to the same contribution to the hydrophobic effect per carbon atom: -3.3 kJ mol^{-1} .

As a consequence of the model employed, values of $\text{Hb}(\text{H}_2\text{O})$ and N ought to be independent of the choice of the cosolvent as long as specific structural effects are absent. Because in NMF structure breaking by tetraalkylammonium halides may occur,¹⁴⁻¹⁶ we cannot test the model with our experimental results⁷ in mixtures of NMF and water. A similar reason¹⁶ prevents use of our results in formamide-water. However, very recently, Fuchs and Hagan¹⁷ reported on enthalpies of solution of $n\text{-Bu}_4\text{NBr}$ in aqueous dimethyl sulfoxide. Because DMSO is a dipolar

aprotic solvent in which specific short-range interactions are absent, it can be compared to DMF and the values given by Fuchs and Hagan can be used likewise to calculate $\text{Hb}(\text{H}_2\text{O})$ and N . Although the enthalpies of solution reported by these authors are restricted to mole fractions above $X = 0.5$ (except the value in pure DMSO) and their experiments carry rather large uncertainties, their excess enthalpies fit eq 7 rather well for $N = 23.2$ and $\text{Hb}(\text{H}_2\text{O}) = -50.3 \text{ kJ mol}^{-1}$. The mean deviation of $\Delta H^E(\text{calcd})$ from $\Delta H^E(\text{obsd})$ is 791 J mol^{-1} . The fit is much better if we omit the value given by Fuchs and Hagan at $X = 0.80$; then the values of N and $\text{Hb}(\text{H}_2\text{O})$ are 25.6 and $-49.2 \text{ kJ mol}^{-1}$, respectively, with a mean deviation of 329 J mol^{-1} . These values are in fair agreement with those given in Table II.

At the moment we can conclude that the outlined procedure fits the experimental enthalpies of solution reasonably well and that this approach gives some additional evidence for the number of water molecules which are necessary for hydrophobic interactions and for the enthalpic effects corresponding with these interactions.

Acknowledgments. The valuable assistances of Miss E. J. Blom and Mr. W. J. H. Heuvelsland in the experimental work are gratefully acknowledged. Moreover, Mr. Heuvelsland substantially contributed to the model calculations.

References and Notes

- W. Y. Wen, "Water and Aqueous Solutions," R. A. Horne, Ed., Wiley-Interscience, New York, N. Y., 1972, p 613.
- S. J. Bass, W. I. Nathan, R. M. Meighan, and R. H. Cole, *J. Phys. Chem.*, **68**, 509 (1964).
- C. V. Krishnan and H. L. Friedman, *J. Phys. Chem.*, **75**, 3606 (1971).
- C. de Visser and G. Somsen, *Recl. Trav. Chim. Pays-Bas*, **91**, 942 (1972).
- J. S. Falcone, Jr., and R. H. Wood, *J. Solution Chem.*, **3**, 233 (1974).
- C. de Visser and G. Somsen, *J. Chem. Thermodyn.*, **4**, 313 (1972).
- C. de Visser and G. Somsen, *J. Solution Chem.*, accepted for publication.
- M. J. Mastroianni, M. J. Pikal, and S. Lindenbaum, *J. Phys. Chem.*, **76**, 3050 (1972).
- E. J. Prosen and M. V. Kilday, *J. Res. Nat. Bur. Stand., Sect. A*, **77**, 581 (1973).
- Ideal behavior in this context means that $\Delta H^E(\text{sol}) = X_A \Delta H_A^E(\text{sol}) + X_B \Delta H_B^E(\text{sol})$ in which $\Delta H_A^E(\text{sol})$ and $\Delta H_B^E(\text{sol})$ are the enthalpies of solution in two pure solvents A and B at infinite dilution. As a consequence, the excess enthalpy of solution $\Delta H^E(\text{sol}) = \Delta H^E(\text{sol}) - \Delta H^E(\text{sol}) = 0$.
- We are grateful to Professor H. L. Friedman of the State University of New York at Stony Brook for drawing our attention to this point.
- J. E. Desnoyers and C. Jolicœur, "Modern Aspects of Electrochemistry," Vol. 5, J. O'M Bockris and B. E. Conway, Ed., Plenum Press, New York, N. Y., 1969, p 1.
- We are indebted to Professor P. Ros from the Department of Theoretical Chemistry of our Laboratory for the use of this program.
- P. P. Rastogi, *Bull. Chem. Soc. Jap.*, **43**, 2442 (1970).
- R. D. Singh and R. Gopal, *Bull. Chem. Soc. Jap.*, **45**, 2088 (1972).
- C. de Visser and G. Somsen, *J. Chem. Soc., Faraday Trans. 1*, **69**, 1440 (1973).
- R. Fuchs and C. P. Hagan, *J. Phys. Chem.*, **77**, 1797 (1973).

Hydrogen Bonding of Water in Organic Solvents. I

O. D. Bonner* and Y. S. Choi

Department of Chemistry, University of South Carolina, Columbia, South Carolina 29208 (Received February 11, 1974)

The $\nu_2 + \nu_3$ combination band of water has been recorded for bulk water and for very dilute solutions of water in various organic solvents. In each instance, the bands due to the organic solvent have been eliminated by placing a matched cell of pure solvent in the reference beam. This also served the purpose of cancelling any trace of moisture in the solvent before adding the measured quantity of water. This particular band was chosen because there is no interference from OH groups in hydroxylic solvents such as alcohols and glycols, and hydroxy or amido compounds of biological interest. The water band has been resolved by a computer program into three Gaussian components which have been identified with the 1:1 water-solvent and the 1:2 water-solvent complexes. The assignments have been verified by dilution of the complexes with CCl_4 and C_6H_6 . The positions of the bands and their widths at half-intensity vary in a predictable manner with the degree of hydrogen bonding and with the basicity of the solvent. The total areas under the curves are dependent, within experimental error, only on the amount of water present. Interactions between water and oxygen-containing organic solvents are strongest in DMSO of all solvents studied and weakest in nitromethane.

Introduction

The effect of hydrogen bonding on the physical properties of liquid water is well known. It is also recognized that the change in the extent of hydrogen bonding caused by the addition of a solute makes a significant contribution to the properties of the solution. The current phase of our research program was initiated with the objective of determining the nature of water in membranes and in biological systems. It was decided that near-infrared spectra would be susceptible to the most unambiguous interpretation. The combination band region was chosen since these bands are better separated than in the fundamental stretching region and because cells of more convenient and reproducible thickness can be used. The $\nu_2 + \nu_3$ combination band of water is convenient in that it avoids interference from the O-H and N-H stretching modes present in alcohols, sugars, amides, etc. It has been observed,¹⁻⁴ for example, that the $\nu_{\text{O-H}}$ band in alcohols occurs in the same region as the ν_1 and ν_3 water bands and that the $2\nu_{\text{O-H}}$ band has almost the same frequency as the $\nu_1 + \nu_3$ water band. The $\nu_2 + \nu_3$ water band is sufficiently far removed from all O-H and N-H modes occurring in organic cosolvents or solutes that no interference is observed. It may also be noted that there are no interfering water bands at neighboring wavelengths. The $\nu_1 + \nu_2$ band which one might consider is not reported in the vapor phase⁵ or in carbon tetrachloride solutions of water.^{6,7}

It is desirable to investigate the extent of water bonding both with itself and with other molecules as a function of concentration since the water content of membranes and tissues varies over a wide range. This report covers only the initial results which have been obtained for low water concentrations. Most of the initial data have also been obtained in aprotic solvents since the number of possible interactions are smaller and the data should be subject to more exact interpretation. This background will be used as a point of departure in future investigations of more complicated systems.

Experimental Section

Spectrophotometric or Reagent Grade solvents were used in all instances without further purification. The spectra were recorded with a Cary Model 14 spectrophotometer equipped with a 0-0.1 and 0.1-0.2 range slidewire. For all solvents except benzene, carbon tetrachloride, chloroform, and methylene chloride, the solutions were prepared containing 0.025-0.2 ml of water in 5 ml of solution. The spectra of the pure solvents (*vs.* CCl_4 in the reference beam) were first recorded in the 1800-2100-nm region. It was noted that few of the solvents had bands in this region and that when they were present their intensity was small compared with that of the $\nu_2 + \nu_3$ water band. Difference spectra of solution *vs.* pure solvent were then obtained in the same wavelength region. An interesting by-product of these preliminary investigations was the ability to detect small amounts ($\sim 0.02\%$ or less) of water in supposedly "dry" solvents. Absorption at the $\nu_2 + \nu_3$ water band could not be removed by further drying, but the addition of a small amount of D_2O would remove the band by converting the water to HDO. In the reported data small traces of moisture in the solvent were cancelled by comparing the solutions with the "pure" solvents in the double beam instrument. Cell thicknesses were 0.1 or 0.5 mm depending on the water concentration. The solutions of water in C_6H_6 , CHCl_3 , CCl_4 , and CH_2Cl_2 were much more dilute and 2- or 5-cm cells were used. The longer cells were also used in the experiments in which the various water-aprotic solvent mixtures were diluted with carbon tetrachloride or benzene. It was observed that Beer's law was obeyed for solutions containing less than 2% water by volume. Studies are presently underway on solutions in which the water concentration is much greater. In solutions containing only water and an aprotic solvent the water concentration was 0.1 ml per 5 ml of solution except for solutions in benzene, chloroform, and methylene chloride in which case the concentration was 10^{-3} ml of water per 5 ml of solution and for nitromethane where solubility limited the concentration to

0.08 ml of water per 5 ml of solution. These solutions were then diluted with varying amounts of CCl_4 or benzene and spectra were obtained *vs.* reference solvent which was diluted in an identical fashion.

Spectral results as recorded were digitized so as to tabulate absorbance as a function of wavelength at 5-nm intervals. The two pen instrument with the special slidewire permitted the recording of absorbance in the range 0–0.2 with chart divisions of 0.001 absorbance unit. Interpolation was easily possible to 0.0005 absorbance unit. A computer program was developed which would fit the experimental data as the sum of three gaussian curves each of which was defined by the equation

$$A_i = A_i^0 \exp \left[\frac{(\lambda_i^0 - \lambda)^2}{0.601(\Delta\lambda_{1/2})} \right]$$

where A_i is the absorbance of specie i at wavelength λ ; A_i^0 is the maximum absorbance at the peak λ_i^0 , and $\Delta\lambda_{1/2}$ is the band width at the half-intensity. The area under a curve is given by the expression

$$\text{area} = 1/2[0.601\sqrt{\pi} A_i^0(\Delta\lambda_{1/2})]$$

It was permitted, of course, for one or more of the bands to have a value of A_i^0 equal to zero or a very small value. The computer program minimizes the sum of the residuals between the calculated and experimentally observed curves at each data point by adjusting the variable parameters A_i^0 , λ_i^0 , and $\Delta\lambda_{1/2}$. This is done in an iterative fashion with no limit placed upon the amount that any parameter can change from an initial guess. It was found that convergence could be obtained with the sum of the absolute values of the residuals being smaller in most instances than the uncertainty in reading the data points.

Results and Discussion

Experimental data and plots of the computer resolution for some of the solvent systems are presented in Figures 1–3. The data for all of the systems are summarized in Tables I and II in the general order of increasing strength of the water–solvent complex. Data are also presented for solutions of water in 1-pentanol and of pure water for the purpose of comparison. One may first note that these data are qualitatively in agreement with those reported by earlier workers for similar systems.^{6–9} The fact that only one water band is observed in carbon tetrachloride does not conflict with the work of Magnusson¹⁰ since he found it necessary to use a double beam cancellation technique to observe the small amount of polymeric water which is present.

At this point one should be concerned about two aspects of the results. First, is the computer resolution correct? Although there is remarkable agreement between the sum of the resolved Gaussian curves and the experimental data, is this resolution unique and are three components the correct number? Second, if this is true, how may one interpret the data? One possibility is, of course, to assign the bands to water molecules having zero, one, or two of the protons participating in hydrogen bonding in a manner similar to that proposed initially by Buijs and Chopin.¹¹ More recent data obtained by Barrow, *et al.*,¹² on the fundamental water bands indicate, however, that this simple interpretation might be incorrect. Additional experiments were therefore performed in which successive dilutions of the water–aprotic solvents were made with CCl_4 (which is com-

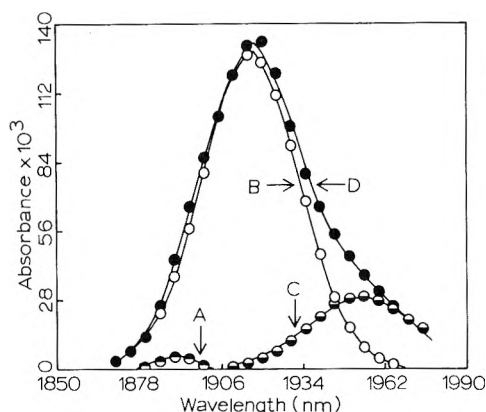


Figure 1. Computer resolutions of a spectrum of a solution of water in dioxane ($1 \mu\text{l}$ of H_2O per 5 ml of solution): curve A, band 1; curve B, band 2; curve C, band 3; curve D, sum of bands 1, 2, and 3; ●, experimental data points.

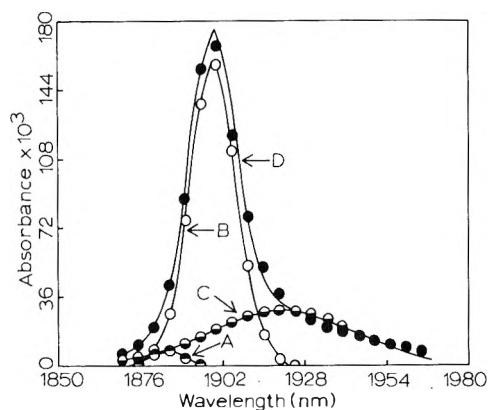


Figure 2. Computer resolution of spectrum of a solution of water in nitromethane ($1 \mu\text{l}$ of H_2O per 5 ml of solution): curve A, band 1; curve B, band 2; curve C, band 3; curve D, sum of bands 1, 2, and 3; ●, experimental data points.

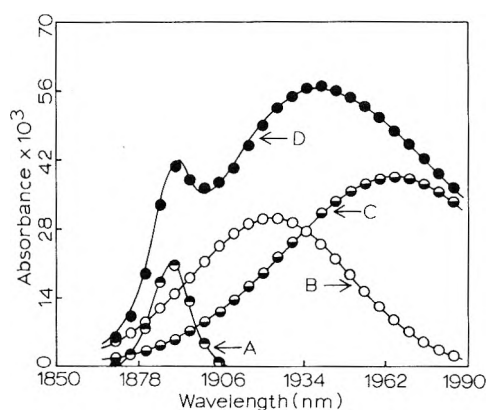


Figure 3. Computer resolution of spectrum of a solution of water in 1-pentanol ($1 \mu\text{l}$ of H_2O per 5 ml of solution): curve A, band 1; curve B, band 2; curve C, band 3; curve D, band 4; ●, experimental data points.

pletely transparent at these wavelengths) and with benzene. The pure reference solvent was likewise diluted with corresponding amounts of CCl_4 or benzene. The family of dilution curves for the tetrahydrofuran–water system is shown in Figure 4. This is typical of the curves obtained for other systems. It may be noted that the band at 1918 nm disappears with dilution while a new band at 1891 nm grows immensely in intensity, although not quite so much

TABLE I: Observed Band Maxima and Computer-Resolved Band Positions and Half-Widths for Water Dissolved in Solvents

Solvent	Exptl obsd max, nm	Band 1		Band 2		Band 3	
		Position, nm	Half-width, nm	Position, nm	Half-width, nm	Position, nm	Half-width, nm
CCl ₄	1893			1893	13.5		
CHCl ₃	1897			1897	12.2		
CH ₂ Cl ₂	1898			1898	14.0		
CH ₃ NO ₃	1899	1882	14.8	1899	17.5	1921	53.0
C ₆ H ₆	1900			1900	16.5		
PC ^a	1904	1888	16.5	1904	26.2	1934	47.0
CH ₃ CN	1905	1888	16.5	1905	27.6	1937	44.9
MEK ^b	1909	1888	15.6	1907	31.6	1939	51.6
Sulfolane	1914	1888	15.4	1913	26.8	1943	37.8
Dioxane	1920	1891	14.2	1916	39.3	1954	40.5
THF ^c	1921	1891	21.7	1920	37.5	1958	36.6
DMSO ^d	1943	1896	16.6	1941	47.3	1983	35.9
Pyridine	1944	1896	14.1	1441	79.1	2001	37.2
H ₂ O	1928	1901	22.4	1923	57.9	1977	70.1
<i>n</i> -AmOH	1940	1889	14.9	1923	64.8	1965	90.2

^a Propylene carbonate. ^b Methyl ethyl ketone. ^c Tetrahydrofuran. ^d Dimethyl sulfoxide.

TABLE II: Band Areas for Water Dissolved in Solvents^a

Solvent	Band areas, nm absorbance × 10 ³			Total area
	Band 1	Band 2	Band 3	
CH ₃ NO ₃	0.8	18.7	10.5	30.0
PC ^b	0.5	21.0	10.2	31.7
CH ₃ CN	0.9	22.6	9.3	32.8
MEK ^c	1.1	20.0	12.1	33.2
Sulfolane	1.0	26.7	6.3	34.0
Dioxane	0.4	27.2	6.4	34.0
THF ^d	4.0	22.3	6.8	33.1
DMSO ^e	1.4	28.6	3.9	33.9
Pyridine	1.6	30.2	1.2	33.0
H ₂ O	0.8	17.2	14.6	32.6
AmOH	1.7	10.7	19.0	31.4

^a Areas normalized to 1 μl of H₂O per 5 ml of solution; cell thickness = 0.5 nm. ^b Propylene carbonate. ^c Methyl ethyl ketone. ^d Tetrahydrofuran. ^e Dimethyl sulfoxide.

in integrated areas because of its narrowness. A third broad but weak band emerges at 1963 nm. This experiment gives strong support to the computer resolution of the original water-aprotic solvent curves in that there are exactly *three* Gaussian components and that the experimentally determined positions of the maxima in the CCl₄ diluted solutions occur at almost those positions calculated by the computer resolution. In similar dilution studies on the other systems, there is never more than a few nanometers difference observed between the positions calculated for the bands (Table I) and those observed in the CCl₄ diluted solutions; an explanation for these deviations will be presented later.

These experiments indicate that the $\nu_2 + \nu_3$ water band may be interpreted in the same fashion as the fundamental modes¹² when water is dissolved in various solvents. The sharp band occurring at 1890–1900 nm can be assigned to the free (or almost free) $\nu_{OH} + \nu_2$ mode of the 1:1 complex, H–O–H–B. The position of this band is almost identical with that of the extremely weakly bonded water in the chlorinated hydrocarbons and benzene. In both instances the band is shifted to the longer wavelengths as the water proton(s) becomes more strongly bonded. The band occurring at wavelengths greater than about 1940 nm is due also to the 1:1 complex as is shown by its increase in intensity relative to the second band upon dilution of the solutions with CCl₄. The fact that this band has an appreciable in-

tensity in solutions in which there are few unbonded protons indicates that it must occur in any unsymmetric situation in which the two protons of a water molecule are participating in hydrogen bonds of unequal strength. This band likewise shifts to longer wavelengths as the basicity of the solvent increases.

The band occurring in the 1905–1945-nm region may be assigned the symmetrical situation, B–H–O–H–B, in which both water protons are hydrogen bonded with bonds of near-equal strength. The intensity of this band decreases upon CCl₄ or benzene dilution as the probability of the 1:1 complex increases. The shift in the position of the band due to symmetrically bonded water from the 1893 nm for the very weakly bonded H₂O–CCl₄ to 1944 nm for water in pyridine is directly related to the strength of the hydrogen bonds which are formed. It may be noted that the position of this band coincides with the experimentally observed maximum for most of the solutions indicating that water is largely doubly bonded. This should be expected since the mole fraction of water in all instances is less than 0.1.

These band assignments, of course, refute all previous interpretations¹¹ in which they were assigned to water molecules containing zero, one, or two hydrogen bonds. A more proper interpretation of our experimental results appears to be the following. Tetrahydrofuran and pyridine, of the aprotic solvents, contain a somewhat larger fraction of dissolved water in which one of the protons is nonbonded or extremely weakly bonded. Steric effects can account for the 1:1 complex in THF because of the bulky nature of the molecule containing only one oxygen. Dioxane, by contrast, shows a much smaller fraction of nonbonded protons. The band in pyridine is probably due to the weak interaction of one proton of some of the water molecules with the π electrons of the aromatic ring. The relative solubilities and band positions of water in CCl₄ and benzene confirms this type of interaction. Perhaps the most interesting aprotic solvent studied is the nitromethane–water spectrum and the dilution studies in CCl₄ indicate that the water is as weakly bonded as when dissolved in benzene. The limited solubility of water in nitromethane is a further indication that any interactions must be very weak. If one does not wish to believe that hydrogen bonding in a water-oxygenated solvent complex can be so weak, there is a possible alternative explanation. It is possible that the attraction between water and nitromethane is purely dipolar in nature

TABLE III: Effect of a Change in the Type of Hydrogen Bonding on Band Intensities^a

Solvent A	Solvent B	Vol % A	Water band area, nm absorbance $\times 10^3$			Total area
			Band 1	Band 2	Band 3	
CH ₃ CN	CCl ₄	100	0.9	22.6	9.3	32.8
		50	5.4	18.1	6.3	29.8
		25	9.1	13.7	6.2	29.0
		12.5	10.8	6.8	4.7	22.3
		6.25	9.6	4.1	3.3	17.0
THF	CCl ₄	100	4.0	22.3	6.8	33.1
		50	5.2	21.5	5.3	32.0
		25	9.3	13.2	6.2	28.7
		12.5	8.6	7.5	4.6	20.7
		6.25	8.4	3.6	3.5	15.5
THF	C ₆ H ₆	100	4.0	22.3	6.8	33.1
		50	9.5	15.5	6.8	31.8
		25	12.9	9.8	6.9	29.6
		12.5	13.7	5.3	5.4	24.4
		6.25	14.0	3.4	3.7	21.1

^a Areas normalized to 1 μ l of H₂O per 5 ml of solution; cell thickness = 0.5 nm.

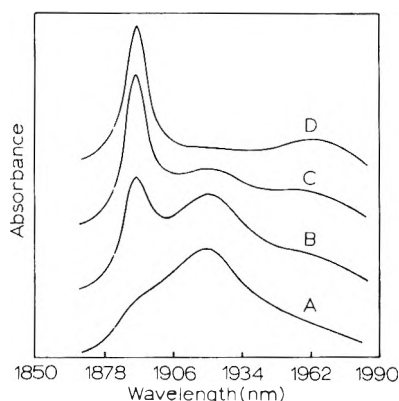


Figure 4. Spectrum of dilutions of tetrahydrofuran-water solutions with carbon tetrachloride. The ratio of THF to H₂O remains constant at 49 to 1: curve A, volume fraction of CCl₄ = 0.00; curve B, volume fraction of CCl₄ = 0.50; curve C, volume fraction of CCl₄ = 0.75; curve D, volume fraction of CCl₄ = 0.94.

and that because of the similar geometry of the H-O-H and O-N-O bonds (with protons being positive in water and nitrogen being positive in CH₃NO₂) the water molecule assumes a position so that the three oppositely charged atoms of each of the molecules are adjacent to one another in the form of two superimposed V's. Hydrogen bonding in the usual sense is thus not possible.

At this point in the interpretation of the spectra, it should be observed in solutions containing only a small amount of water that the band 2 area is larger than the sum of the areas of bands 1 and 3. It is, in general, 10 to 20 times as large as the area calculated for band 1 (Table II). It has been properly pointed out by a reviewer of this paper that the area of bands 1 and 3 may be affected by whether one considers band 2 to be entirely Gaussian or to possess some Lorentzian character. The character of the bands cannot be indisputably determined by computer resolution. One may conclude, however, that the relative areas of bands 2 and 3 will not be greatly disturbed by the character of the bands. It is possible that band 1 might be eliminated or its area doubled if band 2 were essentially Lorentzian but in either case the fraction of nonbonded protons in water would be only a small fraction of the total number.

The sum of the integrated areas under the bands is also of interest. One of the advantages of the near-infrared spectra is that these areas can be determined with a high

degree of accuracy. The absorbance is reported in nm absorbance units normalized to water concentrations of 1 μ l per 5 ml of solution and a cell thickness of 0.5 mm. The total water absorbance is found to be approximately constant for all water-aprotic solvent mixtures (Table II). This may be somewhat fortuitous, however, since most of the water protons are hydrogen bonded in all of the solutions. It has been observed that the intensity of fundamental stretching OH modes is increased by hydrogen bonding. The fact that the absorbance is independent of the solvent and dependent only on the amount of water up to about 2% water by volume recommends this as a convenient and accurate method of determining small quantities of water in organic solvents.

The total area of the three water bands which is obtained when solutions are diluted with CCl₄ (Table III) decreases upon dilution. This is undoubtedly due at least in part to the loss of water by adsorption on the sides of the glass cells which were used and perhaps in part by a difference in molar absorbance of bonded and nonbonded OH groups. Dilutions with benzene confirm that the loss of water to the cell walls is less than when the dilutions are with CCl₄, a poorer solvent. This loss of water upon dilution with CCl₄ or benzene does not, however, negate a comparison of the relative intensities of the three bands. The intensity of the second band due to the symmetrically bonded water definitely decreases as that of the first and third band increases. The slight shift in the position of the band maxima upon dilution results from a decrease in water-THF or water-CH₃CN interactions and an increase in H₂O-CCl₄ or H₂O-benzene interaction. At extreme dilutions the first band position approaches that in pure CCl₄ or pure benzene. The more rapid decrease in the intensity of the band due to symmetric bonding in benzene relative to CCl₄ upon dilution indicates that the benzene is more competitive with THF than to CCl₄ for the H₂O protons.

There has been a considerable difference of opinion concerning the fraction of unbonded protons in pure water. Estimates have ranged from approximately 30% at 25° by Choppin¹¹ and Scheraga¹³ to less than 1% by Stevenson.⁷ We have recorded the spectrum for pure water and have obtained a resolution of the experimental data using the same computer program as was used for water in very dilute solutions. The total area of the bands is identical, within experimental error, with that of water in dilute solutions. The fraction of nonbonded protons appears to be

very small (perhaps 2 or 3%) from the relative areas of the three bands. The band widths at half-intensity are larger than those of water in dilute solutions as one would expect since there are more possible configurations and hydrogen-bond angles in pure water. The large area under the third band indicates that although most of the water is doubly bonded, there are a large fraction of the molecules in which the proton-oxygen bonds are of unequal strength. This suggests that the most appropriate model for water might be that proposed by Pople¹⁴ some years ago in which the majority of the hydrogen bonds are regarded as distorted rather than broken. This would result in a rather broad spectrum of energies for the bonds.

Finally data for water in one alcohol are presented (Figure 3). The ν_{OH} band of the alcohol lies above 2000 nm and is much less intense than the water band so that there is no interference. All three water bands are observed for dilute solutions of water in 1-pentanol. The free ν_{OH} water band could result from water molecules which are adjacent to the hydrocarbon portion of the molecule but more probably results from the hydrogen bonding of the alcohol proton and the water oxygen. The large area of band 3 relative to that of band 2 indicates that many of the water molecules are not symmetrically bonded. This could result from the steric effects of a five carbon alcohol. The band half-widths and band positions are similar to those of pure water.

In conclusion, the $\nu_2 + \nu_3$ water band appears to be better suited for the study of water structure than the fundamental modes for at least three reasons. (1) The data are easier to interpret as there is only *one* band when water is un-bonded or symmetrically bonded rather than the three bands (ν_1 , ν_3 , and $2\nu_2$) which interfere with one another. (2) Interference of other O-H and N-H bands is avoided. (3) Semiquantitative measurements may be made as shown by the agreement in the values of the integrated intensities which were obtained.

References and Notes

- (1) R. M. Badger and S. H. Bauer, *J. Chem. Phys.*, **4**, 469 (1936).
- (2) G. Herzberg and H. Verleger, *Phys. Z.*, **37**, 444 (1936).
- (3) A. R. H. Cole and A. J. Mitchell, *Aust. J. Chem.*, **18**, 46 (1965).
- (4) G. Habermahl, *Angew. Chem.*, **76**, 271 (1964).
- (5) G. Herzberg, "Molecular Spectra and Molecular Structure II. Infrared and Raman Spectra of Polyatomic Molecules," Van Nostrand, Princeton, N. J., 1959, p 281.
- (6) E. Greinacher, W. Luttko, and R. Mecke, *Z. Elektrochem.*, **59**, 23 (1955).
- (7) D. P. Stevenson, *J. Phys. Chem.*, **69**, 2145 (1965).
- (8) W. C. McCabe, S. Subramanian, and H. F. Fisher, *J. Phys. Chem.*, **74**, 4360 (1970).
- (9) A. Burneau and J. Corset, *J. Phys. Chem.*, **76**, 449 (1972).
- (10) L. B. Magnusson, *J. Phys. Chem.*, **74**, 4221 (1970).
- (11) K. Buijs and G. R. Choppin, *J. Chem. Phys.*, **39**, 2035 (1963).
- (12) S. C. Mohr, W. D. Wilk, and G. M. Barrow, *J. Amer. Chem. Soc.*, **87**, 3048 (1965).
- (13) M. R. Thomas, H. A. Scheraga, and E. E. Schrier, *J. Phys. Chem.*, **69**, 3722 (1965).
- (14) J. A. Pople, *Proc. Roy. Soc., Ser. A*, **205**, 163 (1951).

Hydrogen Bonding of Water in Organic Solvents. II. The Change of Water Structure with Composition

O. D. Bonner* and Y. S. Choi

Department of Chemistry, University of South Carolina, Columbia, South Carolina 29208 (Received February 11, 1974)

The $\nu_2 + \nu_3$ combination band of water has been recorded for tetrahydrofuran-water, acetonitrile-water, and dimethyl sulfoxide-water solutions over the entire range of water concentrations. Absorbance of the weak bands of the organic component of the solution has been compensated. It was found that in all solutions the fraction of nonbonded or very weakly bonded OH groups was greater in solutions dilute in water and in pure water than in solutions of intermediate composition. It was also observed that a large fraction of the water molecules bonded with the two protons forming bonds of near equal strength in dilute water solutions but that the bonding became more "unsymmetric" as the mole fraction of water in the solution was increased. Evidence was obtained for the phenomenon of "hydrophobic bonding" in the case of tetrahydrofuran-water solutions. The computer resolution of the bands in the organic solvent-water solutions of various concentrations was substantiated by measurement of the derivative $d(\text{absorbance})/d(\text{water concentration})$ for several solutions over the wavelength region 1850-2050 nm. It was found for these solutions, just as for the dilute solutions reported previously, that the total water absorbance is independent of the cosolvent and dependent only on the amount of water which is present.

Introduction

In a previous paper¹ spectra were reported for small amounts of water in 13 aprotic solvents and one alcohol. The $\nu_2 + \nu_3$ combination band of water involving the bending mode was chosen so as to avoid interference from OH

and NH groups in alcohols, glycols, and amides since it was hoped to extend these studies to systems of biological interest. It is the purpose of this paper to report spectra for some of the organic solvent-water systems which have been recorded over the entire concentration range from very di-

TABLE I: Computer-Resolved Band Positions, Half-Widths, and Areas for the $\nu_2 + \nu_3$ Water Band in Tetrahydrofuran-Water Solutions

Mole fraction of water	0.08	0.21	0.32	0.66	0.82	0.91	0.98	1.00
Band 1								
Position, nm	1891	1891	1892	1894	1897	1897	1900	1901
Half-width, nm	21.7	24.5	24.3	22.9	23.6	22.2	21.6	22.4
Area, nm absorbance $\times 10^3$	4.0	3.3	2.5	0.8	0.8	0.8	0.6	0.8
Band 2								
Position, nm	1920	1921	1923	1924	1925	1924	1923	1923
Half-width, nm	37.5	42.8	46.6	55.5	56.7	56.7	57.7	57.9
Area, nm absorbance $\times 10^3$	22.3	21.0	20.1	18.7	17.7	17.5	17.2	17.2
Band 3								
Position, nm	1958	1963	1966	1971	1975	1975	1977	1977
Half-width, nm	36.6	48.3	53.6	65.8	70.8	69.1	70.0	70.1
Area, nm absorbance $\times 10^3$	6.8	10.0	11.7	12.9	14.2	14.9	14.5	14.6
Total area, nm absorbance $\times 10^3$	33.1	34.3	34.3	32.4	32.7	33.2	32.3	32.6

lute water solutions to pure water and to note the water structure in these solutions.

Experimental Section

Spectrophotometric or Reagent Grade solvents were used in all instances without further purification. For solutions containing only a small amount of water or for solutions in which the water concentration was varied only a small amount a Cary Model 14 spectrophotometer equipped with a 0–0.1 and 0.1–0.2 range slidewire was used. The same instrument equipped with the normal 0–1.0 and 1.0–2.0 range slidewire was used for more concentrated water solutions. In order to be consistent with the data reported in the previous paper, all absorbances were normalized to 1 μ l of H₂O per 5 ml of solution and a cell path length of 0.5 nm. The concentrated solution data may thus be directly compared with that for the very dilute solutions. The two slide wires and the cells of varying path length were, of course, calibrated for internal consistency.

Results and Discussion

It is not possible because of solubility limitations to study aqueous solutions of all of the nonelectrolytes reported in the previous paper¹ over the entire concentration range. Three systems with different organic functional groups were, therefore, chosen and examined in detail.

(A) *Tetrahydrofuran-Water*. The tetrahydrofuran-water system is interesting since the very dilute solution of water in THF exhibited the largest fraction of nonbonded water OH groups of all of the systems reported. Solutions containing various mole fractions of water were prepared and their spectra were recorded in the 1850–2050-nm region with the slight absorbance due to THF being compensated in the reference beam. The absorbances were then normalized to 1 μ l of H₂O per 5 ml of solution and subjected to computer resolution in the same fashion as the dilute solutions. The resultant data are reported in Table I. It may be noted that the position of band 1 shifts in a regular fashion with increasing water concentration from 1891 to 1901 nm. The fraction of nonbonded OH groups, however, appears to decrease to a minimum value at an intermediate concentration and then increase slightly in pure water. The area of band 2 does not change drastically with composition but the position of the band appears to reach a maximum wavelength at an intermediate concentration. If this

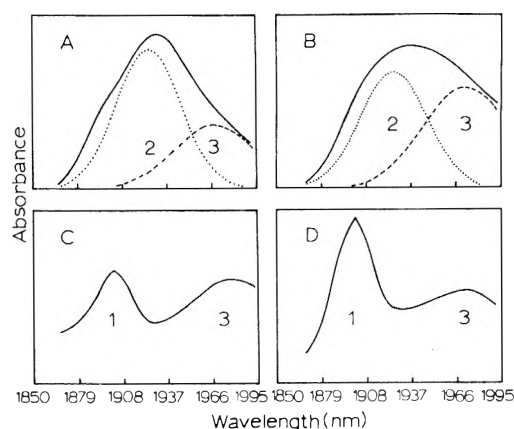


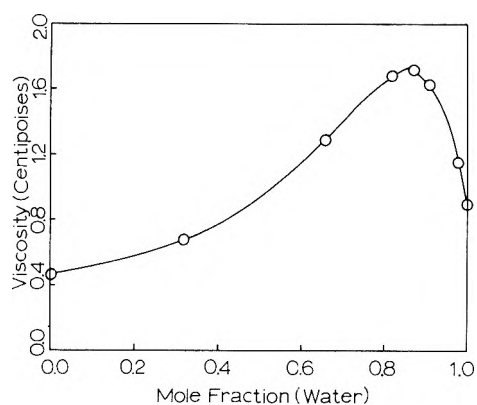
Figure 1. Spectra of the derivative $d(\text{absorbance})/d(\text{H}_2\text{O concentration})$ for tetrahydrofuran-water solutions of various compositions: (A) 0.21 mole fraction water, relative areas band 2/band 3 = 1.8; (B) 0.66 mole fraction water, relative areas band 2/band 3 = 0.9; (C) 0.91 mole fraction water; (D) 0.99 mole fraction water.

is related to the strength of the bonding in the symmetrical complex as was inferred from the earlier work, it indicates that the bonding is stronger in solutions of intermediate concentration than in pure water or in very dilute solutions. This indication will be confirmed by further data. Band 3, which like band 1 is due to the unsymmetrically bonded complex, increases in area and in wavelength as the fraction of water increases. The constancy of the total area of the water band over the entire range of composition is reassuring. The average residual between the calculated sum of the absorbances of the three bands and that observed experimentally was again less than the experimental error in reading the spectra.

The data in Table I give the overall picture for all of the water molecules in a solution of a given water concentration. Because of the unexpected minimum in the fraction of nonbonded OH groups and the maximum in the wavelength of the symmetrically bonded water complex, it was desired to further substantiate the data in Table I. Consequently, a series of experiments was designed in which values of the derivative $d(\text{absorbance})/d(\text{concentration})$ could be measured at various water concentrations. This was done by preparing a solution of a given water concentration and dividing it into two parts. One part was placed

TABLE II: Computer-Resolved Band Positions, Half-Widths, and Areas for the $\nu_2 + \nu_3$ Water Band in Acetonitrile-Water Solutions

Mole fraction of water	0.05	0.15	0.24	0.56	0.74	0.87	0.96	1.00
Band 1								
Position, nm	1888	1889	1894	1898	1900	1900	1900	1901
Half-width, nm	16.5	20.5	21.1	21.6	20.7	20.9	22.1	22.4
Area, nm								
absorbance $\times 10^3$	0.9	0.9	0.9	0.7	0.4	0.6	0.7	0.8
Band 2								
Position, nm	1905	1908	1909	1914	1916	1919	1921	1923
Half-width, nm	27.6	31.9	36.6	43.3	47.0	50.0	54.2	57.9
Area, nm								
absorbance $\times 10^3$	22.6	21.4	20.5	18.6	17.0	17.1	16.5	17.2
Band 3								
Position, nm	1937	1944	1947	1957	1961	1967	1971	1977
Half-width, nm	44.9	49.9	53.3	55.7	63.6	63.4	64.5	70.1
Area, nm								
absorbance $\times 10^3$	9.3	10.7	11.5	12.3	14.2	14.5	14.2	14.6
Total area nm								
absorbance $\times 10^3$	32.8	33.0	32.9	31.6	31.6	32.2	31.4	32.6

**Figure 2.** Viscosities of tetrahydrofuran-water solutions at 25°.

in the reference beam of the spectrophotometer and a very small amount of additional water (*ca.* 1%) was added to the other sample which was placed in the sample beam of the spectrophotometer. The observed spectrum was that resulting from the increment of water which was added to the solution. This procedure is similar to that employed by Magnusson² to study the dimerization of water in CCl₄ and by Bellamy and Pace³ to investigate the polymerization of alcohols. It differs, however, in that the concentrations of water or alcohol in their compensation technique differed by factors of 5–50 while we changed the water concentration only slightly. These spectral data are thus somewhat analogous to partial molal quantities which may be calculated for a solution at a given (constant) composition. The derivatives for some of the solutions are shown in Figure 1. When a small increment of water is added to solutions containing mole fractions of water in the range 0.15–0.82 the appearance of the derivative, $d(\text{absorbance})/d(\text{water concentration})$, is similar to that of the spectrum of pure water except that the wavelength of maximum absorbance gradually shifts from 1925 to 1948 nm. The wavelength of maximum absorbance of pure water is 1928 nm. A computer resolution of the derivatives indicated that the additional increment of water is at first *primarily* symmetrically bonded with the bonds being rather strong as is indicated by the increasing wavelength of both the observed band maximum and also the maximum of resolved band 2 due to the symmetrically bonded water. It is necessary that most of the new hydrogen bonds be water-water rather than the weak-

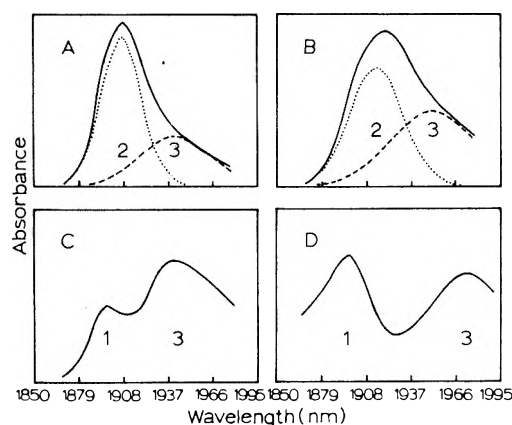
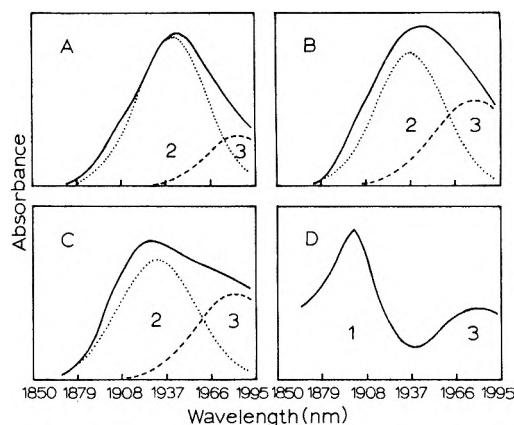
er water-THF bonds since at mole fraction 0.33 the availability of THF oxygen atoms for bonding is exhausted. The strength of the bonds appears to be experimental confirmation of the “cooperative phenomenon” proposed by Frank.⁴ It is also probable that the structure of the water is enhanced by the THF methylene groups. This phenomenon has been referred to as “hydrophobic bonding” by some persons. As the water concentration becomes greater, it becomes increasingly difficult for the water to hydrogen bond in a symmetrical fashion, primarily due to steric effects. In solutions having mole fractions of water greater than 0.9, the added increment of water exhibits completely unsymmetrical hydrogen bonding and this contributes to the larger fraction of nonbonded OH groups present in pure water than in a solution containing 0.8–0.9 mole fraction water. The derivatives thus tend to validate the computer resolutions for the spectra of the various solutions.

The spectral data for the THF-water solutions also correlate with certain physical properties of the solutions. Both the adiabatic compressibility⁵ and the water activity⁶ curves show minima between water mole fractions of 0.9 and 1.0. the viscosity, which is probably a better indicator of structure, shows a maximum at a mole fraction of water of approximately 0.9 indicating that solutions of intermediate concentrations indeed have stronger forces of attraction than are present in the pure liquids. This behavior is similar to that observed in solutions^{7–9} of water with dioxane and alcohols.

(B) *Acetonitrile-Water.* This system seemed to be of interest since the water-solvent hydrogen bonds appeared to be among the weaker of those reported¹ for dilute water solutions as indicated by the wavelengths of both the symmetrically and unsymmetrically bonded water. The spectral data for solutions of various water concentrations are presented in Table II. It may be noted that the positions of the band maxima for the three bands and also the band areas vary in a more regular fashion with water concentration than was the case with the THF-H₂O system except that there again appears to be slightly fewer nonbonded OH groups in solutions of intermediate composition than in either of the pure liquids. There is, however, no solution of intermediate composition in which the wavelength of the symmetrically bonded water band is greater than that for pure water. This confirms the suspicion that the occurrence of this phenomenon in THF-water systems may be due to the enhancement of the water structure (and strength of

TABLE III: Computer-Resolved Band Positions, Half-Widths, and Areas for the $\nu_2 + \nu_3$ Water Band in Dimethyl Sulfoxide-Water Solutions

Mole fraction of water	0.07	0.19	0.31	0.63	0.80	0.90	0.97	1.00
Band 1								
Position, nm	1896	1897	1898	1900	1901	1901	1901	1901
Half-width, nm	16.6	17.5	18.2	18.5	19.2	19.7	21.2	22.4
Area, nm absorbance $\times 10^3$	1.4	1.1	1.0	0.7	0.6	0.7	0.8	0.8
Band 2								
Position, nm	1941	1940	1939	1934	1930	1927	1924	1923
Half-width, nm	47.3	51.0	51.3	57.3	57.7	57.7	57.7	57.9
Area, nm absorbance $\times 10^3$	28.6	27.4	23.9	20.0	17.8	17.0	16.3	17.2
Band 3								
Position, nm	1983	1982	1980	1978	1978	1978	1977	1977
Half-width, nm	35.9	42.3	54.1	62.4	66.0	67.7	69.4	70.1
Area, nm absorbance $\times 10^3$	3.9	5.4	8.8	11.7	12.5	12.9	13.8	14.6
Total area, nm absorbance $\times 10^3$	33.9	33.9	33.7	32.4	30.9	30.6	30.9	32.6

**Figure 3.** Spectra of the derivative $d(\text{absorbance})/d(\text{H}_2\text{O concentration})$ for acetonitrile-water solutions of various compositions: (A) 0.10 mole fraction water, relative areas band 2/band 3 = 1.8; (B) 0.24 mole fraction water, relative areas band 2/band 3 = 1.0; (C) 0.74 mole fraction water; (D) 0.96 mole fraction water.**Figure 4.** Spectra of the derivative $d(\text{absorbance})/d(\text{H}_2\text{O concentration})$ for dimethyl sulfoxide-water solutions of various compositions: (A) 0.19 mole fraction water, relative areas band 2/band 3 = 3.2; (B) 0.31 mole fraction water, relative areas band 2/band 3 = 1.3; (C) 0.63 mole fraction water, relative areas band 2/band 3 = 1.0; (D) 0.97 mole fraction water.

the hydrogen bonds) by the methylene groups of THF. In this connection it may be observed that at comparable water mole fractions the wavelength of the symmetrically bonded water band is always greater in THF-H₂O solutions than in acetonitrile-water solutions. The areas of bands 2 and 3 indicate that the hydrogen bonding becomes less symmetrical as the concentration of water is increased. The spectra of the derivatives for this system (Figure 3) again confirm the data given by the computer resolution. The fairly sharp band at 1909 nm for a mole fraction of water of 0.1 indicates that the added increment of water is still bonding primarily in a symmetrical fashion but with stronger bonds. At a mole fraction of 0.24 the band is much broader and it can be resolved into both a symmetrical and an unsymmetrical bonded portion. The double peaks occurring in the derivative for the 0.74 mole fraction solution confirm that the added water is bonding unsymmetrically. For a mole fraction of water of 0.96 the derivative exhibits a maximum at 1892 nm and a minimum at 1918 nm. This substantiates the increase in free OH group concentration and decrease in the fraction of symmetrically bonded water as one approaches pure water.

(C) *DMSO-Water.* This system was chosen for study since the DMSO-water hydrogen bond strength appears to

be greater than water-water hydrogen bond strength from the dilute solution data. This system also affords a direct comparison of the data obtained from near-infrared spectra with those obtained from Raman spectra¹⁰ of the fundamental vibrational region. The DMSO-water spectral data, which are summarized in Table III, are about those which would be expected in the light of the experience gained with the previous systems. It appears that in all aprotic solvent-water systems that the fraction of non-bonded or very weakly bonded water protons is greater in pure water or in very dilute solutions than in those of intermediate composition. Likewise, the fraction of symmetrically bonded water decreases as the mole fraction of water in any of the solutions increases. The band maxima for the three bands again changes wavelength in a regular manner with water composition although there is a shift of only 2 nm in the position of the symmetrically bonded water band between mole fractions of water of 0.07 and 0.31. This may be taken as further evidence that the added water continues to bond primarily to DMSO molecules rather than to other water molecules. The spectra of the derivatives for this system again confirm the computer resolutions of Table III. Computer resolution of the derivatives which have been made for solutions in which water is the minor

component of the three cosolvent systems reveal that, for solutions of comparable mole fractions, the relative areas of band 1/band 3 are in the order DMSO-H₂O > THF-H₂O > CH₃CN-H₂O. This is the same order as the relative strengths of the aprotic solvent-water hydrogen bond.

Although this study yields data which are more quantitative concerning the state of water in various DMSO-water solutions it is interesting that the model proposed by Scherer, *et al.*,¹⁰ applies rather well. Both studies conclude that the water exists almost entirely dihydrogen bonded with a portion of it having one stronger and one weaker bond and another portion having hydrogen bonds of near equal strength. A very small fraction of the protons are very weakly bonded.

Conclusions

The $\nu_2 + \nu_3$ combination water band is useful for studying the nature of organic solvent-water solutions over the entire range of compositions from pure water to solutions containing very small quantities of water. There is no interference of neighboring bands as is the case in the ν_1 , ν_3 , $2\nu_2$ region and no need to consider¹⁰ the effects of Fermi resonance. The water band of any solution can be resolved into its Gaussian components and from these data one can estimate (1) the relative amounts of symmetrically and asymmetrically bonded water molecules, (2) the fraction of protons which are very weakly bonded, and (3) the strength

of the solvent-water hydrogen bond relative to that of the water-water bond from the wavelength at which the band occurs.

The technique of observing the derivative, $d(\text{absorbance})/d(\text{water concentration})$, should be extremely valuable in that it enables one to observe changes in water-water and water-cosolvent interactions as a function of solution concentration. In cases where water miscibility is not achieved over the entire range of concentrations such as for biological membrane systems and solutions of electrolytes one may observe at what point the additional water molecules begin to bond to other water molecules instead of to the cosolvent molecules. A study of biological systems by successive dehydration might furnish data for distinguishing between so called "bound" and "free" water in these systems.

References and Notes

- (1) O. D. Bonner and Y. S. Choi, *J. Phys. Chem.*, **78**, 1723 (1974).
- (2) L. B. Magnusson, *J. Phys. Chem.*, **74**, 4221 (1970).
- (3) L. J. Bellamy and R. J. Pace, *Spectrochim. Acta*, **22**, 525 (1966).
- (4) H. S. Frank and W. Y. Wen, *Discuss. Faraday Soc.*, **24**, 133 (1957).
- (5) E. K. Baumgartner and G. Atkinson, *J. Phys. Chem.*, **75**, 2336 (1971).
- (6) K. L. Pinder, *J. Chem. Eng. Data*, **18**, 275 (1973).
- (7) R. L. Kay and T. L. Broadwater, *Electrochem. Acta*, **16**, 667 (1971).
- (8) T. L. Broadwater and R. L. Kay, *J. Phys. Chem.*, **74**, 3802 (1970).
- (9) R. L. Kay, C. P. Cunningham, and D. F. Evans, "Hydrogen Bonded Solvent Systems," A. K. Covington and P. Jones, Ed., Taylor and Francis, London, 1968.
- (10) J. R. Scherer, M. K. Go, and S. Kint, *J. Phys. Chem.*, **77**, 2108 (1973).

Coordination and Ionic Solvation

B. G. Cox, A. J. Parker, and W. E. Waghorne*¹

The Research School of Chemistry, Australian National University, Canberra, A.C.T. Australia (Received November 19, 1973; Revised Manuscript Received April 15, 1974)

Free energies of transfer of a variety of ions from pure solvents to binary solvent mixtures have been estimated by the application of an extrathermodynamic assumption to free-energy data from emf and solubility measurements. In addition, the composition of the inner-coordination spheres of several cations in solvent mixtures have been estimated from pmr spectroscopic results. These results have been compared to those calculated from the measured equilibrium constants for the coordination of the cation by the solvents, using a simple coordination model of ionic solvation in which variations in solvation energy are considered to arise solely from differences in the energy of complex formation between the ions and molecules of the component solvents, and in which interactions outside the first coordination sphere are considered to be constant. For ions in a variety of nonaqueous solvent mixtures, the agreement between measured free energies and those predicted by the model is excellent. In aqueous mixtures, deviations from the behavior predicted by the simple model are attributed to the effects of nonideality of the solvent components and interactions between the complexed ion and solvent molecules outside the first coordination sphere.

Introduction

A number of recent studies² have pointed out the inability of the Born equation to account satisfactorily for the changes in solvation energy of electrolytes on transfer from one medium to another. Indeed in many cases the sign of the free-energy change is incorrectly predicted. For

example, the transfer of silver halides from methanol ($\epsilon = 32.6$) to propylene carbonate ($\epsilon = 65$) is energetically unfavorable in all cases,³ while the opposite is predicted by the Born equation.

The unfavorable change in the free energy of anions from protic to dipolar aprotic media has been explained in

terms of hydrogen bond formation between the anion and protic solvents,⁴ and the anomalous free-energy changes of silver and cuprous ions on transfer from water to a variety of nitrile solvents^{5,6} has been interpreted as being the result of specific complexing of the ions by the nitriles.

In view of the failure of Born type treatments and the qualitative success of consideration of specific interactions to account for these changes in ionic solvation energy, it was decided to see if changes in ionic free energy with changes in medium could generally be accounted for in terms of the coordination of the ion by the solvent molecules.

If differences in specific ion-solvent interactions determine a significant part of the free energy of transfer of ions between different media, this should be reflected in the behavior of ions in mixed solvents, where the different solvent molecules can compete for coordination sites on the ion.

The estimation of the free energy of transfer of individual ions between different media can be carried out with a reasonable degree of confidence by the use of several assumptions^{3,7,8} and this technique has been applied to some systems involving binary solvent mixtures.^{9,10} A second useful technique is the estimation of changes in the inner-coordination sphere of the ion, by proton magnetic resonance spectroscopy,¹¹⁻¹³ as the composition of the binary mixture is changed.

In this paper we report studies of a variety of ions in several binary solvent mixtures, by both of these techniques, and relate the results to a simple coordination model of ionic solvation.

Experimental Section

Solvents. Dimethyl sulfoxide and propylene carbonate were twice fractionally distilled under reduced pressure (1-3 mm) from calcium hydride and calcium sulfate, respectively. Acetonitrile was purified by successive distillation from phosphorus pentoxide and calcium hydride, after initial drying with calcium hydride.¹⁴ Water was distilled from an all-glass still. Acetone was fractionally distilled from calcium hydride. Methanol was dried over activated magnesium turnings¹⁵ and fractionally distilled.

Electrolytes. All salts were dried at 1-3-mm pressure for at least 24 hr before use. The purity of salts was determined by silver halide titration, or by atomic absorption spectroscopy, and water content was determined by Karl Fischer titration.

The following salts were analytical grade, having purity greater than 99% of analysis, and were dried at the temperature, and to the hydration numbers, indicated in parentheses.

Silver perchlorate (60°, anhydrous), cupric perchlorate (60°, 5H₂O), ferrous perchlorate (40°, 7-8H₂O), ferric perchlorate, (40°, 10H₂O), sodium perchlorate (100°, anhydrous). Tetraethylammonium picrate (60°, anhydrous) was prepared by neutralizing tetraethylammonium hydroxide (10% aqueous solution, Eastman chemicals) with a methanolic solution of picric acid and recrystallizing the product twice from methanol. Tetrabutylammonium chloride (60°, anhydrous) was recrystallized twice from dimethylacetamide and washed with dry ether. Potentiometric measurements were made with a Radiometer type 26 pH meter, having an expanded scale, accurate to ±1 mV.

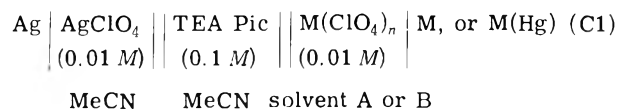
Proton magnetic resonance (pmr) measurements were made with a JEOL Mini Mar 100 spectrometer equipped

with a frequency counter having an accuracy of ±0.1 Hz and were carried out at the normal probe temperature (32°).

Sodium amalgam (0.2% w/w) was prepared by adding triply distilled mercury to the appropriate amount of sodium under a layer of toluene.¹⁵

Results

Free Energies of Transfer of Individual Ions ΔG_{tr} . Values of ΔG_{tr} of silver, sodium, cuprous, and ferrous ions in all solvent systems where they were studied, and of the cupric ion in the DMSO-H₂O systems were estimated by assuming that there is a negligible liquid junction potential in cell C1, where TEA Pic is tetraethylammonium picrate.



It has been shown that this assumption gives acceptable values of ΔG_{tr} for individual ions³ and it is the simplest to use of the available extrathermodynamic assumptions for the estimation of ΔG_{tr} . The assumption is expected to give estimates within ±0.5 kcal of the correct value.³

Values of $\Delta G_{tr}(\text{M})$ between any two solvents A and B were calculated from the potentials of cell C1 and eq 1

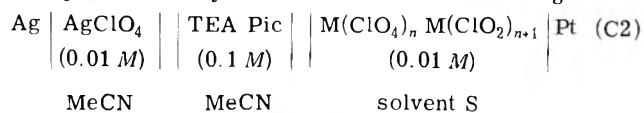
$$\Delta G_{tr}(\text{M}) = \frac{-nF}{4.184}(E_A - E_B) \quad (1)$$

where n is the number of electrons involved in the overall cell reaction, F is Faraday's constant, E_A and E_B are the potentials of cell C1 for the two solvents A and B, and the factor 4.184^{-1} converts the results to calories (from joules).

For cells C1 in which M was copper or silver, the electrodes were metallic wires (99.99% pure) and were cleaned before each measurement by scraping with a mild abrasive. When M was sodium the electrode was a freshly prepared 0.2% sodium amalgam in the form of a dropping amalgam electrode. Measurements on the iron system were carried out at an electrode of reduced iron powder placed over a platinum wire contact.¹⁶ The iron measurements were carried out in a drybox, under an atmosphere of nitrogen, and after a 30-min equilibration period. The results for the ferrous-iron couples were reproducible and stable throughout the period 30-60 min. However, the value for the aqueous system was consistently 20 mV more positive than the literature value.^{16,17}

Randall and Frandsen¹⁶ reported that the potential of the cells used to measure the ferrous-iron couple decreased gradually until it reached a stable value after about 100 days; therefore the high result is most likely due to nonequilibration of the system. No correction was applied for this effect and it was assumed that the difference from the equilibrium value was the same in each solvent mixture.

Values of ΔG_{tr} for ferric ions, and for cupric ions in the acetonitrile containing systems, in which cuprous ions were stable, were estimated from the potentials of cell C2 and eq 2, where all symbols have their usual meanings



$$\Delta G_{tr}(\text{M}^{n+1}) = \frac{-nF}{4.184}(E_A - E_B) + \Delta G_{tr}(\text{M}^n) \quad (2)$$

All cells gave steady reproducible potentials provided that sufficient care was taken to deaerate the solutions with nitrogen.

Measurements involving cupric and ferrous perchlorates in anhydrous media were complicated by the presence of water in the solid salts. In the cases of ferrous and cupric potentials in MeCN, it is likely that the true potentials in the anhydrous media would be higher than those measured in the presence of this water.¹⁸ In the MeCN-PC system the presence of water would lower the potential in all solvent mixtures, and would tend to reduce the changes in the solvation energy of the cupric ion. While this would affect the values determined, it would not be expected to change the form of the variations, which show the same qualitative behavior as those involving some anhydrous salts in the same media.

Values of ΔG_{tr} for anions were determined from the solubility products of silver halides in the appropriate media, and the values of ΔG_{tr} by eq 3 where A and B are the reference and test solvents, respectively.

$$\Delta G_{tr}(X^-) = RT \ln \frac{K_{sp}(AgX)A}{K_{sp}(AgX)B} - \Delta G_{tr}(Ag^+) \quad (3)$$

For this work no corrections were made to the solubility products for Debye-Hückel activity effects, but as these corrections are commonly 0.1–0.3 kcal mol⁻¹ for dilute solutions in solvents having moderate dielectric constants,³ and in addition largely cancel when values are compared, no significant change in the results would arise from such corrections.

Table I lists the cell potentials of each of the redox couples studied, the solubility products of silver chloride in MeCN-H₂O mixtures, and the values of ΔG_{tr} of the ions studied.

Equilibrium Constants. Equilibrium constants for the complexes formed between silver ions and acetonitrile or dimethyl sulfoxide in propylene carbonate were calculated¹⁹ from the results of potentiometric titrations of 0.01 M solutions of silver perchlorate in propylene carbonate with solutions containing 0.5 M ligand and 0.01 M silver perchlorate. These results are shown in Table II, together with results for a variety of other systems reported in the literature.¹⁹ Ligand concentrations are expressed as volume fractions (ϕ) and are simply related to the corresponding molar concentration (c) by $\phi_A = c_A M_A / 1000 \rho_A$, where for ligand A, M_A is the molecular weight of A and ρ_A is the density of pure A.

Solvation Numbers of Ions. The fraction of the inner-sphere solvation sites occupied by one of the solvent components was estimated by pmr spectroscopy from the difference in the chemical shift of the solvent protons in the solvent mixture and in an electrolyte solution in the solvent mixture.

Chemical shifts (δ) were measured relative to either cyclohexane or sodium 3(trimethylsilyl)propanesulfonate (TPS) as an internal standard. TPS was used as standard in solvent mixtures in which cyclohexane was too insoluble. Where both standards could be used, agreement between the measurements based on the two standards was within experimental error for all electrolytes except cupric perchlorate, where the two values differed by ~ 2.5 Hz.

Changes in the chemical shift of the solvent protons, due to the presence of electrolytes, were found to vary linearly with electrolyte concentration up to 1.0 M for silver and sodium perchlorates and to 0.15 M for cupric perchlorate.

The difference in the chemical shift of the solvent protons in the presence and absence of an electrolyte ($\Delta\delta$) is caused by changes in the chemical shift of solvent molecules in the inner-solvation spheres of the anion and cation, and of those in the bulk solvent. Since there is rapid exchange of solvent molecules among these three environments, only one line is observed and its chemical shift is given¹¹ by

$$\Delta\delta = p^+\delta^+ + p^-\delta^- + p^0\delta^0 \quad (4)$$

where δ^+ , δ^- , and δ^0 are the chemical shifts of solvent molecules around the cation, anion, and in the bulk solvent, respectively, and p^+ , p^- , and p^0 are the fractions of the solvent molecules in each environment. It was assumed that the effects of the addition of an electrolyte on the bulk solvent and internal standard were the same so that $\Delta\delta$ is given by

$$\Delta\delta = p^+\delta^+ + p^-\delta^- \quad (5)$$

The measured values of $\Delta\delta$ for silver perchlorate in pure DMSO (+3.3) and MeCN (+4.1) were divided into contributions from $p^+\delta^+$ and $p^-\delta^-$ by the method of Strehlow and Schneider.¹¹ The chemical shifts (δ) of the protons in MeCN and DMSO were measured in solutions containing 2% of these solvents, and varying concentrations of silver perchlorate in PC. Since DMSO and MeCN form complexes with silver ions in PC they are preferentially included in the inner coordination of the silver ions. Extrapolation of plots of the inverse of the chemical shift (δ^{-1}) against the inverse of the electrolyte concentration, to infinite electrolyte concentration ($[AgClO_4]^{-1} = 0$) at which point all of the MeCN or DMSO would be in the inner-coordination sphere of the silver ions, gave values of 40.3 and 33.3 for δ^+ in DMSO and MeCN, respectively, in the presence of silver ions. Assuming a value of 4 for the coordination number of silver ions these give values of +3.5 and +5.7 for $p^+\delta^+$ in pure MeCN and DMSO containing 0.5 M silver ions. These values, combined with the measured $\Delta\delta$ values, give +0.6 and -2.4 for $p^-\delta^-$ in these solutions containing 0.5 M perchlorate ions.

A second possibility for determining $p^+\delta^+$ would be to replace the solvent molecules in the inner-coordination sphere of the cation with a stronger complexing ligand, and observe the change $\Delta\delta$, which results from the reduction of p^+ . Dimethylthioformamide (DMTF) complexes strongly with silver ions in the first and second coordination positions and less strongly in the third and fourth positions.²⁰ The values of $\Delta\delta$ for 0.5 M silver perchlorate solutions in the presence of 2.5 M DMTF in MeCN and DMSO were -0.4 and +1.2, respectively. If the DMTF replaced three of the solvent molecules from the inner-coordination sphere of the silver ions, these values would be expected to be -1.0 and +1.5, respectively. The agreement between these calculated and measured results lends good support to the values determined by the methods of Schneider and Strehlow.¹¹

In the remaining work the values of $p^+\delta^+$ of 5.7 in DMSO and 3.5 in MeCN determined from the method of Schneider and Strehlow¹¹ were used.

To determine the variation in $p^+\delta^+$ through a range of solvent compositions from the measured $\Delta\delta$ values it was necessary to estimate the change in $p^-\delta^-$ over the same range. The simplest systems to consider were those involving the paramagnetic cupric ion, since the $\Delta\delta$ values are much larger than the $p^-\delta^-$ values due to the perchlorate anion so that the measured $\Delta\delta$ can be equated with

Cu^{2+}	(+14) ^a	-137	-311	-344	-380	-454	-492	-519	-593
$\Delta E, \text{Cu}/\text{Cu}^+$	0.0	-3.5	-7.5	-8.0	-9.1	-10.8	-11.7	-12.3	-14.0
ΔG_{tr}									
Cu^{2+}	+338	+439	+519	+579	+620	+652	+673	+690	+729
$\Delta E, \text{Pt}/\text{Cu}^+$	0.0	-1.2	-3.4	-2.5	-2.6	-3.6	-3.8	-4.2	-5.0
ΔG_{tr}									
Me₂CO									
Ag^+	+308	+255	+220	+169	+105	+79	+51	0	0
$\Delta E, \text{Ag}/\text{Ag}^+$	0.0	-1.2	-2.0	-3.2	-4.7	-5.3	-5.9	-7.1	-7.1
ΔG_{tr}									
MeOH									
Ag^+	+270	+239	+210	+185	+153	+95	+73	+50	0
$\Delta E, \text{Ag}/\text{Ag}^+$	0.0	-0.8	-1.4	-2.0	-2.7	-4.1	-4.6	-5.1	-6.3
ΔG_{tr}									
DMSO-MeCN									
$\phi(\text{DMSO})$	0.0	0.02	0.04	0.06	0.09	0.13	0.17	0.23	0.33
Na^+	-2294	-2324	-2349	-2368	-2399	-2423	-2441	-2467	-2497
$\Delta E, \text{Na}^+$	0.0	-0.7	-1.3	-1.7	-2.4	-3.0	-3.4	-4.0	-4.7
$(\text{Hg})/\text{Na}^+$									
ΔG_{tr}									

^a Abbreviations DMSO, dimethyl sulfoxide, PC, propylene carbonate. All values at 25°, emf values are for 0.01 M solutions of the perchlorate salt and are measured against the Ag|AgClO₄(0.01 M)|| couple in MeCN. ΔG_{tr} values in kcal mol⁻¹. ^b Measured against a 0.2% sodium amalgam. ^c Measured in the presence of 0.01 M HClO₄. ^d Measured in the presence of 0.01 M NEt₄ClO₄. ^e From B. Kratochvil and R. Long, *Anal. Chem.*, **42**, 43 (1970). ^f These apply to MeCN-PC, MeCN-Me₂CO, and MeCN-MeOH mixtures. ^g By extrapolation of the measured curve to [MeCN] = 0. ^h $\phi(\text{MeCN})$ values are the same for each of the cosolvents.

the $p^+\delta^+$ values. The $\Delta\delta$ values (see paragraph at end of paper regarding supplementary material) of the cupric ion vary in the same way as the ΔG_{tr} values listed in Table I in both MeCN-H₂O and DMSO-H₂O solvent systems. In addition, if $\Delta G_{\text{tr}}(\text{ClO}_4^-)$ parallels those of other anions in the solvent mixtures, the $\Delta\delta$ values of the electrolytes involving diamagnetic ions parallel the corresponding ΔG_{tr} values, and it could be reasonably assumed that the $\Delta\delta$ values due to the individual ions would vary in the same way as their ΔG_{tr} values. Thus, it was assumed that $p^-\delta^-$ of the perchlorate ion would parallel $p^+\delta^+$ of the sodium ion in MeCN-H₂O mixtures, and would be constant in the DMSO-H₂O and MeCN-PC systems, since free-energy changes in these systems would be expected to be small (<1 kcal mol⁻¹).^{3,7}

From the measured $\Delta\delta$ values and $p^-\delta^-$ values estimated in the above way, $p^+\delta^+$ values were calculated for the cuprous, silver, and sodium ions in the various media from eq 5. The fraction of the inner-solvation sphere sites of an ion occupied by one of the component solvents, B, [$n(\text{B})/n$] was calculated from eq 6, where c is the molar concentration of the component solvent, B, and the subscript zero refers to values in pure solvent B.

$$n(\text{B})/n = (p^+\delta^+)c / (p^+\delta^+)_0 c_0 \quad (6)$$

Despite some uncertainty about the assumptions used to divide the measured $\Delta\delta$ values into anion and cation contributions, several factors make the calculated $n(\text{B})/n$ values appear reasonable. The corrections for $p^-\delta^-$ in the MeCN-H₂O and MeCN-PC systems were small, so that errors could have only minor effects; and in the DMSO-H₂O systems there was good qualitative agreement between the variation in $p^+\delta^+$ values for the cupric ion, which were essentially independent of the assumptions, and those of the sodium ion. Moreover, the relative changes in $p^+\delta^+$ for any two cations in a solvent system are independent of the assumptions used to determine $p^-\delta^-$, so that qualitative conclusions about the relative preferences of two cations for the component solvents are unaffected by these assumptions.

Discussion

(i) *Coordination Model of Ionic Solvation.* In this section the implications of an idealized model in which the free energy of transfer (ΔG_{tr}) of ions between different solvents results entirely from differences in energy of coordination of the solvents with the ions are considered. It is assumed that the interactions of the ion with solvent molecules outside its primary coordination sphere are independent of the medium. It is further assumed that, in mixed solvent, the differences in the intermolecular forces are small so that solvent concentrations rather than activities may be used to describe the solvent composition. In mixed solvents the concentration of each component solvent is expressed as a fraction of its molar concentration in the pure solvent and is given the symbol ϕ (this fraction is equivalent to the volume fraction).

The solvation of an ion M, with a coordination number n , in solvents A and B may be considered in terms of equilibria I and II, where M₀ represents the unsolvated ion in a common reference state (e.g., *in vacuo*) and MA_n and MB_n refer to ion M coordinated by A and B respectively.

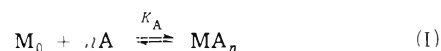


TABLE II: Equilibrium Products^a for Complex Formation at 25°

Ion	Ligand	Solvent	Log β_1	Log β_2	Log β_3	Log β_4
Ag ⁺ ^b	MeCN	MeOH	2.4	3.8	5.0	
Ag ⁺ ^b	MeCN	Me ₂ CO	2.3	4.1	5.5	
Ag ⁺ ^b	MeCN	EtNO ₂	2.4	5.4	7.8	9.6
Ag ⁺ ^b	MeCN	H ₂ O	2.0	3.4		
Ag ⁺ ^c	MeCN	PC	3.0	5.2	6.9	
Ag ⁺ ^c	DMSO	PC	3.3	5.9	7.9	9.5
Cu ⁺ ^b	MeCN	H ₂ O		6.5	8.0	

^a Solvent and ligand concentrations expressed in volume fraction concentrations scale (eq 8). ^b Values from ref 19. ^c This work.

TABLE III: Comparison of ΔG_{tr} for Ions between a Variety of Solvents from Eq 7 and from the Potentials of Cell A

Ion	Solvent A	Solvent B	ΔG_{tr} , kcal mol ⁻¹ (calcd from eq 7)	ΔG_{tr} , kcal mol ⁻¹ (meas by $E_{ij} = 0$ for cell C1)
Ag ⁺	MeOH	MeCN	-6.8	-6.3 ^a
Ag ⁺	Me ₂ CO	MeCN	-7.5	-7.3 ^a
Ag ⁺	R-NO ₂ ^c	MeCN	-13.1	-12.4 ^a
Ag ⁺	H ₂ O	MeCN	-4.6	-4.2 ^a
Ag ⁺	PC	MeCN	-9.4	-9.5 ^d
Ag ⁺	PC	DMSO	-12.9	-12.9 ^d
Cu ⁺	H ₂ O	MeCN	-10.9	-11.5 ^d

^a Reference 3. ^b From β_n values in Table II. ^c β_n were measured in EtNO₂ while ΔG_{tr} was measured for MeNO₂. ^d This work.

from the assumption of negligible liquid junction potential in cell C1. The agreement between the two sets of values is excellent.

Figure 1 shows the variation of $\Delta G_{tr}(Ag^+)$ in four solvent mixtures as estimated from the assumption of negligible liquid junction potential in cell C1, and as calculated from the equilibrium constants listed in Table II (eq 16). The agreement between these pairs of curves, which is better than 0.5 kcal in virtually all instances, provides strong support for the coordination model of solvation. Thus, for example, from equilibrium constants for complex formation between Ag⁺ and CH₃CN at infinite dilution in propylene carbonate it is possible to reproduce the free energy of transfer of Ag⁺ from pure propylene carbonate to mixtures of propylene carbonate and acetonitrile and to pure acetonitrile. This means that the free energy of the coordinated silver ions must be essentially independent of the surrounding medium as deviations from ideality of the component solvents should be small.²¹

In addition to the four sets of data for the silver ion, Figure 1 shows the variation of $\Delta G_{tr}(Cu^+)$ in the MeCN-PC system as estimated from the assumption of negligible liquid junction potential. This curve can be duplicated by calculation of eq 16 using the equilibrium products $\log \beta_1 = 7.4$, $\log \beta_2 = 8.9$, $\log \beta_3 = 10.3$, $\log \beta_4 = 11.3$.

Figure 2 shows the variation in the inner-coordination sphere of silver and cuprous ions as estimated from pmr measurements and as calculated *via* eq 19 from the appropriate equilibrium products. The estimated curves agree qualitatively with the calculated ones, and show the type of behavior predicted above. However, the quantitative agreement is not nearly so good as for the ΔG_{tr} values. This may be due to problems inherent in the estimation of $n(B)/n$ values. The estimated values depend upon the assumption that the solvent molecules outside the coordination sphere of the ion are affected to the same degree as

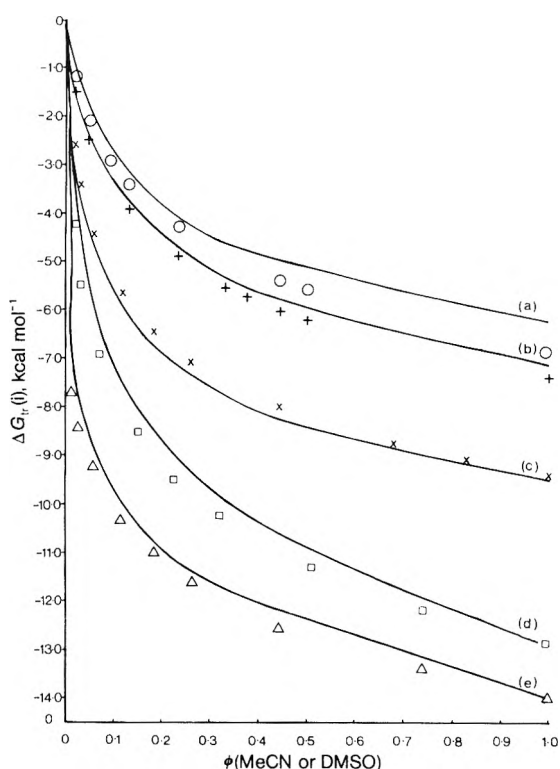


Figure 1. Comparison of calculated free energies of transfer of ions with those estimated from measurements in cell A. Solid lines refer to measured values: (a) O, Ag⁺ in MeCN-MeOH; (b) +, Ag⁺ in MeCN-Me₂CO; (c) x, Ag⁺ in MeCN-PC; (d) □, Ag⁺ in DMSO-PC; (e) Δ, Cu⁺ in MeCN-PC.

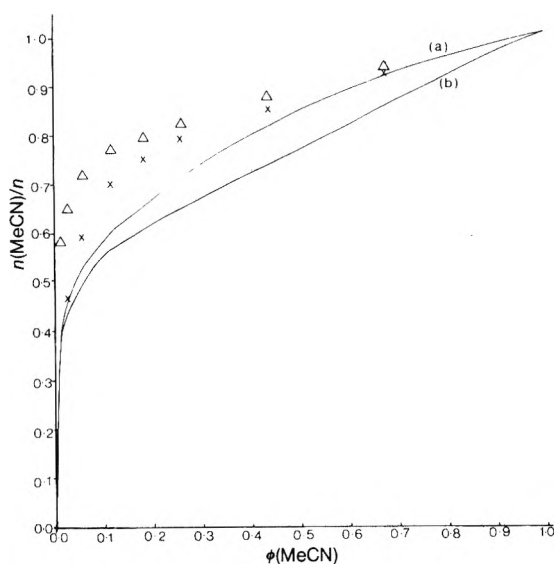


Figure 2. Comparison of calculated $n(\text{MeCN})/n$ values for Ag⁺ and Cu⁺ in MeCN-PC mixtures with values estimated from pmr measurements (solid lines): (a) x, Ag⁺; (b) Δ, Cu⁺.

the internal standard, by the field of the ion. Since the solvent molecules are polar and the internal standard (cyclohexane) is nonpolar, it is possible that the solvent molecules are slightly more affected than the standards by the fields of the ions. This would lead to effective solvation numbers greater than the number of molecules in the primary coordination sphere and so would cause the measured $n(B)/n$ values to change more slowly than the composition of the coordination sphere. Calculated values of $n(B)/n$ are also more susceptible to errors in β_i and effects

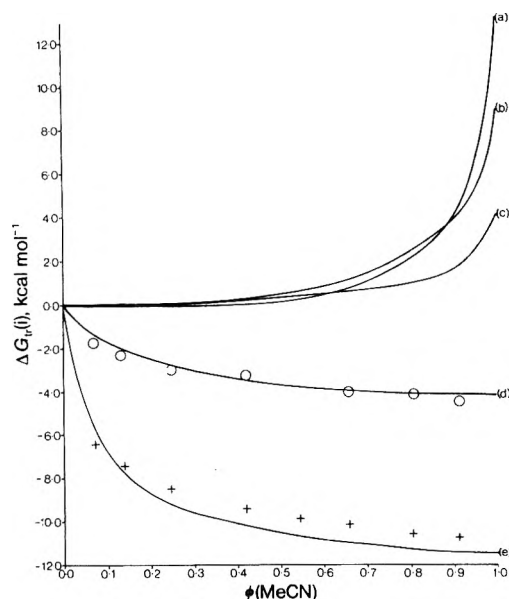


Figure 3. Free energies of transfer of ions from water to mixtures of water and acetonitrile. Solid lines refer to measured values: (a) Cu^{2+} ; (b) Cl^- ; (c) Na^+ ; (d) Ag^+ , \circ calculated; (e) Cu^+ , $+$ calculated.

due to solvent-solvent interactions than are ΔG_{tr} values which are logarithmically related to the equilibrium constants.

It should be noted that the cupric and sodium ions where they have been studied (see Table I) have the same general variation in ΔG_{tr} as those shown in Figure 1. That is, the type of behavior shown in Figure 1 is not specific to those ions which would be expected to form strong complexes but is a more general phenomenon.

The solvent systems considered in Figures 1 and 2 are those for which the mutual heats of solution are small²¹ and so, presumably, there are not large differences in the intermolecular forces for the components and their mixtures. Therefore these systems would be expected to be described by eq 16 and 19 without using the activities of the component solvents. The mutual heats of solution of MeOH and MeCN are considerably larger than those of the other systems, and it is this system for which there is the greatest difference between the calculated and estimated $\Delta G_{\text{tr}}(\text{Ag}^+)$ values.

Studies of ionic solvation involving aqueous media are complicated by the strong hydrogen bond interactions between water molecules which cause considerable solvent structuring of high water concentrations, and by the strong interactions which can occur between water molecules and those of other component solvents which are strong acids or bases. The MeCN-H₂O and DMSO-H₂O solvent systems can be considered in terms of these interactions.

Figures 3 and 4 show the variation in $\Delta G_{\text{tr}}(M)$ for the chloride ion, and several cations in MeCN-H₂O mixtures and the variation in the composition of the inner-coordination sphere for silver, sodium, and cupric ions in the same mixtures.

It is clear that in this system the behavior of all of the ions studied is in qualitative agreement with the predictions of the simple coordination model. Thus, considering the sodium ion, which is typical of those ions having an unfavorable free-energy change from water to MeCN ($\Delta G_{\text{tr}} > 0$) there is little increase in the fraction of the

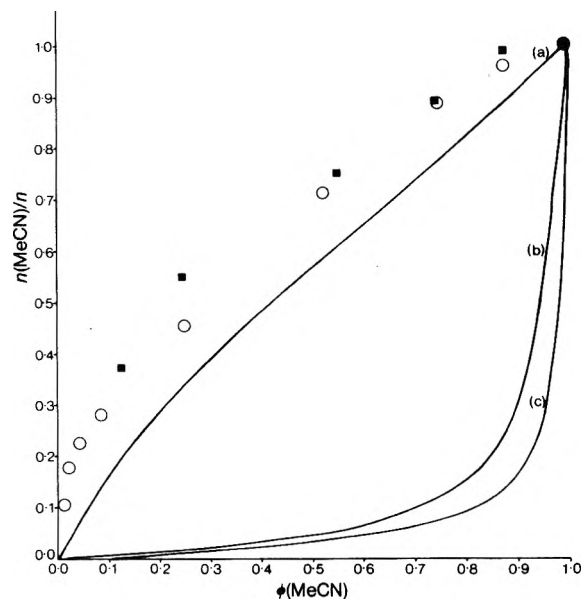


Figure 4. $n(\text{MeCN})/n$ values for ions in mixtures of acetonitrile and water estimated from pmr measurements (solid lines): (a) Ag^+ , \circ , calculated values, \blacksquare , values from ref 11; (b) Na^+ ; (c) Cu^{2+} .

inner-coordination sphere occupied by MeCN until the H₂O concentration becomes very low, and then there is a rapid rise in $n(\text{MeCN})/n$ to unity in pure MeCN. Accompanying the variation in $n(\text{MeCN})/n$ is the change in $\Delta G_{\text{tr}}(\text{Na}^+)$, which is slightly unfavorable until the low water region is reached, and then becomes rapidly more unfavorable as the H₂O concentration decreases to zero. This behavior contrasts strongly with that of the silver ion which, like the cuprous ion, has a favorable free-energy change from H₂O to MeCN ($\Delta G_{\text{tr}} < 0$). In this case there is a relatively rapid inclusion of MeCN in the inner-coordination sphere, and an accompanying favorable change in the free energy of the ion.

Equilibrium constants for complex formation of Ag^+ and Cu^+ with CH_3CN in dilute aqueous solutions have previously been reported¹⁹ and indicate that the major energy changes accompany formation of $\text{Ag}(\text{CH}_3\text{CN})_2^+$ and $\text{Cu}(\text{CH}_3\text{CN})_3^+$ species, respectively. By assuming that replacement of the remaining water in the coordination sites of Ag^+ and Cu^+ by CH_3CN occurs without further change in free energy, i.e., ($K_i = 1$), $\Delta G_{\text{tr}}(\text{Ag}^+)$, $\Delta G_{\text{tr}}(\text{Cu}^+)$, and $n(\text{CH}_3\text{CN})/n$ have been calculated from eq 16 and 19. It can be seen from Figures 3 and 4 that the agreement with the simple model is better than expected, as it is known from vapor pressure studies²² that the activities of CH_3CN and H_2O in the mixtures are considerably higher than their concentrations. This behavior can be understood if it is assumed that there are unfavorable interactions, such as those between the component solvents, between some of the solvent molecules coordinated to the ion and those of the surrounding medium raising the activities of the coordinated ions.

In the absence of measured values, we attempted to find a reasonable set of equilibrium constants that, when used in eq 16, would reproduce the estimated variation in ΔG_{tr} for the cupric and sodium ions (which are preferably coordinated by water) in the acetonitrile-water mixtures. This, however, was not possible as in all cases, if the concentration of the component solvents were used, the calculated values varied more slowly than those estimated from experiments, whereas if the activities of the compo-

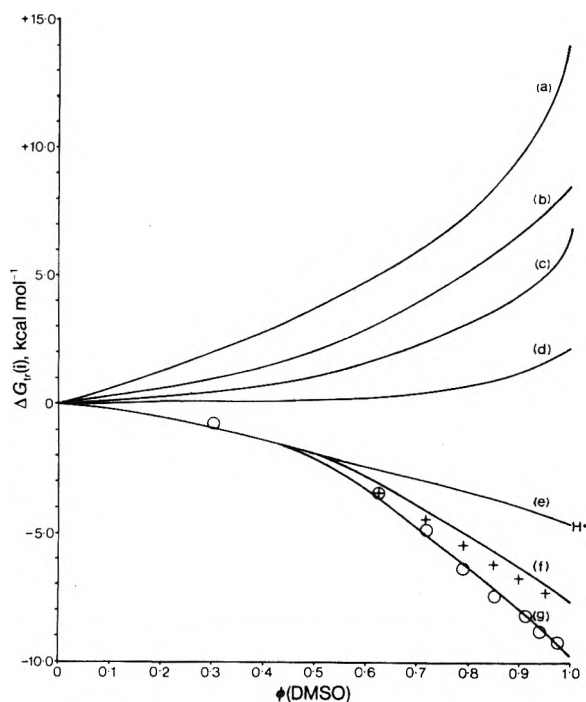


Figure 5. Free energies of transfer of ions from water to mixtures of water and dimethyl sulfoxide. Solid lines refer to measured values: (a) OAc^- (ref 9); (b) Cl^- (ref 9); (c) N_3^- (ref 9); (d) I^- (ref 9); (e) H^+ (ref 9); (f) Ag^+ , + calculated values; (g) Cu^{2+} , O calculated values.

nents, which are considerably greater than their concentrations,²² were used, the calculated values varied too rapidly. It seems that the activity coefficients of these coordinated ions are varying in a similar manner to those of the component solvents leading to partial, but not complete cancellation of the effects.

Figures 5 and 6 show the variation of ΔG_{tr} for a number of cations and anions from H_2O to $\text{DMSO-H}_2\text{O}$ mixtures, and the variation in the coordination sphere of the silver, cupric, and hydrogen ions in these mixtures. The variation of ΔG_{tr} of the anions in these mixtures agrees qualitatively with that predicted by the model. However, that of the cations is apparently significantly different from that predicted by the model and observed in the other solvent systems. The variation in the cation results can be simply explained in terms of the strong $\text{DMSO-H}_2\text{O}$ interactions which vapor pressure studies indicate²³ significantly lower the DMSO activity in aqueous media (for example, when ϕ_{DMSO} is 0.30, the DMSO activity is only 0.013 of its value in pure DMSO) although the H_2O activity closely approximates its concentration in the mixtures. When the solvent concentrations were replaced by their activities it was possible to find reasonable equilibrium products (for Cu^{2+} , $\log \beta_1 = 2.60$, $\log \beta_2 = 5.00$, $\log \beta_3 = 6.00$, $\log \beta_4 = 6.60$, $\log \beta_5 = 7.00$, and $\log \beta_6 = 7.20$; for Ag^+ , $\log \beta_1 = 2.24$, $\log \beta_2 = 3.93$, $\log \beta_3 = 5.06$, and $\log \beta_4 = 5.63$) which when used in eq 16 would reproduce the ΔG_{tr} variations of the silver and cupric ions in these mixtures (Figure 5). While this ability to "fit" the estimated curves with calculations based on eq 16 and the activities of the component solvents does not prove that the above explanation is correct, it strongly supports it.

The variation of $n(\text{DMSO})/n$ for the proton and to a lesser degree those for the cupric and silver ions (Figure 6) in the $\text{DMSO-H}_2\text{O}$ mixtures indicates that more H_2O is included in the ionic coordinations sphere than would be

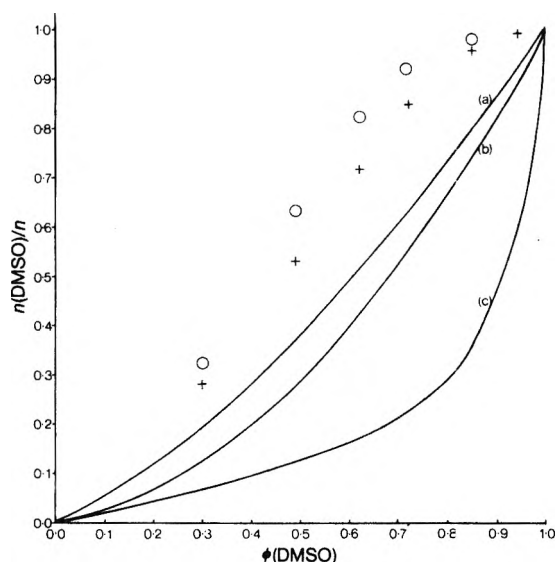


Figure 6. $n(\text{DMSO})/n$ values for ions in mixtures of dimethyl sulfoxide and water (solid lines): (a) Ag^+ , O calculated values; (b) Cu^{2+} , + calculated values; (c) H^+ (ref 24).

expected on the basis of the coordination model. This behavior for the proton, which actually shows preferential solvation by H_2O , although $\Delta G_{tr}(\text{H}^+)$ from H_2O to DMSO is favorable (-4.8 kcal),⁹ has been explained in terms of greater stabilization of H_3O^+ which can form three hydrogen bonds to the surrounding medium²⁴ than of DMSO-H^+ which can form only one such bond. Similar stabilization should be available to those coordinated species containing H_2O in the coordination sphere relative to those containing DMSO , and this would increase the amount of H_2O above that predicted by the coordination model. Since this stabilization affects only the higher energy species $\text{M}(\text{H}_2\text{O})^{n+}$, and not the energy of the more stable species $\text{M}(\text{DMSO})^{n+}$, it would not be expected to have large effects on the total energy of the system. This is in contrast to the $\text{MeCN-H}_2\text{O}$ system where the unfavorable interactions apply to both coordinated species $\text{M}(\text{H}_2\text{O})^{n+}$ and $\text{M}(\text{CH}_3\text{CN})^{n+}$ and so considerably affect the energy of the whole system.

It is clear from the preceding discussion that the solvation of ions in the various pure solvents and solvent mixtures studied here can be explained largely and in some cases quantitatively in terms of the relative coordination energies between the various ions and solvents. That the variation of ΔG_{tr} values is not a function of a change in some bulk physical property of the system, such as dielectric constant, but rather is related to the changes in concentration of the component solvents is perhaps most clearly seen in the $\text{CH}_3\text{CN-H}_2\text{O}$ system. In this system two of the ions (Cu^+ and Ag^+) have favorable ΔG_{tr} values from H_2O to MeCN while the remaining ions studied (Cu^{2+} , Fe^{3+} , Fe^{2+} , Na^+ , H^+ , and Cl^-) all have unfavorable ΔG_{tr} values from H_2O to MeCN . In each case the free-energy changes little across the range of solvent composition in which the concentrations of the "better" solvent (i.e., MeCN for Cu^+ and Ag^+ and H_2O for the rest) is high; and then changes rapidly to the more unfavorable value as the last few per cent of the better solvent is removed. It is interesting that the chloride ion, which would be expected to hydrogen bond to H_2O molecules, shows the same sort of variation as do the proton, cupric, ferric, and ferrous ions which are strongly complexed through the

oxygen of the H₂O molecules, indicating that the type of specific ion solvent interaction has little effect on the variation of ΔG_{tr} with solvent composition. Similar variations are seen for the sodium ion for which interactions are presumably mainly electrostatic in nature.

Throughout this work the concentrations of the component solvents have been expressed as fractions of their concentrations in the pure liquid, on a molar scale (this is equivalent to the volume fraction scale), rather than the alternative mole fraction scale. This choice is largely dictated by the results of this work, that is, it is the concentration of the better solvent relative to its concentration in the pure liquid (volume fraction) and not the relative concentrations of "good" and "bad" solvent (mole fraction) which determines the solvation behavior of the ions in the solvent mixtures.

Supplementary Material Available. A table of the chemical shifts of solvent protons (in Hz) in the electrolyte solutions and the fractional solvation numbers of the ions in the mixed solvents will appear following these pages in the microfilm edition of this volume of the journal. Photocopies of the supplementary material from this paper only or microfiche (105 × 148 mm, 24 × reduction, negatives) containing all of the supplementary material for the papers in this issue may be obtained from the Journals Department, American Chemical Society, 1155 16th St., N.W., Washington, D. C. 20036. Remit check or money order for \$3.00 for photocopy or \$2.00 for microfiche, referring to code number JPC-74-1731.

References and Notes

- (1) Author to whom enquiries should be addressed at Department of Chemistry, University College, Belfield, Dublin 4.
- (2) J. I. Padova, "Modern Aspects of Electrochemistry," Vol. 7. J. O'M Bockris, Ed., Butterworths, London, 1972, p 1, and references therein.
- (3) R. Alexander, A. J. Parker, J. H. Sharp, and W. E. Waghorne, *J. Amer. Chem. Soc.*, **94**, 1148 (1972).
- (4) A. J. Parker, *Chem. Rev.*, **69**, 1 (1969).
- (5) R. C. Larson and R. T. Iwamoto, *J. Amer. Chem. Soc.*, **82**, 3239, 3526 (1960).
- (6) B. G. Cox, G. R. Hedwig, A. J. Parker, and D. W. Watts, *J. Amer. Chem. Soc.*, submitted for publication.
- (7) I. M. Kollhoff and M. K. Chantooni, *J. Phys. Chem.*, **76**, 7104 (1972).
- (8) O. Popovych, *Crit. Rev. Anal. Chem.*, **1**, 73 (1970).
- (9) J. Courtot-Coupes, M. le Demezot, A. Laouenan, and C. Madec, *J. Electroanal. Chem.*, **29**, 21 (1971).
- (10) O. Popovych, A. Gibofsky, and D. H. Berne, *Anal. Chem.*, **44**, 811 (1972).
- (11) H. Schneider and H. Strehlow, *Z. Phys. Chem.*, **49**, 44 (1966).
- (12) L. S. Frankel, J. R. Stengle, and C. H. Langford, *Can. J. Chem.*, **46**, 3183 (1968).
- (13) Y. Haas and G. Navon, *J. Phys. Chem.*, **76**, 1449 (1972).
- (14) J. F. Coetzee, G. P. Cunningham, D. K. McGuire, and G. R. Podmanashan, *Anal. Chem.*, **34**, 1139 (1962).
- (15) A. I. Vogel, "Textbook of Practical Organic Chemistry," Longmans, London, 1956.
- (16) Randall and M. Frandsen, *J. Amer. Chem. Soc.*, **54**, 40 (1932).
- (17) W. M. Latimer, "Oxidation Potentials," Prentice-Hall, Englewood Cliffs, N. J., 1952.
- (18) H. C. Mruthyunijaya and A. R. V. Murthy, *J. Electroanal. Chem.*, **15**, 200 (1967).
- (19) S. E. Manahan and R. T. Iwamoto, *J. Electroanal. Chem.*, **14**, 213 (1967).
- (20) W. E. Waghorne, unpublished results.
- (21) B. G. Cox, A. J. Parker, and W. E. Waghorne, *J. Amer. Chem. Soc.*, **95**, 1010 (1973).
- (22) A. M. von Vierk, *Z. Anorg. Chem.*, **261**, 283 (1950).
- (23) (a) J. Kenttamaa and J. Lindberg, *Suom. Kemistilehti B.* **33**, 98 (1960); (b) B. G. Cox and P. T. McTigue, *Aust. J. Chem.*, 1815 (1967).
- (24) P. T. McTigue and A. R. Watkins, *Aust. J. Chem.*, **25**, 777 (1972).

Effect of Structure on the Mesomorphic Properties of Cholesteryl Alkanoates. V. Electric Field Effects on a Uniaxial Smectic Phase of Mixtures of Cholesteryl Alkanoates¹

John M. Pochan* and Harry W. Gibson

Webster Research Center, Xerox Corporation, Webster, New York 14580 (Received March 20, 1974)

Publication costs assisted by Xerox Corporation

A uniaxial smectic phase has been studied in binary mixtures of cholesteryl esters. A branched ester is prerequisite for formation of the texture in mixtures. Surface interactions are also necessary but were not investigated in detail. The electric field induced transition between the uniaxial smectic texture and a birefringent scattering texture is not dependent upon a critical field, but rather appears analogous to nucleation phenomena in polymers, showing sporadic points of transformation, followed by growth of the transformed areas. Addition of a room temperature nematic material with negative anisotropy lowers the field required for the transition. The results are compared to the familiar cholesteric-nematic field induced transition.

Introduction

In previous work from this laboratory cholesteryl alkanoate structure has been related to the rate of nucleation of crystals in the supercooled liquid crystalline phases,^{2,3}

to the phase transition thermodynamic parameters of both the pure materials and binary mixtures of them,⁴ and to the pitch of the cholesteric mesophase.⁵ In the course of these studies a number of phase diagrams have been con-

structed,^{3,4,6} in several instances the existence of a unique spontaneously formed, thermally reversible uniaxially aligned smectic phase was noted.

Liquid crystals have been used in a variety of imaging systems.⁷ Most devices incorporating liquid crystals are made from nematic and/or cholesteric materials. Imaging and display systems utilize changes in the molecular alignment of the various textures of the mesophases by external perturbations. However, few studies of the effect of external perturbations, *i.e.*, electric and magnetic fields, on the smectic mesophase have been reported,⁸ probably because of the high viscosity of the phase.

Our interest in the effects of shear⁹⁻¹⁴ and combinations of shear and electric field¹⁵ on texture transformations in liquid crystalline systems led us to a study of the effect of electric field on the spontaneously uniaxially aligned smectic mesophase mentioned above. The effects of molecular structure on the formation of this uniaxial phase as well as the effects of doping with a nematic material on the field assisted transition of the phase are also reported.

Experimental Section

Cholesteryl alkanoates were prepared and purified as previously reported.^{3,4,6b} *p*-Methoxybenzylidene-*p*-*n*-butylaniline (MBBA), Eastman, was used as obtained.

Mixtures were produced by melt mixing of the components. Optical observations were made with a Leitz Ortholux microscope containing a Mettler heating stage.

Field effect experiments were conducted at room temperature in tin oxide coated glass cells in order that optical observation could be made simultaneously. A 5490-Å filter was used with the microscope source to eliminate the possibility of infrared pick-up in a photocell mounted within the microscope (see Figure 1). Polarized light transmitted through the sample was monitored as a function of time and applied electric field. The effect of field is observed microscopically because of molecular realignment from the uniaxial phase (dark field in cross polars) to a scattering birefringent texture. This latter texture does not resemble any of the general smectic textures and is referred to herein as the birefringent texture.

Results and Discussion

Uniaxial Phase. Binary mixtures of cholesteryl nonanoate (CN) and cholesteryl 2(*S*)-methylbutyrate (C2MB*)^{6b} at certain compositions exhibit a stable smectic phase (Figure 2). As the temperature of the phase is lowered below the smectic-cholesteric transition, a focal conic texture of the smectic mesophase is observed. This is followed by a spontaneous, thermally reversible realignment of the phase to a uniaxial texture on a clean glass substrate. The phase is characterized as a positive uniaxial material, implying it is a smectic phase. X-Ray diffraction studies on a 50 wt % mixture of CN in C2MB* indicate that the room temperature thickness of the smectic planes is 23 ± 3 Å. This distance is approximately equivalent to the molecular length and this indicates a uniaxial phase with no molecular tilt. This uniaxial smectic phase may be the more generally labeled the smectic A phase.¹⁶ Similar uniaxial smectic phases have been found in other systems.^{6a} The common structural feature of all these systems is the presence of at least one branched cholesteryl alkanoate.^{6a} While all these systems have not been studied in detail, the results presented here are representative of the electric field effects.

It was noted that a requirement for this uniaxial phase

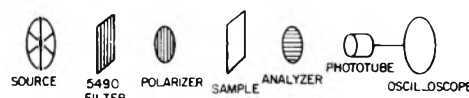


Figure 1. Experimental set-up for electrooptic field effect study.

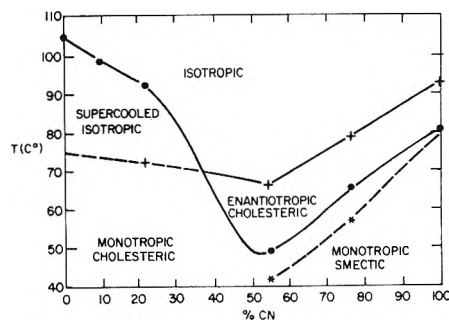


Figure 2. Phase diagram for cholesteryl nonanoate and cholesteryl 2(*S*)-methylbutyrate.

was the glass or tin oxidized coated surface of microscope slides and cover glasses used in these experiments. With thin samples ($<10 \mu$) the phase formed spontaneously. In thicker samples, movement of a cover glass was sometimes necessary to produce the uniaxial state from the smectic focal conic state. The uniaxial texture was also observed in a free standing drop of the mixture; however, spontaneous molecular alignment occurred only to a finite depth near the glass substrate. The effect of surface preparation was not studied systematically; however, it appears that surface interactions do control molecular arrangement and that these interactions are temperature dependent.

Electric Field Effects. Electric fields would be expected to affect the uniaxial smectic phase in one of two ways. (1) If the dielectric anisotropy of the molecule is negative, the application of field will cause molecular realignment with the long molecular axis perpendicular to the applied field. This orientation will be isotropic in a plane perpendicular to the applied field and the viewer and the sample will appear birefringent. (2) Impurities in the sample may cause ionic conduction and produce disturbances similar to the dynamic scattering mode in nematic liquid crystal systems.⁷ The latter effect would be expected to be dependent on the mobilities of such ionic materials within the liquid crystal matrix.

Figure 3 is a photograph of a phototube response during the field assisted birefringent texture transition for a 47.8 wt % mixture of CN in cholesteryl 2-ethylbutyrate (C2EB). In Figure 4 is a sequence of photomicrographs showing behavior of the sample as a function of time after electric field was applied. The phototube response is an S-shaped curve and is characteristic of all response curves obtained as a function of applied field. The field dependence of this curve was characterized by correlating the slope of the curve at 50% change in light intensity (dV/dt)_{50%} and the time needed to attain 50% change in light intensity ($t_{1/2}$) with applied electric field. The results are shown in Figure 5. The field dependences of the two variables are approximately inverse (Table I).

The S-shaped time dependence of the transformation is noteworthy. It is similar to that of the field assisted cholesteric-nematic transition;¹⁷ however, the time response in Figure 4 indicates that random areas within the uniaxial phase nucleate to a birefringent texture which then ad-

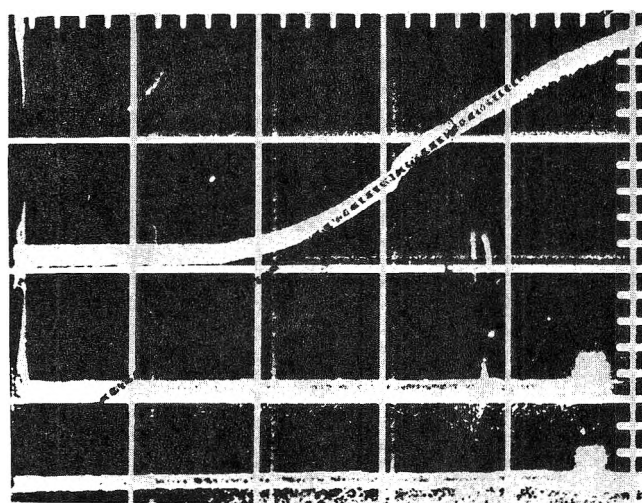


Figure 3. Oscilloscope response as a function of time for field induced uniaxial to birefringent texture transformation in smectic mesophase of 47.8% cholesteryl nonanoate-52.2% cholesteryl 2-ethylbutyrate. Horizontal scale is 1 sec per division.

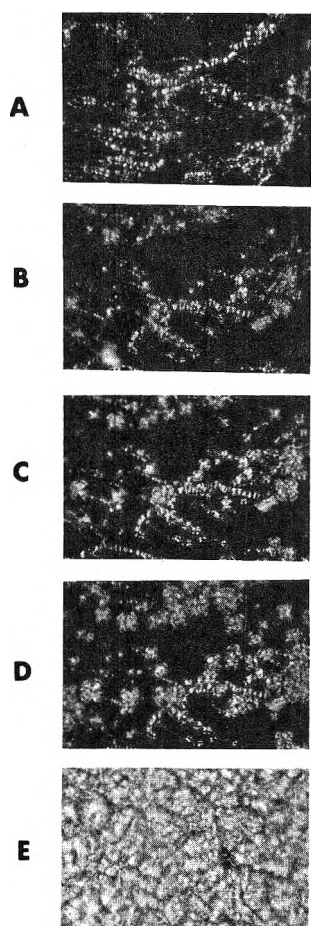


Figure 4. Photomicrograph sequence of field induced uniaxial to birefringent texture transformation in smectic mesophase (of 47.8% cholesteryl nonanoate-52.2% cholesteryl 2-ethylbutyrate) as a function of time after field ($20 \text{ V}/\mu$) application.

vances in place of the uniaxial state. This is in contrast to the cholesteric-nematic field assisted transition in which the entire state transforms at once.⁷ The S-shaped response is similar to that observed in nucleation studies of crystalline polymers.^{18,19} An induction period is appar-

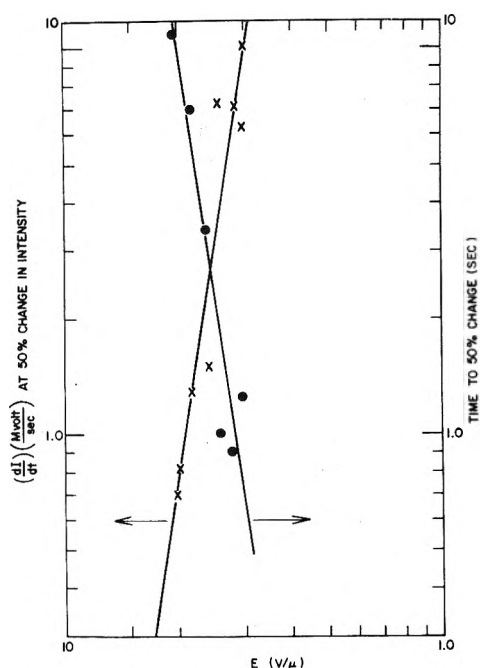


Figure 5. Log $(dV/dt)_{50\%}$ and log $t_{1/2}$ vs. electric field for 47.8/52.2 wt % cholesteryl nonanoate-cholesteryl 2-ethylbutyrate.

TABLE I: Slopes of Log $(dV/dt)_{50\% \text{ transmission}}$ and Log $(t_{1/2})$ vs. Log Electric Field for a Binary Mixture of Cholesteryl 2-Ethylbutyrate and Cholesteryl Nonanoate and Mixtures of the Two with MBBA

Mixture (CN/C2EB/MBBA), wt %	Slope	R (correlation coefficient)
A. $(dV/dt)_{50\%}$		
(47.8/52.2/0)	4.91 ± 1.58	0.84
(44.2/45.4/10.4)	3.88 ± 0.61	0.90
(42.0/44.3/13.7)	4.75 ± 0.78	0.93
B. $t_{1/2}$		
(47.8/52.2/0)	-5.41 ± 1.39	0.91
(44.2/45.4/10.4)	-3.59 ± 0.54	0.91
(42.0/44.3/13.7)	-5.23 ± 0.50	0.98

ently required before the transition takes place. The induction and growth may be similar to spontaneous nucleation followed by crystalline growth in supercooled systems.^{2,3,19,20} It appears in this system that the transition begins at specific spots and these spots grow in time (see Figure 4). With this type of transformation it appears that the transition is not a critical phenomenon, but one that occurs when enough perturbing force is present to cause certain areas to transform. These transformed areas do not appear to be the normal focal conic smectic texture.

The transformation time is on the order of seconds or less, while relaxation times to the initial uniaxial state are much longer, in the order of minutes to tens of minutes depending on the samples studied. The response times are at least an order of magnitude higher than those observed for the field induced cholesteric to nematic phase transition.²⁰ In order to facilitate the transformation from the birefringent texture to uniaxial smectic phase the sample was sheared. This process caused uniaxial alignment to take place almost immediately.

The transformation times in these binary systems are impractical for many imaging or display systems. In order

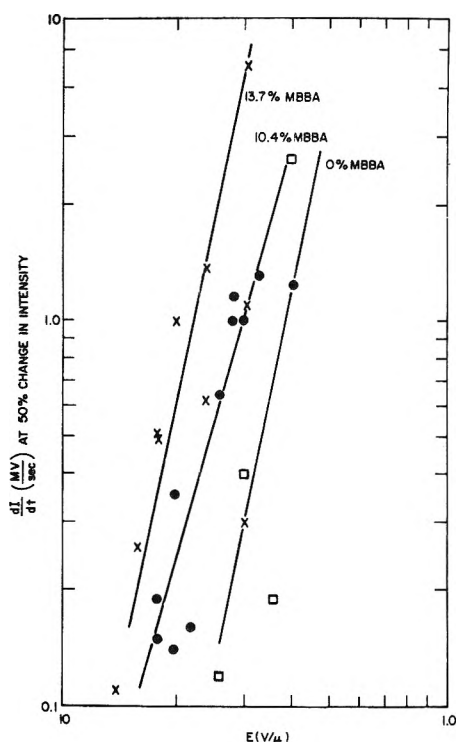


Figure 6. Log $(dV/dt)_{50\%}$ vs. electric field for ternary mixtures of cholesteryl nonanoate, cholesteryl 2-ethylbutyrate, and MBBA containing 0, 10.4, and 13.7 wt % MBBA (Table I).

to decrease the response time of the system, the room temperature nematic MBBA was added to binary mixtures of CN/C2EB. It was felt that the lower viscosity and negative dielectric anisotropy of MBBA would facilitate the field induced transition. The ternary system still exhibited the smectic phase at room temperature. At the higher MBBA concentrations, the uniaxial state was not as stable, *i.e.*, could be induced by shearing of the system, but relaxed to the normal focal conic in some areas. When this happened, experiments were conducted on the mixed systems. Results are displayed in Table I and in Figures 6 and 7. These data indicate the high field dependence of the transition. Nucleation and growth of the transformed areas occurred as in the binary system. Increasing the MBBA concentration in the mixtures lowered the field required for transition. Unfortunately, scatter in the data prevented determination of whether the speed of the system $(dV/dt)_{50\%}$ is also increased with increasing MBBA concentration.

Conclusions

In conclusion, a uniaxial smectic phase has been studied in binary mixtures of cholesteryl esters. A branched ester is prerequisite for formation of the texture in mixtures. Surface interactions are also necessary as the uniaxial state will form only near surface boundaries in a free standing mixture.

An electric field induced transition between the uniaxial smectic texture and a birefringent scattering texture has been studied. The transition is not dependent upon a critical field, but rather appears analogous to nucleation phenomena in polymers, showing sporadic points of transformation, followed by growth of the transformed areas. Addition of a room temperature nematic material with

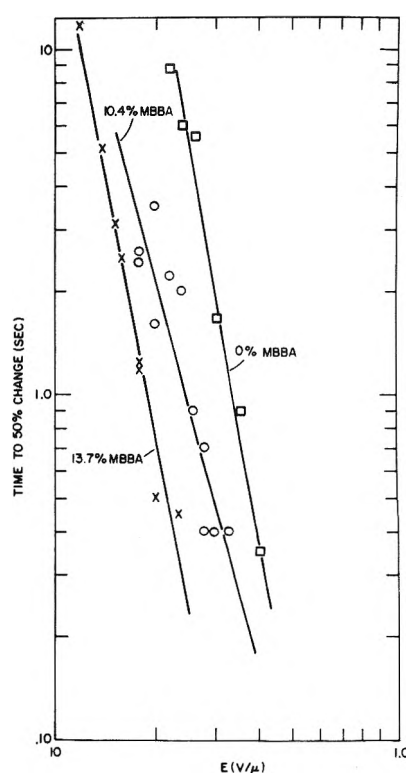


Figure 7. Log $t_{1/2}$ vs. electric field for ternary mixtures of cholesteryl nonanoate, cholesteryl 2-ethylbutyrate, and MBBA containing 0, 10.4, and 13.7 wt % MBBA (Table I).

negative anisotropy lowers the field required for the transition.

Acknowledgment. The authors wish to thank Dr. G. Fekete for the X-ray data and Professor P. DeGennes for helpful discussions concerning the uniaxial phase.

References and Notes

- (1) Parts I thru IV of this series are listed as ref 2 thru 5.
- (2) J. M. Pochan and H. W. Gibson, *J. Amer. Chem. Soc.*, **93**, 1279 (1971).
- (3) J. M. Pochan and H. W. Gibson, *J. Amer. Chem. Soc.*, **94**, 5573 (1972).
- (4) H. W. Gibson and J. M. Pochan, *J. Phys. Chem.*, **77**, 837 (1973).
- (5) H. W. Gibson, J. M. Pochan, and D. Hinman, "Liquid Crystals and Ordered Fluids," J. F. Johnson and R. S. Porter, Ed., Plenum Press, New York, N. Y., 1974, p 593.
- (6) (a) Additional phase diagrams for the new compounds reported in ref 5 and 6b will be presented in detail in future publications. (b) The synthesis of the cholesteryl esters of a number of chiral alkanic acids discussed in ref 5 are reported in a forthcoming paper: H. W. Gibson, *Mol. Cryst. Liquid Cryst.*, in press.
- (7) R. A. Soref, *Proc. Symp. Phys. Opto-Electronic Materials*, 1971, 207 (1972); *Chem. Abstr.*, **77**, 25748c (1972).
- (8) J. A. Costellano and M. T. McCaffrey, "Liquid Crystals and Ordered Fluids," J. H. Johnson and R. S. Porter, Ed., Plenum Press, New York, N. Y., 1970.
- (9) J. M. Pochan and P. F. Erhardt, *Phys. Rev. Lett.*, **27**, 790 (1971).
- (10) J. M. Pochan and D. G. Marsh, *J. Chem. Phys.*, **57**, 1143 (1972).
- (11) P. F. Erhardt, J. M. Pochan, and W. C. Richards, *J. Chem. Phys.*, **57**, 3596 (1972).
- (12) J. M. Pochan and D. G. Marsh, *J. Chem. Phys.*, **57**, 5154 (1972).
- (13) D. G. Marsh and J. M. Pochan, *J. Chem. Phys.*, **58**, 2835 (1973).
- (14) D. Marsh, J. Pochan, and P. Erhardt, *J. Chem. Phys.*, **58**, 5795 (1973).
- (15) J. M. Pochan, P. F. Erhardt, and W. C. Richards, *Mol. Cryst. Liquid Cryst.*, in press.
- (16) D. Coates and G. W. Gray, *J. Chem. Soc., Chem. Commun.*, 101 (1974).
- (17) J. Wysocki, *Mol. Cryst. Liquid Cryst.*, **14**, 71 (1971).
- (18) A. D. Jenkins, Ed., "Polymer Science," American Elsevier, New York, N. Y., 1972, p 306.
- (19) F. W. Billmeyer, Jr., "Textbook of Polymer Science," Wiley-Interscience, New York, N. Y., 1972, p 166.
- (20) J. J. Wysocki, *et al.*, *J. Sci. Ind. Res.*, **13**, 2 (1972).

Dipole Moment and Far-Infrared Studies on the Dimethyl Sulfoxide–Iodine Complex¹

A. Eugene Pekary²

Department of Chemistry, University of California, Berkeley, California 94720 (Received March 13, 1974)

Publication costs assisted by the National Institute of General Medical Sciences

Ground state properties of the dimethyl sulfoxide (DMSO)–iodine (I₂) charge-transfer complex have been studied by dielectric, refractometric, conductivity, and far-infrared measurements. The dipole moments obtained in carbon tetrachloride for the DMSO–I₂ complex, (5.8 ± 0.1) D, and for DMSO, (4.06 ± 0.05) D, suggest that electronic charge is actually transferred from DMSO to iodine in the ground state of the complex. Experimental conditions for the dipole moment measurements were arranged to eliminate any contributions from ion-pair formation. The far-infrared molecular iodine stretch absorption for DMSO–I₂ in carbon tetrachloride shifts to lower frequency with increasing DMSO concentration. This frequency shift results from a progressive increase in the solution dielectric constant which favors additional DMSO electron donation to molecular iodine.

Spectroscopic studies of Klaeboe³ demonstrated the formation in carbon tetrachloride of a 1:1 charge-transfer complex between the oxygen atom of dimethyl sulfoxide (DMSO) and iodine. While considerable theoretical⁴ and experimental^{5,6} interest in the dipole moment of such complexes has developed in recent years, doubts about the identity of the measured species have also been raised because some charge-transfer complexes dissociate into ion pairs.^{7,8} No crystallographic data concerning DMSO–iodine have appeared, due, presumably, to the difficulties of preparing stable crystals.⁹ A further characterization of the solution properties of the DMSO–iodine molecular complex seemed desirable because of this absence of definitive information concerning the intermolecular geometry.

The equilibrium association constant for DMSO–iodine in carbon tetrachloride,³ 11.17 M⁻¹, was considered ideal for a dipole moment determination of the corresponding 1:1 complex. It is sufficiently strong to provide a significant concentration of DMSO–iodine at very low total mole fraction of DMSO but not large enough to induce spontaneous ion-pair formation.¹⁰ This was an important experimental consideration since ion-pair formation in DMSO–iodine solutions can be avoided only with anhydrous conditions³ and low DMSO concentrations.¹⁰ The effect of DMSO self-association^{11–14} on the dipole moment determinations could also be minimized by the use of very dilute DMSO solutions.

Dipole moment and far-infrared measurements for the DMSO–iodine complex have not been reported previously despite the chemical and biological importance of DMSO¹⁵ and iodine¹⁶ intermolecular interactions. Dipole moment values for charge-transfer complexes provide valuable information concerning the nature of intermolecular bonding and are indispensable for checking theoretical calculations.⁴ Studies with far-infrared and Raman spectroscopy, on the other hand, provide information concerning the motional dynamics of the complex which are usually quite sensitive to environmental influences such as the solvent dielectric constant.¹⁷

Experimental Section

Materials. Matheson Coleman and Bell (MCB) anhydrous DMSO and Mallinckrodt resublimed iodine, stored

over phosphorus pentoxide, were used without further purification. MCB spectrograde carbon tetrachloride was freshly distilled over anhydrous calcium sulfate before use. Infrared absorption indicated water content to be below 0.0005% in all DMSO and DMSO–iodine in carbon tetrachloride solutions.

Dipole Moment Studies. Dielectric constants of carbon tetrachloride solutions containing 0–0.216 mole fraction per cent, X%, (0–0.021 M) DMSO with and without 0.76X% (0.081 M) iodine were measured by the frequency deviation method at 25 ± 0.1° and 1.050 MHz. An immersion refractometer was used to measure the refractive indices for DMSO–iodine and DMSO solutions in carbon tetrachloride. The DMSO concentration range was 50-fold greater than that for the dipole moment measurements.

Far-Infrared Studies. A Beckman IR 11 was used in the double beam mode with 2.0- and 1.0-mm path Beckman polyethylene cells and 0.4- and 0.2-mm path Beckman liquid cells with polyethylene windows. (See Table II for DMSO and iodine concentrations.)

Dielectric Studies. The dielectric constants and conductivities of solutions of the same DMSO–iodine concentration as used in the far-infrared studies were measured on a General Radio R-F Bridge Type 1806-A using a General Radio Bridge Oscillator Type 1330-A and a radio receiver as detector. A mica capacitor was introduced in series with the platinum concentric electrode cell when necessary to keep the measurements on scale. The measurements were carried out at 1.00 MHz and 30°.

Dipole Moment Calculations

Because of the hygroscopic nature of DMSO and its tendency to self-associate, dipole moment measurements were made with molecular iodine at the highest attainable concentration in carbon tetrachloride¹⁸ and the concentration of DMSO limited to a very dilute concentration range (0–0.021 M). Even though the molecular iodine concentration used was near its solubility limit it could be shown that DMSO was not completely associated with iodine at any DMSO concentration.

A generalized version of the Halverstadt–Kumler extrapolation procedure¹⁹ for analyzing dielectric constant measurements was applied to this four-component system con-

TABLE I: Results of Polarization Measurements on (a) DMSO-Iodine Complex and (b) DMSO in Carbon Tetrachloride

	α	ϵ_1	ν_1	β	P_{2e}^0	P_{2e}^0	μ
a	30.75 ^a	2.235	0.6285	0.00	535.9	39.5	(5.8 ± 0.1) D
b	20.67	2.228 ^b	0.6328	0.00	352.1	15.4	(4.06 ± 0.05) D ^c

^a Experimental value, 29.17, corrected for iodine depletion. ^b See ref 43. ^c Gas-phase dipole moment, (3.96 ± 0.04) D.⁴³

sisting of DMSO, DMSO-I₂, molecular iodine, and carbon tetrachloride. We find

$$P_2^0 = \frac{3\alpha\nu_1 \sum_{j=1}^2 M_{1j} X_{1j}}{(\epsilon_1 + 2)^2} + \left[\frac{\nu_1 \sum_{i=1}^2 M_{2i} X_{2i}}{X_2} + \beta \sum_{j=1}^2 M_{1j} X_{1j} \right] \frac{(\epsilon_1 - 1)}{(\epsilon_1 + 2)} \quad (1)$$

where P_2^0 corresponds to the combined molar polarizations of DMSO and DMSO-I₂ attained on infinite dilution of DMSO with 0.76 mole fraction per cent iodine in carbon tetrachloride. The measured value of α was corrected for change in the [DMSO-I₂]/[DMSO] ratio which results from the depletion of molecular iodine upon the addition of finite amounts of DMSO (see Table I).

Equating P_2^0 to the "solute" molar polarization calculated by the general formula²¹

$$P_2^0 = \frac{4\pi}{3} \sum_i \left(\alpha_{e_i} + \alpha_{a_i} + \frac{\mu_i^2}{3kT} \right) N_i = \sum_i (P_{e_i} + P_{a_i} + P_{\mu_i}) N_i \quad (2)$$

we can then solve explicitly for $\mu_{\text{DMSO-I}_2}$ with all P_{a_i} assumed equal to zero and P_{2e}^0 and P_{DMSO}^0 calculated from eq 1 using Maxwell's equation, $\epsilon = n^2$.

The factors

$$\frac{X_{\text{DMSO}}}{X_{\text{DMSO}} + X_{\text{DMSO-I}_2}} \quad \text{and} \quad \frac{X_{\text{DMSO-I}_2}}{X_{\text{DMSO}} + X_{\text{DMSO-I}_2}} \quad (3)$$

appearing in eq 1 and 2 were calculated from the DMSO-iodine in carbon tetrachloride association constant,³ 11.17 M⁻¹ (25°).

Dielectric and Conductivity Results

The dielectric constant for DMSO-iodine solutions (Table II) increased linearly with the DMSO concentration up to about 2.5 M DMSO. The solution with 0.068 M (about 4.5X%) DMSO and 0.086 M iodine, for example, contained more than 20 times the amount of DMSO as the solution of highest DMSO content used for dipole moment measurement. No change was detected in the dielectric constant or conductivity of this solution during repeated measurement over a 2-hr interval. The dielectric constant and conductivity for the DMSO-iodine solution containing 4.36 M DMSO, on the other hand, increased rapidly during the measurement interval. The conductivity data of Table II are readily extrapolated to the DMSO concentration range of the dipole moment solutions (0–0.021 M). It is apparent from such an extrapolation that the conductivity of no dipole moment solution could have exceeded about 10⁻¹⁰ ohm⁻¹ cm⁻¹.

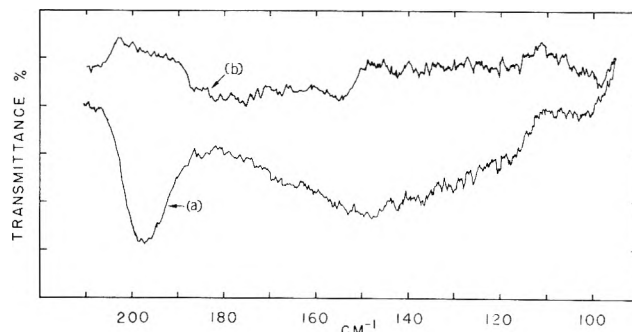


Figure 1. Far-infrared difference spectrum for (a) 0.068 M DMSO + 0.086 M iodine vs. 0.068 M DMSO and (b) 0.086 M iodine. Carbon tetrachloride was used as solvent.

Far-Infrared Results

Two absorption bands were observed in far-infrared difference spectra of DMSO and iodine in carbon tetrachloride solutions. In Figure 1, for example, they occur at 197 and 150 cm⁻¹, respectively. The 197-cm⁻¹ absorption is due to the stretching vibration of iodine molecules complexed with DMSO.²² This molecular iodine stretch absorption shifted monotonically to lower frequency with solution dielectric constant increase, as revealed in Table II.

The very broad 200–95-cm⁻¹ absorption region may arise either from a resonant dipole pair absorption transition for DMSO-I₂ pairs^{12–14,23–25} or interionic vibrations.²⁶ Free and DMSO-complexed²⁷ triiodide asymmetric and symmetric stretching modes, which have been assigned to the 148- and 114-cm⁻¹ regions, respectively,^{22,28} may contribute to this absorption region at DMSO concentrations above 0.2 M.¹⁰

DMSO-I₂ intermolecular vibration should occur at a frequency below that for pyridine- and substituted pyridine-I₂ complexes,²⁹ 94–65 cm⁻¹, since the pyridine-I₂ association constant,³⁰ ≈100 M⁻¹, and therefore the intermolecular stretching force constant,³¹ is greater than that for DMSO-I₂. This region below 95 cm⁻¹ was not accessible by the present difference absorption technique because of increased carbon tetrachloride absorption³² between 100 and 33 cm⁻¹.

Discussion

Infrared^{33a} visible and ultraviolet³ (uv) studies of Augdahl and Klæboe demonstrated the formation in carbon tetrachloride of a 1:1 charge-transfer complex between the oxygen atom of DMSO and iodine. However, spectroscopic^{3,22} and conductivity data³ have revealed the presence of triiodide ions in concentrated DMSO-iodine solutions. Giordano, *et al.*,¹⁰ found a reversible formation of triiodide ion which was related to the solvent polarity. Other iodine complexes^{17,33b} have also been shown to form highly polar reaction products.

Molar conductivity data for dilute iodine in pure DMSO solutions indicate that ionization increases very slowly in parallel with the iodide uv absorption.³⁴ No triiodide was

TABLE II: Averaged Results of Far-Infrared and Dielectric Studies on DMSO-Iodine Solutions in Carbon Tetrachloride at 30° during 1-hr Period Following Preparation

Concn, <i>M</i>	Iodine stretch frequency, cm ⁻¹	Dielectric constant (ϵ)	Conductivity (<i>K</i>), ohm ⁻¹ cm ⁻¹
0.068 <i>M</i> DMSO + 0.086 <i>M</i> I ₂	197.0 ± 0.6	2.4	4.8 × 10 ⁻¹⁰
0.546 <i>M</i> DMSO + 0.020 <i>M</i> I ₂	193.1 ± 0.9	3.4	3.7 × 10 ⁻⁹
1.09 <i>M</i> DMSO + 0.02 <i>M</i> I ₂	191.1 ± 0.4	4.8	4.3 × 10 ⁻⁷
2.18 <i>M</i> DMSO + 0.02 <i>M</i> I ₂	190.3 ± 0.6	6.9	5.7 × 10 ⁻⁶
4.36 <i>M</i> DMSO + 0.04 <i>M</i> I ₂	187.3 ± 1.9	37	2.8 × 10 ⁻⁵
8.72 <i>M</i> DMSO + 0.20 <i>M</i> I ₂	185.7 ± 0.5	80	1.2 × 10 ⁻⁵
15.0 <i>M</i> DMSO + 0.20 <i>M</i> I ₂	186.0 ± 1.1	72	5.3 × 10 ⁻⁶

observed for dilute DMSO-iodine solutions in carbon tetrachloride and triiodide formation at high DMSO concentration in carbon tetrachloride was completely reversed on dilution with carbon tetrachloride.³ Therefore, to eliminate concentration effects¹⁹ and DMSO and water catalyzed^{3,22} triiodide formation from DMSO-iodine in carbon tetrachloride polarization measurements the solution components must be anhydrous and the DMSO concentrations kept as low as experimental accuracy will permit.

The comparison, in Table I, between the present DMSO-I₂ and DMSO dipole moment measurements in carbon tetrachloride, which were obtained in the absence of significant conductivity, suggests that charge is actually transferred from DMSO to molecular iodine on formation of the 1:1 complex. Polarization by quadrupole-induced-dipole and other electrostatic forces,³⁵⁻³⁹ and solvent dielectric effects,^{40,41} undoubtedly contribute to the measured dipole moment and help stabilize the complex.

The shift to lower frequency of the molecular iodine stretch vibration with increased solution dielectric constant is also consistent with the concept of charge transfer from DMSO to iodine. Electrons donated by DMSO to molecular iodine occupy an iodine antibonding orbital.⁴ These antibonding electrons weaken the iodine intermolecular bond and thereby reduce the vibration frequency below the value 207 cm⁻¹ observed for uncomplexed molecular iodine in carbon tetrachloride.⁴² This polar, "charge-transferred" configuration of the complex will be at lower energy in a high dielectric constant medium.¹⁷ The observed iodine stretch frequency shift is thus a measure of the greater electron transfer from DMSO to iodine induced by the polarizing effects of neighboring DMSO molecules.

Acknowledgments. The author wishes to thank Professor Chester T. O'Konski for suggesting the present investigation, for providing the dielectric instrumentation, and for many helpful discussions concerning the theory of dielectric constant measurement and its interpretation. The present infrared measurements were carried out in Dr. Herbert L. Strauss's laboratory and assisted by Heleen Gabelnick and Mac Pickett.

References and Notes

- (1) This research was supported under USPHS Research Grant No. GM 12082 (to Professor Chester T. O'Konski) and USPHS Training Grant No. 2 T01 GM 00829 from the National Institute of General Medical Sciences.
- (2) NIH Biophysics Training Grant Fellow, 1966-1970. Address correspondence to the Endocrinology Laboratory, Wadsworth VA Hospital, Los Angeles, Calif. 90073.
- (3) P. Klaeboe, *Acta Chem. Scand.*, **18**, 27 (1964).
- (4) R. S. Mulliken and W. B. Person, "Molecular Complexes," Wiley-Interscience, New York, N. Y., 1969.
- (5) S. N. Bhat and C. N. R. Rao, *J. Amer. Chem. Soc.*, **90**, 6008 (1968).
- (6) G. Briegleb, "Electronen-Donator-Acceptor Komplexe," Springer-Verlag, Berlin, 1961.
- (7) P. Boule, *J. Amer. Chem. Soc.*, **90**, 517 (1968).
- (8) K. Toyota and W. B. Person, *J. Amer. Chem. Soc.*, **88**, 1629 (1966).
- (9) R. Reid and B. Musulin, *Trans. Ill. State Acad. Sci.*, **59**, 48 (1966).
- (10) M. C. Giordano, J. C. Bazan, and A. J. Arvia, *J. Inorg. Nucl. Chem.*, **28**, 1209 (1966).
- (11) Z. Yoshida and N. Yoshida, *Kogyo Kagaku Zasshi*, **73**, 2296 (1970).
- (12) R. L. Amey, *J. Phys. Chem.*, **72**, 3358 (1968).
- (13) R. H. Figueroa, E. Roig, and H. H. Szmant, *Spectrochim. Acta*, **22**, 587 (1966).
- (14) R. J. Jakobsen and J. W. Brasch, *J. Amer. Chem. Soc.*, **86**, 3571 (1964).
- (15) C. D. Leake, *Ann. N.Y. Acad. Sci.*, **141**, 1 (1967).
- (16) V. Cody, W. L. Duax, and D. A. Norton, *Acta Crystallogr., Sect. B*, **28**, 2244 (1972).
- (17) S. G. W. Ginn and J. L. Wood, *Trans. Faraday Soc.*, **62**, 777 (1966).
- (18) J. H. Hildebrand and R. L. Scott, "Regular Solutions," Prentice-Hall, Englewood Cliffs, N. J., 1962.
- (19) I. F. Halverstadt and W. D. Kumler, *J. Amer. Chem. Soc.*, **64**, 2988 (1942).
- (20) The symbols are *M*₁₁, molecular weight (MW) CCl₄; *M*₁₂, MW I₂; *M*₂₁, MW DMSO; *M*₂₂, MW DMSO-I₂; *X*, mole fraction (subscripts correspond to those for *M*); ϵ_1 , dielectric constant of 0.76 mole fraction per cent (X%) I₂ in CCl₄; v_1 , specific volume, 1/density, of 0.76X% I₂ in CCl₄; $\alpha = d\epsilon_{12}/dX_2$, $\beta = dv_{12}/dX_2$, where subscript 12 refers to DMSO + 0.76 X% I₂ in CCl₄ and *X*₂ is initial mole fraction of DMSO; *N*_i = (*X*₂/*X*₂)*N*₀, where *N*₀ is Avogadro's number, μ , dipole moment, Debye units, *k*, Boltzmann constant; *T*, absolute temperatures; *n*, refractive index.
- (21) P. Debye, "Polar Molecules," Dover Publications, New York, N. Y., 1929.
- (22) P. Klaeboe, *J. Amer. Chem. Soc.*, **89**, 3667 (1967).
- (23) H. Margenau, *Rev. Mod. Phys.*, **11**, 1 (1939).
- (24) B. J. Bulkin, *Helv. Chim. Acta*, **52**, 1348 (1969).
- (25) J. R. Durig, C. M. Player, Jr., and J. Bragin, *J. Chem. Phys.*, **52**, 4224 (1970).
- (26) W. F. Edgell, A. T. Watts, J. Lyford, IV, and W. M. Risen, Jr., *J. Amer. Chem. Soc.*, **88**, 1815 (1966).
- (27) C. H. Paulson, Jr., Ph.D. Thesis, Department of Chemistry, University of California, Berkeley, Calif., 1965, p 45.
- (28) A. G. Maki and R. Forneris, *Spectrochim. Acta*, **23**, 867 (1967).
- (29) R. F. Lake and H. W. Thompson, *Proc. Roy. Soc., Ser. A*, **297**, 440 (1967).
- (30) W. J. McKinney and A. I. Popov, *J. Amer. Chem. Soc.*, **91**, 5215 (1969).
- (31) J. Yarwood and W. B. Person, *J. Amer. Chem. Soc.*, **90**, 594 (1968).
- (32) H. S. Gabelnick and H. L. Strauss, *J. Chem. Phys.*, **46**, 396 (1967).
- (33) (a) E. Augdahl and P. Klaeboe, *Acta Chem. Scand.*, **18**, 18 (1964); (b) C. Reid and R. S. Mulliken, *J. Amer. Chem. Soc.*, **76**, 3869 (1954).
- (34) T. Soda and J. H. Hildebrand, *J. Phys. Chem.*, **71**, 4561 (1967).
- (35) M. J. Mantione, *Theor. Chim. Acta*, **15**, 141 (1969).
- (36) M. J. Mantione, *Int. J. Quantum Chem.*, **3**, 185 (1969).
- (37) J. L. Lippert, M. W. Hanna, and P. J. Trotter, *J. Amer. Chem. Soc.*, **91**, 4035 (1969).
- (38) J. P. Malrieu and P. Claverie, *J. Chim. Phys.*, **65**, 735 (1968).
- (39) M. J. S. Dewar and C. C. Thompson, Jr., *Tetrahedron, Suppl.*, **No. 7**, 97 (1966).
- (40) P. V. Huang, N. Platzter, and M. L. Josien, *J. Amer. Chem. Soc.*, **91**, 3669 (1969).
- (41) O. K. Rice, *Int. J. Quantum Chem.*, **11S**, 219 (1968).
- (42) R. Stammerich, R. Forneris, and Y. Tameris, *Spectrochim. Acta*, **17**, 1173 (1961).
- (43) A. A. Maryott and E. R. Smith, *Nat. Bur. Stand. (U. S.), Circ.*, **No. 514** (1951).
- (44) H. Driezler and G. Dendl, *Z. Naturforsch. A*, **19**, 512 (1964).

Nuclear Magnetic Resonance Studies of the Interaction of Molecular Oxygen with Organic Compounds

M. Polak and G. Navon*

Department of Chemistry, Tel-Aviv University, Tel-Aviv, Israel (Received January 25, 1974)

Proton nmr line broadenings and chemical shifts due to dissolved molecular oxygen were measured for various organic compounds. After corrections for the extra broadening in spin-spin multiplets, due to T_1 spin decoupling effects, the observed oxygen-induced broadening was similar for all compounds studied. It was concluded that there was no complex formation between the oxygen and the organic molecules. Small oxygen-induced chemical shifts could be observed and some possibilities for their origin were discussed.

Introduction

Since the original observation by Evans¹ of the appearance of a new uv optical absorption spectrum when oxygen is dissolved in aromatic solvents, similar spectra were observed for solutions of oxygen in a variety of other organic substances as well.²⁻⁴ Tsubomura and Mulliken³ and Jortner and Sokolov⁴ concluded that the new oxygen-induced absorption spectra are not a result of the formation of stable complexes, but are due to contact charge-transfer interactions.⁵ More quantitative studies made by Lim and Kowalski⁶ in benzene solutions, as well as those of King and Bradely in the gas phase,⁷ confirmed this general conclusion. A negligible stability constant was also found for the charge-transfer optical absorption due to oxygen interaction with halide ions.⁸

While all previous conclusions were based mainly on solubility and thermochemical data, the application of the nmr technique gives information on the molecular level, and is sensitive to the presence of preferred structures even in weak complexes. Measurements of proton nmr relaxation times of water saturated with oxygen were reported by Hausser and Noack.⁹

Experimental Section

Nmr spectra were measured on a Varian HA-100 spectrometer using 2% v/v TMS as an internal lock. Relaxation times T_1 and T_2 of single-line spectra were measured by the methods of Carr and Purcell¹⁰ and of Meiboom and Gill¹¹ using a pulsed spin-echo attachment to the HA-100 spectrometer.¹²

In early experiments where atmospheric pressures of oxygen or nitrogen were used, the gas was bubbled through the solutions for 5 min in a syringe and the solutions were injected into a thin walled 5-mm nmr tube. In order to obtain larger oxygen effects, which could be measured more precisely, higher pressures of oxygen were used in later experiments. For such experiments, pure oxygen at atmospheric pressure was introduced into a rubber tube of a known volume, which was connected to three-limb vacuum stopcock at one end and to a thick-walled nmr tube (Wilmad 523-PP, 3.5-mm internal diameter and 5-mm external diameter) containing the solution at the other end. The stopcock could be linked either to the oxygen tank or to a vacuum line, thereby enabling the air to be replaced by the oxygen gas. The oxygen was then trapped in the nmr tube

by inserting the tube into liquid nitrogen, and the tube was sealed and brought to room temperature. Oxygen pressures were estimated from the ratios of the initial volume to the volume inside the sealed nmr tube.

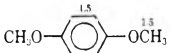
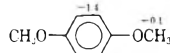
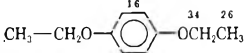
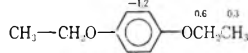
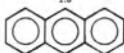
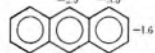
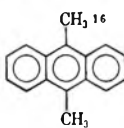
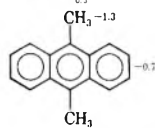
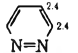
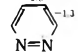
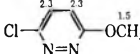
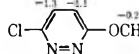
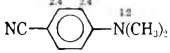
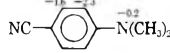
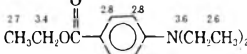
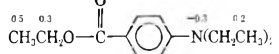
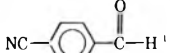
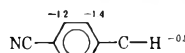
Bulk susceptibilities were estimated using peak separations of spectra obtained in a coaxial cell without spinning.¹³ The cell (Wilmad No. 517) consisted of two coaxial tubes with internal diameters of 2.3 and 4.2 mm and external diameters of 3.3 and 5.0 mm for the inner and the outer tubes, respectively. The proton nmr signal of the solute in the inner tube which consisted of a single line was used for locking the spectrometer. In all experiments the outer tube contained a solution of 1.5 M benzene in CCl_4 . Its spectrum consisted of two broad peaks the separation of which is related to the bulk magnetic susceptibilities of the solutions in the inner and the outer tubes.¹³ A calibration curve was obtained using various liquids with known magnetic susceptibilities.^{14,15} In order to estimate the bulk magnetic susceptibility due to dissolved oxygen, the peak separation of the benzene solution in the outer tube was measured while the inner tube contained a solution of 1.5 M acetone in CCl_4 in which oxygen was dissolved at various pressures. The uncorrected shifts were obtained by spinning the same sample, thereby obtaining a single sharp peak from the outer solution.

Results and Discussion

In preliminary experiments line broadenings and chemical shifts were observed after bubbling oxygen through solutions of organic compounds in CCl_4 . All these effects could be reversed after bubbling nitrogen gas through the same solutions, thus eliminating the possibility that the observed effects are due to the introduction of impurities or to oxidation products. Furthermore, both line broadenings and chemical shifts were found to be proportional to oxygen pressure.

Since many of the samples contained oxygen at a pressure of 3.6 atm all the other results listed in Table I were normalized to this particular pressure. In order to eliminate errors due to inaccurate estimations of oxygen pressures, spectra were run for solutions each containing a mixture of three or four of the compounds listed in Table I. The results for one compound in different mixtures were consistent within the experimental error, and the values given in Table I are the average results.

TABLE I: Differential Line Broadenings and Chemical Shifts of Various Organic Molecules Due to Dissolved Oxygen^a

	Line broadening, ^b Hz	Chemical shifts, ^c Hz
Acetone	1.4	-0.3
Dioxane	1.4	-0.1
Methylene dichloride	1.2	-0.9
Chloroform	1.3	-2.8
Benzene	1.4	-0.6
<i>p</i> -Diiodobenzene	1.5	-1.7
<i>p</i> -Dimethoxybenzene		
<i>p</i> -Diethoxybenzene		
Anthracene		
9,10-Dimethylantracene		
Pyridazine		
3-Chloro-6-methoxy-pyridazine		
<i>N,N</i> -Dimethyl- <i>p</i> -aminobenzonitrile		
Ethyl <i>p</i> - <i>N,N</i> -diethylaminobenzoate		
<i>p</i> -Cyanobenzaldehyde		

^a All results are for 0.125 *M* solution in CCl₄ and are normalized to oxygen pressure of 3.6 atm. ^b Estimated error, 0.3 Hz. ^c Estimated errors 0.2 Hz for singlets and 0.4 Hz for multiplets.

Line Broadening Well-defined complexes of oxygen with the organic molecules should result in differential broadening effects: ordered structures should produce different broadenings of different functional groups within one molecule and unequal binding constants of such complexes should result in different broadening effects for the various organic molecules in the same solution. However, from the results listed in Table I another trend may be noted: while all singlets exhibited the same amount of broadening (within experimental error) spin-spin multiplets exhibited greater amount of broadening which increased in the order doublets, triplets, quartets. Moreover, an apparent decrease of the spin-spin splitting, *J*, was noted for the multiplets. This decrease was more pronounced at higher oxygen pressures and paralleled the amount of the line broadening.

All these results can be nicely interpreted by an equal oxygen effect on all proton groups together with a "*T*₁ spin-decoupling" effect by which an extra broadening occurs to a proton group due to a *T*₁ relaxation process of another group, spin-spin coupled to it. According to the treatment given previously¹⁶ for first-order spectra, the broadening of the "A" portion of an A_{*m*}X_{*n*} multiplet is given by

$$\frac{1}{T_{2A}'} = \frac{1}{T_{2A}} + \frac{n}{2T_{1X}} \quad (1)$$

provided that the broadening is smaller than the spin-spin splitting, *J*. According to this equation the apparent broadening $1/T_{2A}'$ of a group of nuclei A, coupled to *n* nuclei X, having spins of one-half, consists of an intrinsic broadening $1/T_{2A}$ and an extra broadening effect due to *T*₁ spin decoupling, $n/2T_{1X}$, where *T*_{1X} is the longitudinal relaxation time of the proton group X. For the specific case of *n* = 1 eq 1 was given also by Abragam.¹⁷

Measurements of the ratio T_{1p}/T_{2p} (T_{1p}^{-1} and T_{2p}^{-1} are the relaxation rates due to dissolved oxygen) were performed for acetone by a pulse nmr technique at 100 MHz and the result was $T_{1p}/T_{2p} = 1.17 \pm 0.15$. We calculated this ratio, applying Pfeifer equations,¹⁸ which are based on a translational diffusion mechanism (see below) obtaining an estimated value of 1.06. Assuming that these ratios apply also for the intrinsic relaxation times of all other compounds, one expects for singlets, triplets, and quartets broadening ratios of 1:1.86:2.29, respectively, for $T_{1p}/T_{2p} = 1.17$ and of 1:1.94:2.41 for $T_{1p}/T_{2p} = 1.06$. These are in good agreement with the average experimental broadening ratios of 1:1.87:2.46.

As a further check a 4.5-atm O₂ broadened spectrum of the aliphatic residue of *p*-diethoxybenzene is compared in Figure 1 with a spectrum computed as described before.¹⁶ The agreement seems satisfactory. Accordingly, the apparent reduction of *J* is fully explained.

From the above treatment it can be concluded that all

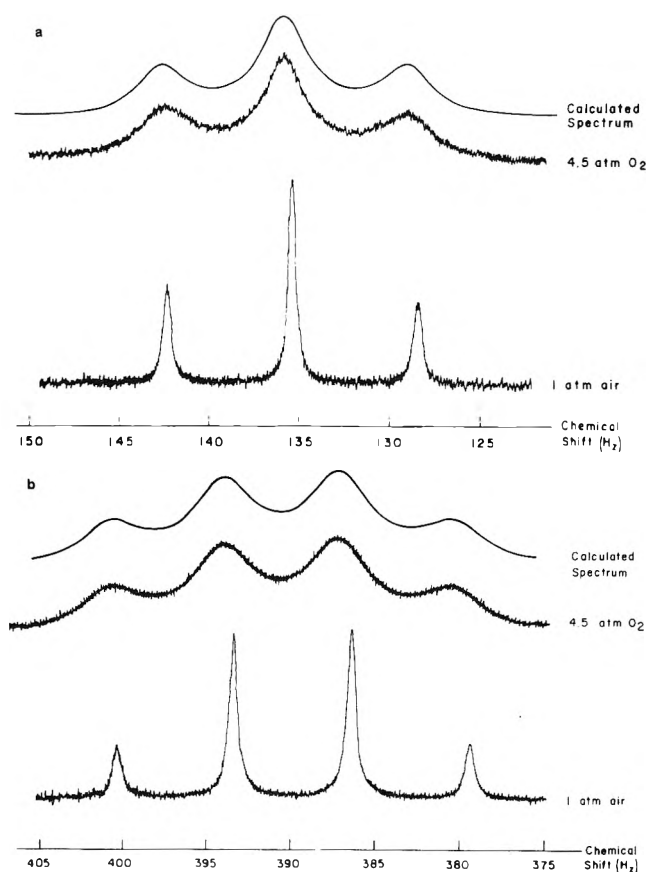


Figure 1. Calculated and experimental spectrum of *p*-diethoxybenzene under 4.5 atm of O₂: (a) methyl spectrum, (b) methylene spectrum. (All shifts are relative to TMS which was used as an internal reference.)

broadening data can be accounted for, within experimental error, by equal oxygen effect on the relaxation rates of all the molecules measured and for all proton groups within each molecule. This rules out any specific binding of oxygen to the organic molecules in solution. There are only statistical encounters with *equal probability* for all protons belonging to the various molecules and functional groups. This result is in agreement with previous suggestions for negligible stability of oxygen complexes with organic molecules.^{3,4,6,7} Moreover, it gives evidence on the molecular level for the nonspecificity of their interaction.

The equality of the relaxation times of various proton types indicates also that the dominant relaxation mechanism due to oxygen is through dipolar interaction. Scalar interaction should depend on the induced spin densities of the various proton groups and it is expected to have a large variation among groups of different chemical nature.

In the absence of stable complexes of oxygen and organic molecules the dipolar interaction can be modulated by their mutual translational diffusion and by the electronic spin relaxation of the paramagnetic oxygen. Such a relaxation mechanism was treated by Pfeifer,¹⁸ whose equations were used for the calculation of the T_1/T_2 ratio. As was mentioned above the calculated ratio for 100 MHz is in agreement with the experimental value within our experimental error. Moreover, frequency dependence studies of the proton nmr relaxation times of oxygen solutions in water⁹ and organic solvents¹⁹ were in accordance with the above mechanism.

Chemical Shifts. The chemical shift data given in Table

TABLE II: Susceptibilities and Chemical-Shift Corrections of Acetone-O₂ Benzene

O ₂ pressure, atm	$\Delta\delta_{\text{obsd}},^a$ Hz	$\Delta\nu,^b$ Hz	$-\chi \times 10^4,^c$ cgs	$\Delta\delta_{\text{corr}},$ Hz
0.21		65.6	0.673	
2.0	10.3	47.2	0.628	-0.9
0.21		61.4	0.662	
3.0	15.1	27.2	0.578	+2.5

^a Chemical shift differences between solutions containing oxygen under high pressures and air saturated solutions (0.21 atm of oxygen). ^b The separation of the two peaks obtained for a nonrotating coaxial nmr tube. ^c Estimated by using a calibration curve.

I are relative to internal TMS. The shifts are small but beyond experimental error. Especially noticeable are the diamagnetic shifts exhibited by aromatic protons and by methylene chloride and chloroform.

In order to estimate the absolute values of the chemical shifts caused by the dissolved oxygen, the shifts were measured against an external reference, and a bulk susceptibility correction was applied. The results are shown in Table II. The chemical shifts relative to the external reference were highly reproducible with an average value of 6.0 ± 0.6 Hz per 1 atm of oxygen. On the other hand, high precision could not be obtained for the bulk susceptibility corrections. This only allows us to conclude that dissolved oxygen does not induce large absolute chemical shifts in the nmr spectra of the organic solutes.

Two explanations can be tentatively suggested for the observed chemical shifts. (a) Anisotropy in the paramagnetism of the oxygen molecules which are close to the measured proton. It can be seen in Table I that the shifts are pronounced for protons to which the approach is relatively sterically hindered. Examples are the phenyl protons in the para-substituted benzenes which have shifts greater than benzene, and the shifts of the substituted methyl groups which increase in the order methyl, methylene chloride, chloroform. Oxygen molecules having a possible paramagnetic anisotropy would induce proton chemical shifts by approaching the sterically hindered proton in a unique way. It should be stressed that an asymmetrical encounter complex alone cannot induce any shift because of orientational averaging. Only an anisotropy in the magnetic susceptibility would lead to a nonzero average. (b) A transferred hyperfine interaction induced by the oxygen molecule during the short encounters could also occur. A possible mechanism for such an interaction might involve a mixing with charge-transfer states in which the oxygen may serve as an acceptor and the organic molecules as donors. In such a case a correlation is expected to exist between the induced chemical shifts and the spin densities on the corresponding protons in the cation radicals of the organic molecules. This mechanism is consistent with the sign of the shift induced by oxygen; the shifts of the aromatic protons are more diamagnetic than those of the methyl protons (see Table I), in line with the negative spin densities on the aromatic protons in aromatic radicals.

The hyperfine constants of the aromatic protons in the cation radical of *N,N*-dimethyl-*p*-aminobenzonitrile have not been measured, but they are expected to be in the reverse order of that of the corresponding anion radical. The hyperfine constants in similar anion radicals as, e.g., *p*-nitroaniline²⁰ and *N,N*-dimethyl-*p*-nitroaniline²¹ are about 3.3 and -1.1 G for the protons in positions ortho and meta to the nitro group, respectively. Thus, the hyperfine cou-

pling constant in the cation radical is expected to be higher for protons adjacent to the dimethylamino group. Such an order was, in fact, observed also for the chemical shifts.

The hyperfine coupling constant for the positive ion of dimethoxybenzene is slightly smaller than that of the benzene cation (2.4 vs. 2.9 G, respectively)^{22,23} in contrast to our chemical-shift results. However, as the dimethoxybenzene is a better donor than benzene, it is reasonable that a higher amount of charge transfer occurs during the encounter with an oxygen molecule. However, the relatively high hyperfine constant of the methyl protons in the cation radical of 9,10-dimethylanthracene (8.0 G^{24,25}) is not reflected in the oxygen-induced chemical shift of these protons, which is similar to the chemical shifts of methyl groups in all other compounds. This last result renders the correlation between the oxygen-induced chemical shifts and the proton hyperfine constants of the cation radicals incomplete. Obviously, further study is needed before a firm conclusion about the origin of the chemical shifts can be made.

Conclusions

The equal relaxation rates induced by dissolved O₂ on proton groups in the same or different molecular species lead to the conclusion that no stable complexes of oxygen with the organic molecules are present in the solutions. The relaxation is caused by a nonspecific dipolar interaction. The small but reproducible shifts, the origin of which is

still unknown, may indicate, however, some specific interaction during the short encounters.

References and Notes

- (1) A. D. F. Evans, *J. Chem. Soc.*, 345 (1953); (b) *ibid.* 1351, 3885 (1957).
- (2) A. U. Munck and J. R. Scott, *Nature (London)*, **177**, 587 (1956).
- (3) H. Tsubomura and R. S. Mulliken, *J. Amer. Chem. Soc.*, **82**, 5966 (1960).
- (4) J. Jortner and U. Sokolov, *J. Phys. Chem.*, **65**, 1633 (1961).
- (5) L. E. Orgel and R. S. Mulliken, *J. Amer. Chem. Soc.*, **79**, 4839 (1957).
- (6) E. C. Lim and V. L. Kowalski, *J. Chem. Phys.*, **36**, 1729 (1962).
- (7) H. Bradely, Jr., and A. D. King, Jr., *J. Chem. Phys.*, **47**, 1189 (1967).
- (8) (a) G. Navon, *J. Phys. Chem.*, **68**, 969 (1964); (b) H. Levanon and G. Navon, *ibid.*, **73**, 1861 (1969).
- (9) R. Hausser and F. Noack *Z. Naturforsch. A*, **20**, 1668 (1965).
- (10) H. Y. Carr and F. M. Purcell, *Phys. Rev.*, **94**, 630 (1954).
- (11) S. Meiboom and D. Gill, *Rev. Sci. Instrum.*, **29**, 688 (1958).
- (12) A. Ginsburg, A. Lipman, and G. Navon, *J. Phys. E*, **3**, 699 (1970).
- (13) C. A. Reilly, H. M. McConnell, and R. G. Meisenheimer, *Phys. Rev. A*, **98**, 264 (1955).
- (14) J. W. Emsley, J. Feeney, and L. H. Sutcliffe, "High Resolution Nuclear Magnetic Resonance Spectroscopy," Vol 1, Pergamon Press, New York, N. Y., 1965, Appendix c.
- (15) "Handbook of Chemistry and Physics," 50th ed, The Chemical Rubber Publishing Company, Cleveland, Ohio, 1969.
- (16) G. Navon and M. Polak, *Chem. Phys. Lett.*, **25**, 239 (1974).
- (17) A. Abragam, "The Principles of Nuclear Magnetism," Oxford University Press, London, 1961, pp 445 and 509.
- (18) H. Pfeifer, *Ann. Phys.*, **8**, 1 (1961).
- (19) M. Polak and G. Navon, to be submitted for publication.
- (20) P. L. Kolker and W. A. Waters, *J. Chem. Soc.*, 1136 (1964).
- (21) D. H. Geske, J. L. Ragle, M. A. Bambenek, and A. L. Balch, *J. Amer. Chem. Soc.*, **86**, 987 (1964).
- (22) W. F. Farbes and P. D. Sullivan, *J. Amer. Chem. Soc.*, **44**, 1501 (1966).
- (23) J. R. Bolton and A. Carrington, *Proc. Chem. Soc.*, 174 (1961).
- (24) J. R. Bolton, A. Carrington, and A. D. McLachlan, *Mol. Phys.*, **5**, 31 (1962).
- (25) J. A. Brivati, R. Hulme, and M. C. R. Symons, *Proc. Chem. Soc.*, 384 (1961).

Cation Radical Salts of *N*-Methylphenothiazine and Its Analogs. Synthesis and Characterization

M. H. Litt* and J. Radovic

Department of Macromolecular Science, Case Western Reserve University, Cleveland, Ohio 44106 (Received September 4, 1973; Revised Manuscript Received April 17, 1974)

Publication costs assisted by the National Science Foundation

10-Methylphenothiazine and dibenzo-*N*-methylphenothiazine were oxidized with silver perchlorate, hexafluoroantimonate, and tetrafluoroborate to give stable ion-radical salts. All compounds exhibit exponential dependence of conductivity on temperature. Their magnetic behavior has been interpreted on the basis of a linear Ising model involving antiferromagnetic interaction of the unpaired electrons. Only a small fraction of the unpaired electrons participate in conduction.

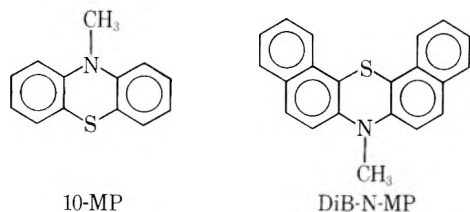
Introduction

Organic salts of TCNQ radical anions have attracted much attention due to their low electrical resistivities, particularly when incorporating an apparently neutral molecule of TCNQ.¹ Recently it has been shown that some simple radical-ion salts of TCNQ exhibit an insulator-metal transition below room temperature.^{2,3}

We have been looking for compounds that could form

cation radical ions by appropriate oxidation. The low ionization potential of phenothiazine and related compounds made them worth investigating. These form charge-transfer complexes with several electron acceptors.^{4,5} It was felt that stable salts of substituted phenothiazines could be formed using strong oxidizing agents. We report here the preparation of several salts based on 10-methylphenothiazine (10-MP) and 3,4:5,6-dibenzo-*N*-methylphenothiazine (DiB-N-MP) and their electrical and magnetic

behavior. The structural formulas of the two compounds are shown.



Experimental Section

Preparation. *10-Methylphenothiazine* was obtained by a procedure developed in this laboratory by Litt and Summers.⁶

10-Methylphenothiazine Perchlorate (10-MPClO₄). 10-MP (3.3220 g, 0.0156 mol) was dissolved in sufficient 95% ethanol to get an almost saturated solution at about 60° and 1.9760 g (0.0077 mol) of iodine dissolved in 20 ml of ethanol was added. After a few minutes a solution of 3.2280 g (0.0156 mol) of silver perchlorate in 10 ml of ethanol was poured in. A precipitate of AgI formed immediately. The precipitate was allowed to agglomerate and then was filtered off, leaving a red solution of 10-methylphenothiazine perchlorate. After evaporation to dryness *in vacuo* at room temperature the salt had the appearance of a black powder. The crude yield was 4.8232 g (99.3%). The product was recrystallized by dissolving in acetone (saturated solution) adding dioxane (1/3 the volume of acetone) and precipitating the crystals out by slow evaporation of acetone under reduced pressure. After two recrystallizations the yield was 4.2697 g or 87.9%. The ir spectrum shows the presence of water despite prolonged drying under vacuum. The element analysis indicates that the salt exists as a hydrate rather than as a simple salt.

Anal. Calcd for a 1:1 salt hydrated by one water molecule, C₁₃H₁₁NSClO₄·H₂O: C, 47.10; H, 3.92; N, 4.22; S, 9.67; Cl, 10.69. Found: C, 48.48; H, 3.96; N, 4.08; S, 9.58; Cl, 10.08.

The nonhydrated salt decomposes in several hours. This was seen when the synthesis was attempted using a solvent such as acetone. The compound starts decomposing above 120°.

10-Methylphenothiazine Tetrafluoroborate (10-MPBF₄). The salt was prepared in the same way as 10-MPClO₄. The respective quantities of reactants were 3.3220 g of 10-MP (0.0156 mol), 1.9760 g of I₂ (0.0077 mol), and 4.6668 g of AgBF₄ (0.0156 mol). The yield after recrystallization was 4.3048 g or 80.0%.

Anal. Calcd for a 1:1 salt, C₁₃H₁₁NSBF₄: C, 52.04; H, 3.66; F, 25.30; S, 10.68. Found: C, 53.40; H, 4.31; F, 23.74; S, 11.04.

Anal. Calcd for the 1:1 salt (+0.10 10-MP): C, 54.1; H, 3.85; F, 23.95; S, 11.10.

The compound decomposes above 120°.

10-Methylphenothiazine Hexafluoroantimonate (10-MPSbF₆). This was prepared as the salts above. The respective amounts of reagents were 3.3220 g of 10-MP, 1.9760 g of I₂, and 5.295 g of AgSbF₆. After recrystallization the yield was 4.456 g or 64.4%.

Anal. Calcd for a 1:1 salt, C₁₃H₁₁NSSbF₆: C, 34.77; H, 2.47; S, 7.14; F, 25.39. Found: C, 36.54; H, 2.46; S, 6.82; F, 24.86.

The compound decomposes above 145°.

Dibenzo-*N*-methylphenothiazine (DiB-*N*-MP). Dibenzophenothiazine was prepared from 2,2'-dinaphthylam-

TABLE I: Optical Spectra of Cation Radicals in Acetonitrile Showing Band Maxima Positions and Extinction Coefficients

Compound	Band maximum		Extinction coefficient
	mμ	eV	
10-MPClO ₄	850	1.46	1320
	760	1.63	1320
	512	2.42	7830
	480	2.58	6480
	312	3.98	2400
10-MPSbF ₆	Same as above		
DiB-N-MPClO ₄	720	1.72	9050
	568	2.18	2830
	500	2.48	3580

ine,⁷ and subsequently methylated by the same procedure as phenothiazine. The melting point of dibenzophenothiazine was 230° (lit.⁷ 232°). The yield was 77%. The melting point of the methylated compound was 287° and the yield was 85.1%. It was recrystallized from pyridine.

Anal. Calcd for C₂₁H₁₅NS: C, 80.43; H, 4.79; N, 4.47; S, 10.24. Found: C, 79.43; H, 5.00; N, 4.45; S, 10.39.

Dibenzo-*N*-methylphenothiazine Perchlorate (DiB-*N*-MPClO₄). DiB-*N*-MP being poorly soluble in ethanol, only 0.4690 g was dissolved in 750 ml at ~60° and 0.1889 g of I₂ in 30 ml of ethanol was added. After stirring the solution for 5 min, 0.3086 g of AgClO₄ in 5 ml of ethanol was poured in. The solution turned blue-black and a precipitate of AgI settled slowly to the bottom. Unfortunately DiB-*N*-MPClO₄ partly precipitated too; many extractions with ethanol were required to dissolve it from the silver iodide. After filtration and evaporation of the solvent, the salt was a black crystalline powder similar to the 10-MP salts. The yield was only 0.2764 g (44.8%). The salt was recrystallized from the same solvent-nonsolvent mixture as the 10-MP salts. It decomposes above 125°. The ir spectrum shows the presence of water not removed after several days of drying *in vacuo*.

Anal. Calcd for a hydrated 1:1 salt, C₂₁H₁₅NS·ClO₄·H₂O: C, 58.53; H, 3.94; N, 3.25; S, 7.44; Cl, 8.23. Found: C, 59.15; H, 3.81; N, 3.11; S, 7.16; Cl, 8.20.

All synthesized compounds were stable in air for months.

Characterization. Optical Spectra. The uv and visible spectra of the salts in acetonitrile solution were taken on a Cary 14 spectrophotometer at concentrations of 2 × 10⁻⁵ to 10⁻⁴ *M*. Transmission spectra on the solids were taken in Nujol mulls on the same instrument.

Table I shows the band positions and extinction coefficients for 10-methylphenothiazine perchlorate and dibenzo-*N*-methylphenothiazine perchlorate. Beer's law is obeyed.

Esr Spectra. The solid salts were diluted with NaCl (1% of the salt). The concentration of the solutions was 8 × 10⁻⁴ *M*. The measurements were made at room temperature on a Varian E-3 spectrometer.

Electrical resistances were measured on pellets of compressed powder. The ac resistance was measured on a Tektronix curve tracer, Type 576, at 60 Hz. The higher resistances were measured in dc using a Keitney 610C electrometer. The oscilloscope display was a simple straight line indicating that the compounds obey Ohm's law.

Magnetic susceptibility measurements were made by Mr. Lever, Department of Chemistry, York University, Downview, Ontario. He used the Faraday method.

X-Ray spectra were run on powders using the General Electric XRD-6 wide angle diffractometer.

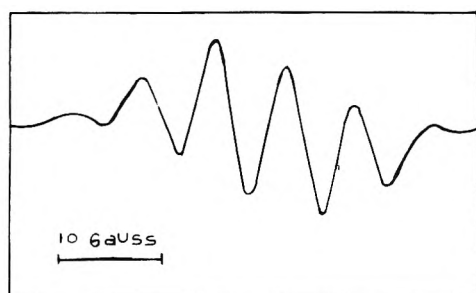


Figure 1. ESR spectrum of 10-MPClO₄ in acetonitrile: concentration 8×10^{-4} M.

Results

Esr Spectra. The esr spectrum of 10-MPClO₄ in acetonitrile is shown in Figure 1. The spectrum is exactly the same as obtained by other workers who oxidized the compound in sulfuric acid^{8,9} or electrochemically.¹⁰ The relative intensities of the lines are 1:4:7:7:4:1. The coupling constants of the electron with the nitrogen nucleus and the protons are $A_N = 8.5$ G and $A_H = 7.4$ G. DiB-N-MPClO₄ exhibits exactly the same solution spectrum.

The solid state spectra reduce to single lines of 4.95 and 5.3 G width respectively, indicating a large exchange effect.

X-Ray Data. Powder diagrams of the neutral 10-MP and its perchlorate salt are compared in Table II. The relative intensities of the strongest reflections are given.

Conductivity. All salts obey an exponential temperature dependence characteristic of semiconductors (Figure 2). The 10-MP salts exhibit very high σ_0 values and high activation energies. Many, Harnik, and Gerlich¹¹ postulated the relation

$$\sigma = \epsilon \mu N_0 \exp(-E/kT)$$

where μ is the drift mobility, ϵ the electron charge, and N_0 the effective density of states in the conducting levels of the crystal. N_0 was taken as 10^{21} from the number of molecules per cm³ and the multiplicity of the first excited electronic level of each molecule. We used this relation to estimate maximum possible intrinsic drift mobilities. Table III summarizes the data obtained from conductance measurements.

Magnetic Susceptibility. The magnetic susceptibility of 10-MPClO₄ follows the Curie-Weiss law, as shown in Figure 3. The concentration of spins calculated from the Curie constant indicates one unpaired electron per cation radical. The constant θ was -175°K showing antiferromagnetic interactions. In order to determine the energy of the interaction we applied the linear Ising model¹² which has been shown to fit similar crystalline organic free-radical systems reasonably well.¹³ (The singlet-triplet model was also tested but proved unsatisfactory.) The susceptibility is given by

$$\chi_M = \frac{Ng^2\mu_B^2}{4kT} \exp \frac{-J}{kT}$$

where N is the total number of spins, μ_B is the Bohr magneton, g the usual g factor, and J is the energy of interaction, often called exchange energy. The plot of $\log(\chi_M T)$ vs. $1/T$ gave a straight line (Figure 4), from the slope of which J was calculated to be 0.011 eV. Figure 5 shows the agreement between the experimental values of susceptibility and those calculated from the above equation using

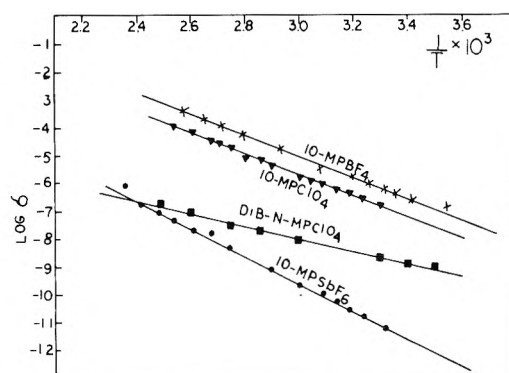


Figure 2. Temperature dependence of conductivity for the cation radical salts.

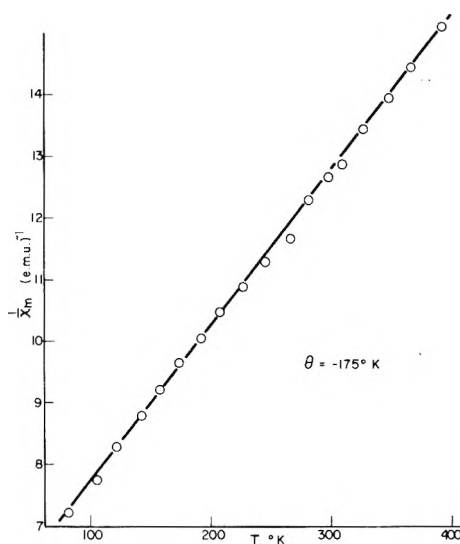


Figure 3. Reciprocal magnetic susceptibility vs. temperature for 10-MPClO₄.

TABLE II: Relative Intensities of Strongest X-Ray Reflections of 10-MP and 10-MPClO₄

Compound	d spacings of strongest reflections	Relative ^a intensity
10-MP	8.92	0.066
	4.97	0.056
10-MP	4.45	0.116
	3.72	0.200
10-MPClO ₄	5.33	0.027
	4.97	0.048
	4.45	0.065
	3.54	0.110

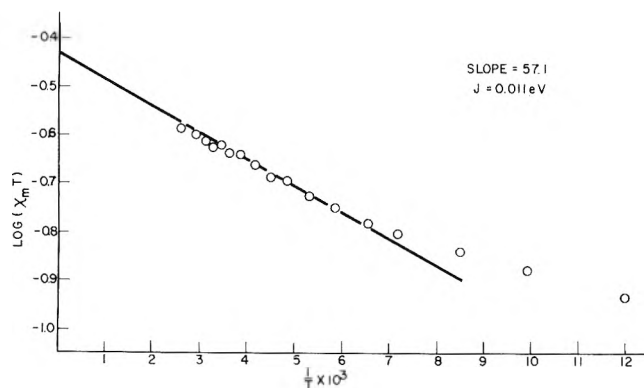
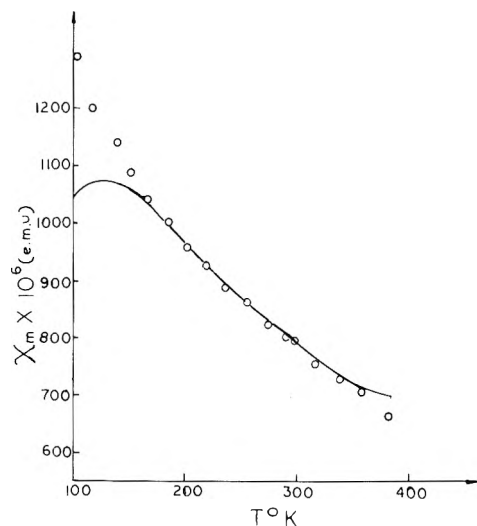
^a The intensities were corrected for Lorentz and polarization factors.

$J = 0.011$ eV. The low temperature divergence of the experimental points is attributed to a small amount of paramagnetic impurity. The overall behavior of the salt is, therefore, one of an antiferromagnetic substance in the ground state, which becomes progressively paramagnetic with increasing temperature.

DiB-N-MPClO₄, however, gave the susceptibility temperature dependence shown in Figure 6 (points). The curve can be reproduced to a large extent if we assume the material to act as an Ising solid with $J = 0.036$ eV, which contains about 15% of a paramagnetic impurity (Figure 6, solid line). The calculated higher temperature

TABLE III: Data Obtained from Conductance Measurements

Compound	Conductivity at 25°, ohm ⁻¹ cm ⁻¹	Activation energy, <i>E</i> , eV	σ_0 , ohm ⁻¹ cm ⁻¹	N_0	Estimated maximum drift mobility, μ , cm ² sec ⁻¹ V ⁻¹	Interaction energy, <i>J</i> , eV
10-MPClO ₄	1.8×10^{-7}	0.73	1.8×10^5	1.9×10^{21}	5.8×10^2	0.011
10-MPSbF ₆	1.6×10^{-11}	0.98	2.5×10^5	1.3×10^{21}	1.2×10^3	
10-MPBF ₄	7.0×10^{-7}	0.75	1.8×10^6	2.0×10^{21}	5.5×10^3	
DiB-N-MPClO ₄	2.5×10^{-9}	0.43	0.035	1.4×10^{21}	1.5×10^{-4}	0.036

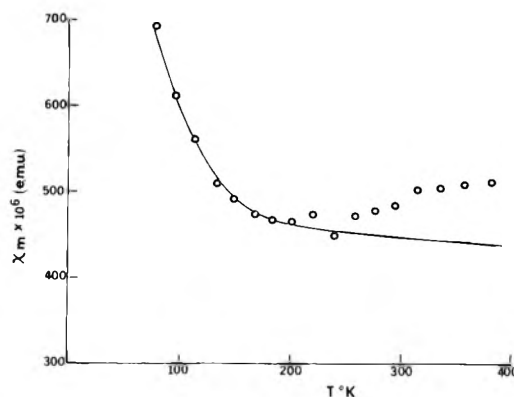
Figure 4. Ising model plot for 10-MPClO₄.Figure 5. Magnetic susceptibility vs. temperature for 10-MPClO₄: solid line, calculated from Ising model equation using $J = 0.011$ eV; points, experimental.

susceptibilities deviate from the experimental curve. This may be due to a change in J with temperature caused by lattice expansion. Other workers have also reported that the interaction energy is a function of temperature.^{1,14}

Discussion and Conclusions

Although the crystal structure of these salts has not been elucidated, the strongest reflection in the X-ray spectrum of 10-MPClO₄ was at 3.54 Å. This value is only slightly smaller than the strongest reflection for 10-MP itself (3.72 Å) the latter being the distance between parallel 10-MP molecules.

It has been recently shown that *N*-methylphenazinium tetracyanoquinodimethane, as well as TCNQ salts with

Figure 6. Magnetic susceptibility vs. temperature for DiB-N-MPClO₄: points, experimental; line, calculated from Ising model for $J = 0.036$ eV, assuming 15% of a paramagnetic impurity.

inorganic cations, consist of linear chains of TCNQ⁻ anions stacked essentially face to face, the interplanar distance between TCNQ molecules within a given chain being 3.26 Å.^{3,15} It is worthwhile pointing out that *N*-methylphenazinium cations also formed linear arrays between TCNQ⁻ chains.

Therefore it seems very likely that 10-MP and DiB-N-MP cation radical salts are also built up of alternating columns of cations and anions. The electronic structure becomes pseudo one dimensional with maximum π -electron interaction along the 10-MP⁺ chains.

It follows that the state of the solid is largely paramagnetic at room temperature. However, the salts exhibit moderate electrical conductivities. Obviously not all the paramagnetic electrons are participating in conduction. Only those that can be excited to conduction levels behave as carriers. The paramagnetism is, therefore, due to the uncoupled electrons in the lowest antibonding π orbitals. The population of the conduction band is very small at room temperature or slightly above. The activation energy for conduction can probably be related to the Coulomb repulsion energy for the double cation as elucidated in the modified Hubbard model for one-dimensional conductors.¹⁶ As would be expected, the conduction activation energy is lower for DiB-N-MP than for the smaller molecules since a double positive charge can be accommodated more easily in the larger molecule.

Under our conditions, the solid state spectra of 10-MPClO₄ did not show evidence of an absorption edge at 0.73 eV. The solution absorption at 1.46 eV is reproduced in the solid state spectrum. However, we feel that though it is twice the conduction activation energy, they are probably not related.

Acknowledgment. We thank the NSF for support of this research under Grant No. GK 13612.

References and Notes

- (1) R. G. Kepler, *J. Chem. Phys.*, **39**, 3528 (1963).
- (2) A. J. Epstein, *et al.*, *Solid State Commun.*, **9**, 1803 (1971).
- (3) A. J. Epstein, *et al.*, *Phys. Rev. B*, **5**, 952 (1972).
- (4) R. Foster and P. Hanson, *Biochim. Biophys. Acta*, **112**, 482 (1966).
- (5) Y. Matsunaga, *Helv. Phys. Acta*, **36**, 800 (1963).
- (6) M. Litt and J. Summers, *J. Polym. Sci., Part A-1*, **11**, 1359 (1973).
- (7) "Beilsteins Handbuch der Organischen Chemie," Vol. 27, 86, I 243, II 51.
- (8) C. Lagercrantz, *Acta Chem. Scand.*, **15**, 1545 (1961).
- (9) J. M. Lhoste and F. Tannard, *J. Chim. Phys.*, **63**, 678 (1966).
- (10) J. P. Billen, *J. Chim. Phys.*, **61**, 374 (1964).
- (11) A. Many, E. Harnik, and D. Gerlich, *J. Chem. Phys.*, **23**, 1733 (1955).
- (12) J. W. Stout and R. C. Chisholm, *J. Chem. Phys.*, **36**, 979 (1962).
- (13) Y. Sato, M. Kinoshita, *et al.*, *Bull. Chem. Soc. Jap.*, **40**, 2539 (1967).
- (14) R. M. Lynden-Bell and H. M. McConnell, *J. Chem. Phys.*, **37**, 794 (1962).
- (15) S. Hirama, H. Kuroda, and H. Akamota, *Bull. Chem. Soc. Jap.*, **44**, 3 (1971).
- (16) Z. G. Soos and D. J. Klein, *J. Chem. Phys.*, **55**, 3284 (1971).

Structure of Aqueous Solutions. Structure Making and Structure Breaking in Solutions of Sucrose and Urea

David W. James*

Chemistry Department, University of Queensland, St. Lucia, Australia

and Ray L. Frost

Chemistry Department, Queensland Institute of Technology, Brisbane, Australia (Received April 8, 1974)

The effect of sucrose and urea on the librational band of water has been studied by infrared spectroscopy. Sucrose is found to produce little change in the band while all band characteristics are changed by the addition of urea. Comparison with changes produced by electrolytes indicates that the structural change produced by urea is different from that observed in electrolyte solutions.

The terms structure making and structure breaking have been used to describe aqueous solutions containing various solutes. From various measurements it was concluded that urea was a structure breaker while sucrose was a structure maker.^{1,2} The region of the vibrational spectrum which corresponds to the librational energy of water molecules has been little studied although it may be expected to yield significant information on the hydrogen bonded structure in solutions. We present here a preliminary report of a study of the librational spectrum of water in solutions of sucrose and urea using a thin film infrared technique.

The spectra were obtained using a Perkin-Elmer 457 spectrometer and a thin film transmission technique in which a film of $\sim 7 \mu$ thickness was held between KRS-5 plates. Appropriate corrections were made for reflection losses and variations in film thickness and reproducibility of better than 1% in band intensity could be maintained from run to run. Band intensities are adjusted to unit concentration of water and all intensities are quoted relative to that of pure water at 20°. The technique is reported in detail elsewhere.³ The collected results for urea and sucrose at various concentrations and temperatures are collected in Table I. Also shown, for comparison, are results for selected ionic salts.^{3,4}

Three of the four band characteristics reported in Table I show different behavior for urea and sucrose. The shift in band maximum with added solute shows a small decrease in energy with either sucrose or urea. This decrease is similar to that noted for a number of ionic salts. The

band intensity increases much faster with added urea than it does for added sucrose. In this respect urea is similar to tetraethylammonium nitrate and potassium iodide; sucrose on the other hand resembles potassium nitrate. The decrease of intensity with temperature rise noted for urea is unique among the solutes studied; pure water and all other solutions examined show an intensity increase. The band asymmetry as measured by the asymmetry index⁵ is markedly different for urea for which the asymmetry goes from negative for pure water to appreciably positive. The only other solutes for which positive asymmetry indices have been measured are LiNO₃, NaClO₄, LiCl, BaBr₂, NaI, and KI at very high salt concentrations (*e.g.*, for LiNO₃ concentration of 10 *m* the asymmetry index is +8).

Examination of the spectrum of water as the temperature is raised indicates that a gradual disruption of the water structure produces a small increase in band intensity, a marked decrease in the band maximum, and little effect on the band asymmetry. The salts NH₄Cl, NH₄Br, and to a lesser extent NH₄NO₃ and NH₄ClO₄ show concentration-dependent behavior which resembles this. The behavior of all other solutes is more complex.

Intensity increase with added solute is frequently large; the largest increases are noted when there is a great size difference between anion and cation (*e.g.*, LiI) or when the cation has aliphatic side chains (tetraalkylammonium cation). The former may be ascribed to the structure disruption produced by the dissimilar ion sizes while the latter may generally be ascribed to hydrophobic bonding. In

TABLE I: Characteristics of the Librational Band of Water with Added Urea and Sucrose

Sample	Concn, <i>M</i>	20°				40°				60°			
		<i>I</i> _{rel} ^c	ν_{\max}	<i>W</i> /2	ν_{As}	<i>I</i> _{rel} ^c	ν_{\max}	<i>W</i> /2	ν_{As}	<i>I</i> _{rel} ^c	ν_{\max}	<i>W</i> /2	ν_{As}
H ₂ O	Pure	1.00	690	445	-20	1.03	660	433	-25	1.05	625	420	-30
Urea	2	1.10	670	440	0								
	5	1.23	640	432	+20	1.15	605	430	+20	1.10	600	420	+22
	9	1.44	595	425	+20	1.25	585	425	+20	1.19	580	415	+20
Sucrose	0.5	1.01	685	440	-20	1.02	655	425	-30	1.00	628	415	-24
	1	1.01	680	452	-20	1.02	650	425	-28	1.03	620	420	-20
	2	1.03	675	418	-20	1.03	640	430	-25	1.05	610	420	-18
Et ₄ NNO ₃ ^a	2	1.12	676	422	-25								
KNO ₃ ^a	2	1.01	690	485	-40								
KCl ^a	2	1.05	650	505	-40								
KBr ^a	2	1.03	645	503	-30								
KI ^a	2 ^b	1.08	640	518	-40								

^a Intensities increase with temperature rise. V_M decreases with temperature rise (small); *W*/2 increases with temperature rise (small). ^b At high concentrations KI has a positive ν_{As} . ^c *I*_{rel} is the integrated intensity relative to that of pure water.

any case the intensity increase can be associated with a disruption of water structure. In the case of urea there is a marked intensity increase with added urea but neither disparate ion size nor aliphatic side chains can be responsible. If the urea acted to disrupt the hydrogen bonded network there would be increased librational freedom which would result in greater amplitude of the librational motion. This would result in an increase in band intensity. The changes noted in the energy of the band maximum may also be attributed to a decrease in the hydrogen bonded forces holding the water molecules in the mean librational position. The asymmetry of the librational band shows considerable variation as solutes are added to water. For most electrolytes (except ammonium salts) the asymmetry decreases (and may change sign) as the electrolyte concentration increases. This decrease in asymmetry is most pronounced for iodides where the large anion is expected to contribute to the absorption of water structure.

The change in band symmetry is more pronounced for urea than for any other solute studied. We feel that it gives a clear indication that the average environment of water molecules has been drastically altered by the addition of urea. This change is more pronounced than that produced by other solutes studied.

The spectroscopic changes induced by addition of sucrose to water are, in general, small. They indicate that the forces acting on water molecules do not show great change as the sucrose is added. Thus the intermolecular water-water interactions appear to be similar to the intermolecular water-sucrose interactions.

The use of the terms "structure making" and "structure breaking" to describe our results does not appear to be appropriate. It is obvious that urea produces pronounced changes in the forces acting on water molecules but whether this should be termed structure breaking is not obvious. This work is currently being extended to a range of substituted ureas and thioureas in an attempt to clarify the factors contributing to changes in the intermolecular forces influencing water in solution.

Note Added in Proof. It has been suggested that a more extensive discussion of the band variations observed, together with a comparison with findings from other techniques, would be useful. The factors influencing the librational band are not adequately illustrated by sucrose and urea. However, the findings from a study of solutes structurally related to urea has enabled a much more satisfactory discussion to be developed and this will be published shortly.

References and Notes

- (1) D. V. Beauregard and R. E. Barrett, *J. Chem. Phys.*, **49**, 5241 (1968); G. A. Vidulich, J. R. Andrade, P. B. Blanchette, and T. J. Gilligan, *J. Phys. Chem.*, **73**, 1621 (1969); V. I. Khamova, A. M. Ponomareva, and K. P. Mishchenko, *Russ. J. Phys. Chem.*, **40**, 748 (1966); H. S. Frank and F. Franks, *J. Chem. Phys.*, **48**, 4746 (1968); G. Barone, E. Rizzo, and V. Vitagliano, *J. Phys. Chem.*, **74**, 2230 (1970).
- (2) G. E. Walrafen, *J. Chem. Phys.*, **44**, 3726 (1966).
- (3) R. F. Armishaw and D. W. James, submitted for publication; R. F. Armishaw, Ph.D. Thesis, University of Queensland, St. Lucia, 1972.
- (4) D. W. James and R. F. Armishaw, to be submitted for publication.
- (5) The asymmetry index is defined as the difference in wave numbers between the band maximum and the middle of the isoabsorbance chord at half-band height.

Self-Diffusion Coefficients for Chloride Ion in Aqueous Solutions of Sodium Polyacrylate Containing Sodium Chloride

Shelini Menezes-Affonso and Paul Ander*

Department of Chemistry, Seton Hall University, South Orange, New Jersey 07079 (Received January 21, 1974)

Publication costs assisted by Seton Hall University

The concentration dependence of the self-diffusion coefficients of the coion in polyelectrolyte solutions containing simple salts was studied at two concentrations of sodium polyacrylate at several concentrations of sodium chloride in water at 25°. At constant polyelectrolyte concentration, the self-diffusion coefficients of the coion increase with the added salt concentration, whereas at a fixed salt concentration the coion self-diffusion coefficients decrease with increasing polymer concentration. Good correlation has been obtained between the predictions for the self-diffusion coefficient of the coion obtained from the Manning line charge polyion model and the data presented in this study.

It is well recognized that the interactions of small ions with polyelectrolytes in aqueous solution govern many of the solution properties of polyelectrolytes. Attention has been focused on the long-range electrostatic and short-range specific interactions of the counterions with the polyion.¹⁻⁵ However, no systematic experimental investigations have been reported concerning the interactions of the coion with the polyion. This interaction has been dismissed by many by their insistence that the coion, being of the same charge as the polyion, would hardly be affected by the polyion. Yet, the literature contains some results⁶⁻¹⁴ that indicate that the coion has a noticeable effect on the solution properties of polyelectrolytes.

A model for polyelectrolyte solutions developed by Manning¹⁵⁻¹⁷ presents simple limiting laws for both thermodynamic and transport properties for both the counterion and the coion. According to this theory, a fraction of the counterions condense onto the polyion above a critical charge density for the polyion. The coions interact with the polyion by Debye-Hückel interactions, as do the uncondensed counterions.

While the Manning theory has not been tested extensively, a few good correlations between the theory and experimental results have been discussed.⁴ Recently, Dixler and Ander¹⁸ reported excellent agreement between the theoretical and experimental values of the self-diffusion coefficient of sodium ions in aqueous solutions of sodium polyacrylate in sodium chloride. Here, we discuss the results of the self-diffusion coefficients of chloride ions in aqueous solutions of sodium polyacrylate containing sodium chloride. A capillary method^{19,20} was used along with an equation developed by McKay²¹

$$D = \frac{\pi}{4} \left(1 - \frac{C}{C_0}\right)^2 \frac{l^2}{t} \quad (1)$$

where D is the self-diffusion coefficient, C/C_0 is the ratio of final to the initial chloride activities in the capillary, l is the length of the capillary, and t is the time of diffusion. The experimental conditions employed in this work were such that $0.5 < C/C_0 < 0.7$, for which range McKay's equation has been shown to be valid.

Experimental Section

Material. The sodium polyacrylate used in this investigation was the same used in a previous study.¹⁸ The radioactive ³⁶Cl (half-life 3×10^5 years) was obtained from New England Nuclear as a 2.68 N H ³⁶Cl aqueous solution, which was neutralized with aqueous NaOH.

Diffusion Measurements. All diffusion measurements were carried out in a bath thermostated at $25.00 \pm 0.01^\circ$. The diffusion assembly was the same as used previously.¹⁸ Precision bore capillaries of 1.60 mm i.d. and 3.00 cm length were used. After time was allowed for diffusion, usually 1 day, each capillary solution was quantitatively transferred to a planchet. All planchets were dried under an infrared lamp while rotating slowly on a sample spinner. After being emptied of the diffused contents, the capillary was rinsed with the original tracer solution and refilled. This was again quantitatively transferred to another planchet and dried. The two planchets were subsequently counted in a Geiger counter to give C and C_0 .

Sample Counting and Validation of Technique. Since ³⁶Cl emits high energy β particles, a Geiger-Muller Counter was selected as a detector. The counting assembly consisted of a Nuclear Chicago G-M counter, timer, and a scaler Model 181B.

The counting parameter used to calculate the diffusion coefficient according to eq 1 is the square of the ratio C/C_0 and consequently the error is magnified substantially. In order to minimize the counting errors, each sample was counted at least six times, each count for a duration of 15 min. The diffusion coefficients reported were calculated from the total count obtained from the six measurements for each sample. Each D_2 value reported is the average value and the standard deviation obtained for three to six samples.

Prior to the self-diffusion measurements in NaPA solutions, the validity of the transfer of capillary contents, the counting techniques, and the diffusion procedure were tested using aqueous NaCl solutions. The diffusion technique described above and eq 1 were used to determine the diffusion coefficients of Cl⁻ in 0.050 and 0.030 N NaCl solutions. The results obtained were $1.93 \pm 0.01 \times 10^{-5}$ and $1.97 \pm 0.01 \times 10^{-5}$ cm²/sec for the 0.050 and 0.030 N NaCl,

respectively. Since these are in good agreement with the corresponding literature values of 1.94×10^{-5} and 1.96×10^{-5} cm²/sec,²² the technique was concluded to be adequate for use in this study.

Results and discussions

Self-diffusion coefficients for Cl⁻ D_2 were determined in dilute aqueous solutions of NaPA containing NaCl at 25°. Completely neutralized NaPA at concentrations of 0.0100 and 0.0300 *N* were used. The NaCl concentrations ranged from 0.0011 to 0.0300 *N*. Thus the value of *X*, defined by

$$X = n_e/n_s \quad (2)$$

where n_e and n_s are equivalent concentrations of the polyelectrolyte and sodium chloride, respectively, ranged from 1 to 9 for both polyelectrolyte concentrations.

From the experimental results depicted in Table I it is evident that the D_2 values decrease with increasing values of *X*, leveling off to a constant value at high *X* values. Also the D_2 values decrease with a decrease in concentration of the added salt, at constant polymer concentration. (It should be noted that this tendency is in contrast with the behavior in simple salt solutions^{23,24} where the opposite trend is observed.) Inspection of the data in Table I further reveals that at a fixed concentration of simple salt, the diffusion coefficients decrease with increasing polymer concentration. Most important is that D_2 is found to be a function of *X* only under the conditions studied.

A test of the Manning theory is to compare the experimental self-diffusion coefficients of the counterion and the coion with those predicted. Very good agreement has been observed in the case of the counterion.¹⁸ The experimental data obtained for the self-diffusion coefficients of the Cl⁻ ion were correlated with Manning's theoretical predictions. Based on the assumption that the condensed counterions have negligible mobility while all the uncondensed small ions are subject to Debye-Hückel interactions with the polyions, Manning derived expressions to calculate the self-diffusion coefficients of the mobile ions. The diffusion coefficient on an *i*th ion is given by

$$\frac{D_i}{D_i^0} = 1 - \frac{1}{3} A \quad (3)$$

where *i* = 1 and 2 represents the uncondensed counterions and the coions, respectively; D_i is the self-diffusion coefficients of small ions in the polyelectrolyte solution and D_i^0 is its value at infinite dilution in the absence of polyelectrolyte; and the quantity *A* is given by the series

$$A = \sum_{m_1=-\infty}^{\infty} \sum_{m_2=-\infty}^{\infty} [\pi(m_1^2 + m_2^2) + 1 + 2\xi^{-1}]^{-2} \quad (4)$$

where $m_1, m_2 \neq 0, 0$; $\xi > 1$; m_1 and m_2 are integers and ξ is a linear charge density parameter given by

$$\xi = Z_p e^2 / \epsilon k T b$$

and Z_p is the valence of a charged group on the polyion, *e* is the unit of electrical charge, *k* is the Boltzmann constant, *T* is the absolute temperature, and *b* the distance between charges on the polyion, 2.5 Å for a fully charged vinylic polyelectrolyte making $\xi = 2.85$ for the present study. Since the series *A* was rapidly convergent, the summation for values of (m_1, m_2) was evaluated only from -10 to +10, ex-

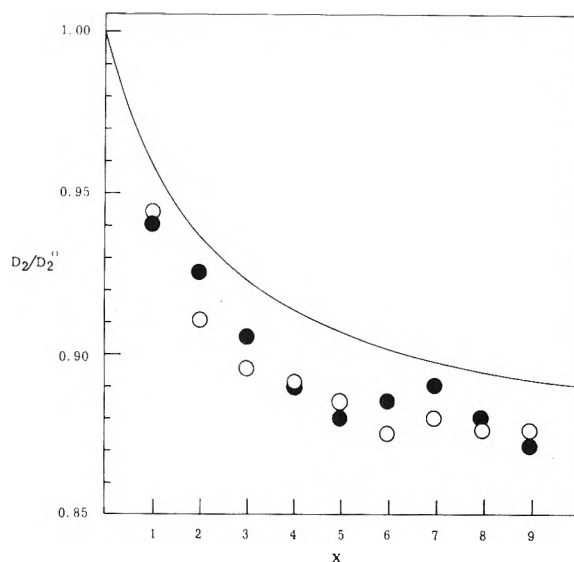


Figure 1. Plot of D_2/D_2^0 vs. *X*. Comparison of theoretical curve (solid line) with experimental D_2 values for $n_e = 0.0100$ *N*, O, and 0.0300 *N*, ●, with $D_2^0 = 2.033 \times 10^{-5}$ cm²/sec.

TABLE I: Self-Diffusion Coefficients for Cl⁻ in NaPA-NaCl-H₂O Solutions at 25°

<i>X</i>	$D_2 \times 10^6$, cm ² /sec	
	$n_e = 0.0100$ <i>N</i>	$n_e = 0.0300$ <i>N</i>
1	1.92 ± 0.02	1.91 ± 0.03
2	1.85 ± 0.03	1.88 ± 0.01
3	1.82 ± 0.01	1.84 ± 0.03
4	1.81 ± 0.00	1.81 ± 0.01
5	1.80 ± 0.01	1.79 ± 0.03
6	1.78 ± 0.03	1.80 ± 0.02
7	1.79 ± 0.01	1.81 ± 0.01
8	1.78 ± 0.00	1.79 ± 0.01
9	1.78 ± 0.01	1.77 ± 0.02

TABLE II: Values for *X* = 1 to 9

$\xi^{-1}X$	<i>A</i>	$\xi^{-1}X$	<i>A</i>
0.351	0.125	2.105	0.298
0.702	0.194	2.456	0.310
1.053	0.235	2.807	0.319
1.403	0.263	3.150	0.326
1.754	0.283		

cluding the point (m_1, m_2) = (0, 0). The values obtained for *A* for *X* values from 1 to 9 are given in Table II.

The limiting laws are specifically formulated to be strictly valid at infinite dilution. However, the properties of polyelectrolyte solutions at the lowest measurable concentrations are taken to be very close to those at infinite dilution. The range of *X* values was chosen because according to Manning theory the "polyelectrolyte effect" on the diffusion coefficients of the coion is especially evident at high values of *X*.

Using the limiting value for $D_2^0 = 2.033 \times 10^{-5}$ cm²/sec²² and the values obtained as described above for *X* and *A*, theoretical values were computed from eq 3 for D_2 . It can be seen from Figure 1 that the D_2/D_2^0 values obtained from self-diffusion experiments are in close agreement with the values calculated from eq 3, within range of concentrations investigated. This lends confirmation to Manning's theory for self-diffusion, since both the self-diffusion coefficients

of the counterion and the coion are found to be in good agreement with the predicted values.

The general trend predicted is for the D_2 of the coion to rapidly decrease with increasing X values and then to level off to a constant value at higher values of X over a wide range of concentrations. To investigate the validity of this conclusion two sets of data were obtained keeping X constant and varying the values of n_e and n_s . From Figure 1 it can be seen that the D_2 values for the two sets of points are in good agreement and also display the expected trend. It should be noted from Figure 1 that the experimental points fall about 3% below the theoretical curve. This small discrepancy may be thought to be due to the neglect of small ion-small ion interactions in the theory, which was discussed by Wells.²⁵ However, Dixler and Ander¹⁸ found no need to consider small ion-small ion interactions since this small correction would be hard to detect in the larger scatter of the points.

Theoretically the limiting value of D_2 at $n_s = 0$, i.e., a polyelectrolyte with no simple salt present, could be obtained by evaluating A at $X = \infty$, which is 0.40, and inserting this value into eq 3. This gives $D_2/D_2^0 = 0.87$ and hence $D_2 = 1.78 \times 10^{-5}$ cm²/sec for the limiting value. It is interesting that for both polyelectrolyte concentrations employed in this study, a constant value of $1.79 \pm 0.03 \times 10^{-5}$ cm²/sec was obtained for D from $X = 4$ to $X = 9$. At $X = 4$, D_2/D_2^0 has a theoretical value of 0.91, which is approximately 5% greater than 0.87, the limiting value at $X = \infty$ which is predicted from the theory.

One additional prediction to be made from Manning relationship is that

$$D_1/D_1^0 < D_2/D_2^0$$

that is, for a maximally charged polyelectrolyte the relative decrease in the self-diffusion coefficient of the counterion is larger than that for the coion. For this case the diffusion coefficients of the condensed counterions are assumed to

be zero and those of the uncondensed counterions are given by the equation

$$\frac{D_1}{D_1^0} = (\xi^{-1}X + 1)(X + 1)^{-1} \left(1 - \frac{1}{3}A\right) \quad (5)$$

The experimental data for D_{Na^+} ¹⁸ and D_{Cl^-} confirm the above result. Furthermore, these self-diffusion results justify an assumption of the Manning model that the mobility of the condensed counterions is negligible.

Acknowledgment. We are grateful to Dr. G. S. Manning for his stimulating discussions.

References and Notes

- (1) S. A. Rice and M. Nagasawa, "Polyelectrolyte Solutions," Academic Press, New York, N. Y., 1961, Chapter 9.
- (2) F. Oosawa, "Polyelectrolytes," Marcel Dekker, New York, N. Y., 1971, p 160.
- (3) R. W. Armstrong and U. P. Strauss, "Polyelectrolytes," in "Encyclopedia of Polymer Science and Technology," Vol. X, Wiley, New York, N. Y., 1969.
- (4) G. S. Manning, *Annu. Rev. Phys. Chem.*, **23**, 117 (1972).
- (5) A. Katchalsky, *Pure Appl. Chem.*, **26**, 327 (1971).
- (6) P. H. von Hippel and T. Schleigh, *Accounts Chem. Res.*, **2**, 257 (1969).
- (7) H. Eisenberg and G. R. Mohan, *J. Phys. Chem.*, **63**, 671 (1959).
- (8) H. Eisenberg and D. Woodside, *J. Chem. Phys.*, **36**, 1844 (1962).
- (9) A. Takahashi, S. Yamori, and T. Kagawa, *Nippon Kagaku Zasshi*, **83**, 11, 14 (1962).
- (10) J. T. G. Overbeek, A. Vrij, and H. F. Huisman, in "Electromagnetic Scattering," M. Kerker, Ed., Macmillan, New York, N. Y., 1962, p 321.
- (11) R. L. Gustafson, *J. Phys. Chem.*, **67**, 2549 (1963).
- (12) M. Nagasawa, I. Kagawa, and M. I. Izumi, *J. Polym. Sci.*, **37**, 375 (1959).
- (13) T. J. Podlas and P. Ander, *Macromolecules*, **2**, 432 (1969).
- (14) T. J. Podlas and P. Ander, *Macromolecules*, **3**, 154 (1970).
- (15) G. S. Manning, *J. Chem. Phys.*, **51**, 924 (1969).
- (16) G. S. Manning, *J. Chem. Phys.*, **51**, 934 (1969).
- (17) G. S. Manning, *J. Chem. Phys.*, **51**, 3249 (1969).
- (18) D. S. Dixler and P. Ander, *J. Phys. Chem.*, **77**, 2684 (1973).
- (19) J. A. Anderson and D. J. Saddington, *J. Chem. Soc.*, S381 (1949).
- (20) R. Fernandez-Prini, E. Baumgarter, S. Liberman, and A. E. Lagos, *J. Phys. Chem.*, **73**, 1420 (1969).
- (21) R. McKay, *Proc. Phys. Soc.*, **42**, 547 (1930).
- (22) J. H. Wang and S. Miller, *J. Amer. Chem. Soc.*, **74**, 1611 (1952).
- (23) R. Mills, *J. Phys. Chem.*, **61**, 1631 (1957).
- (24) R. S. Robinson and R. H. Stokes, "Electrolyte Solutions," Butterworths, London, 1959.
- (25) J. D. Wells, *Biopolymers*, **12**, 223 (1973).

Effect of Ethanol on Hydrophobic Interactions. Conductometric Study of Ion-Pair Formation by Double-Long-Chain Electrolytes

D. G. Oakenfull* and D. E. Fenwick

Division of Food Research, CSIRO, North Ryde, New South Wales 2113, Australia (Received December 27, 1973)

Publication costs assisted by the Commonwealth Scientific and Industrial Research Organization

The equivalent conductance (Λ) of double-long-chain electrolytes such as decyltrimethylammonium deca-noate was measured in a series of ethanol-water mixtures in which the mole fraction of ethanol was 0.05, 0.10, 0.15, and 0.20. With increasing electrolyte concentration, Λ was found to decrease by more than was predicted by the Onsager equation. This discrepancy was treated as resulting from ion-pair formation, and ion-pair association constants (K) were calculated. The electrostatic and hydrophobic contributions to the free energy of ion-pair formation ($\Delta G_{\text{ion pair}} = -RT \ln K$) were separated by examining the effect of hydrocarbon chain length on $\Delta G_{\text{ion pair}}$. The change of the electrostatic contribution with ethanol concentration, as a result of accompanying change in the dielectric constant, agreed with Bjerrum's equation. The hydrophobic contribution (ΔG_{HI}) initially decreased (hydrophobic interactions became stronger) with increasing concentration of ethanol, with the minimum value observed when the mole fraction of ethanol was 0.10. A linear relationship was obtained when ΔG_{HI} was plotted against the reciprocal of the isothermal compressibility (a measure of the free energy required to make a cavity in the solvent to accommodate a hydrophobic solute). Contrary to popular belief, ΔG_{HI} does not appear to be related to the surface tension of the solvent.

Introduction

The importance of hydrophobic interactions in maintaining the viability of living organisms is widely recognized.¹⁻⁸ Studies of effects of solutes on hydrophobic interactions are important since they further our theoretical understanding of these interactions and also provide a means of distinguishing hydrophobic from other forces (such as electrostatic and hydrogen bonding) involved in stabilizing the native conformation of proteins and nucleic acids.

While studying the effects of hydrophobic interactions on the kinetics of reactions of some long-chain alkylamines with long-chain carboxylate esters of *p*-nitrophenol, we noticed that low concentrations of ethanol (mole fraction ≤ 0.1) apparently increased the effect of hydrophobic interaction between the hydrocarbon chains, compared with the effect in pure water.⁹ In this paper we report a more detailed investigation of this phenomenon.

This investigation is based on measurements of the equivalent conductance of solutions of hydrophobic ions. Some preliminary experiments¹⁰ on purely aqueous solutions of decyltrimethylammonium undecanoate, decanoate, nonanoate, etc. had suggested that hydrophobic interaction between the hydrocarbon chains might lead to the formation of ion pairs (at concentrations below the critical micelle concentration), but the effect was too small to obtain reliable ion-pair association constants. Addition of ethanol can be expected to favor formation of ion pairs because it lowers the dielectric constant of the solvent.¹¹ Our investigation shows that when the mole fraction of ethanol is ≥ 0.05 , ion-pair formation is sufficiently increased to obtain reliable association constants and consequently to obtain an estimate of the free energy of hydrophobic interaction between the hydrocarbon chains.

Experimental Section

1. *Materials.* Decyltrimethylammonium bromide (Eastman) was recrystallized from 50% (v/v) ethanol-ether. Car-

boxylic acids were redistilled before use. Water was distilled from glass and passed through a mixed-bed ion-exchange column [Bio-Rad AG 501-X8 (D)]. The conductivity was always below $1 \times 10^{-4} \text{ ohm}^{-1} \text{ cm}^{-1}$.

Decyltrimethylammonium hydroxide was prepared by shaking a solution of the bromide (0.15 M) with a twofold excess of freshly precipitated silver hydroxide, for 2 hr. The filtrate was titrated potentiometrically (Radiometer PHM26/ABU 1c), and carboxylate solutions were prepared by neutralizing ($6 < \text{pH} < 7$) aliquots with the appropriate amount of neat carboxylic acid. An appropriate weighed quantity of ethanol was added at this point.

2. *Methods.* Conductance measurements were made with a Wayne-Kerr universal bridge (B224). The cell was fitted with platinized platinum electrodes and was of a type designed for use with solutions which have a tendency to froth (see Figure 13 of ref 12). The cell constant (15.72) was checked before and after each set of experiments by using standard potassium chloride.¹¹ The carboxylate solutions were diluted by weight with the appropriate mixture of ethanol and water. All solutions were thermostated at $25^\circ (\pm 0.05^\circ)$. We could detect no change in conductance with time, once the test solution had reached the thermostat temperature. When appropriate, the conductivity was corrected for the conductivity of the solvent.

An Olivetti Programma 101 programable calculator was used for the repetitive calculations.

Results

Figure 1 shows equivalent conductance (Λ) plotted against the square root of the molar concentration, in 0.1 mole fraction ethanol-water, for decyltrimethylammonium dodecanoate, undecanoate, decanoate, nonanoate, octanoate, heptanoate, and acetate. The long-chain carboxylates form micelles within the concentration range of these experiments (indicated by a sharp decrease in Λ), but as the points observed above the critical micelle concentration (cmc) are not relevant here, we have simplified the figure

TABLE I: Decyltrimethylammonium Carboxylates in 0.10 Mole Fraction Ethanol–Water at 25°

Carboxylate ion	$\Lambda_0^{\text{RCO}_2\text{K}^a}$	Λ_0^b	Λ_0^c	K, M^{-1}	C_{mc}, M
Acetate	64.27		36.40 ^d		>0.02
Heptanoate	57.59	29.72	29.83	5.8 ± 1.2	>0.02
Octanoate	57.42	29.55	29.71	10.6 ± 1.2	0.014
Nonanoate	56.50	28.63	28.66	38.6 ± 1.2	0.0080
Decanoate	55.88	28.01	28.03	91.6 ± 1.7	0.0056
Undecanoate	55.42	27.55	27.53	190 ± 2	0.0046
Dodecanoate	54.89	27.02	27.05	192 ± 3	0.0036

^a Limiting equivalent conductance ($\text{cm}^2 \text{ohm}^{-1} \text{mol}^{-1}$) of the potassium salt. ^b Limiting equivalent conductance of the decyltrimethylammonium salt, calculated from eq 2. ^c Limiting equivalent conductance obtained by using Davies' procedure. ^d Obtained, directly, from the Onsager equation.

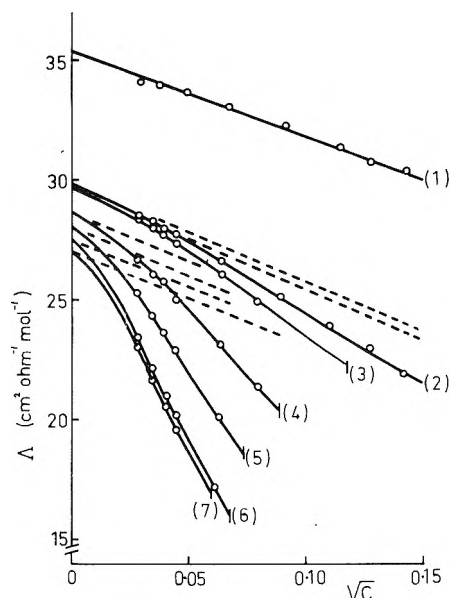


Figure 1. Equivalent conductance (Λ) of decyltrimethylammonium carboxylate solutions in 0.1 mole fraction ethanol–water at 25° plotted against \sqrt{C} where C is the molar concentration: (1) acetate, (2) heptanoate, (3) octanoate, (4) nonanoate, (5) decanoate, (6) undecanoate, (7) dodecanoate. Broken lines show the theoretical (Onsager) slope. Vertical lines represent the cmc.

by terminating the plots at the cmc. (Approximate values of the cmc are given in Table I.)

The points for the acetate conform with the Onsager equation¹¹ (within the limits of experimental error) but those for the long-chain carboxylates lie consistently below the theoretical lines, indicated in Figure 1 by broken lines. The discrepancy is large enough (<25% for the dodecanoate) to be confidently explained as resulting from ion-pair formation,^{11,13} and such an explanation is supported by the fact that consistent values of the ion-pair association constant (K) were obtained for each set of values of electrolyte concentration and Λ (see below).

Modified to take ion-pair formation into account, the Onsager equation is usually given as

$$\Lambda = \alpha[\Lambda_0 - (P + Q\Lambda_0)\sqrt{\alpha c}] \quad (1)$$

where P and Q are the constants which give the Onsager slope, α is the fraction of dissociated ions, c is the molar concentration (for a 1:1 electrolyte), and Λ_0 is the limiting equivalent conductance.

For this particular concentration of ethanol (mole fraction of 0.10), values of Λ_0 were obtained independently of the data of Figure 1 by measuring Λ_0 for the potassium salt of each of the carboxylic acids. Λ_0 for the decyltrimethylammonium carboxylate was then given by

TABLE II: Calculation of K for Decyltrimethylammonium Decanoate in 0.10 Mole Fraction Ethanol–Water at 25°

C, M	Λ^a	α^b	f_{\pm}^{2c}	K, M^{-1}
0.00397	20.70	0.804	0.854	89.5
0.00199	22.97	0.872	0.887	94.8
0.00156	23.81	0.898	0.897	90.1
0.00120	24.49	0.918	0.908	88.6
0.00079	25.25	0.938	0.923	95.0

^a Observed equivalent conductance ($\text{cm}^2 \text{ohm}^{-1} \text{mol}^{-1}$). ^b Fraction of dissociated ions, calculated from eq 1. ^c Mean activity coefficient calculated from the Debye–Hückel equation, ^d Mean value is 91.6 with standard error ±1.2.

TABLE III: Comparison of Observed and Calculated Values of Λ for Decyltrimethylammonium Decanoate in 0.10 Mole Fraction Ethanol–Water at 25°

C, M	Obsd Λ	Calcd ^a Λ	
		Onsager	Fuoss and Onsager
0.00397	20.70	20.69	20.91
0.00199	22.97	23.14	23.26
0.00156	23.81	23.85	23.94
0.00120	24.49	24.51	24.60
0.00079	25.25	25.41	25.45

^a $\Lambda_0 = 28.09 \text{ cm}^2 \text{ohm}^{-1} \text{mol}^{-1}$, $K = 91.6 M^{-1}$, $a = 0.352 \text{ nm}$.

$$\Lambda_0 = \Lambda_0^{\text{CH}_3\text{CO}_2\text{D}} + \Lambda_0^{\text{RCO}_2\text{K}} - \Lambda_0^{\text{CH}_3\text{CO}_2\text{K}} \quad (2)$$

where $\Lambda_0^{\text{CH}_3\text{CO}_2\text{D}}$ is the limiting equivalent conductance of decyltrimethylammonium acetate, $\Lambda_0^{\text{RCO}_2\text{K}}$ is the limiting equivalent conductance of the potassium carboxylate, and $\Lambda_0^{\text{CH}_3\text{CO}_2\text{K}}$ is the limiting equivalent conductance of potassium acetate. An iterative procedure was then used to calculate from eq 1 α for each set of values of c and Λ . The association constant (K) was then calculated from

$$K = (1 - \alpha)/f_{\pm}^2 \alpha^2 c \quad (3)$$

in which f_{\pm} is the mean activity coefficient of the free ions as given by the Debye–Hückel equation.¹¹ Table II shows a typical set of results. The values of K were considered sufficiently close to each other to substantiate our interpretation of the results in terms of ion-pair formation.

Alternatively, Λ_0 and K can be obtained without recourse to the equivalent conductance of the potassium salts by using the procedure suggested by Davies.^{13,14} This gave values of Λ_0 almost identical with those obtained by using the potassium salts (see Table I); hence we felt justified in using this less laborious procedure for the other concentrations of ethanol.

Instead of using the Onsager equation to calculate K , we considered using the more exact version of Onsager and

TABLE IV: Decyltrimethylammonium Carboxylates in Ethanol–Water Mixtures at 25°

Carboxylate ion	$X_{\text{EtOH}}^a = 0.05$		$X_{\text{EtOH}}^a = 0.15$		$X_{\text{EtOH}}^a = 0.20$	
	$\Lambda_0, \text{cm}^2 \text{ohm}^{-1} \text{mol}^{-1}$	K, M^{-1}	$\Lambda_0, \text{cm}^2 \text{ohm}^{-1} \text{mol}^{-1}$	K, M^{-1}	$\Lambda_0, \text{cm}^2 \text{ohm}^{-1} \text{mol}^{-1}$	K, M^{-1}
Acetate	47.37	<0.6	27.31		27.43	
Hexanoate	40.00		23.06	1.8 ± 0.2		
Heptanoate	38.77	1.4 ± 0.4	22.39	2.9 ± 0.1	22.49	2.4 ± 0.2
Octanoate	38.55	3.2 ± 0.2	22.22	6.6 ± 0.2	22.37	3.7 ± 0.2
Nonanoate	37.20	7.5 ± 0.2	21.78	12.5 ± 0.4	21.60	5.6 ± 0.1
Decanoate	36.46	17.1 ± 0.2	21.08	23 ± 1	21.18	9.1 ± 0.1
Undecanoate			20.79	43 ± 1	20.72	12.3 ± 0.1

^a Mole fraction of ethanol.

Fuoss,¹⁵ but a comparison (see Table III) of the observed values of Λ , for decyltrimethylammonium decanoate, with values of Λ calculated from both the original Onsager equation (eq 1) and the extended version of Onsager and Fuoss leads to the conclusion that our results were not of sufficient precision to justify the more elaborate treatment.

The results obtained in ethanol–water mixtures containing 0.05, 0.15, and 0.20 mole fraction of ethanol are summarized in Table IV.

Discussion

1. *The Free Energy of Hydrophobic Interaction in Ethanol–Water Mixtures.* The free energy of ion-pair formation by the hydrophobic ions is given by

$$\Delta G_{\text{ion pair}} = -RT \ln K \quad (4)$$

The term $\Delta G_{\text{ion pair}}$ can be split into two components: the contribution from the interaction between the charged head groups ($\Delta G_{\text{electrostatic}}$) and the contribution from the interaction between hydrocarbon chains ($\Delta G_{\text{hydrophobic}}$).

$$\Delta G_{\text{ion pair}} = \Delta G_{\text{electrostatic}} + \Delta G_{\text{hydrophobic}} \quad (5)$$

The value of $\Delta G_{\text{hydrophobic}}$ must increase with increasing length of contact between the hydrocarbon chains. If we assume that the free energy increment for each additional contact between two methylene groups is constant, then

$$\Delta G_{\text{hydrophobic}} = n\Delta G_{\text{HI}} \quad (6)$$

where n is the number of methylene groups in contact in the ion pair and ΔG_{HI} is the free energy of hydrophobic interaction between two methylene groups (which includes contributions from both the hydrocarbon–hydrocarbon attraction and the solvent). This assumption would obviously be incorrect if the free hydrocarbon chains were curled up, by *intramolecular* hydrophobic interaction. However, the free energy of transfer of hydrocarbons to water, from the gas phase or from an organic solvent, varies linearly with the length of hydrocarbon chain from C_4 to C_{16} .¹⁶ Consequently intramolecular hydrophobic interaction must be insignificant for chain lengths below at least C_{16} . Combining eq 5 and 6, then, gives

$$\Delta G_{\text{ion pair}} = \Delta G_{\text{electrostatic}} + n\Delta G_{\text{HI}} \quad (7)$$

The interaction between the charged head groups, *i.e.*, $\Delta G_{\text{electrostatic}}$, is presumably constant and independent of the interaction between the hydrocarbon chains, so that $\Delta G_{\text{electrostatic}}$ and ΔG_{HI} can be separated by plotting $\Delta G_{\text{ion pair}}$ against n .

Figure 2 shows the four plots of $\Delta G_{\text{ion pair}}$ against n . (The values of n assume maximum contact between the hydro-

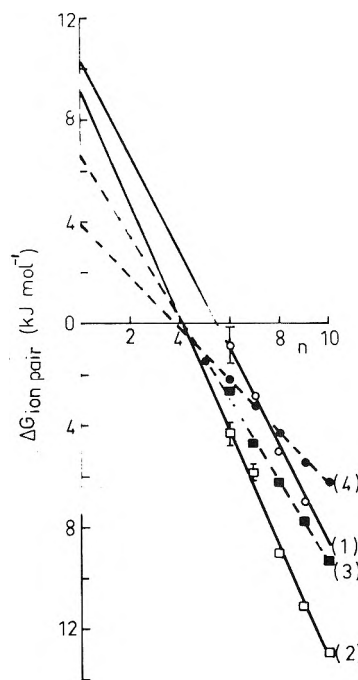


Figure 2. $\Delta G_{\text{ion pair}}$ plotted against the maximum number of methylene groups in contact (n). The lines refer to the following mole fractions of ethanol: (1) 0.05, (2) 0.10, (3) 0.15, (4) 0.20.

carbon chains.) These plots are indeed linear (correlation coefficients are given in Table V) and the intercepts ($\Delta G_{\text{electrostatic}}$) are consistent with Bjerrum's theory of ion-pair formation (see below). The values of $\Delta G_{\text{electrostatic}}$ and ΔG_{HI} are given in Table V. The table also includes a value of ΔG_{HI} for pure water ($-1.40 \text{ kJ}/(\text{mol methylene group})$). This value was obtained from a study of the binding of long-chain counterions to cationic micelles¹⁰ and is identical with that obtained from Némethy and Scheraga's theoretical treatment of hydrophobic interaction.¹⁷

The value of ΔG_{HI} initially becomes more negative (*i.e.*, hydrophobic interactions become *stronger*) with increasing concentration of ethanol, and this is in agreement with the qualitative trend previously observed in a kinetic study of reactions between hydrophobic molecules.⁹ The minimum value was observed when the mole fraction of ethanol was 0.10.

This was a surprising result because it has been argued that hydrophobic interactions are always *weakened*, by the addition of even dilute ethanol, and indirect evidence such as effects of ethanol on the cmc of nonionic detergents¹⁸ or on the solubility of amino acids¹⁹ has been brought to support this contention. We suggest that the similar argu-

TABLE V: Values of $\Delta G_{\text{electrostatic}}$ and ΔG_{HI} (Eq 7) at 25°

Mole fraction of ethanol	$\Delta G_{\text{electrostatic}}$, kJ mol ⁻¹	\bar{a} , ^a nm	ΔG_{HI} , kJ mol ⁻¹	Correln coeff
0			-1.40 ^b	
0.05	10.3 ± 1.0	0.352	-2.06 ± 0.13	0.837
0.10	9.2 ± 0.8	0.322	-2.24 ± 0.11	0.991
0.15	6.7 ± 0.3	0.352	-1.61 ± 0.04	0.997
0.20	4.0 ± 0.1	0.382	-1.03 ± 0.04	0.996

^a Effective distance between the charged groups in the ion pair, calculated according to Bjerrum. ^b From sources other than this work; see text.

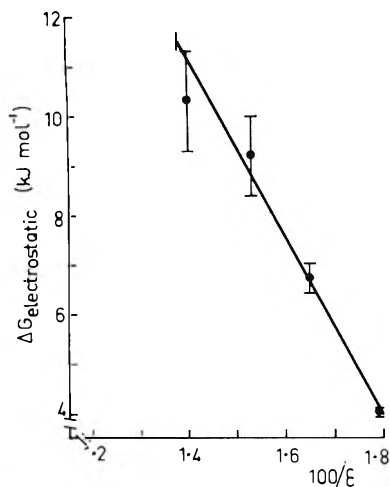


Figure 3. $\Delta G_{\text{electrostatic}}$ plotted against the reciprocal of the dielectric constant. (The curve was calculated according to Bjerrum.)

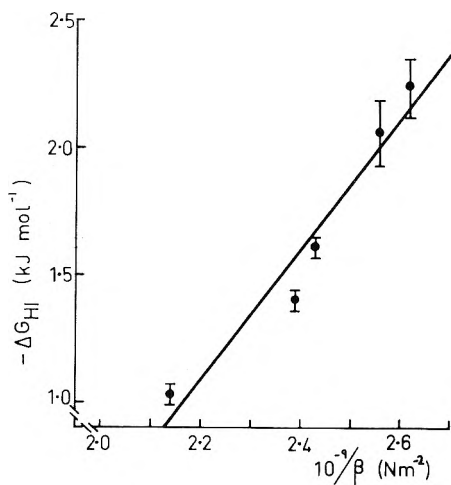


Figure 4. ΔG_{HI} plotted against $10^{-9}/\beta$, where β is the isothermal compressibility of the solvent at 25° (obtained from K. H. Jung, Thesis, University of Calgary, 1969).

ments which have been applied to determining the effect on hydrophobic interactions of other solutes, such as urea,^{20,21} guanidine hydrochloride,²⁰ or "chaotropic salts,"²² should be regarded with suspicion.

2. *The Variation of $\Delta G_{\text{electrostatic}}$ with Dielectric Constant.* Bjerrum¹¹ has developed a theoretical relationship between the free energy of formation of a simple ion pair, the dielectric constant of the solvent (ϵ), and the distance of closest approach of the two ions (\bar{a}). We have used Bjerrum's equations to calculate, from $\Delta G_{\text{electrostatic}}$, the distance between the two charged groups in a hydrophobic ion pair, in each of the four solvent mixtures. These distances (shown in Table V) are as consistent among themselves as

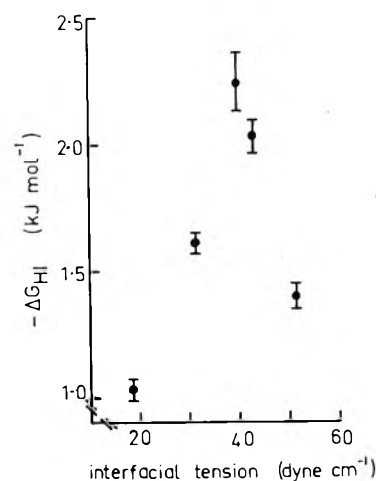


Figure 5. ΔG_{HI} plotted against the interfacial tension of the solvent and *n*-hexane. Values of interfacial tension, at 25°, were estimated by using the drop-weight method (J. T. Davies and E. K. Rideal, "Interfacial Phenomena," Academic Press, New York, N. Y., 1963).

can be expected¹¹ and inspection of molecular models shows that their mean value (0.352 nm) is physically reasonable. When this mean value was used to calculate the theoretical curve relating $\Delta G_{\text{electrostatic}}$ to $1/\epsilon$, there was excellent agreement between the theoretical curve and the experimental points (see Figure 3).

3. *Correlation of ΔG_{HI} with the Compressibility of the Solvent.* Several authors have suggested that the free energy required to make a cavity in the solvent, to accommodate the hydrophobic solute, might be a useful practical index for comparing hydrophobic interactions in different media.²²⁻²⁴ The free energy of cavity formation can be estimated from the isothermal compressibility (β) of the solvent by using the relationship⁹

$$\left(\frac{\partial G}{\partial V}\right)_T = -V\left(\frac{\partial P}{\partial V}\right)_T = -\frac{1}{\beta}$$

from which

$$\Delta G_{\text{cavity}} \approx -V_m/\beta \quad (8)$$

where V_m is the molar volume of the hydrophobic solute. If ΔG_{cavity} is proportional to ΔG_{HI} , then ΔG_{HI} should be linearly related to $1/\beta$. Figure 4 shows a plot of $-\Delta G_{\text{HI}}$ against $1/\beta$. This plot is sufficiently linear (the correlation coefficient is 0.946) to suggest that compressibility data might be used to predict effects of other media on hydrophobic interactions.

4. *Correlation of ΔG_{HI} with the Interfacial Tension of the Solvent and Hexane.* Figure 5 shows how ΔG_{HI} varies with the interfacial tension of the solvent and *n*-hexane. There is clearly no support here for the notion that interfacial tension is largely what determines hydrophobic inter-

actions.^{25,26} This is hardly surprising because it is inappropriate to apply a bulk surface tension to a very small surface consisting of a relatively small number of molecules. This was recognized as long ago as 1870 by Lord Kelvin when he stated that his equation for the equilibrium vapor pressure over a curved surface could not be expected to apply over distances of less than 500 molecular diameters.²⁷ Surface tension results from the fact that molecules at, or near, the surface of a liquid are subject to intramolecular forces more from one side (the interior of the liquid) than the other.²⁸ However, the maximum distance between water molecules at a "surface" surrounding a hydrophobic molecule need never be more than about 1 nm. At this distance the force between two water molecules is still about 10% of its maximum.²⁹ Consequently, the net force on the water molecules around a hydrophobic molecule must be quite different from that experienced by water molecules at the interface between water-hydrocarbon *bulk* phases.

It might be argued that interfacial tension is simply being used as a measure of the intramolecular forces that must be overcome to make a cavity in the solute. This again is doubtful because, although surface tension is undoubtedly controlled by intramolecular forces, it is only at the triple point that it can be *directly* related to the bulk properties of the liquid.^{30,31}

Acknowledgment. We thank Professor J. B. Hyne for supplying us with values of the isothermal compressibility of ethanol-water mixtures from K. H. Jung's thesis.

References and Notes

- (1) M. J. Tait and F. Franks, *Nature (London)*, **230**, 91 (1971).
- (2) G. Némethy, *Angew. Chem., Int. Ed. Engl.*, **6**, 195 (1967).
- (3) D. Chapman, "Biological Membranes," Academic Press, London, 1968.
- (4) V. N. Dorovska, S. D. Varfolomeyev, N. F. Kazanskaya, A. A. Klyosov, and K. Martinek, *FEBS (Fed. Eur. Biochem. Soc.) Lett.*, **23**, 122 (1972).
- (5) D. Pörschke and F. Eggers, *Eur. J. Biochem.*, **26**, 490 (1972).
- (6) W. P. Jencks, *Annu. Rev. Biochem.*, **32**, 639 (1963).
- (7) W. P. Jencks, "Catalysis in Chemistry and Enzymology," McGraw-Hill, New York, N. Y., 1969, pp 393-436.
- (8) W. Kauzmann, *Advan. Protein Chem.*, **14**, 1 (1959).
- (9) D. G. Oakenfull, *J. Chem. Soc., Perkin Trans. 2*, 1006 (1973).
- (10) D. G. Oakenfull and D. E. Fenwick, *Aust. J. Chem.*, **26**, 2649 (1973).
- (11) R. A. Robinson and R. H. Stokes, "Electrolyte Solutions," Butterworths, London, 1955.
- (12) T. Shedlovsky, "Physical Methods of Organic Chemistry," Vol. 1, A. Weissberger, Ed., 2nd ed, Interscience, New York, N. Y., 1949, Part II, p 1651.
- (13) C. W. Davies, "Ion Association," Butterworths, London, 1962.
- (14) C. W. Davies, *J. Chem. Soc.*, 645 (1933).
- (15) R. M. Fuoss and L. Onsager, *J. Phys. Chem.*, **61**, 668 (1957); **62**, 1339 (1958).
- (16) P. Mukerjee, *Advan. Colloid Interface Sci.*, **1**, 243 (1967).
- (17) G. Némethy and H. A. Scheraga, *J. Phys. Chem.*, **66**, 1773 (1962).
- (18) P. Becher, *J. Colloid Sci.*, **20**, 728 (1965).
- (19) C. Tanford, *J. Amer. Chem. Soc.*, **84**, 4240 (1962).
- (20) W. Bruning and A. Holtzer, *J. Amer. Chem. Soc.*, **83**, 4865 (1961).
- (21) W. B. Gratzer and G. H. Beaven, *J. Phys. Chem.*, **73**, 2270 (1969).
- (22) E. Wilhelm and R. Battino, *J. Chem. Phys.*, **55**, 4012 (1971).
- (23) A. Ben-Naim, *J. Chem. Phys.*, **54**, 1387 (1971).
- (24) R. B. Hermann, *J. Phys. Chem.*, **76**, 2754 (1972).
- (25) O. Sinanoglu and S. Abdulnur, *Fed. Proc.*, **24**, Suppl. 15, S-12 (1965).
- (26) S. Lewin, *Nature (London), New Biol.*, **231**, 80 (1971).
- (27) Sir W. Thomson, *Proc. Roy. Soc. Edinburgh*, **7**, 63 (1870).
- (28) S. Glasstone, "Textbook of Physical Chemistry," 2nd ed. Van Nostrand, New York, N. Y., 1947.
- (29) A. Ben-Naim, "Water: A Comprehensive Treatise," Vol. 1, F. Franks, Ed., Plenum Press, New York, N. Y., 1972, p 413.
- (30) S. Fisk and B. Widom, *J. Chem. Phys.*, **50**, 3219 (1969).
- (31) P. A. Egelstaff and B. Widom, *J. Chem. Phys.*, **53**, 2667 (1970).

Matrix Isolation Infrared Study of the Reaction between Germanium Vapor and Molecular Oxygen. The Characterization and Mechanism of Formation of Molecular Germanium Dioxide and Ozone

A. Bos, J. S. Ogden,*¹ and L. Orgee

Inorganic Chemistry Laboratory, South Parks Road, Oxford, England (Received January 28, 1974)

When germanium vapor is cocondensed at 16°K with an excess of krypton containing a few mole per cent O₂, the principal products are found to be O₃ and molecular GeO. In nitrogen matrices, however, significant concentrations of molecular GeO₂ are also produced, and a normal coordinate analysis for this molecule based on the available germanium and oxygen isotope frequencies indicates that GeO₂ is linear *D_{∞h}* with a principal Ge-O stretching force constant of 7.32 mdyn/Å. A study of the oxygen isotope distributions in the O₃ and GeO₂ in ¹⁸O enrichment experiments clearly shows that the formation of GeO₂ involves insertion of a Ge atom into the O-O bond of the oxygen molecule, while in the formation of O₃, ground-state ³P oxygen atoms effectively add end-on to molecular O₂.

Introduction

Several recent papers have described how matrix isolation techniques may be used to study the chemistry of metal atoms and, in particular, reactions with molecular

oxygen have attracted considerable attention. The alkali metal atom-O₂ reactions have been studied extensively by Andrews, *et al.*,²⁻⁵ and it is clear that a considerable amount of new information concerning the stoichiometries

and vibration frequencies of the reaction products can be obtained. In a few cases it has been possible to carry out fairly detailed normal coordinate analyses and to establish molecular geometries. Studies on some transition metal-O₂ reactions in low temperature matrices have also been reported by Ozin, *et al.*,^{6,7} and by Darling, *et al.*^{8,9}

One feature common to practically all these studies is the characterization of small superoxide or peroxide molecules with typical stoichiometries M_x(O₂)_y in which the O-O bond appears to remain intact throughout the reaction sequence. However, when tin atoms react with molecular oxygen under these conditions,¹⁰ an insertion reaction takes place to produce linear (*D_{∞h}*) SnO₂ in which the O-O bond is ultimately broken, and a number of other reaction products such as O₃ can also be produced. It is therefore of considerable interest to investigate whether this alternative type of reaction is a common feature of group IV atom chemistry, and this paper describes the results of analogous studies on the Ge atom-O₂ reaction in low temperature matrices. The reaction products are detected using ir spectroscopy, and extensive use of both germanium and oxygen isotope data is employed in the vibrational analyses.

Experimental Section

The Knudsen furnace and low temperature cryotip used for the matrix isolation studies have been described previously.¹¹ In the present experiments, germanium metal (Koch-Light, 99.999%) was heated to *ca.* 1500°K and the vapor deposited on a cooled CsI window with an excess of Kr or N₂ containing between 1 and 25 mol % O₂. The sample holders used (2.5 cm × 0.5 cm i.d. tubes, with 1-2-mm orifice) were made from either tantalum, graphite, or alumina; none was found to be completely satisfactory, although the spectroscopic results obtained were identical in each case. The tantalum holders alloyed with the germanium, crumbling to a powder after two to three runs; the graphite holders gave too great a quantity of CO₂, presumably by reaction with some of the matrix gas which had diffused back into the furnace; and the alumina holders were porous to the molten germanium, leading to fracture of the saturated holders, on cooling.

Research grade ¹⁶O₂, Kr, and N₂ gases were obtained from the British Oxygen Co., and ¹⁸O enriched oxygen gas (86% ¹⁸O₂, 14% ¹⁶O¹⁸O) was supplied by Miles Laboratories Inc. The method for making up isotopically scrambled (*e.g.*, 25% ¹⁶O₂, 50% ¹⁶O¹⁸O, 25% ¹⁸O₂) and "unscrambled" (*e.g.*, 46% ¹⁶O₂, 8% ¹⁶O¹⁸O, 46% ¹⁸O₂) oxygen mixtures has been described previously.¹⁰

Most experiments were carried out using oxygen concentrations of between 5 and 10 mol % in the matrix. Experiments carried out using smaller or larger proportions gave essentially the same products, but the rate of product formation was too slow when the proportion was ~1% and the yield of product based on oxygen content was uneconomical for higher concentrations. The gas samples were made up using a Toepler pump and flow rates were varied between 2 and 10 mmol/hr. The rate of growth of product peaks was less sensitive to the matrix gas flow rate (for N₂) than was previously found for the system Sn-O₂. Germanium deposition rates were equivalent to weight losses from the holder of *ca.* 10-50 mg/hr, which when combined with the matrix gas flow rate and the geometry of the set-up gave estimated matrix ratios of ~500:1. The CsI deposition window was maintained at either 16 or 20°K during deposition, and at higher temperatures for diffusion studies, by

adjusting the H₂ back pressure in the cryotip. Ir spectra were recorded at 20°K using a Perkin-Elmer 225 spectrophotometer, calibrated in the wave number region of interest with gaseous NH₃ (IUPAC Tables).

Results and Band Assignments

Over 30 experiments were carried out using either krypton or nitrogen as matrix gases, but the ir spectra obtained were found to be markedly dependent on the matrix gas used, and the results from the two systems Ge-N₂-O₂ and Ge-Kr-O₂ are therefore discussed separately.

Nitrogen Matrices

Nitrogen matrix depositions were carried out over a range of window temperatures from 16 to 20°K, and oxygen concentrations of between 1 and 10% were employed. All spectra showed traces of H₂O, CO, and CO₂ after deposition, but several additional features were also produced. Figure 1a shows a typical ir spectrum obtained after cocondensing germanium vapor at 20°K with a large excess of nitrogen containing 5% ¹⁶O₂. Apart from the presence of matrix isolated CO₂, and a window impurity band (labeled ×), this spectrum shows five important features: a very closely spaced triplet at ~1060 cm⁻¹, a sharp singlet at 1042.4 cm⁻¹, and three broader bands at 974, 824, and 599 cm⁻¹. Figure 1b shows the 980-1080-cm⁻¹ region under higher resolution, and the "triplet" feature now appears as a quintet with three intense components at 1070.6, 1065.8, and 1061.6 cm⁻¹, and two weaker bands at 1063.6 and 1057.3 cm⁻¹. This intensity pattern corresponds closely to the natural abundance of germanium isotopes which is also shown on this diagram.

These results may be compared with the earlier matrix isolation studies on molecular germanium oxides by Ogden and Ricks,¹² and on the basis of this earlier work, the bands at 974, 824, and 599 cm⁻¹ are assigned to GeO, Ge₂O₂, and Ge₃O₃ (Table I). The absorption at 1042.4 cm⁻¹ and the quintet pattern are provisionally assigned to O₃ and molecular GeO₂ respectively by analogy with corresponding studies on the tin atom-O₂ matrix reactions,¹⁰ and these assignments are discussed in detail below.

When depositions were carried out at 16°K, the bands assigned to GeO₂, GeO, and O₃ were still prominent, but the absorptions of Ge₂O₂ and Ge₃O₃ were considerably less intense, and in some experiments they could hardly be detected. In an attempt to confirm the identification of GeO₂ and O₃ produced in these cocondensations, a number of experiments were carried out using both scrambled and unscrambled samples of ¹⁸O enriched oxygen. Depositions were generally carried out at 16°K in order to maximize the relative intensity of these bands and, in the majority of experiments, the proportion of total oxygen in the matrix gas was kept constant at 5%.

When a scrambled oxygen mixture was used (95% N₂, 1.2% ¹⁶O₂, 2.5% ¹⁶O¹⁸O, 1.3% ¹⁸O₂) two moderately intense GeO bands were observed at 974 (Ge¹⁶O) and 928 cm⁻¹ (Ge¹⁸O) together with several sharp bands in the 980-1080-cm⁻¹ region. The absorptions of Ge₂O₂ and Ge₃O₃ were not detected. Figure 1c shows the 980-1080-cm⁻¹ region of the spectrum under high resolution, and if our assignment of the 1042.4-cm⁻¹ band to O₃ is correct, then six of the bands in this spectrum must be assigned to ν₃ vibrations of the six possible isotopically scrambled ozone molecules. The vibrational spectra of these molecules have recently been studied in inert matrices by Andrews and Spik-

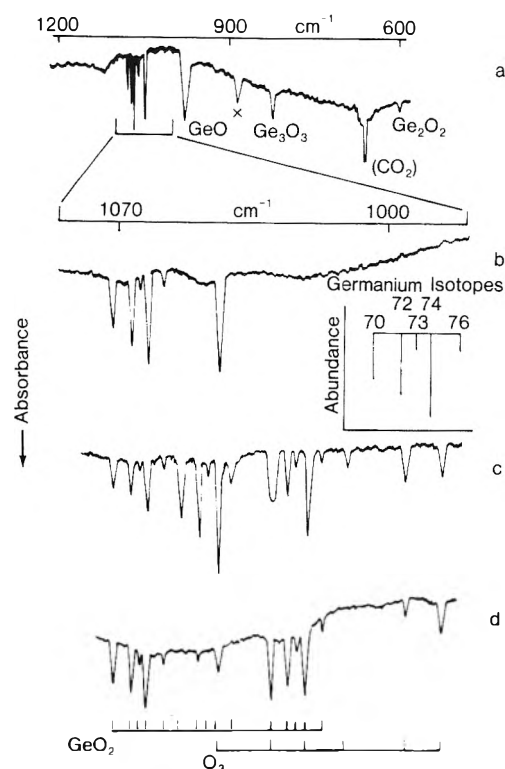


Figure 1. Ir spectrum obtained (a) after condensing germanium vapor at 20°K in a nitrogen matrix containing 5% ¹⁶O₂; (b) part of the above spectrum under higher resolution; (c) after condensing germanium vapor at 16°K with nitrogen containing 1.2% ¹⁶O₂, 2.5% ¹⁶O¹⁸O, 1.3% ¹⁸O₂; (d) after condensing germanium vapor at 16°K with nitrogen containing 2.2% ¹⁶O₂, 0.4% ¹⁶O¹⁸O, 2.4% ¹⁸O₂.

TABLE I: Ir Absorptions (cm⁻¹) Observed after Condensing Germanium Vapor in a Nitrogen Matrix Containing 5% ¹⁶O₂

This work ^a	Previous related studies	Assignment
1070.6		¹⁶ O ⁷⁰ Ge ¹⁶ O
1065.8		¹⁶ O ⁷² Ge ¹⁶ O
1063.6		¹⁶ O ⁷³ Ge ¹⁶ O
1061.6		¹⁶ O ⁷⁴ Ge ¹⁶ O
1057.3		¹⁶ O ⁷⁶ Ge ¹⁶ O
1042.4	1042.5 ^b	¹⁶ O ₃
974	973.4 ^c	GeO
824	824 ^c	Ge ₃ O ₃
599	599.0 ^c	Ge ₂ O ₂

^a Frequency accuracy ±0.2 cm⁻¹ for GeO₂ and O₃, ±0.5 cm⁻¹ for the remaining bands. ^b Reference 13. ^c Reference 12.

er¹³ and it is clear from the frequency comparison in Table II that the four bands at 1042.4, 1009.2, 994.5, and 985.3 cm⁻¹ may immediately be assigned to ozone.

The remaining bands consist basically of a pattern of three quintets, in which the intensity of the central group is approximately twice that of the outer pair. This 1:2:1 intensity ratio using 50% scrambled ¹⁸O enrichment is characteristic of a dioxide in which the two oxygen atoms are equivalent and it is evident from the general intensity pattern in each quintet that the vibration involves one atom of germanium. However, it is also clear that the two components of the lower frequency quintet at 1029.1 and 1019.9 cm⁻¹ appear to be more intense than would be expected on the basis of the known germanium isotope distribution, in addition to which two remaining ozone bands remain un-

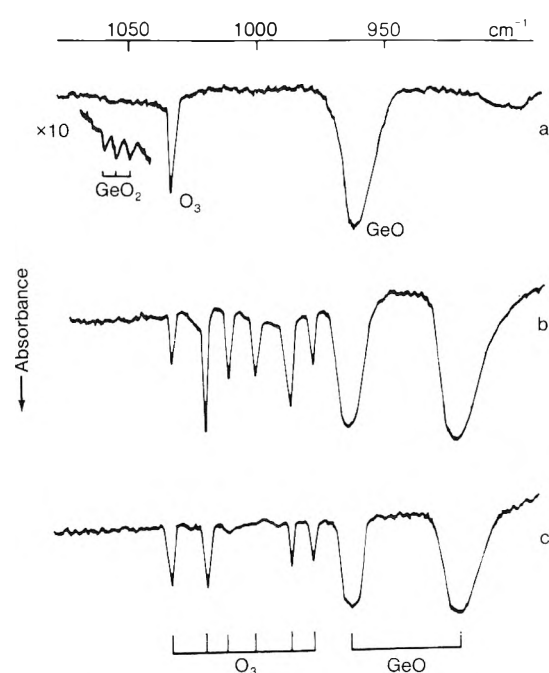


Figure 2. Ir spectrum obtained (a) after condensing germanium vapor at 16°K with krypton containing 10% ¹⁶O₂; (b) after condensing germanium vapor at 16°K with krypton containing 1.2% ¹⁶O₂, 2.5% ¹⁶O¹⁸O, 1.3% ¹⁸O₂; (c) after condensing germanium vapor at 16°K with krypton containing 2.3% ¹⁶O₂, 0.4% ¹⁶O¹⁸O, 2.3% ¹⁸O₂.

counted for. Two experiments were therefore carried out using optimum ¹⁸O enrichment (95% N₂, 4.2% ¹⁸O₂, 0.8% ¹⁶O¹⁸O) and in these experiments, a normal lower frequency quintet pattern was observed, together with a prominent ¹⁸O₃ band. Table II shows that two ozone bands are expected at ~1029 and ~1020 cm⁻¹, and it is clear that in ¹⁶O-¹⁸O experiments, there is accidental overlap between these two bands and two of the components of the Ge¹⁸O₂ quintet.

Figure 1d shows the same spectral region in a corresponding experiment using unscrambled oxygen (95% N₂, 2.2% ¹⁶O₂, 0.4% ¹⁶O¹⁸O, 2.4% ¹⁸O₂) and it is evident that very little Ge¹⁶O¹⁸O is produced, and that bands due to ¹⁶O¹⁸O¹⁶O and ¹⁸O¹⁶O¹⁸O are absent. By analogy with our previous tin atom-O₂ matrix experiments, this observation provides information on reaction mechanisms, and this is discussed below. A complete tabulation of the GeO₂ and O₃ vibrations observed in these experiments is given in Table II together with their isotopic assignments.

Krypton Matrices

Figure 2a shows part of a typical ir spectrum obtained after cocondensing germanium vapor with a large excess of krypton containing 10% ¹⁶O₂. In contrast with the corresponding nitrogen matrix experiments this spectrum shows virtually no absorption due to GeO₂, although bands due to O₃ and GeO are relatively intense. Traces of Ge₂O₂ and Ge₃O₃ could also be observed in these experiments when depositions were carried out at 20°K, but these were essentially absent in 16°K depositions even though the O₃ and GeO bands remained prominent. The proportion of O₂ in the matrix was varied from 1 to 25% in an attempt to obtain conditions under which GeO₂ could be observed, but in no case could a prominent GeO₂ absorption be detected. Two experiments were, however, carried out under optimum noise level and sensitivity conditions in an attempt to locate the characteristic quintet at ~1060 cm⁻¹. Under

TABLE II: Vibration Frequencies (cm^{-1}) of Isotopically Labeled GeO_2 and O_3 in Low Temperature Matrices

	Germanium isotopes				
	70	72	73	74	76
	$\nu_3 \text{ GeO}_2(\text{N matrix})^{a,h}$				
$^{16}\text{Ge}^{16}\text{O}$ obsd	1070.6	1065.8	1063.6	1061.6	1057.3
calcd	1070.8	1066.1	1063.8	1061.7	1057.4
$^{16}\text{Ge}^{18}\text{O}$ obsd	1052.6	1047.8	1045.6	1043.5	1039.4
calcd	1052.5	1047.8	1045.5	1043.3	1039.1
$^{18}\text{Ge}^{18}\text{O}$ obsd	1029.1	1024.6	1022.4	1019.9	1015.6
calcd	1029.2	1024.3	1021.9	1019.7	1015.3
	Ozone isotopes				
	16-16-16	16-16-18	18-16-18	16-17-16	16-18-18
	$\nu_3 \text{ Ozone}$				
N_2 matrix ^a	1042.4	1029.2 ^d	1020.2 ^d	1009.2	994.5
Ar matrix ^c	1040.0	1026.2	1017.1	1006.5	992.0
Kr matrix ^a	1034.6	1020.9	1012.1	1001.5	986.8

^a This work. ^b GeO_2 vibrations calculated assuming a linear $D_{\infty h}$ structure with principal and interaction Ge-O force constants of 7.32 and -0.094 mdyn/Å, respectively. Frequency accuracy for observed values ± 0.2 cm^{-1} . ^c Reference 13. ^d Partly overlapped by Ge^{18}O_2 absorptions.

these conditions, three very weak absorptions ($\text{OD} \sim 0.002$) could just be detected at 1050, 1054, and 1058 cm^{-1} (Figure 2a) and these are assigned to $^{74}\text{Ge}^{16}\text{O}_2$, $^{72}\text{Ge}^{16}\text{O}_2$, and $^{70}\text{Ge}^{16}\text{O}_2$. They would not have been located without prior knowledge of their approximate position.

The results of ^{18}O enrichment using krypton as a matrix are shown in Figure 2a and 2b. These experiments were carried out principally to investigate the distribution of oxygen isotopes in the ozone under conditions where the ozone bands would not be overlapped by GeO_2 . Using a scrambled oxygen mixture (95% Kr, 1.2% $^{16}\text{O}_2$, 2.5% $^{16}\text{O}^{18}\text{O}$, 1.3% $^{18}\text{O}_2$) six ozone peaks were observed at 1034.6, 1020.9, 1012.1, 1001.5, 986.8, and 977.7 cm^{-1} with relative intensities $\sim 1:2:1:1:2:1$. This intensity pattern is thus very close to that predicted by simple statistics and found experimentally by Andrews.¹³ The frequencies are uniformly ~ 8 cm^{-1} lower than the corresponding absorptions in nitrogen (Table II) and this observation has also been reported previously.¹⁰ In contrast, Figure 2c shows the corresponding spectrum obtained using isotopically unscrambled oxygen (95% Kr, 2.3% $^{16}\text{O}_2$, 0.4% $^{16}\text{O}^{18}\text{O}$, 2.3% $^{18}\text{O}_2$). Four bands of comparable intensity were observed, and the absorptions of $^{16}\text{O}^{18}\text{O}^{16}\text{O}$ and $^{18}\text{O}^{16}\text{O}^{18}\text{O}$ were again absent. The Ge^{16}O and Ge^{18}O bands were prominent in both types of ^{18}O enrichment experiment.

Discussion

These results indicate that when germanium vapor is condensed with krypton matrices containing a few mole per cent oxygen, ozone is produced together with GeO and traces of Ge_2O_2 and Ge_3O_3 . In nitrogen matrices, however, molecular GeO_2 is formed in addition to the above species, and the isotopic data obtained may be used to deduce its structure.

GeO_2

The assignment of the 15 bands ascribed to various isotopic GeO_2 molecules (Table II) is made on the basis of isotope intensity patterns and simple statistics. By analogy with our previous studies on molecular SnO_2 , GeO_2 must have either $D_{\infty h}$ or C_{2v} symmetry, and the observed bands are assigned to antisymmetric stretching vibrations. The apex angle 2α may then be estimated¹⁰ from the relationship

$$4\pi^2\omega_3^2 = (F_r - F_{rr})(\mu_{\text{O}} + 2\mu_{\text{Ge}} \sin^2 \alpha)$$

and frequency data from pairs of molecules such as $^{72}\text{Ge}^{16}\text{O}_2$ and $^{72}\text{Ge}^{18}\text{O}_2$ or $^{72}\text{Ge}^{16}\text{O}_2$ and $^{76}\text{Ge}^{16}\text{O}_2$. As in our previous analysis for SnO_2 , the neglect of anharmonicity is expected¹⁴ to produce upper and lower limits for $\sin \alpha$ depending upon which atom undergoes isotopic substitution, and Table III shows the results of product rule calculations and experimental ratios for three pairs of isotopically substituted GeO_2 molecules. It is clear that isotopic substitution at oxygen has, as expected, produced a higher value of $\sin \alpha$ than substitution at germanium, and the value $\sin \alpha = 1.023$ obtained from oxygen isotope substitution is interpreted as indicating a linear GeO_2 molecule. The lower limit for the apex angle is estimated to be $\sim 170^\circ$ from the germanium isotope effect.

The principal and interaction Ge-O force constants (F_r and F_{rr}) may be obtained from the observed frequencies of Ge^{16}O_2 and $\text{Ge}^{16}\text{O}^{18}\text{O}$ using standard equations¹⁵ and the values obtained are 7.32 and -0.094 mdyn/Å, respectively. Table II compares the 15 frequencies observed for isotopically substituted GeO_2 species with those calculated using these parameters and assuming a linear $D_{\infty h}$ structure and, in all cases, agreement is to within 0.5 cm^{-1} . The totally symmetric stretching vibrations are inactive in the ir for this molecular symmetry, but are predicted to lie at 875.6 (Ge^{16}O_2), ~ 848 ($\text{Ge}^{16}\text{O}^{18}\text{O}$), and 825.5 cm^{-1} (Ge^{18}O_2) using the above force constants.

The value of F_r GeO_2 found here (7.32 mdyn/Å) is very close to that for matrix isolated GeO (7.34 mdyn/Å),¹² and the corresponding bond length estimated from the appropriate Herschbach-Laurie equation¹⁶

$$r_{\text{Ge-O}} = 2.15 - 0.60 \log F_r$$

is 1.63 Å. A similar calculation for GeO also gives $r_{\text{Ge-O}} = 1.63$ Å compared with the accurate value¹⁷ of 1.65 Å and, although the above equation appears to give a slightly low estimate of the bond length, it is significant that $r_{\text{Ge-O}}$ in both GeO_2 and GeO is considerably less than the sum of the single bond covalent radii¹⁸ of Ge and O (1.22 + 0.66 Å). Molecular GeO_2 would therefore seem to be rather similar, as regards its general electronic structure, to the related molecules CO_2 , SiO_2 , and SnO_2 all of which adopt a linear configuration,^{10,19} and show a considerable shortening or strengthening²⁰ of the M-O bond compared with the corresponding single bond values.

One final point remains concerning the bending mode in GeO_2 . This vibration is active in the ir but was not ob-

TABLE III: Observed and Calculated Frequency Ratios for Isotopic GeO₂ Species in N₂ Matrices

Species	Obsd frequency	Obsd ^a ratio	Sin α^b	Calculated ratio	
				$D_{\omega h} (\alpha = 90^\circ)$	$C_{2v} (\alpha = 75^\circ)$
¹⁶ O ⁷² Ge ¹⁶ O	1065.8	1.0402	1.023	1.0408	1.0418
¹⁸ O ⁷² Ge ¹⁸ O	1024.6				
¹⁶ O ⁷⁰ Ge ¹⁶ O	1070.6	1.01258	0.997	1.01263	1.01203
¹⁶ O ⁷⁶ Ge ¹⁶ O	1057.3				
¹⁸ O ⁷² Ge ¹⁸ O	1024.6 ^c	1.00886	0.997	1.00891	1.00849
¹⁸ O ⁷⁶ Ge ¹⁸ O	1015.6 ^c				

^a Error limits ± 0.0002 . ^b Error limits ± 0.003 . ^c Not overlapped by ozone peaks.

served in these experiments. By comparison with ν_3/ν_2 for CO₂, it would be expected to lie within the range of our spectrometer, and we conclude that its extinction coefficient is at least one order of magnitude smaller than that for ν_3 .

Ozone

The bands assigned to isotopically substituted ozone are very close to those recently obtained by Andrews and Spiker,¹³ Brewer and Wang,²¹ and Spoliti, *et al.*,²² in similar matrix studies. The frequencies obtained here in krypton and nitrogen matrices need not be discussed in detail, but the intensity patterns obtained are very significant.

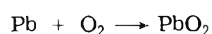
Reaction Mechanisms

The experiments with scrambled and unscrambled oxygen show interesting intensity patterns which provide important information concerning the mechanisms both of the Ge–O₂ reaction and of ozone formation in matrix reactions. We shall consider the Ge–O₂ reaction first.

The reaction products obtained when group IV atoms react with molecular oxygen are typified by the two reactions



and



which have been found to occur in the gas phase.^{23,24} For the intermediate element, tin, previous matrix isolation studies¹⁰ have indicated that both abstraction and addition products are present, and that small amounts of ozone, as well as Sn₂O₂ and Sn₃O₃ are produced depending upon the matrix gas used.

In the analogous germanium–O₂ system, the reaction products are found to be strongly dependent on the nature of the matrix gas, and at 16°K, in krypton–O₂ matrices, the principal species observed are O₃ and GeO. This suggests that the most important reactions here are



followed by



At higher deposition temperatures, small amounts of Ge₂O₂ and Ge₃O₃ are produced, and although no detailed isotope studies were made on these bands owing to their low intensities, we believe that they are formed by the stepwise polymerization of GeO.

In N₂–O₂ matrices, GeO and O₃ are still observed, but GeO₂ is now an important product. Again very few Ge_nO_n polymers are observed at the lower deposition tempera-

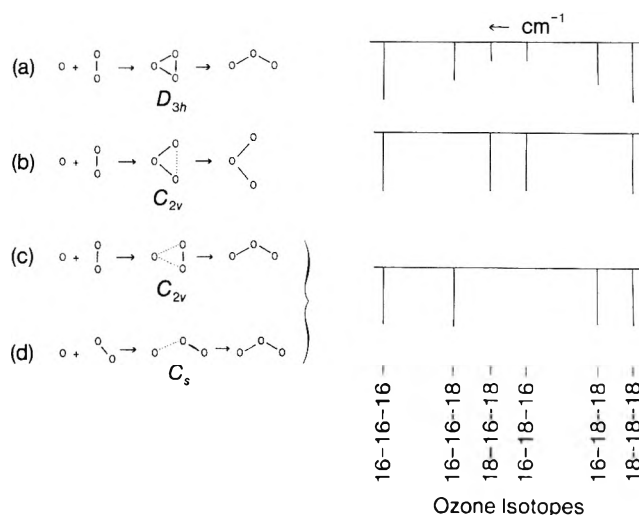
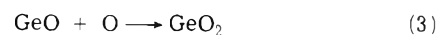


Figure 3. Ozone isotope intensity patterns for four possible mechanisms $O + O_2 \rightarrow O_3$ in experiments involving 50% ¹⁸O enriched unscrambled oxygen (¹⁶O₂ + ¹⁸O₂).

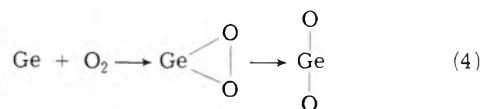
tures. By analogy with the corresponding tin atom–O₂ matrix reaction,¹⁰ two mechanisms would seem possible



followed by diffusion and further reaction to give



and/or



Just as in the formation of SnO₂, the Ge atom–unscrambled oxygen results (Figure 1d) clearly indicate an insertion mechanism (4) in which the O–O bond is retained in the transition state. If the alternative step (3) were important, one might expect to observe significant amounts of Ge¹⁶O¹⁸O in these experiments, since this mechanism provides an opportunity for isotope scrambling.

The bond dissociation energy in diatomic GeO is 156 kcal/mol²⁰ and the heat of atomization of molecular GeO₂ may therefore be estimated as ~ 220 kcal/mol by comparison with the corresponding values²⁰ for SiO₂ (with respect to SiO) and CO₂. The overall enthalpy change for the reaction $Ge + O_2 \rightarrow GeO_2$ is thus ~ -100 kcal/mol, and it is clear that both the cyclic intermediate and the final product are likely to contain a large amount of excess energy.

For a molecule in the gas phase, this energy might easily be lost through dissociation, which would result in an overall reaction in the gas phase $\text{Ge} + \text{O}_2 \rightarrow \text{GeO} + \text{O}$, $\Delta H = -38$ kcal/mol, but for a matrix isolated species there is the possibility of transferring the energy to a vibrational mode of the matrix. In krypton matrices only the lattice modes are available, and very little GeO_2 was in fact observed, but in nitrogen, where there is the additional possibility of energy transfer to the high-frequency $\text{N}\equiv\text{N}$ vibration, GeO_2 was produced in much higher concentrations. If this form of stabilization is important for the product of $\text{M} + \text{O}_2 \rightarrow \text{MO}_2$ reactions, one might expect that it would be increasingly more difficult to produce SiO_2 and CO_2 in this way, and that the products would be $\text{MO} + \text{O}$ ($\rightarrow \text{O}_3$). Conversely, the stabilization of SnO_2 or PbO_2 would be relatively easier, and it is interesting to note that in our earlier paper SnO_2 could be established in both krypton and nitrogen and that ozone was only observed in krypton matrices.

In contrast to the tin atom- O_2 matrix reactions, very little M_2O_2 was produced in this work, and there is no evidence that this comes from the reaction $\text{GeO}_2 + \text{Ge} \rightarrow \text{Ge}_2\text{O}_2$. Instead, experiments at different window temperatures (16 or 20°K) indicate that any Ge_2O_2 present is formed by dimerization of GeO . In the Sn- O_2 system, the majority of the Sn_2O_2 (D_{2h} isomer) was produced from SnO_2 , and this difference in behavior may partly be accounted for in that although germanium vapor contains a large proportion²⁵ of monatomic Ge, one might expect germanium atoms to be more reactive than tin atoms and to be removed by oxygen in reactions 1 or 4 leaving little possibility for subsequent reaction with GeO_2 .

Ozone Formation

The identification of ozone in all the experiments indicates that the overall reaction 1 does occur and, as the net enthalpy change is -38 kcal/mol, the oxygen atoms produced in (1) must be in the ^3P ground state (the promotion energy $\text{O}(^3\text{P}) \rightarrow \text{O}(^1\text{D})$ is 45.5 kcal/mol²⁶).

Two general mechanisms might be considered for the matrix reaction of ^3P oxygen atoms with O_2 to form O_3 . The first of these could involve a cyclic transition state



in which the intermediates had C_{2v} or D_{3h} symmetry, while the second might involve end-on attack *via* a linear or bent (C_s) intermediate. The overall ΔH for the reaction under matrix conditions is ~ -25 kcal/mol.

Wright²⁷ has suggested that a cyclic form of ozone might be an intermediate in the reverse decomposition reaction, and that such a structure might even be more stable than the usual open C_{2v} form by ~ 6 kcal/mol. Reaction 5 might therefore also be the pathway adopted in the formation of ozone, and it is interesting to examine our oxygen isotope results in this context.

Experiments with completely scrambled oxygen would be expected to yield the statistical distribution of isotopically labeled ozone molecules irrespective of mechanism, and Figure 2b shows this pattern for $\sim 50\%$ ^{18}O enrichment. However, in unscrambled oxygen mixtures, only the reactions $^{16}\text{O} + ^{16}\text{O}_2$, $^{16}\text{O} + ^{18}\text{O}_2$, $^{18}\text{O} + ^{16}\text{O}_2$, and $^{18}\text{O} + ^{18}\text{O}_2$ can lead directly to ozone formation, since these mixtures contain virtually no $^{16}\text{O}^{18}\text{O}$. In practice, it is found that essentially no $^{16}\text{O}^{18}\text{O}^{16}\text{O}$ or $^{18}\text{O}^{16}\text{O}^{18}\text{O}$ is produced in this type of experiment, and that the four other

ozone molecules are produced (Figure 2c) in approximately equal amounts.

Figure 3 shows the intensity patterns expected in "unscrambled" oxygen enrichment experiments (50% ^{18}O enrichment) for four possible mechanisms $\text{O} + \text{O}_2 \rightarrow \text{O}_3$. The first of these (a) considers the possibility of a D_{3h} cyclic intermediate in which there is no preferential bond breaking in the final step. Simple statistics then predict that all six isotopically substituted ozone molecules should be observed with relative intensities as shown.²⁸ Two other cyclic transition states of lower symmetry are also possible, and the isotope patterns expected for these are shown in Figure 3b and 3c. Reaction scheme b should be described as an insertion reaction in which the final step involves preferential fission of the *original* O-O bond, while c shows the effect of *retaining* the original O-O linkage and breaking one of the other two bonds in the ring. This particular mechanism (c) produces an intensity pattern which is very similar to that observed experimentally, but the same pattern would also be predicted for simple end-on attack (d).

These experiments therefore indicate that the formation of ozone takes place here either by end-on attack, or by side-on attack involving a C_{2v} intermediate in which the original O_2 bond remains intact throughout. There is no evidence for either a D_{3h} cyclic intermediate or for a simple insertion reaction. It is impossible to assess whether the matrix cage imposes any particular restrictions on either the geometry of the intermediate or on the overall reaction mechanism, but matrix perturbations of molecular geometry are generally considered to be small,¹⁴ and we believe that the above conclusions concerning the mechanism of the $\text{O} + \text{O}_2$ matrix reaction will remain valid for the corresponding gas-phase reaction.

Conclusions

A pronounced third body effect has been observed in the reaction between germanium atoms and molecular oxygen under matrix isolation conditions. In nitrogen matrices, the principal products are the molecular species GeO_2 , O_3 , and GeO , but only traces of GeO_2 are observed in krypton matrices, and it is suggested that energy transfer is an important factor in stabilizing molecular GeO_2 .

A normal coordinate analysis based on the frequencies of a large number of isotopically substituted species indicates that GeO_2 is linear $D_{\infty h}$ and thus isostructural with the other group IV oxides CO_2 , SiO_2 , and SnO_2 . The relatively high value of the principal Ge-O stretching constant indicates that GeO_2 contains appreciable multiple bonding.

Experiments with both isotopically scrambled and unscrambled oxygen indicate that the mechanism of formation of GeO_2 involves insertion of a Ge atom into the O-O bond to form a cyclic transition state. Ozone formation, on the other hand, is shown to proceed with retention of the O-O bond throughout the reaction $\text{O} + \text{O}_2 \rightarrow \text{O}_3$, and the possibility of a D_{3h} triangular intermediate is discounted.

Acknowledgments. We gratefully acknowledge the financial support of the Science Research Council and the Central Electricity Generating Board for this work.

References and Notes

- (1) Author to whom correspondence should be addressed.
- (2) L. Andrews and R. R. Smardzewski, *J. Chem. Phys.*, **58**, 2258 (1973).
- (3) L. Andrews, *J. Phys. Chem.*, **73**, 3922 (1969).
- (4) L. Andrews, *J. Chem. Phys.*, **54**, 4935 (1971).

- (5) R. R. Smardzewski and L. Andrews, *J. Phys. Chem.*, **77**, 801 (1973).
- (6) H. Huber and G. A. Ozin, *Can. J. Chem.*, **50**, 3746 (1972).
- (7) H. Huber, W. Klotzbücher, G. A. Ozin, and A. Vander Voet, *Can. J. Chem.*, **51**, 2722 (1973).
- (8) J. H. Darling, Ph.D. Thesis, Oxford, 1973.
- (9) J. H. Darling, M. G. Garton-Sprenger, and J. S. Ogden, *Discuss. Faraday Soc.*, in press.
- (10) A. Bos and J. S. Ogden, *J. Phys. Chem.*, **77**, 1513 (1973).
- (11) J. S. Anderson and J. S. Ogden, *J. Chem. Phys.*, **51**, 4189 (1969).
- (12) J. S. Ogden and M. J. Ricks, *J. Chem. Phys.*, **52**, 352 (1970).
- (13) L. Andrews and R. C. Spiker, Jr., *J. Phys. Chem.*, **76**, 3208 (1972).
- (14) J. Overend, *Annu. Rev. Phys. Chem.*, **21**, 265 (1970).
- (15) J. L. Griggs, Jr., K. N. Rao, L. H. Jones, and R. M. Potter, *J. Mol. Spectrosc.*, **18**, 212 (1965).
- (16) D. R. Herschbach and V. W. Laurie, *J. Chem. Phys.*, **35**, 458 (1961).
- (17) G. Herzberg, "Molecular Spectra and Molecular Structure," Vol. 1, Van Nostrand, Princeton, N. J., 1959.
- (18) See, e.g., F. A. Cotton and G. Wilkinson, "Advanced Inorganic Chemistry," Interscience, New York, N. Y., 1962, p 93.
- (19) M. Kaufman, J. Muentner, and W. Klemperer, *J. Chem. Phys.*, **47**, 3365 (1967).
- (20) See, e.g., J. Drowart and P. Goldfinger, *Angew. Chem., Int. Ed. Engl.*, **6**, 581 (1967).
- (21) L. Brewer and J. L.-F. Wang, *J. Chem. Phys.*, **56**, 759 (1972).
- (22) M. Spoliti, S. N. Cesaro, and B. Mariti, *J. Chem. Phys.*, **59**, 985 (1973).
- (23) R. F. Peterson, Jr., and R. Wolfgang, *Advan. High Temp. Chem.*, **4**, 43 (1971).
- (24) P. R. Ryason and E. A. Smith, *J. Phys. Chem.*, **75**, 2259 (1971).
- (25) J. Drowart and R. E. Honig, *J. Phys. Chem.*, **61**, 980 (1959).
- (26) H. S. Johnston, *Nat. Stand. Ref. Data Ser., Nat. Bur. Stand.*, **No. 20**, (1968).
- (27) J. S. Wright, *Can. J. Chem.*, **51**, 139 (1973).
- (28) These line spectra are calculated on the basis of relative molecular abundances. An exact calculation of relative band intensities would require two additional refinements: the effect of the molecular mass on isotope intensities, and in the case of ¹⁶O¹⁶O¹⁸O and ¹⁶O¹⁸O¹⁸O, the effect of coupling with the symmetric O-O stretching modes. The first of these may be calculated precisely²⁹ and shown to be relatively unimportant, while the second is also small as indicated by Andrews' work¹³ and by the isotope intensity pattern observed here in Figure 2b.
- (29) E. B. Wilson, Jr., J. C. Decius, and P. C. Cross, "Molecular Vibrations," McGraw-Hill, New York, N. Y., 1955, p 191.

COMMUNICATIONS TO THE EDITOR

Electron Spin Resonance Study of Chlorine Dioxide Adsorbed on the Alkali-Cation-Exchanged X-Type Zeolites

Publication costs assisted by Tokyo Institute of Technology

Sir: As has been suggested by Rabo, *et al.*,¹ the catalytic activity on zeolite surfaces is, in some cases,²⁻⁴ associated with the polarization of the adsorbed molecules by the intense electrostatic field in the adsorption sites. Gardner⁵ first applied the esr technique to the study of these surface fields. Coope, *et al.*,⁶ have recently reported that esr spectra of ClO₂ and Cl₂⁻ adsorbed on the zeolites exhibit significant shifts in the hyperfine splittings, caused by the large electrostatic field of the zeolite surfaces. Thus it is of considerable interest to investigate systematically the effect of the exchanged cations on esr spectra of the adsorbed radicals, since the surface field is related to the poor shielding of cations in the zeolite structure. In this communication we will report our recent results of the esr study on the effect of the cations, and adsorbed water upon the hyperfine splitting of ClO₂ adsorbed on the cation-exchanged X-type zeolites.

All forms of the X-type zeolites were prepared from Linde 13X (sodium form) by ion exchange in the conventional manner and were pretreated under vacuum at various temperatures for 6 hr. The ClO₂ was allowed to adsorb onto the samples at 0.1 Torr, and then evacuated for a few minutes at room temperature. The esr measurements were made at 77 K and a JES 3BSX X-band spectrometer was employed.

In Figure 1a is shown the spectrum of ClO₂ adsorbed on NaX pretreated at 350°. As has been reported by Coope, *et al.*,⁶ the spectrum indicates the presence of two types of ClO₂ with different hyperfine splittings. The relative intensity of both species, however, was changed, as is shown in Figure 1b, when the zeolite was exchanged further with sodium by immersing the 13X into a sodium nitrate solution for 12 hr. The two-site spectra were also obtained in the zeolites exchanged partially (10%) with lithium and potassium. It was found that, when the 10% LiX was pretreated at 600°, the hyperfine splittings were increased, while in the 10% KX treated at 350 and 600° and the 10% LiX treated at 350° the spectra were the same as NaX. In other exchanged zeolites studied, the spectra indicated the presence of a single species of ClO₂, as is shown in Figure 1c. However, the hyperfine splittings of these spectra were dependent upon the cations and the pretreatments of zeolites.

According to the model proposed,⁶ the ClO₂ is adsorbed on the cationic sites, whose negative (oxygen) end is closest to the cation, and the large electric field due to the cation causes the change of the electron-density distribution in the molecule to give an increase in the spin density on chlo-

rine nucleus. Therefore we could make use of the hyperfine splitting of chlorine as a measure of the electric fields. The observed hyperfine splittings on the cation-exchanged zeolites pretreated at various temperatures are listed in Table I. For the sake of simplicity, we chose the splitting of an outermost component, which corresponds to the principal axis perpendicular to the radical plane in the anisotropic hyperfine structure.^{6,7}

The electrostatic fields in these zeolites are, as has been reported by Ward,⁴ dependent on the ionic polarization power, which is proportional to the charge (e) and inversely to the cationic radius (r_i). However, the polarizing power may be better correlated with the field by taking into consideration the shielding of nuclear charge by electrons on cation. The correction due to this effect can be made by including a factor $S_{\text{eff}} = (5e^{1.27})/(r_i^{1/2}I)$ (I is the ionization potential), derived by Ahrens,⁸ and the usefulness of which has been confirmed by Brooker and Bredig⁹ in their study of some metal nitrates. For alkali metal ions the value of S_{eff} is approximately unity except for lithium, in which the value is 1.12. Figure 2 shows the hyperfine splittings of the spectra observed in the zeolites pretreated at 200 and 350° as a function of $e/(r_i S_{\text{eff}})$. Except for the presence of the two-site spectra in NaX and 10% LiX, evidently there exists a good correlation between the splitting and the polarization power ($e/r_i S_{\text{eff}}$), as might be expected from above discussion. Similar relationship has also been obtained by Ward⁴ in the systematic study on the infrared spectra of water adsorbed on the X-type zeolites. The linear relation in Figure 2 may give experimental support of the linear Stark shift⁶ of the hyperfine couplings with the electric field.

The effect of dehydration on the splittings can be interpreted by taking into consideration the shielding of the cations by adsorbed water. From the data listed in Table I, it may be suggested that, although the evacuation at 200° cannot eliminate the water adsorbed on the cations and the electric field on the radical is reduced to some extent by the water, the splittings still reflect the polarization power of the cations. However, since the adsorbed water, as is well known, cannot be effectively removed by evacuation at 25°,

TABLE I: Hyperfine Splittings of ClO₂ Adsorbed on Zeolites (G)

Sample	Evacuation temperature			
	25° ^a	200°	350°	600°
LiX (10%)	74.7	82.5	85.1, 77.6	88.1, 80.8
LiX	75.4	76.5	76.9	76.9
NaX	74.7	82.1	85.1, 77.6	85.1, 77.6
KX	73.5	78.9	79.9	79.9
RbX	72.8	77.4	78.8	78.8
CsX	74.3	76.5	77.6	77.6

^a Room temperature.

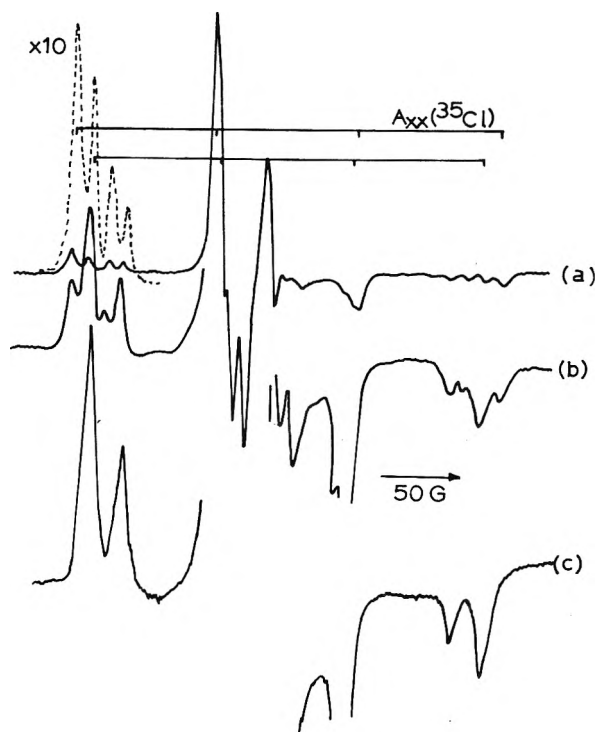


Figure 1. ESR spectra of ClO_2 adsorbed on the alkali-cation-exchanged X-type zeolites; (a) NaX, (b) NaX after treatment in NaNO_3 aqueous solution; and (c) KX.

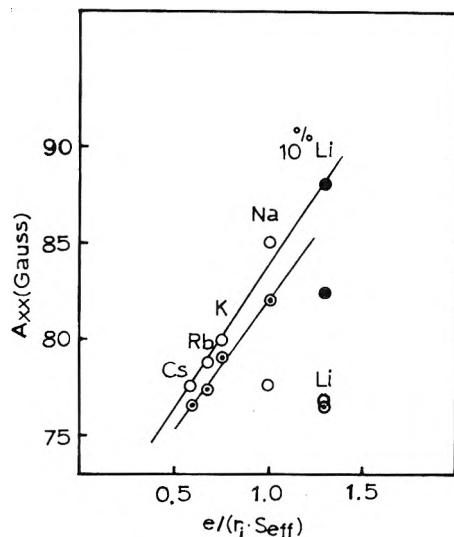


Figure 2. The hyperfine splittings of ClO_2 on the alkali-cation-exchanged zeolites as a function of the polarization power ($e/r_1 S_{\text{eff}}$) of the cations with the samples pretreated at 200° (\circ), 350° (\circ), and 600° (\bullet) (10% LiX).

the radicals are almost free from the effect of the cationic fields because of the water adsorbed not only on cations, but on the other sites in the zeolites. This effect may interpret the least and nearly equivalent hyperfine splittings as is listed in the second column of the table.

In the LiX the splitting was smaller than those in the other zeolites, even when the sample was evacuated at 600° . This probably means, as Pelman¹⁰ has suggested in his esr study of ClO_2 on LiX, that the accessible distance of the radical to Li^+ is different from those in the other cations, because decreased size of the cation decreases the extent of exposure of the cation to the cavities in the stabi-

lized form of the exchanged zeolites. In the partially exchanged LiX, however, the splittings of both species were larger than those of NaX when pretreated at 600° . Therefore it is suggested that the Li^+ in the 10% LiX is sited in the more exposed position than that in LiX, possibly due to the interaction with Na^+ to give the larger splittings. The result that the observed splittings in 10% LiX treated at 350° was the same as NaX may imply the preferential adsorption of ClO_2 on Na^+ sites due to the difficulty in eliminating the adsorbed water on the Li^+ site.

References and Notes

- (1) J. A. Rabo, C. L. Angell, P. H. Kasai, and V. Schomaker, *Discuss. Faraday Soc.*, **41**, 328 (1966).
- (2) J. T. Richardson, *J. Catal.*, **9**, 182 (1967).
- (3) J. W. Ward, *J. Catal.*, **10**, 34 (1968).
- (4) J. W. Ward, *J. Catal.*, **14**, 365 (1969).
- (5) C. L. Gardner, *J. Chem. Phys.*, **46**, 2991 (1967); C. L. Gardner, E. J. Casey, and C. W. M. Grant, *J. Phys. Chem.*, **74**, 3273 (1970).
- (6) J. A. R. Coope, C. L. Gardner, C. A. McDowell, and A. I. Pelman, *Mol. Phys.*, **21**, 1043 (1971).
- (7) T. Cole, *Proc. Nat. Acad. Sci. U. S.*, **46**, 506 (1960).
- (8) L. H. Ahrens, *Nature (London)*, **74**, 644 (1954).
- (9) M. H. Brooker and M. A. Bredig, *J. Chem. Phys.*, **58**, 5319 (1973).
- (10) A. I. Pelman, Ph.D. Thesis, The University of British Columbia, 1971.

Department of Chemistry
Tokyo Institute of Technology
Meguro-ku, Tokyo, Japan 152

K. Shimokoshi*
H. Sugihara
I. Yasumori

Received February 20, 1974

Equilibrium Studies by Electron Spin Resonance. VIII. The Use of Time Averaged Coupling Constants to Determine Free Ion-Ion Pair Equilibrium Constants

Publication costs assisted by the University of Puerto Rico

Sir: ESR spectroscopy has proven itself to be the most useful tool for probing the nature of ion pairing in solution and has been used by several workers to investigate the actual equilibrium constants controlling the dissociation of ion pair β to form the free ion α .¹



The number of systems for which this equilibrium constant for ion pair dissociation is known, however, is still quite small. This is due to the fact that it has been necessary to observe the free ion (α) and the ion pair (β) simultaneously. That is, the esr signal for the two species must be observed together.² Further, simultaneous observation of α and β is rarely encountered, since in most cases there is a rapid interchange between the free ion and ion pair that is fast on the esr time scale.³ This results in an esr spectrum that is a weighted average between that for α and that for β .

Here we wish to report the first use of weighted average equations in terms of esr coupling constants for the determination of an equilibrium constant for ion pair dissociation to form free ion and the conditions under which these equations can be used.

It has been previously observed that anion radicals in hexamethylphosphoramide (HMPA) are virtually fully dis-

- (3) N. Hirota, *J. Phys. Chem.*, **71**, 127 (1967).
 (4) G. Levin, J. Jaugar-Grodzinski, and M. Szwarc, *J. Amer. Chem. Soc.*, **92**, 2268 (1970).
 (5) G. R. Stevenson and L. Echegoyen, *J. Phys. Chem.*, **77**, 2339 (1973).
 (6) It has been previously observed that salts such as KI are fully dissociated in HMPA, see P. Bruno, M. D. Monica, and E. Righetti, *J. Phys. Chem.*, **77**, 1258 (1973).
 (7) The potassium ion concentration was taken as that of the added KI, since this concentration is several orders of magnitude larger than the concentration of potassium used for the reduction.
 (8) D. A. Deranleau, *J. Amer. Chem. Soc.*, **91**, 4044 (1969).
 (9) G. R. Stevenson, J. G. Concepción, and J. Castillo, *J. Phys. Chem.*, **77**, 611 (1973).

Department of Chemistry
 University of Puerto Rico
 Rio Piedras, Puerto Rico 00931

Gerald R. Stevenson*
 Antonio E. Alegría

Received May 6, 1974

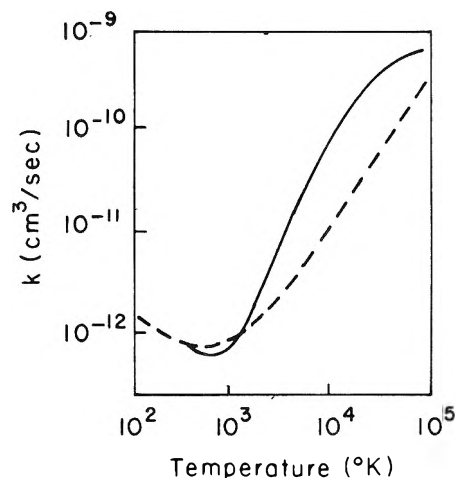


Figure 1. Temperature dependence of the rate constant for the reaction $O^+ + N_2 \rightarrow NO^+ + N$. Experimental data (—) are taken from ref 13; (---) calculated using TST. Calculated rate constant arbitrarily scaled to equal experimental rate constant at $T = 300^\circ K$.

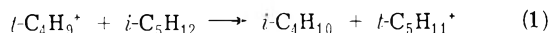
On the Negative Temperature Dependence of Slow Ion-Molecule Reactions

Publication costs assisted by the National Science Foundation

Sir: With the equipment and techniques developed over the past few years it has become possible to study "slow" ion-molecule reactions under conditions which permit the determination of the order of the reaction and the dependence of the rate on temperature. For many of these reactions the temperature dependence is unequivocally negative, that is, the rate increases as the temperature is lowered. In most cases the data best fit not the Arrhenius equation, but the equation $k_r = AT^n$ where n has been found experimentally to have values from 0 to -4.6 .

Two kinds of theoretical explanations have been proposed for these observations. In the first,¹ it is assumed that the reaction proceeds in two stages, the formation of an intermediate, followed by the unimolecular decay of that intermediate. The assumption is made that the longer the lifetime of the intermediate, the higher the probability of its dissociation into the observed products. The other theoretical explanation is quantum chemical and analyzes the reaction path along potential energy surfaces in terms of symmetry and selection rules.²

In the study of one ion-molecule reaction³



for which $n = -3.0$, we have found that ordinary transition state theory (TST) accounts satisfactorily for the observed temperature dependence. We have, therefore, applied TST to other known slow ion-molecule reactions. The results are reported herein.

The basic equation of TST⁴ may be written as

$$k_r(T) = c \frac{kT}{h} \frac{Q_{\text{trans}}^\ddagger Q_{\text{rot}}^\ddagger Q_{\text{vib}}^\ddagger Q_{\text{elec}}^\ddagger}{\prod_i (Q_i)_{\text{trans}} (Q_i)_{\text{rot}} (Q_i)_{\text{vib}} (Q_i)_{\text{elec}}} \times \exp(-E_0/kT) \quad (2)$$

where k_r is the reaction rate constant, c is the transmission coefficient, the Q^j are the partition functions for the activated complex, and the Q_i are the partition functions for the reactants. The temperature dependence of the transmission coefficient and the electronic and vibrational parti-

tion functions will be assumed to be sufficiently small to be neglected as a first approximation.⁵ The partition functions of any internal vibrations that remain unchanged in the complex will cancel out. Labeling the origins of the temperature dependent terms, eq 2 may be rewritten as

$$k_r(T) = AT \frac{(T_{\text{trans}}^{3/2})^\ddagger (T_{\text{rot}}^{j/2})^\ddagger}{\prod_i (T_{\text{trans}}^{3/2})_i (T_{\text{rot}}^{j/2})_i} T_{\text{int rot}}^{r/2} \times \exp(-E_0/kT) \quad (3)$$

Here A is a constant with respect to temperature; r is the total number of new internal rotations created upon the formation of the complex, *i.e.*, the number of new internal rotations present in the complex minus the number of internal rotations that became hindered upon the formation of the complex; j is 3 for nonlinear molecules, 2 for linear molecules, and 0 for atoms.

If E_0 is negligible, eq 3 reduces to the form $k_r = AT^n$. The only reaction of neutrals for which there is a large negative temperature coefficient, that of nitric oxide with oxygen, was treated by Gershinowitz and Eyring.⁶ In that case, as in the case of the ion-molecule reactions which we are here discussing, attractive potentials between the reactants balance the zero point energy of the newly formed vibrations, giving an effectively zero activation energy. Although we wish to reserve a discussion of absolute rates for a more detailed consideration at a later time, we would like to point out here that the same factors which introduce negative exponents for T also explain the slowness of such reactions.

For the ion-molecule reactions, other than reaction 1 reported in the literature, those which have the most markedly negative temperature coefficients are those which have been found to be third order. Table I gives the observed temperature dependences and those predicted from TST for reactions for which experimental data are available. It will be seen that the agreement is very good, considering the accuracy of the experimental data quoted and the approximations involved in the present calculations.

We have already mentioned the reaction of *tert*-butyl ion with isopentane, in which the temperature dependence of T^{-3} indicates that about two free rotations of the methyl

TABLE I: Calculated and Experimental Temperature Dependence of the Rate Constants Expressed as $k_r = AT^n$ for Trimolecular Ion-Molecule Reactions

Type of reaction ^a	Examples	Calcd temperature dependence ^b		Exptl temperature dependence ^c	Ref
		Linear complex	Nonlinear complex		
A ⁺ + A + A	He ⁺ + He + He → He ₂ ⁺ + He	T ⁻¹	T ^{-0.5}	T ⁻¹	7
A ⁺ + L + A	N ⁺ + N ₂ + He → N ₃ ⁺ + He	T ⁻²	T ^{-1.5}	T ^{-1.7}	8
L ⁺ + L + A	N ₂ ⁺ + N ₂ + He → N ₄ ⁺ + He			T ^{-1.6}	8
or					
A ⁺ + L + L	N ⁺ + N ₂ + N ₂ → N ₃ ⁺ + N ₂			T ^{-2.5}	9
L ⁺ + L + L	O ₃ ⁺ + O ₂ + O ₂ → O ₄ ⁺ + O ₂	T ⁻⁴	T ^{-3.5}	T ⁻³	10
	N ₃ ⁺ + N ₂ + N ₂ → N ₄ ⁺ + N ₂			T ^{-4.4}	9
NL ⁺ + L + L	H ₃ ⁺ + H ₂ + H ₂ → H ₅ ⁺ + H ₂	T ^{-4.5}	T ⁻⁴	T ^{-4.6}	11
NL ⁺ + NL + NL	H ₃ O ⁺ + H ₂ O + CH ₄ → H ₅ O ₂ ⁺ + CH ₄	T ^{-5.5}	T ⁻⁵	T ^{-4.2}	12

^a Here A denotes an atomic, L a linear, and NL a nonlinear species. ^b Calculated from eq 3, with $r = 0$. ^c Calculated from the data given in the corresponding references.

groups are restricted in the activated complex. The bimolecular reaction



has been studied over a wide temperature range.¹³ It has been observed that the temperature coefficient changes from negative at low temperatures to positive at high temperatures. This can be accounted for on the basis that at higher temperatures the effect of the vibrational partition functions can no longer be neglected and, consequently, there is no need to introduce arbitrarily a change in the mechanism at higher temperatures.

We have assumed that the activated complex is a linear N₂O⁺. As a first approximation, we take the vibration frequencies of the activated complex to be those of the stable N₂O⁺ ion,¹⁴ and we have calculated the temperature dependence of the rate constant. The results, compared with the experimental data, are shown in Figure 1. The agreement is again gratifying, but more detailed study will be needed to determine whether this explanation based on TST or one of the alternatives proposed by Ferguson¹ or by Kaufman² is the correct one.

The fact that we now have on hand a large amount of experimental data for reactions of small molecules with little or no activation energy makes possible new attempts to calculate absolute rates from first principles and suggests possibilities for experimental investigations of such phenomena as kinetic isotope effects. We think that the study of ion-molecule reactions will contribute to a better understanding of the preexponential factor in chemical reactions in general.

Acknowledgment. This research was supported in part by a grant from the National Science Foundation.

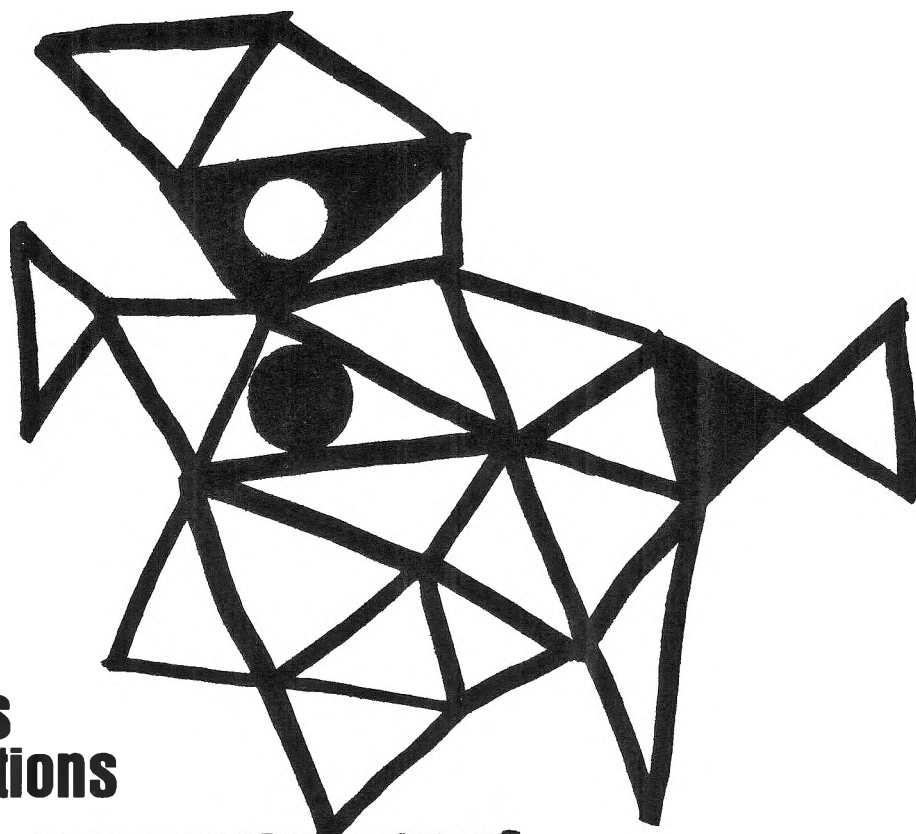
References and Notes

- (1) E. E. Ferguson, "Ion-Molecule Reactions," Vol. 2, J. L. Franklin, Ed., Plenum Press, New York, N. Y., 1972, Chapter 8.
- (2) J. J. Kaufman, "Wave Mechanics, The First Fifty Years," W. C. Price, *et al.*, Ed., Wiley, New York, N. Y., 1973, Chapter 14.
- (3) J. J. Solomon, M. Meot-Ner, and F. H. Field, *J. Amer. Chem. Soc.*, **96**, 3727 (1974).
- (4) For rigorous derivation and comprehensive discussion see H. S. Johnston, "Gas Phase Reaction Rate Theory," Ronald Press, New York, N. Y., 1966, Chapters 8 and 9.
- (5) The partition function for a vibration is $(1 - e^{-h\nu/kT})^{-1}$, which is clearly a function of temperature. Most of the experimental data treated in our Table I were obtained between 80 and 300°K. At 80°K the partition function is unity for practically all vibration frequencies. At 300°K it is equal to 1.097 for $\nu = 500 \text{ cm}^{-1}$, 1.008 for $\nu = 1000 \text{ cm}^{-1}$, and 1.0000005 for $\nu = 3000 \text{ cm}^{-1}$. It is only for frequencies lower than 500 cm^{-1} that one would have an error of 10% or more due to this assumption. One would not expect many such low frequencies in molecules as small as those we are considering. At higher temperatures the value of the partition function begins to change more rapidly and we discuss later in this paper one example for which sufficient data are available.
- (6) H. Gershinowitz and H. Eyring, *J. Amer. Chem. Soc.*, **57**, 985 (1935).
- (7) F. E. Niles and W. W. Robertson, *J. Chem. Phys.*, **42**, 3277 (1965).
- (8) D. K. Bohme, D. B. Dunkin, F. C. Fehsenfeld, and E. E. Ferguson, *J. Chem. Phys.*, **51**, 863 (1969).
- (9) A. Good, D. A. Durden, and P. Kebarle, *J. Chem. Phys.*, **52**, 212 (1970).
- (10) D. A. Durden, P. Kebarle, and A. Good, *J. Chem. Phys.*, **50**, 805 (1969).
- (11) R. C. Pierce and R. F. Porter, *Chem. Phys. Lett.*, **23**, 608 (1973).
- (12) A. J. Cunningham, J. D. Paysant, and P. Kebarle, *J. Amer. Chem. Soc.*, **94**, 7627 (1972).
- (13) M. McFarland, D. L. Albritton, F. C. Fehsenfeld, E. E. Ferguson, and A. C. Schmeltekopf, *J. Chem. Phys.*, **59**, 6620 (1973).
- (14) G. Herzberg, "Electronic Spectra of Polyatomic Molecules," Van Nostrand, Princeton, N. J. 1967, p 593.

Department of Chemistry
The Rockefeller University
New York, New York 10021

M. Meot-Ner
J. J. Solomon
F. H. Field
H. Gershinowitz*

Received April 11, 1974

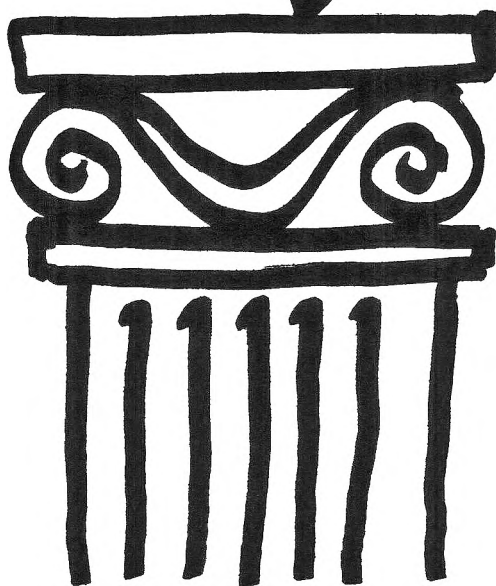


**New concepts
new techniques
new interpretations**

**... together
with valuable reports
on classical areas**

They are all waiting for you between the covers of our well-balanced JOURNAL OF PHYSICAL CHEMISTRY. Whatever your particular interest in physical chemistry, you'll find the JOURNAL's broad range of experimental and theoretical research reports are relevant and beneficial to your work. Each biweekly issue brings you an average of 30 authoritative, comprehensive reports on fundamental aspects of atomic and molecular phenomena, as well as timely notes, communications and reports plus the proceedings of selected symposia.

Join your fellow physical chemists who rely on JPC as an excellent biweekly source of data in both new and classical areas. Just complete and return the form to start your own subscription.



**Journal of
Physical
Chemistry**

**The Journal of Physical Chemistry
American Chemical Society**
1155 Sixteenth Street, N.W.
Washington, D.C. 20036

1974

Yes, I would like to receive the JOURNAL OF PHYSICAL CHEMISTRY at the one-year rate checked below:

	U.S.	Canada**	Latin America**	Other Nations**
ACS Member One-Year Rate*	<input type="checkbox"/> \$20.00	<input type="checkbox"/> \$25.00	<input type="checkbox"/> \$25.00	<input type="checkbox"/> \$26.00
Nonmember	<input type="checkbox"/> \$60.00	<input type="checkbox"/> \$65.00	<input type="checkbox"/> \$65.00	<input type="checkbox"/> \$66.00

Bill me Bill company Payment enclosed

Air freight rates available on request.

Name _____

Street _____ Home
Business

City _____ State _____ Zip _____

*NOTE: Subscriptions at ACS member rates are for personal use only. **Payment must be made in U.S. currency, by international money order, UNESCO coupons, U.S. bank draft, or order through your book dealer.



... another ACS service

NEW

CHEMICAL PHYSICS BOOKS FROM WILEY-INTERSCIENCE.

1. THE EXCITED STATE IN CHEMICAL PHYSICS

Edited by J. William McGowan, *The University of Western Ontario*

Advances in Chemical Physics, Vol. 28

This book consolidates material from many fields in order to familiarize people from other areas with the problems and general literature of excited states in chemistry and physics. It emphasizes collisions of neutral species, chemical reactions, some molecular structure, and energy transfer. Physicists in the chemical, atomic, laser, and upper atmosphere fields, as well as photochemists and physical chemists, will find it an excellent source of information for areas that might not be their specialty.

1974 432 pages \$25.50

2. ADVANCES IN CHEMICAL PHYSICS, Vol. 27

Edited by I. Prigogine, *University of Brussels*, and Stuart A. Rice, *University of Chicago*

Contains original papers by leading scientists on the basic property problems of individual molecules and atoms, and on the behavior of statistical ensembles of molecules and atoms. Topics include: Determination of the Structure and Properties of Solid Surfaces by Electron Diffraction and Emission . . . Electron Spectroscopy of Chemisorption on Metals . . . Surface Plasma Oscillations and Related Surface Effects in Solids . . . Theory of Dynamical Properties of Dielectric Surfaces . . . and Some Comments on the Electronic Properties of Liquid Metal Surfaces.

1974 approx. 704 pages In Press

3. EXPERIMENTAL ELECTRO-CHEMISTRY FOR CHEMISTS

By Donald T. Sawyer, *University of California, Riverside*, and Julian L. Roberts, Jr., *University of Redlands, California*

Written for research workers, graduate students, and upper division majors in chemistry, this book outlines the basic principles and modern methodology of electrochemistry as applied to the study of chemical systems. Special topics include the design and construction of electrodes and cells . . . purification of solvents and electrolytes . . . and a practical introduction to electrochemical instrumentation and electronics.

1974 approx. 480 pages In Press

4. FINITE GROUPS AND QUANTUM THEORY

By D. B. Chesnut, *Duke University*

Here is a book that makes the basic mathematical ideas and structure behind the theory of point groups easily accessible to readers. By examining the use and application of point group theory in quantum mechanics, it shows how to apply the theory and provides related mathematical background and terminology.

1974 approx. 240 pages \$14.95

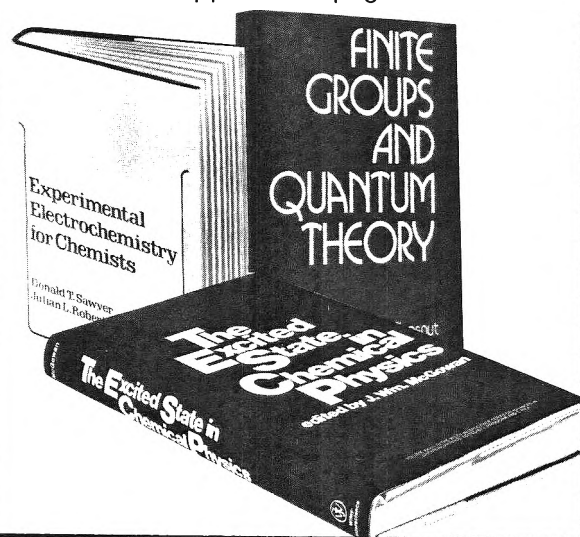
Available from your bookstore or Dept. 265
WILEY-INTERSCIENCE

a division of **John Wiley & Sons, Inc.**

605 Third Avenue, New York, N.Y. 10016

In Canada: 22 Worcester Road, Rexdale, Ontario

Prices subject to change without notice. 092 A 4684-WI



Mail coupon to—

WILEY-INTERSCIENCE, Dept. 265, P.O. Box 4569, Grand Central Station, New York, N.Y. 10017

Please send me the book(s) whose number(s) I have checked:

1 (1-58425-8) 2 (1-69932-2) 3 (1-75560-5) 4 (1-15445-8)

- My check (money order) for \$_____ is enclosed.
 Please bill me. (Restricted to the continental United States.)
 Please send a list of nearest bookstores carrying your titles.

Name _____

Affiliation _____

Address _____

City/State/Zip _____

Please add state and local taxes where applicable. 092 A 4684-WI
Prices subject to change without notice.